Assessing the role of extracellular vesicles in renin-angiotensin system signalling in cardiomyocyte hypertrophy

Laura Downie

BSc (Hons)

Submitted in fulfilment of the requirements for the degree of Doctor of Philosophy to the Institute of Cardiovascular and Medical Sciences, University of Glasgow.

Research conducted at the British Heart Foundation Glasgow Cardiovascular Research Centre, Institute of Cardiovascular and Medical Sciences, College of Medical, Veterinary and Life Sciences, University of Glasgow, U.K.

2019

Author's Declaration

I declare that this thesis was written entirely by myself and is a record of the work performed by me with some exceptions as detailed below. Characterisation of human serum extracellular vesicles by Nanosight, Ang II ELISA and Ang-(1-7) ELISA was carried out in collaboration with Mr Philipp Boder. The echocardiography of animals was carried out by Dr Tamara Martin. The femoral vein injections were carried out by Dr Delyth Graham. Transmission electron microscopy was carried out by the Electron Microscopy Facility, University of Glasgow College of MVLS. This thesis has not been submitted previously for a higher degree. The work included in this thesis was completed at the University of Glasgow Cardiovascular Research Centre in the Institute of Cardiovascular and Medical Sciences under the supervision of Professor Stuart A. Nicklin and Dr Lorraine M. Work.

Laura Downie

2019

Acknowledgements

Firstly, I would like to thank my two supervisors, Professor Stuart Nicklin and Dr Lorraine Work for their support and encouragement throughout this PhD not only academically but also personally. So, thank you, Stu and Lorraine, for giving me the chance to complete my PhD and always believing in me throughout (even when I didn't). I would also like to thank my two independent reviewers, Dr Tom Van Agtmael and Dr Dilys Freeman for going that extra mile for me. Thank you to the Biotechnology and Biological Sciences Research Council and the University of Glasgow, College of MVLS for funding this work.

Many thanks to everyone in the Level 4 lab, past and present, for their help and guidance, and (arguably more importantly) for all the laughs. Particular thanks go to Del, Stacy, Tamara and Nic for their scientific expertise and guidance. Special thanks to Wai for all your IT support. Thanks to Alyson, Arun, Ashton and Ahmad for all the banter – I couldn't have finished this thesis without my regular visits to the banter bay! Long may the pranks continue.

I've been lucky enough to make amazing friends throughout the duration of my PhD and I'm the last of the "Science Besties" to finish! So, thank you to my elders: Lisa, Mags, Emma, Nina, Tall and Small for all the advice and all the amazing memories. Thanks to those I shared the glass office with: Lauren, Tuuli, Aisling and Sonya. And to my write-up office boys, Sammy and Anubhav. Special thanks to Dr Berlin (Julian) for all the coffee, chat and banter.

I couldn't have made it without my non-science friends as well. There are too many to name but a special thanks goes to my aerial people past and present, particularly to Fiona, Becca, Ash, Jody, Claire and Megan for all the fun times – no serious conversations allowed. And also, to Rodolfo for his support with aerial throughout my time at university. Another thanks goes to my hometown bestie, Emma T, who has never once failed to make me laugh.

Finally, a huge thanks must go to my family, in particular to my mum and dad who have been a continual source of support through all of the years I've spent at university – thanks for at least trying to understand what I do!

Table of Contents

List of Figures

List of Tables

List of Publications, Presentations and Awards

Published Abstracts

Downie, L.S., Work, L.M., & Nicklin, S.A. (2018) Endogenous and exogenous loading of extracellular vesicles for therapeutic delivery of the renin-angiotensin system peptide angiotensin-(1-7) in cardiomyocyte hypertrophy, Journal of Extracellular Vesicles, 7(Supplement 1): PT07.14

Downie, L.S., Work, L.M., & Nicklin, S.A. (2018) Endogenous and exogenous loading of extracellular vesicles for therapeutic delivery of renin-angiotensin system peptides in cardiomyocyte hypertrophy, BMJ Heart, 104(Supplement 4):A4

Downie, L.S., Nather, K., Work, L.M., & Nicklin, S.A. (2017) Assessing the role of extracellular vesicles in Renin-Angiotensin System signalling in cardiomyocyte hypertrophy, BMJ Heart, 103(Supplement 2):A2-A3

Presentations

Endogenous and exogenous loading of extracellular vesicles for therapeutic delivery of the renin-angiotensin system peptide angiotensin-(1-7) in cardiomyocyte hypertrophy. International Society for Extracellular Vesicles 7th Annual Meeting, 2018, Barcelona, Spain. [poster communication]

Endogenous and exogenous loading of extracellular vesicles for therapeutic delivery of renin-angiotensin system peptides in cardiomyocyte hypertrophy. Scottish Cardiovascular Forum 21st Annual Meeting, 2018, Dublin, Ireland. [oral communication]

Assessing Renin-Angiotensin System signalling via extracellular vesicles in H9c2 cardiomyocytes. UK Extracellular Vesicle Forum 4th Annual Meeting, 2017, Birmingham, UK. [poster communication]

Assessing the role of extracellular vesicles in Renin-Angiotensin System signalling in cardiomyocyte hypertrophy. Scottish Cardiovascular Forum 20th Annual Meeting, 2017, Glasgow, UK. [oral communication]

Awards

Promoting the Advancement of Physiology Travel Grant, The Physiological Society, March 2018.
Conference Support Award, University of Glasgow College of MVLS, March 2018.
Honor Fell Travel Award, British Society for Cell Biology, February 2018.
Poster communication prize, 4th UK Extracellular Vesicle Forum, December 2017.

List of Abbreviations and Definitions

A779	Mas receptor antagonist
ACE	Angiotensin converting enzyme
ACE2	Angiotensin converting enzyme 2
ACEi	Angiotensin converting enzyme inhibitors
Agt	Angiotensinogen
Akt	Protein kinase B
ALIX	Apoptosis-linked gene 2-interacting protein X
Ang I	Angiotensin I
Ang II	Angiotensin II
Ang-(1-7)	Angiotensin-(1-7)
Ang-(1-9)	Angiotensin-(1-9)
ANOVA	Analysis of variance
ANP	Atrial natriuretic peptide
ARB	Angiotensin II type 1 receptor blocker
ARF6	ADP-ribosylation factor 6
ARRDC1	Arrestin 1 domain-containing protein 1
ARVM	Adult rat ventricular cardiomyocyte
ASK1	Apoptosis signal regulating kinase 1
AT1R	Angiotensin II type 1 receptor
AT2R	Angiotensin II type 2 receptor
ATP	Adenosine triphosphate
B2	Bradykinin B2 Receptor
BCA	Bicinchoninic acid
BNP	Brain natriuretic peptide
BSA	Bovine serum albumin
ß-blockers	Beta blocker
ß-MHC	Beta major histocompatibility complex
cGMP	3'-5'-cyclic guanosine monophosphate
CPC	cardiomyocyte progenitor cell
CPI-17	Protein phosphatase 1 regulatory subunit 14A
Ct	Cycle threshold
CVD	Cardiovascular disease
DAG	Diacylglycerol

DAPI	4′,6-diamidino-2-phenylindole
DMEM	Dulbecco's modified eagle's medium
DMSO	Dimethyl sulfoxide
DNA	Deoxyribonucleic acid
dsDNA	Double stranded DNA
DUSP1	Dual specificity protein phosphatase 1
EDD	End diastolic diameter
EDTA	Ethylenediaminetetraacetic acid
EGFR	Epidermal growth factor receptor
EGTA	Ethylene glycol-bis(ß-aminoethyl ether)-N,N,N′,N′-tetraacetic acid
ELISA	Enzyme-linked immunosorbent assay
eNOS	Endothelial nitric oxide synthase
ErbB	Family of receptor tyrosine kinases
ERK	Extracellular signal-regulated kinase
ESCRT	Endosomal sorting complexes required for transport
ESD	End systolic diameter
EV	Extracellular vesicle
FAK	Focal adhesion kinase
FAM	Fluorescein amidite
FCS	Foetal calf serum
FITC	Fluorescein isothiocyanate
FS	Fractional shortening
gACE	Germinal angiotensin converting enzyme
GAPDH	Glyceraldehyde 3-phosphate dehydrogenase
GPCR	G-protein coupled receptor
Grb2	Growth factor receptor-bound protein 2
GRK	G-protein coupled receptor kinase
GW4869	Inhibitor of neutral sphingomyelinase
Gαi	G-protein
H9c2	H9c2(2-1) cardiomyoblast cell line
HAEC	Human aortic endothelial cells
HEK	Human embryonic kidney
HEp-2	Human epithelial cell line
HEPES	4-(2-hydroxyethyl)-1-piperazineethanesulfonic acid
HETE	Hydroxyeicosatetraenoic acid

HF-pEF	Heart failure with preserved ejection fraction
HF-rEF	Heart failure with reduced ejection fraction
HIF	Hypoxia-inducible factor
HL-1	Mouse cardiac muscle cell line
HSP	Heat shock protein
HW/BW	Heart weight/body weight ratio
ICAM-1	Intercellular adhesion molecule 1
ICC	Immunocytochemistry
IFNGR1	Interferon gamma receptor 1
IGF-1	Insulin-like growth factor 1
IHC	Immunohistochemistry
ILV	Intraluminal vesicle
ISEV	International Society for Extracellular Vesicles
JAK	Janus-activated kinase
JNK	c-Jun N-terminal kinase
LV	Left ventricular
LV/TL	Left ventricular/tibia length ratio
M	Molar
MAPK	Mitogen-activated protein kinase
Mas	MAS1 proto-oncogene, G protein-coupled receptor
MCP-1	Monocyte chemoattractant protein 1
MCT	Monocrotaline
MHC-I	Major histocompatibility complex 1
MI	Myocardial infarction
MEM	Minimal Essential medium
miRNA/miR	Micro ribonucleic acid
mL	Millilitre
MLCK	Myosin light chain kinase
MLCP	Myosin light chain phosphatase
mM	Millimolar
MMP	Matrix metalloproteinase
mRNA	Messenger ribonucleic acid
MSC	Mesenchymal stromal cell
MV	Microvesicle
MVB	Multivesicular body

NADPH	nicotinamide adenine dinucleotide phosphate
NE	Norepinephrine
NFAT	Nuclear factor of activated T cells
NHE-3	Na+/H+ exchanger 3
NKA	Na+/K+ ATPase
nM	Nanomolar
NO	Nitric oxide
NPC	Neural stem precursor cell
Nppa	Natriuretic peptide precursor A
Nppb	Natriuretic peptide precursor B
NRCF	Neonatal rat cardiac fibroblast
NRCM	Neonatal rat cardiomyocyte
nSMase	Neutral sphingomyelinase
NTA	Nanoparticle tracking analysis
P2X7	P2X purinoceptor 7
P38MAPK	P38 mitogen-activated protein kinase
PAH	Pulmonary arterial hypertension
PBS	Phosphate buffered saline
PD123,319	Angiotensin II type 2 receptor antagonist
PDGF	Platelet derived growth factor
PDK1	Phosphoinositide-dependent kinase-1
PDLIM5	PDZ and LIM domain 5
pERK	Phosphorylated extracellular signal-regulated kinase
PFA	Paraformaldehyde
PGE2	Prostaglandin E2
PGH2	Prostaglandin H2
PGI2	Prostacyclin
PI3K	Phosphoinositide 3-kinase
PK	Proteinase K
PKC	Protein kinase C
PKH26	Red lipophilic dye
PLA2	Phospholipase A2
PLC	Phospholipase C
PLP	Proteolipid protein
PM	Plasma membrane

PMSF	Phenylmethylsulfonyl fluoride
PP2A	Protein phosphatase 2A
PTP1b	Tyrosine-protein phosphatase non-receptor type 1
Pyk2	Proline-rich tyrosine kinase 2
Rab	G-protein of Ras superfamily
Rac1	Rac family small GTPase 1
Raf	Rapidly accelerated fibrosarcoma
RAS	Renin-Angiotensin System
Ras	Ras subfamily of proteins
RGS	Regulators of g-protein signalling
ROI	Region of interest
ROS	Reactive oxygen species
RQ	Relative quantification
sACE	Somatic angiotensin converting enzyme
SERCA2	Sarco/endoplasmic reticulum Ca2+-ATPase 2
Shc	SHC Adaptor Protein
SHP-1	Src homology 2 domain phosphatase-1
SHRSP	Stroke-prone spontaneously hypertensive rat
siRNA	Short interfering ribonucleic acid
SOD1	Superoxide dismutase 1
SORBS2	Sorbin and SH3 domain containing 2
SOX4	SRY-Box 4
Src	Proto-oncogene tyrosine-protein kinase Src
STAT	Signal transducer and activator of transcription
TBS	Tris-buffered saline
TEM	Transmission electron microscopy
TSG-101	Tumour-susceptibility gene 101
VEGFR2	Vascular endothelial growth factor receptor 2
VSMC	Vascular smooth muscle cell
v/v	Volume/volume
WGA	Wheat germ agglutinin
WKY	Wistar Kyoto
Wnt	Wingless/integrated
w/v	Weight/volume
YFP	Yellow fluorescent protein

Summary

Cardiovascular disease (CVD) involving the heart or blood vessels is the most common cause of death and disability worldwide. Following development of chronic hypertension, the left ventricular mass of the heart increases adaptively due to increased work load which further increases the risk of adverse cardiac events such as heart failure. Cardiomyocyte hypertrophy is associated with classical renin-angiotensin system (RAS) signalling where increased angiotensin II (Ang II) signalling via the angiotensin II type 1 receptor (AT_1R) exacerbates the hypertrophic response and blockade of Ang II signalling via angiotensin receptor blockers (ARBs) inhibits the hypertrophic response. Experimental models of CVD, including cardiac hypertrophy, have shown that stimulation of the counter-regulatory axis of the RAS, in particular stimulation of the ACE2/Ang-(1-7)/Mas signalling arm, provides cardioprotective effects. Although there is growing evidence for the importance of Ang-(1-7) in cardioprotection, delivery of this peptide to the heart as a therapeutic proves difficult owing to its short half life and thus quick degradation in the circulation. Recently, extracellular vesicles (EVs) have become an area of interest in terms of therapeutic delivery vehicles in a variety of disease settings. Due to their phospholipid bilayer, EVs remain stable and are not immediately degraded in the circulation, however organ-targeting is still a major challenge. As there is a need for new therapeutic delivery strategies for Ang-(1-7), the primary aim of this thesis was to investigate the potential role of EVs in RAS signalling and to determine whether functional Ang-(1-7) could be delivered via EVs in both *in vitro* and *in vivo* models of Ang II-induced cardiomyocyte hypertrophy.

Initially, *in vitro* investigations were carried out in the H9c2 model of Ang II-induced cardiomyocyte hypertrophy. EVs were obtained from the conditioned media of H9c2 cardiomyocytes +/- Ang II stimulation and successfully characterised in terms of size, protein concentration, and concentration of particles released though no significant differences were found upon Ang II stimulation. EVs obtained from cardiac fibroblasts [neonatal rat cardiac fibroblasts (NRCF)] +/- Ang II stimulation were also characterised and found to be significantly larger than those released from H9c2 cardiomyocytes.

Next, the functional effect of the EVs was determined using the H9c2 model of cardiomyocyte hypertrophy. It was found that 1 hr post-treatment with EVs, the EVs could be found associated with the H9c2 cell nucleus. EVs released from FAM-labelled Ang II treated H9c2 cells were shown to co-localise at the recipient H9c2 cell nucleus along with the FAM-Ang II signal. The evidence for Ang II association with EVs was further demonstrated by ELISA, where it was found that Ang II levels were significantly increased in EVs released from Ang II stimulated H9c2 cells vs control cells. Treatment of recipient H9c2 cells with Ang II EVs induced a hypertrophic response in these cells, where a significant increase in cell size was observed along with increased gene expression of the hypertrophy marker, brain natriuretic peptide (BNP). It was found that proteinase K efficiently digests soluble Ang II peptide and that treatment of EVs with proteinase K before addition to recipient cells did not abolish the hypertrophic effect. The hypertrophic response observed by treatment with Ang II EVs could be blocked by pre-treating parental cells with losartan but not by pre-treatment with PD123,319. It was found that EVs derived from Ang II-stimulated NRCF cells could also induce a hypertrophic response in recipient H9c2 cardiomyocytes, and that Ang II was detectable within the EVs.

As the Ang II EVs were shown to have a functional effect in terms of hypertrophy in recipient cells, parental cells were next treated with Ang-(1-7) before EV isolation. It was found that EVs derived from Ang-(1-7) treated H9c2 cardiomyocytes were able to significantly inhibit Ang II-induced hypertrophy in recipient cells, where the Ang II-induced increase in cell size was absent upon co-treatment with Ang-(1-7)-EVs.

As functional Ang II was found at low levels within EVs derived from Ang II-stimulated cells, it was of interest to determine whether Ang II levels could be increased by exogenous loading via electroporation, and if Ang-(1-7) could also be exogenously loaded into EVs. Optimisation of electroporation with Ang II showed significantly higher levels present in Ang II electroporated EVs compared with naïve electroporated EVs. Similarly, it was found that electroporation of EVs in the presence of Ang-(1-7) produced significantly higher levels of Ang-(1-7) within EVs compared to naïve electroporated EVs. These Ang-(1-7)-loaded EVs inhibited Ang II-induced increase in cell size in recipient H9c2 cardiomyocytes.

Next, EVs were derived from the serum of normotensive WKY rats and hypertensive SHRSP rats and characterised. WKY EVs were found to be significantly larger than SHRSP EVs and exhibited a significantly higher protein concentration. WKY EVs were electroporated in the presence of Ang-(1-7) and then found to inhibit Ang II-induced hypertrophy in H9c2 cardiomyocytes. Interestingly, the inhibitory effect was also found after treatment with naïve electroporated EVs, an effect presumed to be due to the detectable levels of endogenous Ang-(1-7).

The protective effect of Ang-(1-7) electroporated serum-derived EVs was next investigated *in vivo* utilising an Ang II-infusion rat model. This involved two 30 µg bolus injections of electroporated EVs into the circulation of WKY rats infused with 200 ng/kg/min Ang II over a 2 week period. It was found that Ang II infusion did not significantly increase blood pressure, percentage fibrosis or cardiomyocyte hypertrophy compared with vehicle infusion. As a result, the protective effects of Ang-(1-7) EV bolus injection could not be established in this study.

Finally, human serum EV populations were analysed between healthy control subjects and coronary artery bypass patients to determine potential differences in size, concentration of particles released, Ang II content and Ang-(1-7) content under normal and CVD conditions. It was found that EVs derived from the serum of patients with coronary artery disease were significantly smaller in size than those from healthy control subjects and there were significantly lower numbers of particles released. It was also found that patient EVs contained significantly higher levels of Ang II compared with healthy controls, however Ang-(1-7) levels did not significantly differ between the two groups.

Overall, these studies provide evidence that different cells of the heart produce different populations of EVs. Additionally, these EVs are able to transport functional effector peptides associated with the RAS, including Ang II and Ang-(1-7), in an *in vitro* model of cardiomyocyte hypertrophy. Finally, for the first time, electroporation was used to load the cardioprotective peptide, Ang-(1-7), into EVs for delivery in an *in vivo* Ang II infusion model with promising effects valuable for future therapeutic studies.

Chapter 1 Introduction

1.1 Cardiovascular Disease

Cardiovascular disease (CVD) is a class of diseases involving the heart or blood vessels and is the number one most common cause of death and disability world-wide with global mortality rates predicted to reach over 23 million by 2030 (Mendis and Norrving, 2011). High blood pressure is arguably one of the most important risk factors in the development of cardiovascular disease. Hypertension is defined as prolonged systolic blood pressure of 140 mmHg or higher or diastolic blood pressure of 90 mmHg or higher (Chalmers et al., 1999). It has been reported that 75% of stroke cases and 50% of coronary heart disease events in developing countries, as well as 25% of myocardial infarctions in Europe were linked to initial development of hypertension (Mathers et al., 2009). This suggests that control and prevention of high blood pressure is key in prevention of further cardiovascular disease events.

Examples of CVD include coronary heart disease (or coronary artery disease), a small group of diseases which include angina, myocardial infarction and sudden cardiac death, and is notably the most common type of cardiovascular disease. These diseases present as limited blood flow to the heart causing ischaemia of myocardial cells. The death of these cells due to lack of oxygen results in occurrence of myocardial infarction, heart muscle damage or death, followed by myocardial scarring where heart muscle is unlikely to regrow (Ambrose and Singh, 2015). Furthermore, chronic stenosis of coronary arteries may induce transient ischaemia leading to ventricular arrhythmia, ventricular fibrillation and finally death (Ambrose and Singh, 2015). Most commonly, coronary artery disease occurs as a response to coronary arteries developing atherosclerosis; where the artery wall thickens and hardens due to deposits of calcium, fatty deposits and irregular inflammatory cells (Ambrose and Singh, 2015).

Another notable cardiovascular disease is stroke. Ischaemic stroke is the most noted in cardiovascular disease, which occurs due to lack of blood flow to the brain. When blood flow to the brain is decreased, the result is brain tissue dysfunction in the affected area of the brain. This may occur due to a number of reasons such as thrombosis (local blood clots obstructing blood vessels in the brain), embolism (an obstruction occurring from elsewhere in the body) or systemic hypoperfusion (a general decrease in blood supply) (Donnan et al.,

2008). In up to 40% of cases, ischaemic stroke occurs without an obvious cause where it is then referred to as cryptogenic stroke (Donnan et al., 2008).

1.1.1 The Heart

The heart is a muscular organ which functions to pump blood through the blood vessels of the circulatory system thus providing the body with oxygen and nutrients while removing metabolic waste. The heart consists of four chambers, the two upper atria which are the receiving chambers, and two lower ventricles which are the discharging chambers. Commonly the right atria and ventricle are referred to as the right heart while the left atria and ventricle are referred to as the left heart. The Frank-Starling law of the heart represents the relationship between stroke volume and end-diastolic volume in the heart (Jacob et al., 1992) which maintains left and right ventricular output equality. The law states that the stroke volume of the heart increases in response to increased volume of blood in the ventricles. As a larger volume of blood enters the ventricle, the cardiac muscle fibres stretch resulting in an increase in the force of contraction (Jacob et al., 1992). Cardiac dysfunction, where weakening, stiffening or loss of elasticity in the heart muscle can result in failure to pump blood efficiently, may culminate in heart failure (Mann and Bristow, 2005). Heart failure is one of the most common causes of death and disability worldwide and is becoming increasingly prevalent in the Western world, estimated to affect 1-2% of the population with generally poor prognosis (Orsborne et al., 2017). Some of the most common causes of heart failure include previous myocardial infarction, chronic hypertension and atrial fibrillation, with risk also increasing with obesity and diabetes mellitis diagnoses. Another contributing factor to the risk of heart failure is the occurrence of adverse cardiac remodelling, or hypertrophy, normally as a response to increased blood pressure (Orsborne et al., 2017).

1.1.2 Cardiac Hypertrophy

Hypertrophy often occurs naturally due to stressors such as haemodynamic overload or strength and aerobic exercise, however this is a type of physiological hypertrophy which is reversible and non-pathological. Pathological ventricular hypertrophy (Figure 1-1) is the thickening of the myocardium of the ventricles of the heart, as opposed to ventricular dilatation, where the ventricle chamber

itself is enlarged. While left ventricular hypertrophy is more common, muscle wall enlargement can also occur on the right side, or in both ventricles at once (Ruilope and Schmieder, 2008). Ventricular hypertrophy is seen as the heart's adaptive response to a chronically increased work load where the risk of cardiovascular disease-related events increases with increasing left ventricular mass however there is no specific cut-off point where mass then indicates pathological hypertrophy (Agabiti-Rosei et al., 2006). In cases of chronic hypertension, pathological ventricular hypertrophy may occur as the heart works to maintain a normal stroke volume. However, over time these changes in the heart cause measurable functional degradation (often resulting in heart failure) and thus can be used as a marker of heart disease (Dominiczak et al., 1997).

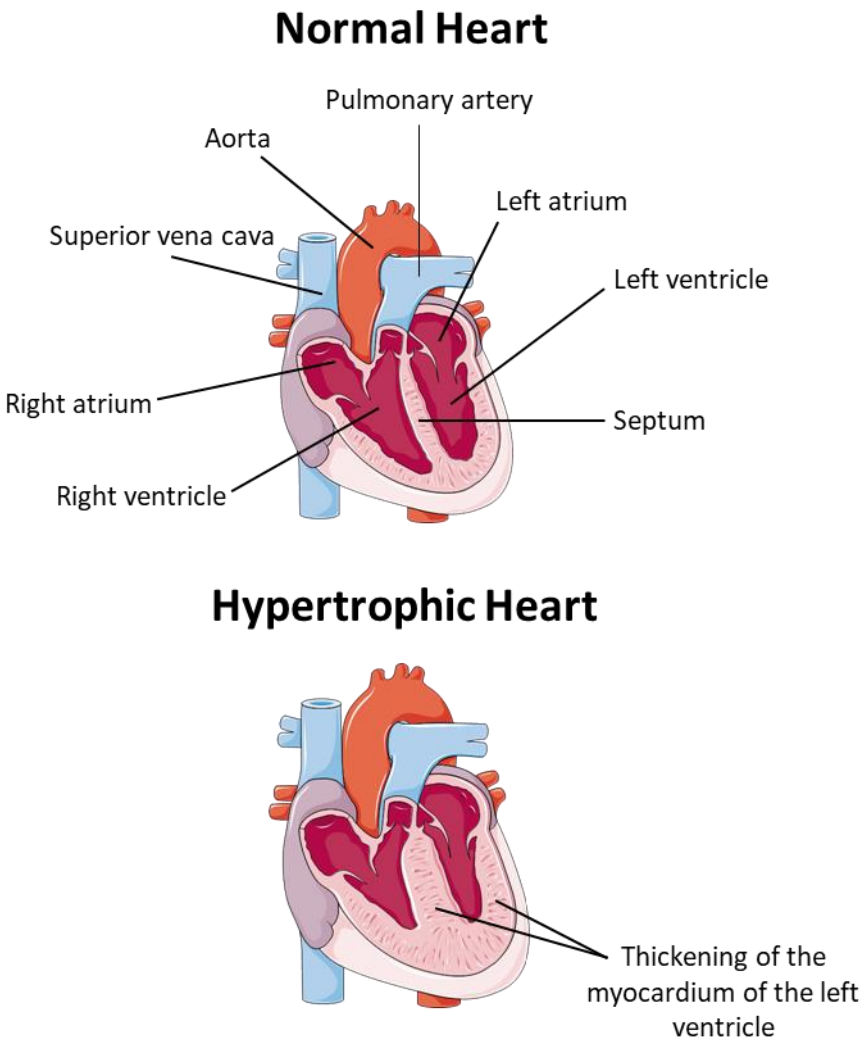

Figure 1-1 Diagram depicting the normal heart vs. the hypertrophied heart. The hypertrophic heart is depicted as having increased ventricular mass in comparison to the healthy heart. Thickening of the myocardium of the left ventricle causes the muscle to lose elasticity and eventually the heart may fail to pump with the force required. This thickening often results in elevation of pressure within the heart and loss of cardiac function.

1.2 The Renin-Angiotensin System

The renin-angiotensin system (RAS) is an important hormone system whereby the body regulates electrolyte concentration and blood pressure. The RAS was first discovered to link renal disease to ventricular hypertrophy in 1836 by Richard Bright, where hypertrophy was shown to be related to an increased resistance to blood flow in small vessels following altered blood conditions (Bright, 1836). Further studies focusing primarily on kidney nephritis (inflammation of the kidneys) showed that fibroids found within renal vessels were caused by blood impurity, which also resulted in left ventricular hypertrophy (Johnson, 1868). High blood pressure was first described in 1872 by Mahomed, who linked this to left ventricular hypertrophy and nephritis, and further reported hypertension in patients who did not have renal impairments (Mahomed, 1877). Although the relationship between renal disease and hypertension had long since been discovered, it was not until 1898 when Tigerstedt and Bergman reported the effects of renal extracts on arterial blood pressure and discovered renin to be the pressor compound involved (Tigerstedt and Bergman, 1898). Years later a second pressor agent was identified as being released into the venous blood of ischaemic kidneys and was shown to have a strong and rapid vasoconstrictor effect, different from renin, this was named hypertensin [later renamed angiotensin I (Ang I)] (Fasciolo et al., 1938). Attempts to investigate the relationship between renin and the newly discovered active compound resulted in the identification of renin as a protease enzyme, a discovery which then led to reports of its substrate, angiotensinogen (Agt), which was found to be formed in the liver (Braun-Menendez et al., 1940). Further studies discovered another pressor protein to be involved in the system, originally termed hypertensin 4 but later renamed angiotensin II (Ang II) (Schwarz et al., 1957), which subsequently has been described as an important effector in the RAS with implications in many cardiovascular disease pathologies.

1.2.1 The Classical RAS

The RAS is a key system with important effects in the regulation of sodium homeostasis and arterial blood pressure stemming from actions in the kidney, central nervous system and cardiovascular system. The major substrate molecule of the RAS is Agt, the only known substrate of renin - an aspartyl protease

enzyme which catalyses the activation of the RAS (Braun-Menendez et al., 1940). RAS activation begins with the release of renin from the juxtaglomerular cells of the kidney, a response which occurs due to a number of different stimuli including detection of a decrease in arterial blood pressure by baroreceptors, (Bock et al., 1992) detection of a decrease in sodium load by the macula densa of the juxtaglomerular complex (Bell et al., 2003) and sympathetic nervous system activity (through ß1 adrenergic receptors). The system is able to rapidly activate under severe stress, for example arterial haemorrhage, where the RAS would be fully activated and producing Ang II within approximately 20 minutes in order to prevent shock via fluid preservation and vasoconstriction (Schalekamp et al., 1989, Michailov et al., 1987). Factors affecting the expression or secretion of renin can impact overall RAS activity due to further effects on Ang II levels in later steps of the RAS. Renin expression is first seen in early mouse kidney development at embryonic day 15 in the developing renal, interlobar and arcuate arteries (Neubauer et al., 2009) though there have been reports of expression as early as embryonic day 11 (Sequeira Lopez et al., 2001). Association of renin producing juxtaglomerular cells (also known as granular cells) with the branching of renal arterioles suggests that in the embryo, renin plays a role in the development of the kidney vasculature (Reddi et al., 1998). At the time of birth, renin expression is found in the newly developed afferent arterioles as well as cells from the inner media layer of renal vessels (Sauter et al., 2008). In the adult kidney, predominant renin expression is found in the juxtaglomerular cells of the juxtaglomerular complex, a type of smooth muscle cell located in the media layer of the afferent arterioles (Rohrwasser et al., 1999). These cells primarily synthesise, store and secrete renin. Once renin has been secreted (constitutively in its inactive form, prorenin) it is cleaved to become activated, where it further acts to cleave Agt, a 12 amino acid glycoprotein produced in the liver (Deschepper, 1994). Renin cleaves the peptide bond between the leucine and valine residues of Agt which creates a 10 amino acid decapeptide known as Ang I, which appears to have no biological activity other than to act as a precursor molecule for Ang II generation (Figure 1-2). When Ang I comes into contact with angiotensin-converting-enzyme (ACE) at the endothelial surface of blood vessels, kidney epithelial cells or epithelial cells within the lung, two C-terminal residues are removed with the resulting product being the biologically active peptide Ang II (Guang et al., 2012).

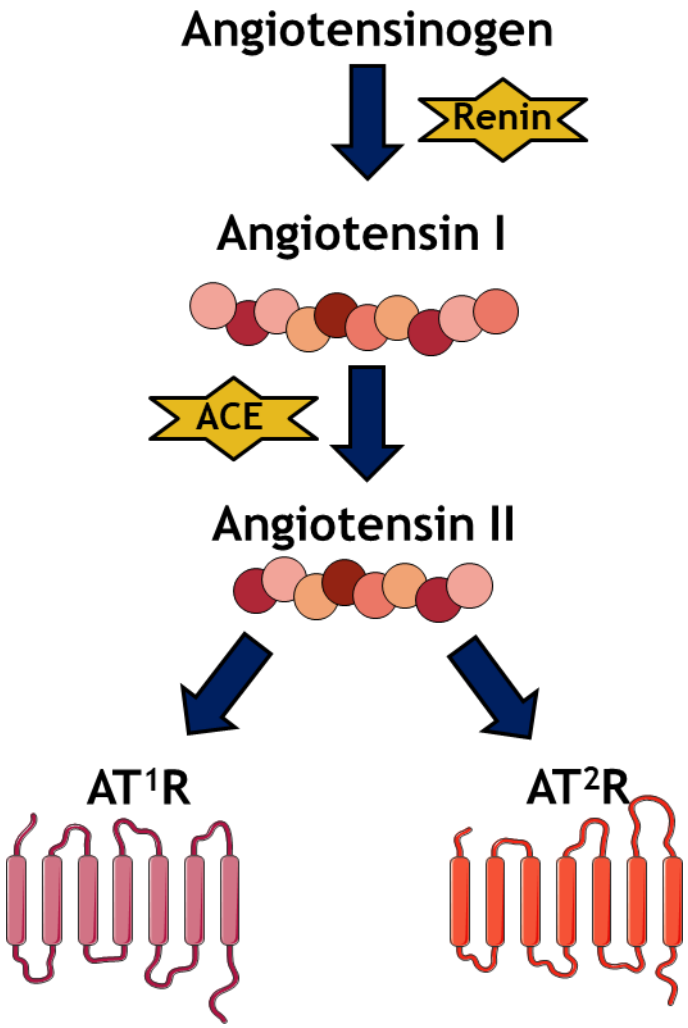

Figure 1-2 The classical renin-angiotensin system pathway.

Agt is cleaved by renin (released by the juxtaglomerular cells of the kidney) to produce Angiotensin I. Ang I is then cleaved by ACE expressed in the endothelial cells of the lung to produce Ang II. Ang II (the main effector of the classical RAS) which binds to the AT_1R resulting in vasoconstriction, cell growth and proliferation, and extracellular matrix remodelling while binding to AT_2R conducts some opposing effects.

1.2.2 Angiotensin Converting Enzyme

ACE was first discovered in 1956 (Skeggs et al., 1956) and is a dicarboxypeptidase found in many tissues and biological fluids, noted to be found along the luminal side of the endothelial membrane (Guang et al., 2012). The ACE gene, ACE, encodes two different isoforms in humans; somatic ACE (sACE) and germinal ACE (gACE). Where sACE is present in many different types of endothelial and epithelial cells (such as in lung, kidney and intestine), gACE is found exclusively in germinal cells of male testis (Rigat et al., 1992). Transgenic studies utilising mice which could only express gACE but not sACE found that the animals were healthy and fertile, comparable to wild-type mice, with normal kidney structure and fluid homeostasis (Kessler et al., 2002). However, although sufficient for normal kidney structure and function, mice expressing only gACE were found to have low blood pressure, suggesting that alone, it is insufficient for restoring normal blood pressure (Kessler et al., 2002). Both ACE isoforms are integral membrane proteins which hydrolyse circulating peptides, for example Ang I; however ACE can also be released into extracellular fluids, such as plasma and seminal fluids, in an enzymatically active form if it undergoes post-translational proteolytic cleavage by membrane protein secretases (Parkin et al., 2004). As well as converting Ang I to Ang II, ACE also degrades bradykinin (an inflammatory mediator) into inactive peptides, resulting in blood pressure increase due to the normal function of bradykinin being dilation of blood vessels causing blood pressure to fall (Dendorfer et al., 2001). Furthermore, aside from mediating blood pressure effects, it has also been shown that, *in vitro,* ACE degrades amyloid beta-protein, the main component of amyloid plaques in the brains of Alzheimer's patients (Hemming and Selkoe, 2005). Amyloid beta-protein levels were also shown to be elevated in the presence of ACE inhibitors, further strengthening the evidence that it is a substrate of ACE (Hemming and Selkoe, 2005).

1.2.3 Angiotensin II

Ang II is the main effector of the classical RAS pathway, generated by cleavage of Ang I by ACE primarily within the lung. Ang II acts as an important endocrine, paracrine and intracrine hormone which raises blood pressure via a number of actions including vasoconstriction, aldosterone biosynthesis and sympathetic

nervous system activation (Fyhrquist et al., 1995). In terms of homeostasis, the expression and secretion of renin is regulated via negative feedback loops involving Ang II. As mentioned previously, renin converts Agt to Ang I, which is then converted by ACE to Ang II. Ang II is then able to rapidly inhibit renin secretion in the kidneys, highlighting its role in negative feedback control of the RAS (Johns et al., 1990, Naftilan and Oparil, 1978). Furthermore, Ang II also stimulates the release of aldosterone from the adrenal cortex, which in turn causes renal tubules to increase reabsorption of sodium and water into the blood while excreting potassium to maintain electrolyte balance (Mulrow, 1999). These actions increase extracellular fluid levels in the body thus increasing blood pressure (Mulrow, 1999).

Ang II also has various effects at the cellular level including stimulation of cell growth, stimulation of cell migration, induction of hypertrophy and fibrosis through increased synthesis of collagen type I and III, and mitosis of vascular smooth muscle cells (Fyhrquist et al., 1995). Once formed from Ang I, Ang II carries out these acts in the heart, brain, kidney, blood vessels and adipose tissues. While circulating, Ang II has a half-life of 30 seconds whereas within tissue it has a half-life of between 15 and 30 minutes (Al-Merani et al., 1978). Most actions of Ang II are mediated through two receptors, the Angiotensin II type 1 receptor (AT_1R) and the Angiotensin II type 2 receptor (AT_2R). The AT_1R and AT_2R share a sequence identity of only 34%, however still share a similar affinity for Ang II binding, which is a primary ligand for both (Li et al., 2012). Both receptors are seven transmembrane G-protein coupled receptors (GPCR) which interact with a variety of G-proteins resulting in activation of a multitude of cell signalling pathways (Mehta and Griendling, 2007). Where actions via the AT_1R include vasoconstriction, proliferation, remodelling and inflammatory responses, actions via the AT_2R tend to result in opposing effects such as vasodilatation and anti-fibrotic, anti-inflammatory and anti-proliferative responses (Li et al., 2012).

1.2.4 The Angiotensin II Type 1 Receptor

The AT_1R is the receptor that mediates the most classically recognised functions of the RAS including, but not limited to, smooth muscle cell contraction, stimulation of renal sodium reabsorption, regulation of renal vascular resistance,

determining blood pressure level and mediating vasoconstrictor responses (Timmermans et al., 1993). The AT_1R is a 359 amino acid, 40kDa receptor that is found in most organs. In humans the AT_1R gene has been mapped to chromosome 17, while in rats two isoforms have been reported which share 95% amino acid sequence identity and have been described as being almost indistinguishable in function. These are the $AT_{1A}R$ on chromosome 17 and the $AT_{1B}R$ on chromosome 2 (Gasc et al., 1994).

The extracellular domain of the AT_1R contains multiple glycosylation sites which are not involved in the binding of Ang II; however, four cysteine residues forming disulphide bridges in this domain have been reported as essential for Ang II binding (Ohyama et al., 1995). Once bound to Ang II at the transmembrane domain, the AT_1R becomes rapidly desensitised and undergoes internalisation into the cell, approximately only 10 minutes post-activation. Following this, receptors may either be recycled back to the plasma membrane (25%) or degraded by lysosomal action (75%) (Griendling et al., 1987). The recycling of AT_1R has been shown to involve a number of proteins including ß-arrestins and the Rab GTPase family (Du et al., 2004). The desensitisation of the AT_1R receptor is mediated by G-protein coupled receptor kinases (GRK), a family of seven kinases which uncouple the receptor from its activated G-protein via serine/threonine phosphorylation sites on the cytoplasmic surface of the AT_1R (Oppermann et al., 1996). After desensitisation occurs, receptor internalisation into clathrin-coated pits then follows (Gaborik and Hunyady, 2004). This is a process which involves the ß-arrestins under normal physiological conditions, however, it has also been demonstrated that receptors may undergo rapid internalisation as a result of agonist-induced phosphorylation, where increased levels of Ang II where shown to cause internalisation of the AT_1R, independent of ß-arrestins *in vitro* (Thomas et al., 1998). Following internalisation, the receptor is then able to induce specific cell signalling pathways, for example when AT_1R is desensitised by GRK5/6, ERK signalling is activated promoting cardiac and vascular remodelling effects (Kim et al., 2005). Conversely, if the AT_1R is desensitised by GRK-2 or GRK-3 as shown in HEK-293 cells, activation of protein kinase C (PKC) is prevented, reducing the vasoconstrictive effects of Ang II/AT_1R signalling (Oppermann et al., 1996).

Although it has been reported that AT_1R internalisation occurs via clathrin-coated pits, it has also been reported to occur via non-coated pits known as caveolae which are related to the caveolin family of integral membrane proteins. Certain signalling molecules associated with the caveolin proteins are found co-localised in these caveolae microdomains, such as epidermal growth factor receptor (EGFR) and proto-oncogene tyrosine-protein kinase (Src) family members (Gratton et al., 2004). It has been shown that Ang II binding promotes the association of AT_1R with caveolin-1 in vascular smooth muscle cells and results in the trafficking of AT_1R into these caveolin-rich domains. Furthermore, this association has been described as essential for the activation of the small signalling GTPase, Rac1, which has been associated with glucose uptake, cell growth, protein kinase activation and cell cycle regulation (Sylow et al., 2016).

The regulation of AT_1R recycling is tightly controlled by cellular trafficking systems to ensure efficient transport of AT_1Rs to the cell membrane. The molecules responsible for this are the Rab family of proteins, a selection of Ras-related GTPases involved in the regulation of intracellular vesicular transport. Transport of AT_1R from the endoplasmic reticulum to the cell surface has been associated with Rab1 in particular (Wu et al., 2003). Furthermore, it has been noted that Rab5 also contributes to the trafficking of AT_1R through fusion of clathrin-coated vesicles with endosomes (Somsel Rodman and Wandinger-Ness, 2000). The packaging of AT_1Rs into either clathrin-coated or non-coated vesicles is likely to be a necessary phenomenon for efficient RAS signalling.

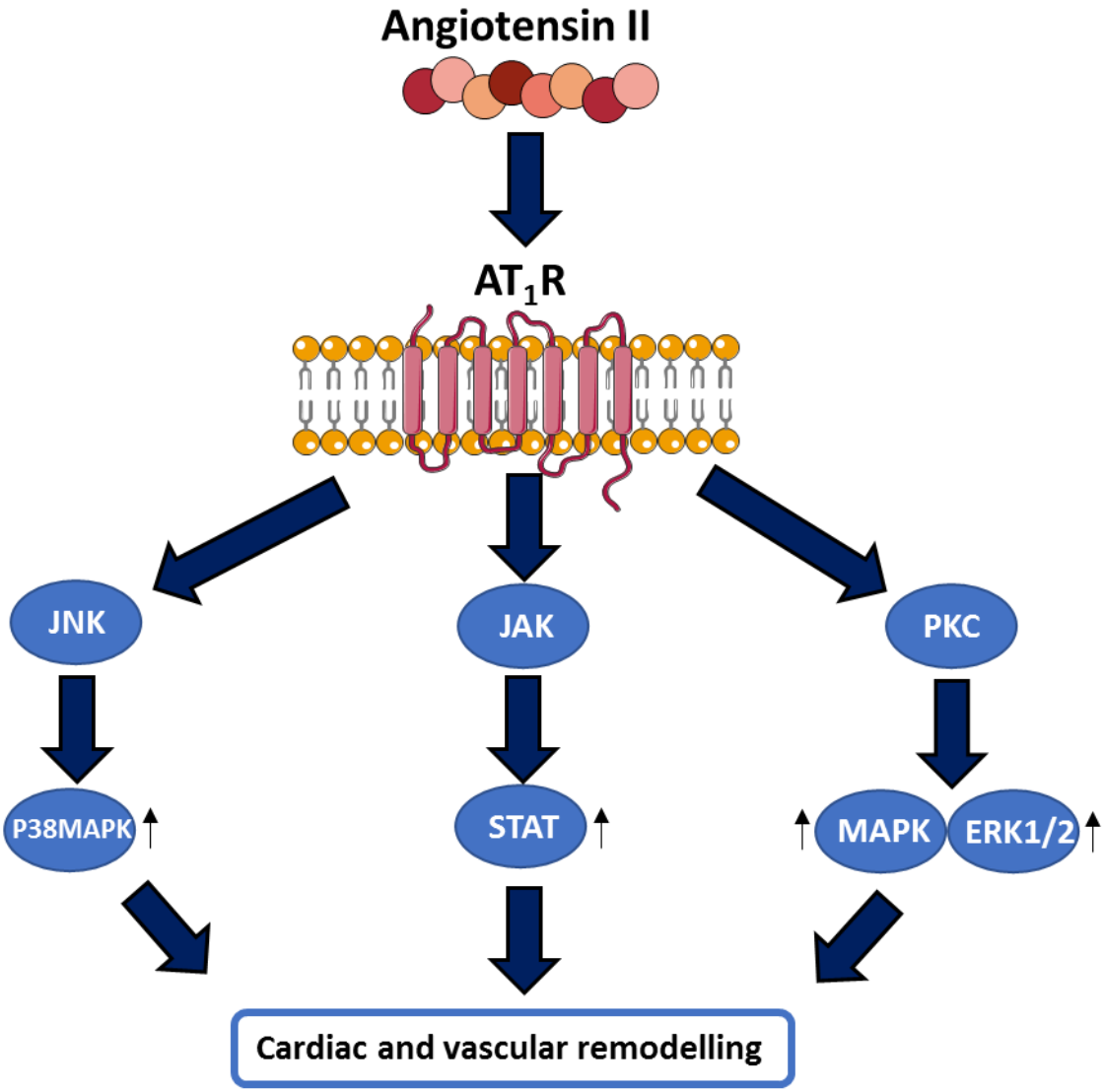

Figure 1-3 Angiotensin II Type 1 Receptor signalling cascades. Cardiac and vascular remodelling is induced via Ang II interaction with the AT_1R resulting in increased signalling through JAK/STAT, PKC/MAPK/ERK1/2 and JNK/P38MAPK signalling pathways (figure information obtained from Ocaranza et al., 2012).

1.2.5 The Angiotensin II Type 2 Receptor

The genes encoding the AT_2R receptor are found on the human X-chromosome. Human AT_2R is a 363 amino acid, 41kDa receptor with more than 92% homology with mouse and rat AT_2R (Mukoyama et al., 1993). The AT_2R is expressed highly in most tissues during foetal development such as the brain, aorta, connective tissue and skeletal system, however expression greatly decreases after birth at which point expression is limited to only a few organs, which includes the renal and cardiovascular systems (Yu et al., 2010). This pattern of expression suggests that the AT_2R plays an important role in foetal development which is then downregulated after birth; however, induction can still occur later in life as a response to pathological stress. Contrary to these findings it has also been shown that total AT_2R protein in tissue is higher in adult rats than in foetuses or neonates for certain tissues including the liver, kidney and brain (Yu et al., 2010). In relation to the cardiovascular system AT_2R expression has been reported in cardiomyocytes and cardiac fibroblasts of the heart, as well as in major blood vessels where, under pathological conditions such as hypertension and heart failure, expression can be regulated (Levy, 2005). For example, studies have shown that AT_2R expression is increased in samples of diseased aortic tissue compared with samples of healthy aortic tissue (Banos et al., 2011). Conversely, AT_2R mRNA and protein expression were found to be decreased in heart tissue during ischaemia/reperfusion injury in a rat model compared with control hearts (Li and Zhang, 2015).

The AT_2R has been reported as having involvement in various signalling pathways where it couples to small G-proteins; associations with Gαi2 and Gαi3 have been shown (Li et al., 2012). Once bound to its ligand, AT_2R may remain constitutively active and is not internalised as seen with the AT_1R receptor (Schluter and Wenzel, 2008). Although the AT_2R is structurally similar to a GPCR, the actual signalling pathways mediated by the AT_2R are not yet fully known. AT_2Rs are unable to recruit or interact with ß-arrestins which are a key mediator of receptor internalisation; furthermore the AT_2R may exert effects independent of ligand binding, again suggesting different signalling mechanisms to those exerted by the AT_1R (Jones et al., 2008). Studies have shown that the AT_2R may interact with other GPCRs and can exist in either a homodimer or a heterodimer form on the plasma membrane. AT_2R/AT_2R homodimers are formed primarily in the

endoplasmic reticulum and are then trafficked to the plasma membrane where biological effects are enhanced due to the homodimer complex (Zhang et al., 2009). Efficient translocation of the AT_2R to the plasma membrane is essential for normal function of the receptor, particularly with regards to renal homeostasis. It has been shown that AT_2R presence on the cell surface is key to the internalisation of Na+/H+ exchanger 3 (NHE-3) and Na+/K+ ATPase (NKA), two important sodium transporters mediating natriuretic effects; when the AT_2R was antagonised by the pharmacological antagonist PD123,319 the natriuretic effects were abolished (Kemp et al., 2014). Studies have shown that abolishing or impairing translocation, where instead AT_2R/AT_2R remains within the intracellular compartment, results in development of sodium retention and hypertension in spontaneously hypertensive rats (Padia et al., 2009). The process by which the AT_2R is translocated to the plasma membrane is not yet fully elucidated, however it has been suggested that nitric oxide (NO) may be a key driving factor, as seen in cardiomyocytes (Jang et al., 2015). This study showed that antagonising the AT_2R with PD123,319 in cardiomyocytes, or treating cardiomyocytes with reactive oxygen species (ROS) scavengers, resulted in blockade of Ang II upregulation of nitric oxide synthase and prevention of AT_2R translocation to the plasma membrane (Jang et al., 2015). It has been shown that the AT_2R may also form a heterodimer complex with the AT_1R (AT_2R/AT_1R) and thus is able to inhibit the adverse effects caused by Ang II signalling through the AT_1R (Porrello et al., 2011). Further to this, activation of the AT_2R was shown to downregulate AT_1R expression through actions of NO and cyclic guanosine monophosphate (cGMP) in renal cells of WKY rats, which may have important effects in the mediation of sodium excretion and regulation of blood pressure (Yang et al., 2012).

AT_2R activation may either activate or inhibit phosphatases involved in regulating the mitogen-activated protein kinase (MAPK) pathway, with particular involvement of the extracellular signal-regulated kinase (ERK) 1/2-dependent pathway. In renal fibroblast cells AT_2R activation has been shown to drive ERK1/2 phosphorylation leading to vasodilatation and inhibition of fibrogenesis in a NO-dependent manner (Chow et al., 2014). Studies have also demonstrated that inhibition of NO synthesis can remove the vasodilatory response promoted by the AT_2R (Zhang et al., 2003). AT_2R activation has also been demonstrated to

inhibit ERK1/2 phosphorylation in both cardiomyocytes and vascular smooth muscle cells through phosphatase stimulation (MAPK phosphatase and protein phosphatase 2) with the end result being inhibition of cell growth and pro-apoptotic effects (Faria-Costa et al., 2014). The effects reported may occur via a G-protein dependent pathway or via activation of Src homology 2 domain phosphatase-1 (SHP-1); a protein phosphatase which inhibits nicotinamide adenine dinucleotide phosphate (NADPH) oxidase activity, producing antioxidant effects mediated by the AT_2R (Faria-Costa et al., 2014).

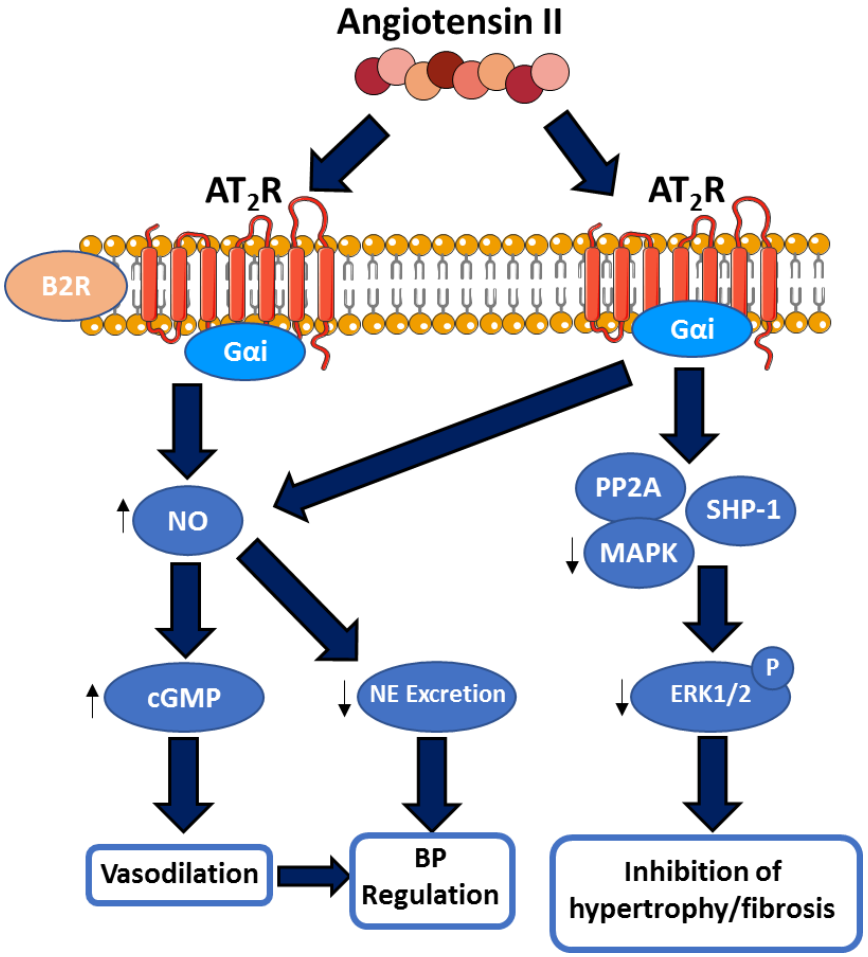

B2: Bradykinin B2 Receptor
Gαi: G-protein
NO: Nitric Oxide
cGMP: 3'-5'-cyclic guanosine monophosphate
NE: Norepinephrine
PP2A: Protein phosphatase 2A
MAPK: Mitogen-activated protein kinase
SHP-1: Src homology region 2 domain-containing phosphatase
ERK1/2: Extracellular signal-regulated kinases 1 and 2

Figure 1-4 Angiotensin II Type 2 Receptor signalling cascades. Ang II interaction with the AT_2R induces protective effects via decreased MAPK/ERK1/2 signalling and increased NO signalling resulting in increased cGMP and decreased NE excretion (figure information obtained from Li et al., 2012).

1.2.6 Angiotensin II Signalling Cascades and Actions

Ang II is able to activate a range of signalling cascades once bound to the AT_1R, which in turn controls the wide range of physiological effects of Ang II (Figure 1-3). There are two categories of pathways regulated by Ang II; G-protein related pathways and non-G-protein related pathways. Alongside these pathways, Ang II is also involved in signalling with a number of tyrosine kinases via the AT_1R including receptor tyrosine kinases [EGFR and platelet derived growth factor (PDGF)] and non-receptor tyrosine kinases [Janus kinases (JAK), focal adhesion kinases (FAK) and calcium-dependent proline-rich tyrosine kinase 2 (Pyk2)] (Mehta and Griendling, 2007). In addition to effects of Ang II related to tyrosine kinase action, many pathological effects of Ang II occur by activation of NADPH oxidases resulting in generation of ROS affecting the vasculature (Griendling et al., 2000). Ang II binding to the AT_1R also plays a role in pathological cell growth and hypertrophy in the cardiac setting where serine/threonine kinases such as MAPK pathways [for example, ERK1/2 and c-Jun NH2-terminal kinase (JNK)] are activated (Hunyady and Catt, 2006). In normal healthy individuals, these aforementioned pathways are under tight regulation; hence aberrant activity of the RAS may result in activation of such pathways leading to pathological disease.

1.2.6.1 G-Protein Coupled Signalling

A well described function of Ang II is vasoconstriction, a process which occurs via a G-protein dependent signalling pathway. Activation of the AT_1R leads to coupling with several G-proteins including Gαq/11, Gα12/13, and Gβγ which further activate downstream pathways. This includes activation of phospholipase C (PLC) which in turn rapidly produces inositol-1,4,5-triphosphate (IP_3) and diacylglycerol (DAG) resulting in calcium flow into the cytoplasm of the cell. Calcium build-up within the cytoplasm causes activation of myosin light chain kinase (MLCK) triggering smooth muscle contraction by enhancing interaction between actin and myosin (Yan et al., 2003). This process is inhibited by myosin light chain phosphatase (MLCP), which prevents sustained contraction of smooth muscle cells; however evidence shows that Ang II (via PKC) increases the phosphorylation of CPI-17 (an inhibitory phosphoprotein of MLCP) which in turn leads to sustained contraction (Seko et al., 2003). This downstream process is

one example of activation of the vasoconstrictive properties of Ang II and the AT_1R, ultimately leading to promotion of aberrant growth by Ang II.

Ang II has also been reported to phosphorylate and activate phospholipase A_2 (PLA_2), an enzyme which catalyses the release of fatty acids from phospholipids. PLA_2 specifically recognises the sn-2 acyl bond of phospholipids and hydrolyses the bond to release arachidonic acid (a polyunsaturated omega-6 fatty acid) and its various metabolites (Mallat et al., 2010). Arachidonic acid and its derivatives have important functions in maintenance of vascular tone and in NADPH oxidation of vascular smooth muscle cells. A group of arachidonic acid metabolites known as hydroxyeicosatetraenoic acids (HETEs) have been reported to have pro-hypertensive actions and to facilitate calcium entry into the cell, leading to Ang II-mediated smooth muscle vasoconstriction (Sarkis et al., 2004). Arachidonic acid may also be metabolised to prostaglandins by cyclooxygenase enzymes, in particular the vasodilatory prostaglandins PGI2 and PGE2, however the actions of these are counteracted by thromboxane A2 and PGH2 (also synthesised from arachidonic acid by cyclooxygenase enzymes) resulting in a vasoconstriction response. Leukotrienes (inflammatory response mediators) are also produced by the oxidation of arachidonic acid by lipooxygenase and have been reported to have implications in hypertension and vasoconstriction, as well as in inflammatory diseases (Sarkis et al., 2004).

Signalling of G-protein dependent pathways is mediated by regulators of G-protein signalling (RGS) which control the duration of the signal produced by the G-protein subunits of the AT_1R which in turn will determine whether, for example, cell growth and migration is enhanced or inhibited. It has been shown that RGS1, 2, 3 and 4 all attenuate Ang II/AT_1R signalling, in particular RGS2 has been shown to inhibit the Gαq subunit and its downstream actions (Cho et al., 2003).

1.2.6.2 Non-G-Protein Coupled Signalling

As well as activating G-protein dependent signalling cascades, Ang II also plays an important role in NADPH and ROS signalling. Oxidative stress has been implicated in a range of cellular pathologies which include vascular smooth muscle cell growth and extracellular matrix formation. Ang II is a potent

mediator of oxidative stress which activates NADPH oxidases in vascular smooth muscle cells and as a result promotes production of superoxide and hydrogen peroxide which have involvement in the pathological effects of Ang II (Yan et al., 2003). ROS have been reported as potent second messengers involved in hypertension and vessel inflammatory responses (whereas previously they were merely thought to be toxic by-products of metabolism). ROS have been shown to have involvement in many Ang II-mediated effects. For example, it has been shown that Ang II-mediated activation of p38MAPK is dependent on hydrogen peroxide as when it is broken down in vascular smooth muscle cells by catalase, activation of p38MAPK is inhibited (Chen et al., 2006). It has been demonstrated that the interaction between ROS and Ang II signalling can lead to significant changes in vascular characteristics and thus these interactions are significant players in vascular pathologies.

Ang II also plays an important role in activating MAPK signalling cascades, pathways which are key to cell growth and cellular protein metabolism and synthesis. For example, Ang II may activate the ERK1/2 pathway, involved in vascular smooth muscle cell proliferation, fibrosis and migration. When Ang II binds to the AT_1R, ERK1/2 is rapidly activated and may then induce a range of effects on cells. It has been shown that ERK activation leads to vascular smooth muscle cell contraction by interaction with calcium-dependent pathways (Touyz et al., 1999) and has been described as anti-apoptotic, where activation of ERK1/2 inhibits apoptosis (Allen et al., 2005). Ang II has also been shown to activate MAPK cascades linked to environmental stress such as apoptosis signal regulating kinase 1 (ASK1), an inducer of JNK and p38MAPK signalling. JNK and p38MAPK are known to influence cell survival and differentiation as well as being mediators of Ang II-induced inflammation and vascular remodelling (Force et al., 1996).

The AT_1R may associate with non-receptor tyrosine kinases that initiate a multitude of signalling pathways leading to phosphorylation and protein activation. When AT_1R becomes activated it may in turn activate the JAK/STAT (Janus Kinase and Signal Transducer and Activator of Transcription) pathway, a signal that mediates transcription of growth genes. The interaction of AT_1R with JAK2 has shown to be enhanced by Ang II (Frank et al., 2002). Ang II has also

been shown to stimulate formation of focal adhesion complexes in the cytoskeleton by inducing phosphorylation of focal adhesion kinase (FAK). This allows for cell adhesion to the extracellular matrix and also activation of proteins found in the cytoskeleton, including Pyk2 which interacts (in the presence of Ang II) with other cytoskeletal proteins to determine cell shape and movement (Rocic et al., 2001).

Ang II is also involved in signalling with receptor tyrosine kinases via the AT_1R. PDGF stimulates the proliferation and migration of vascular smooth muscle cells through the PDGF receptor, and it has also been shown that Ang II may stimulate cell growth signalling at this receptor, though independent of PDGF itself. Evidence has shown that Ang II stimulation of rat aortic smooth muscle cells causes the PDGF receptor to form a complex with Shc (an adaptor protein) and Grb2 (Growth factor receptor-bound protein 2) independent of PDGF (Linseman et al., 1995) and that this complex initiated smooth muscle cell responses. Ang II also initiates cell growth pathways through activation of EGFR within caveolae. Once EGFR is activated it becomes a docking site for Grb2 and Shc complexes which further induce signalling pathways involved in cellular growth, metabolism and remodelling (PI3K/PDK1/Akt) and hypertrophy and inflammation (Ras/Raf/ERK) (Kagiyama et al., 2002).

1.2.7 The Counter-Regulatory Axis of the RAS

It was first assumed that the RAS was a linear step process with Ang II as the major effector peptide driving the system. However, several major discoveries led to a drastic change in how the RAS is viewed. It was discovered that the RAS was expressed in specific tissues ie. a local RAS where Ang II was generated within those specific tissues, rather than being recruited from the circulation. For example it was shown that both renin and Agt were expressed at low levels in the heart (Paul et al., 1993) and that ACE was expressed in the hearts of both rats and humans (Hirsch et al., 1991). Furthermore it was demonstrated that Ang I and Ang II were both synthesised within cardiomyocytes, a discovery made by tracking radio-labelled peptides within plasma and tissue (van Kats et al., 1998). Further studies showed that the AT_1R and AT_2R could also be found expressed in specific tissues, for example, it was demonstrated that both the AT_1R and AT_2R were expressed in all cardiac cells and played a specific role in Ang II-induced

cardiomyocyte hypertrophy (Booz and Baker, 1996). Discovery of the expression of RAS components within specific tissues suggested that generation of Ang II and its ability to initiate signalling through the AT_1R and AT_2R was a process that could occur within specific tissues (such as the heart, in specific cardiac cell types) without the requirement of RAS components drawn from the systemic circulation.

The second major discovery that changed the conventional view of the RAS was the identification of novel components of the RAS within specific tissues, the most noted discovery being Angiotensin Converting Enzyme 2 (ACE2), a homolog of ACE which has a vastly different substrate specificity (Donoghue et al., 2000). It was reported that ACE2 catalysed the conversion of Ang II to Ang-(1-7), another new player in the RAS. ACE2 may also convert Ang I to Ang-(1-9), a protective peptide which signals via the AT_2R (Flores-Muñoz et al., 2011) and may be subsequently converted to Ang-(1-7) by ACE (Rice et al., 2004). However, ACE2 has a 400-fold greater affinity for Ang II than Ang I (Tipnis et al., 2000). It was discovered that ACE2 was the main key to the generation of Ang-(1-7) which was further shown to antagonise the detrimental effects of Ang II signalling via its receptor Mas. These findings describe the ACE2/Ang-(1-7)/Mas axis of the RAS, known as the counter-regulatory axis of the RAS (Figure 1-5).

These two major discoveries revolving around the RAS led to the reasoning that there is both a “local” or “tissue-specific” RAS and also a “systemic” or “circulatory” RAS. The discovery of the local tissue-specific RAS led to many studies dedicated to elucidating the components and their actions along with attempts to isolate these actions from those involved in the classical systemic RAS. The local tissue-specific RAS has been identified in numerous organs since its discovery including the heart, kidney, blood vessels, central nervous system, digestive system, skin, reproductive system, lymphatic system and adipose tissue (Yim and Yoo, 2008). Discovery of the counter-regulatory axis of the RAS has since led to many studies of it as a therapeutic target for various pathological diseases involving the heart, kidney, brain and other organs, combating the detrimental effects of Ang II signalling in the classical RAS.

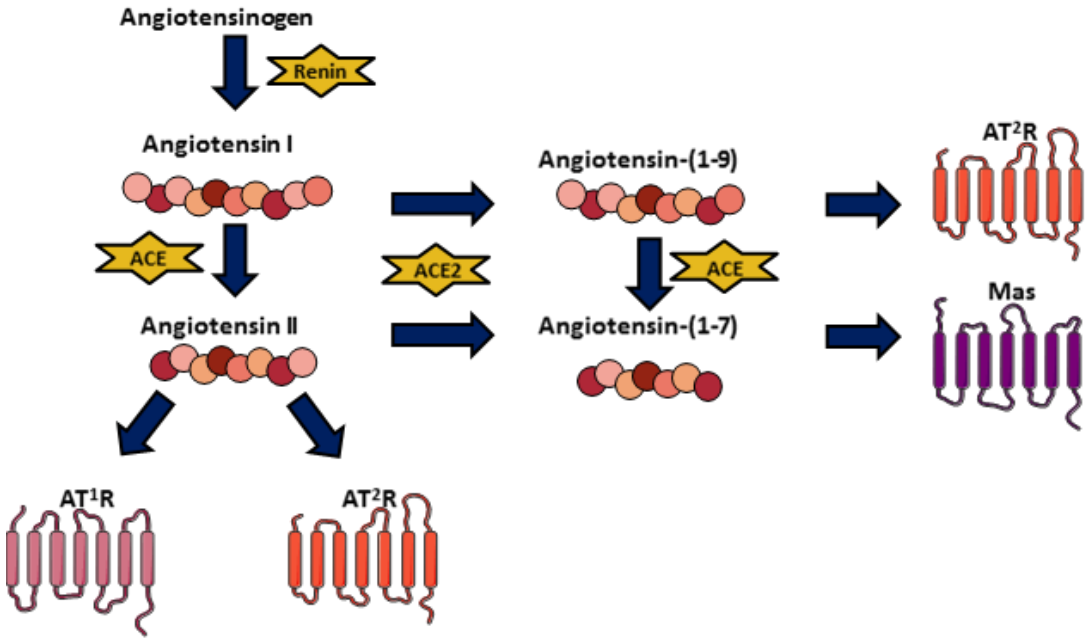

Figure 1-5 The counter-regulatory axis of the renin-angiotensin system. Angiotensin I is converted to Ang-(1-9) by ACE2, while Angiotensin II is converted to Ang-(1-7). Ang-(1-9) then either acts on the AT_2R producing anti-fibrotic, anti-proliferative and anti-hypertrophic effects, or is converted to Ang-(1-7) by ACE. Ang-(1-7) acts on the Mas receptor also resulting in anti-hypertrophic, anti-fibrotic, anti-proliferative and vasodilatory effects.

1.2.8 Angiotensin Converting Enzyme 2

ACE2 was discovered to be a human homolog of ACE in 2000 which constituted a new and different enzymatic pathway to that of ACE (Donoghue et al., 2000). ACE2 is a type 1 transmembrane glycoprotein consisting of 805 amino acids and one extracellular catalytic domain, the gene for which is mapped to the human and rodent X chromosome (Crackower et al., 2002). Similarly to ACE, ACE2 consists of two domains; a carboxy-terminal domain and an amino-terminal catalytic domain, which has only one active site. The ACE2 active site is a zinc metallo-peptidase domain which shares approximately 42% sequence identity with the catalytic domain of ACE (Tipnis et al., 2000). ACE2 is mainly expressed in the heart, testis and kidney; however, is also found to be expressed in low levels in various other tissues including the lung and colon (Tipnis et al., 2000). ACE2 catalyses enzymatic reactions mainly through the use of zinc ions which are coordinated by conserved histidine residues within the active site of the catalytic domain. Although similar to ACE, ACE2 functions in a different manner. While ACE cleaves a C-terminal dipeptide from its substrate and thus is known as a dipeptidylpeptidase, ACE2 only cleaves a single amino acid from its substrate and is known as a monocarboxypeptidase (Tipnis et al., 2000). The binding specificity of ACE and ACE2 differs greatly; while ACE binds to Ang I converting it to Ang II, ACE2 binds predominantly to Ang II converting it to Ang-(1-7). Crystal structure analysis of both enzymes showed that this difference in binding specificity is due to the smaller binding pocket seen in ACE2 where arginine-273 forms a salt bridge with the substrate C-terminal while in ACE-substrate binding this residue is a smaller glutamine (Towler et al., 2004).

Early evidence suggested that ACE2 played a protective role in the RAS, as part of the counter-regulatory axis. Studies in hypertensive rats showed that they had lower expression of ACE2 compared to healthy animals, while over-expression of ACE2 could reduce blood pressure in stroke-prone spontaneously hypertensive rats (SHRSP) as well as improve endothelial function (Rentzsch et al., 2008). These studies suggested that ACE2 played in important role in the regulation of blood pressure. It has been shown that ACE2 is expressed at high levels in the heart and thus has been linked to heart failure. One key study showed that ACE2 null mice had severely impaired cardiac function, and alongside cardiac impairment high levels of cardiac and circulating Ang II were found, a phenotype

which was reversed in ACE/ACE2 double knockout mice (Yamamoto et al., 2006, Crackower et al., 2002). These findings suggested that ACE2 null mice displayed high levels of detrimental Ang II while ACE/ACE2 knockout mice displayed low levels (Crackower et al., 2002, Yamamoto et al., 2006). These key findings proposed an important role for ACE2 in counterbalancing the detrimental effects of the classical RAS signalling pathway.

1.2.9 Angiotensin-(1-7)

The discovery of Ang-(1-7) as a key component of the RAS has been viewed as one of the most significant changes regarding this hormonal system in recent years. Ang-(1-7) is a seven amino acid peptide, the majority of which is produced from Ang II by ACE2, though also produced less effectively by hydrolysis of Ang-(1-9) by ACE. Ang-(1-7) has a very short half-life of approximately 10 seconds while in the circulation [after which it is cleaved by ACE to form inactive Ang-(1-5)] and circulation levels recorded in humans are reported to be approximately 20 pg/mL (Vilas-Boas et al., 2009). It has been reported that Ang-(1-7) may exert effects in a variety of different tissues such as the heart and coronary vessels. The presence of Ang-(1-7) immunoreactivity was first noted in cardiomyocytes of rat hearts alongside Ang-(1-7) immunoreactivity in blood taken from the canine coronary sinus (Averill et al., 2003, Santos et al., 1990). Following this, more recent discoveries showed that both Ang-(1-7) and its receptor could be found in the sinoatrial node, providing a link to the antiarrythmogenic effect of Ang-(1-7) (Ferreira et al., 2011). The presence of ACE2 discovered in cardiomyocytes suggests that Ang-(1-7) may be generated locally in the hearts of various different species (Crackower et al., 2002). Along with ACE2, several other enzymes known to generate Ang-(1-7) have also been described in the heart such as cathepsin-A and prolyl-oligopeptidase, again suggesting local generation of Ang-(1-7) (Jackman et al., 2002, Cicilini et al., 1994). It has been shown that in cardiomyocytes, short term exposure to Ang-(1-7) does not affect calcium levels, however does increase NO release via activation of endothelial nitric oxide synthase (eNOS) and neuronal nitric oxide synthase (nNOS) (Costa et al., 2010). Further to this information, it was discovered that chronic treatment with Ang-(1-7) resulted in significant effects on calcium-handling proteins and calcium levels (Gomes et al., 2012). It has been shown in rats that chronic exposure to Ang-(1-7) via an Ang-(1-7)-

generating fusion protein [whereby the proteolytic action of a furin enzyme cleaves the engineered protein to release Ang-(1-7) (Santos et al., 2004)] showed increased calcium transient and rapid calcium uptake in the heart along with increased expression of sarco/endoplasmic reticulum Ca^{2+}-ATPase 2 (SERCA2), a calcium ATPase functioning to transfer calcium from the cytosol of the cell to the lumen of the sarcoplasmic reticulum during muscle relaxation (Gomes et al., 2012). When the receptor for Ang-(1-7), Mas, was knocked out in mice it resulted in reduced calcium handling and uptake, reduced expression of SERCA2 and a general decrease in heart function suggesting that when Ang-(1-7) cannot bind its receptor to elicit functions it may result in cardiac pathology (Gomes et al., 2012).

Ang-(1-7) has also been shown to have effects in the coronary vessels of various species. It was shown that Ang-(1-7) produced a vasorelaxation effect in the coronary arteries of both dogs and pigs, however when tested in rodents the effect originally observed was the opposite, a possible reasoning being due to the high concentrations (10^{-7} to 10^{-4} mol/L) used in initial experiments (Brosnihan et al., 1998, Gorelik et al., 1998, Santos et al., 2000). In further experiments when lower concentrations (2×10^{-11} mol/L) of Ang-(1-7) peptide where used, evidence showed that the peptide could produce a significant vasodilatory effect in rat hearts (Souza et al., 2013). Early studies described the formation of Ang-(1-7) in the endothelial layer of human blood vessels, while also being found in the vascular wall in various species along with its receptor. As well as Ang-(1-7) formation occurring in blood vessels, this is also a key site where it elicits its effects. Evidence has shown that Ang-(1-7) may cause vasodilation in aortic rings and vascular walls, an effect which leads to a decrease in vessel resistance leading to an increase in cardiac output (Botelho-Santos et al., 2012).

Originally, Ang-(1-7) was thought to function via interaction with the AT_1R and AT_2R receptors with exact mechanisms unknown, however due to the AT_1R and AT_2R having a low affinity for Ang-(1-7) binding it was suggested that this was not the case (Rowe et al., 1995). It was later discovered that Ang-(1-7) binds to the GPCR Mas with high affinity and studies using Mas-deficient rodents provided evidence of Ang-(1-7) being the endogenous ligand for this receptor (Santos et

al., 2003). Although binding of Ang-(1-7) to Mas was confirmed, it has also been suggested more recently that the Mas receptor may have some constitutive activation regardless of Ang-(1-7) presence (Burghi et al., 2019). Despite low affinity, some studies have also shown that Ang-(1-7) can in fact bind the AT_2R to elicit certain effects, for example when mouse hearts were exposed to the AT_2R antagonist PD123,319, Ang-(1-7) was able to increase perfusion pressure independently of the AT_1R and Mas receptors suggesting a role in AT_2R signalling (Castro et al., 2005). Even more recent evidence has suggested that Ang-(1-7) may act as a ligand for the AT_1R. It was shown that Ang-(1-7) binds the AT_1R in a competitive manner against several Ang II G-protein signalling pathways (such as the Ang II/Gq pathway) (Galandrin et al., 2016). Evidence suggested that Ang-(1-7) behaves as an AT_1R-biased agonist which promotes ß-arrestin activation as well as inhibiting the classical effects of Ang II/AT_1R/G-protein signalling (Galandrin et al., 2016) despite being a known Mas-specific ligand. Although this evidence suggests a protective effect for Ang-(1-7) signalling via the AT_1R, these studies were carried out *in vitro* and in whole organ models. As such, it is not clear how these individual peptide-receptor interactions may occur *in vivo,* where peptide levels undergo constant change and difficulty lies in determining the relative contribution of each peptide at each receptor.

1.2.10 Mas Receptor Signalling

Since the discovery of the ACE2/Ang-(1-7)/Mas axis of the RAS, many studies have been dedicated to elucidating the signalling pathways following activation of Mas. Signal transduction pathways following Mas activation have not been fully characterised in the heart, though several examples have been suggested. It has been shown that Ang-(1-7) is able to attenuate 3H-leucine uptake in neonatal rat cardiomyocytes via a mechanism involving inhibition of ERK1/2 and MAPK pathways following activation of Mas, a process which resulted in inhibition of cell growth (Tallant et al., 2005). Furthermore, it has been shown that deletion of the Mas receptor gene caused significant impairment of cardiac function which also resulted in accumulation of collagen type 1, collagen type 3, and fibronectin in the heart which suggests a role for Mas signalling in the prevention of fibrosis (Gava et al., 2012).

Mas is known to be involved in most noted vascular effects of Ang-(1-7). It has been shown that in Mas-deficient mice relaxation occurring in aortic rings due to Ang-(1-7) is absent (Savergnini et al., 2010). Furthermore, various studies have described a link between the Mas receptor and NO release pathways. It has been shown in several cell types including human aortic endothelial cells (HAEC) that Ang-(1-7) promotes the release of NO by phosphorylation or dephosphorylation of eNOS. The phosphorylation of the Ser1777 site (stimulatory) and dephosphorylation of the Thr495 site (inhibitory) results in the release of NO (an effect possibly involving the PI3K–AKT pathway) however this effect is abolished when in the presence of the Mas receptor antagonist A779 (Sampaio et al., 2007). Other studies have shown that in Mas-deficient mice there is a reduction in superoxide catalase activity suggesting that antioxidant processes in these animals is impaired and furthermore it was shown that oxidative stress markers could be found in the urine of these Mas-deficient mice (Xu et al., 2008). In multiple strains of Mas-deficient mice it was also shown that ROS could be found in increased levels, and that these mice exhibited increased blood pressure and endothelial dysfunction (Xu et al., 2008). Various studies have shown the importance of NADPH oxidase in cell signalling leading to oxidative stress and impaired endothelial function related to hypertension (Wong et al., 2010). It has been demonstrated in human endothelial cells that the activation of NADPH oxidase signalling by Ang II can be attenuated by Ang-(1-7). It is suggested that this inhibition occurs through activation of Mas by Ang-(1-7) further leading to AKT signalling, the kinase known to mediate the aforementioned phosphorylation and dephosphorylation of eNOS, stimulating an increase in NO production and protecting against endothelial dysfunction and oxidative stress (Sampaio et al., 2007).

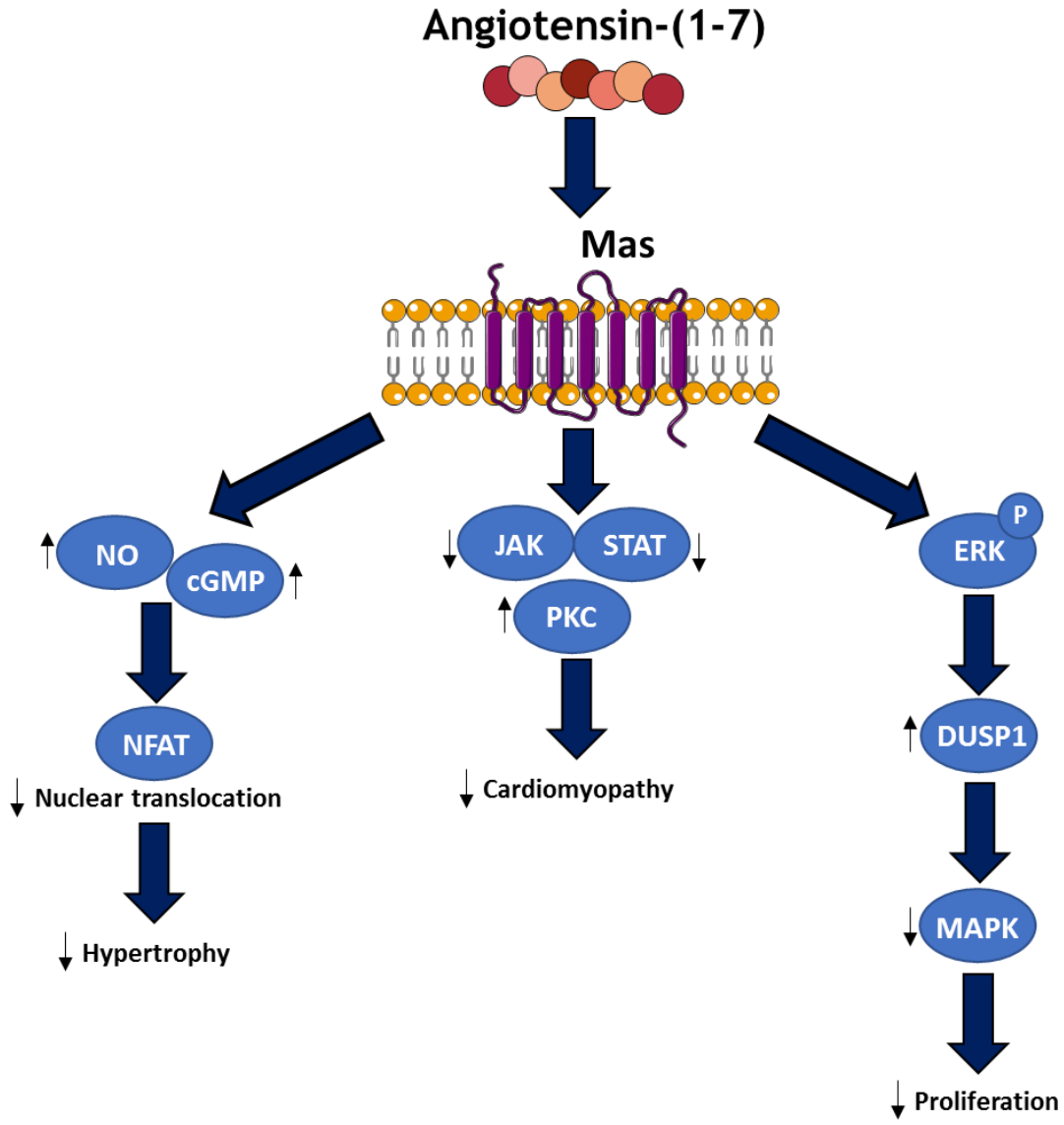

NO: Nitric Oxide
cGMP: 3'-5'-cyclic guanosine monophosphate
NFAT: Nuclear factor of activated T cells
JAK: Janus-activated kinase
STAT: signal transducer and activator of transcription
PKC: Protein kinase C
MAPK: Mitogen-activated protein kinase
ERK: Extracellular signal-regulated kinase
DUSP1: Dual specificity protein phosphatase 1

Figure 1-6 Mas receptor signalling cascades. Ang-(1-7) signalling via the Mas receptor induces cardioprotective effects via downregulation of JAK/STAT and MAPK signalling pathways, and upregulation of NO synthesis (figure information obtained from McKinney et al., 2014).

1.2.11 Other Angiotensin Peptides

Ang-(1-9) is a nine amino acid peptide generated by cleavage of Ang I by several carboxypeptidase enzymes including cathepsin-A, carboxypeptidase A and most notably ACE2, the key enzyme in the counter-regulatory axis of the RAS (Donoghue et al., 2000). It has been shown that in human heart tissue Ang I is degraded to either Ang-(1-9) or Ang II, however specifically in platelet cells, Ang I is mainly degraded to Ang-(1-9) and not Ang II (Snyder et al., 1985). Evidence has suggested that Ang-(1-9) is hydrolysed much slower than both Ang I and Ang-(1-7) which may suggest a longer half-life than other peptides involved in the RAS (Chen et al., 2005). Ang-(1-9) can also be cleaved by several enzymes to produce Ang-(1-7) (although this process of Ang-(1-7) generation is far less efficient than by ACE2); these enzymes include prolyl endopeptidase (POP), thimet-oligopeptidase (TOP) and neutral endopeptidase (NEP) (Rice et al., 2004). Evidence has shown that Ang-(1-9) binds and signals through the AT_2R, though at 100-fold lower affinity than Ang II binding (Flores-Muñoz et al., 2011). Studies in the SHRSP model showed that Ang-(1-9) could significantly reduce cardiovascular damage caused by Ang II-induced hypertension (Ocaranza et al., 2014). The AT_2R was further implicated in Ang-(1-9) signalling in these studies when the known AT_2R inhibitor, PD123,319, was co-administered alongside Ang-(1-9) and the beneficial effects were abolished (Ocaranza et al., 2014).

It has also been established that ACE may convert Ang-(1-7) to Angiotensin-(1-5) [Ang-(1-5)], a pentapeptide associated with the RAS which was recently proven to be biologically active (Yu et al., 2016). This study found that Ang-(1-5) was able to stimulate atrial natriuretic peptide (ANP) secretion which could be attenuated by antagonising the Mas receptor (but not the AT_1R or AT_2R) and by inhibition of PI3K or NOS, suggesting Ang-(1-5) acts via the Mas receptor and PI3K-Akt-NOS pathway (Yu et al., 2016). Although this study suggests potential protective effects of Ang-(1-5), no other evidence has yet been reported on the biological effects of this peptide.

1.3 The RAS and Cardiovascular Disease

The RAS has been heavily implicated in cardiovascular disease pathology and thus has been a key target for various therapies and trials aiming to treat CVDs. Many studies involving blocking classical RAS signalling have resulted in reduction of tissue and organ damage in the heart, kidney and blood vessels. Drugs known to block the classical RAS include ß-blockers inhibiting the release of renin from the kidney, ACE inhibitors which reduce levels of Ang II generated from Ang I by ACE cleavage and angiotensin receptor blockers which competitively bind to the AT_1R preventing Ang II contact (Mehta and Griendling, 2007). These drugs are of notable clinical importance owing to the fact that they are the first line therapies in patient populations for treatment of various CVDs such as hypertension and heart failure. Ang II has been shown to mediate effects in most cardiovascular cell types by inducing a variety of signalling pathways, many of which contribute to the development of CVDs (Mehta and Griendling, 2007). Furthermore, it has been shown that the counter-regulatory axis of the RAS is implicated in the prevention and protection against many CVDs. Key peptides involved in this axis of the RAS, Ang-(1-7) and Ang-(1-9), have both been shown to elicit protective effects mainly by inhibiting or competing against the effects of Ang II in the classical RAS. This has led to many studies and trials involved in adjusting the balance between the classical RAS and counter-regulatory RAS in cardiovascular disease in attempts to evoke protective effects.

1.3.1 The RAS and Hypertension

One of the most important systems involved in regulating blood pressure is the RAS, and aberrant RAS signalling is a key cause of hypertension. Elevated RAS activity results in overactivity of aforementioned homeostatic actions and, if sustained, trigger chronic hypertension. Many studies have confirmed that Ang II promotes vasoconstriction via the AT_1R, for example use of an AT_1R blocker (losartan) is able to abolish the vasoconstrictor effects of Ang II (Cosentino et al., 2005). A further example was described in AT_1R-knockout mice where it could be shown that blood pressure was reduced in these animals and that this was a direct effect of the inability of Ang II to signal through the AT_1R (Audoly et al., 2000). As mentioned previously it is possible for Ang II to mediate the baroreceptor reflex in the sympathetic nervous system to control blood pressure.

Studies have shown that Ang II may be produced in the brain where it then elicits effects on the sympathetic nervous system, for example in the SHRSP elevated levels of Ang II have been described in the brain (as well as elevated systemic levels) (Ferguson and Washburn, 1998). Furthermore, it has been shown that vast numbers of neurones contain Ang II while also expressing the AT_1R, promoting the effects of Ang II in the nervous system and suggesting a role for blood pressure control (Paton and Kasparov, 1999).

More recent studies have shown that the counter-regulatory axis of the RAS can also have effects on blood pressure level and hypertension. Ang-(1-7) is known to exert most of its effects through the Mas receptor, for example activation of Mas induces signalling through the AKT pathway which promotes the synthesis of NO in the endothelium. This NO synthesis allows for the relaxation of VSMCs and vasodilation of the vasculature, promoting blood flow and reducing blood pressure (Verano-Braga et al., 2012). Mas receptor activation by Ang-(1-7) also prevents the detrimental effects of Ang II signalling by inhibiting pathways such as ERK1/2, which is activated by Ang II action at the AT_1R and normally promotes vasoconstriction (Verano-Braga et al., 2012). This evidence suggests that Ang-(1-7) and Mas work to reduce blood pressure both by NO synthesis and by inhibiting the effects of Ang II at the AT_1R, shifting the balance to vasodilation.

1.3.2 The RAS and Heart Failure

Heart failure is a clinical syndrome which often occurs as a result of coronary artery disease, however may also occur due to a variety of other conditions such as congenital heart defects, heart arrythmias, or chronic diseases such as diabetes or HIV (McMurray and Pfeffer, 2005, Chobanian et al., 2003). Heart failure falls into two categories; heart failure with reduced ejection fraction (HF-rEF) and heart failure with preserved ejection fraction (HF-pEF) with diagnosis dependent on whether or not left ventricular contraction is affected (McMurray and Pfeffer, 2005). Currently, there are no treatments for HF-pEF patients and modulation of the RAS has no effect (McMurray and Pfeffer, 2005), however there have been various successes in treating HF-rEF patients. Studies have shown that inhibiting the classical RAS pathway successfully decreases morbidity and mortality associated with this type of heart failure, with treatments such as antagonism of the RAS using ACE inhibitors (ACEi) and AT_1R

blockers (ARBs) being the major contributors to current heart failure therapies (Latini et al., 2000). ACE inhibitors were the first class of drugs shown to be significantly associated with reduced mortality in patients with heart failure symptoms, where the earliest studies compared enalapril with placebo treatment in highly symptomatic patients (New York Heart Association Class IV) showing that active treatment resulted in a reduction of all-cause mortality by 31% (CONSENSUS, 1987). Further studies in less symptomatic patients (New York Heart Association Class II & III) showed that enalapril treatment resulted in a 16% decrease in all-cause mortality (Yusuf et al., 1991). Following the success of ACE inhibitors in both severe and moderate cases of symptomatic heart failure, studies were carried out in patients with minimal symptoms (New York Heart Association Class I & II) demonstrating that enalapril still caused a 20% reduction in heart failure mortality or related hospitalisation (Yusuf et al., 1992). Although studies have proven the beneficial effects of ACE inhibitors in heart failure, research suggested that Ang II could still be produced regardless of ACE inhibition (Petrie et al., 2001). Studies have highlighted the existence of the Ang II escape phenomenon which suggests that Ang II levels may increase in CVD patients regardless of long term ACE inhibition (Shamkhlova et al., 2008). In this case, lack of reno- and cardio-protective effects generally associated with ACE inhibition correlated with higher plasma Ang II levels in CVD patients compared to control healthy subjects, suggesting that Ang II production had escaped inhibition (Shamkhlova et al., 2008). To further the availability of therapeutic intervention in heart failure, studies began into examining specific blockade of the AT_1R using ARBs. Initial studies, in particular the CHARM-Alternative trial, found that using ARBs instead of ACE inhibitors showed a significant reduction in heart failure hospitalisation and cardiovascular death when patients were treated with candesartan compared to placebo, but with no significant increase in all-cause mortality (Granger et al., 2003). Generally, ACE inhibitors were thought to be the most robust treatment option for symptomatic heart failure, with ARBs used when patients are intolerant to ACE inhibitors (Granger et al., 2003). A second part of this study, the CHARM-Added trial, which focused on patients taking both ACEi and the ARB candesartan, found that this combination led to further reductions in cardiovascular events in patients with chronic heart failure (McMurray et al., 2003). More recently, dual angiotensin receptor and neprilysin inhibition (ARNI) treatment has been reported to be a viable

alternative to ACE inhibition in patients with chronic systolic heart failure (McMurray et al., 2013). Neprilysin is an enzyme which metabolises the natriuretic peptides [such as ANP and brain natriuretic peptide (BNP)] involved in promotion of vasodilation and natriuresis, inhibition of abnormal growth and suppression of the RAS (McMurray et al., 2013). As such, this newer class of drugs allows for inhibition of the RAS while also augmenting natriuretic peptides, providing an alternative treatment for heart failure (McMurray et al., 2013)

While ACE inhibitors and ARBs remain as key treatments for heart failure, newer studies have focused on targeting the counter-regulatory axis of the RAS for therapeutic benefit. The role of ACE2/Ang-(1-7) has been researched in HF-pEF using Ang II-induced diastolic dysfunction in animal models. Basic studies found that loss or inhibition of ACE2 resulted in cardiac hypertrophy and fibrosis leading to greater diastolic dysfunction in Ang II-induced models (Zhong et al., 2010, Alghamri et al., 2013). Furthermore, it was found that treatment with recombinant human ACE2 could attenuate the pathological effects of Ang II in these models, where a decrease in Ang II and an increase in Ang-(1-7) was noted in mouse plasma (Alghamri et al., 2013). A reduction in myocardial Ang II levels was also demonstrated (Zhong et al., 2010). It was also found that loss of ACE2 was associated with increased production of ROS, a phenomenon known to be associated with progression of CVD (Zhong et al., 2010) suggesting a role for ACE2 in cardiac protection. Other studies showed that overexpression of ACE2 has protective benefits against myocardial injury in an Ang II-induced rat model (Huentelman et al., 2005) further demonstrating the protective role of ACE2 in the heart. In an Ang II-induced murine model of heart failure, it was found that inhibition of Ang-(1-7)/MAS signalling prevented the protective effects of recombinant human ACE2 treatment seen in previous studies suggesting an important role for this signalling pathway (Patel et al., 2015) in prevention and protection against heart failure.

Although targeting of the classical axis of the RAS with ACE inhibitors and ARBs has been a key medical therapy for heart failure patients over the past 20 years, many studies relating to targeting the counter-regulatory axis of the RAS remain in the pre-clinical phase, but with protective benefits being highlighted in a vast variety of *in vitro* and *in vivo* models.

1.3.3 The RAS and Cardiac Remodelling

As well as the clinical consequences of RAS activation in the heart in relation to hypertension and coronary artery disease (such as angina, myocardial infarction and HF-rEF), RAS activation may also have direct effects on the heart in terms of left ventricular hypertrophy resulting in HF-rEF or HF-pEF. Cardiac hypertrophy is one of the most crucial risk factors of heart disease and is commonly an adaptive response to haemodynamic overload caused by hypertension. Changes in activity or tissue expression of major RAS components such as Ang II as a result of hypertension (or other risk factors, such as diabetes) have been attributed to the development of aberrant cardiac remodelling and cardiovascular disease pathology (Verdecchia et al., 1998, Cohn et al., 2000). Binding of Ang II to the AT_1R is known to initiate various signalling cascades resulting in fibrosis due to increased collagen synthesis by cardiac fibroblasts, and cardiomyocyte hypertrophy, both of which contribute to overall development of cardiac hypertrophy (Gray et al., 1998, Weber, 1989). It has been shown that expression of the AT_1R is increased in cardiac hypertrophy (Reiss et al., 1993) allowing for the increased action of Ang II in the heart leading to its pathological effects. As a result, inhibition of the classical axis of the RAS has been researched in depth and proposed as an important target in the treatment and prevention of cardiac remodelling and heart failure.

As most detrimental effects of Ang II have been shown to occur via AT_1R stimulation, direct inhibition of this receptor has been studied in detail in various models. It has been shown that AT_1R inhibition reduces both cardiac hypertrophy and cardiac remodelling in a transgenic rat model of renin-dependent hypertension, where a clear reduction in interstitial cardiac fibrosis was observed (Whaley-Connell et al., 2013). There are also various other points within the RAS that may be blocked in order to prevent cardiac remodelling, for example use of aliskiren, an inhibitor of renin, prevents the conversion of angiotensinogen to Ang I early on in the pathway (Pilz et al., 2005). Inhibiting the conversion of angiotensinogen to Ang I with aliskiren showed significantly lowered blood pressure and cardiac hypertrophy index score as well as a decrease in hypertrophy marker ANP and beta-myosin heavy chain (B-MHC)] gene expression, suggesting that inhibition of renin early in the RAS signalling pathway is successful in reducing cardiac remodelling and end-organ damage (Pilz et al.,

2005). Clinical studies have also described the importance of renin inhibition by aliskiren treatment. It was shown that treatment with aliskiren was as effective in reducing left ventricular mass as treatment with the well-known ARB, losartan, in hypertensive patients (Solomon et al., 2009). Although aliskiren has shown promising effects as a therapeutic, it has been reported that its use where kidney disease or diabetes is present results in increased risk of hyperkalaemia and renal impairment in these patients (Harel et al., 2012, Zheng et al., 2017). As a result, it is contraindicated in these cases and therefore cannot wholly replace ACE inhibition or ARBs (Harel et al., 2012). Further studies have also shown that use anti-hypertensive agents such as ACE inhibitors (preventing the hydrolysis of Ang I to Ang II) may have some inhibitory effect on cardiac remodelling (Schmieder et al., 1996). These studies suggested that a greater reduction in blood pressure correlated with a more pronounced decrease in left ventricular hypertrophy, and that use of ACE inhibitors, specifically, showed a greater decrease in LV mass compared to use of other blood pressure lowering agents such as beta blockers or calcium channel blockers (Schmieder et al., 1996). Collectively these studies highlight the importance of targeting the classical RAS pathway in reduction and prevention of cardiac hypertrophy.

The counter-regulatory axis of the RAS, centred on the actions of ACE2/Ang-(1-7) signalling via MAS has also become an important target with implications in the prevention of cardiac remodelling. It has been demonstrated that the Ang-(1-7) peptide itself has beneficial effects in terms of structural and functional remodelling in the cardiac setting, and that the role of ACE2 in determining levels of peptide is also important (Crackower et al., 2002). Studies have shown that in ACE2-knockout mice, both tissue levels of Ang II (particularly the heart and kidney) as well as plasma levels of Ang II are increased and are associated with an increase in cardiac remodelling following myocardial infarction (Crackower et al., 2002, Kassiri et al., 2009). Further studies in diabetic mouse models with reduced ACE2 expression showed increased levels of plasma and tissue Ang II associated with systolic dysfunction, a phenotype which could be rescued by using the AT_1R blocker, Irbesartan (Patel et al., 2012). These studies suggest an important role for ACE2 in protection against cardiac remodelling via control of Ang II peptide levels in the tissue and circulation.

Various studies have shown that decreased levels of Ang-(1-7) or Mas expression result in poorer cardiac outcome or loss of a previously observed protective effect. For example, in a rat model of salt-induced cardiac remodelling, it was found that increased collagen deposition in remodelling was associated with decreased levels of Ang-(1-7) and Mas compared to controls (Varagic et al., 2010). Furthermore, studies using Mas-deficient mice found an increase in collagen levels in cardiac tissue suggesting increased remodelling (Gava et al., 2012). These studies suggest that loss of Ang-(1-7) or the Mas receptor have important implications in cardiac remodelling, various studies have also investigated the potential for over-expression of counter-regulatory RAS components in cardiac protection. It was found that transgenic mice over-expressing an Ang-(1-7) fusion protein showed a reduction in both fibrosis and cardiomyocyte hypertrophy induced by Ang II infusion (Mercure et al., 2008). It was also found that lentiviral gene transfer of Ang-(1-7) directly to the heart resulted in attenuated cardiac hypertrophy in a rat model of myocardial infarction, where MI-induced impairments such as decreased fractional shortening, increased LV end-diastolic pressure and increased ventricular hypertrophy were all attenuated, and an increase in cardiac ACE2 expression was observed (Qi et al., 2011).

Ang-(1-9), another effector peptide of the counter-regulatory axis of the RAS, has also been implicated as having anti-hypertrophic effects in the heart. Studies using *in vivo* rat models of MI showed that continuous infusion of Ang-(1-9) via osmotic minipump decreased circulating levels of Ang II and ACE activity in a manner independent of Ang-(1-7) as shown using Mas receptor antagonist A779, a marked decrease in cardiomyocyte hypertrophy was also observed (Ocaranza et al., 2010). *In vitro* studies have also suggested an anti-hypertrophic role for Ang-(1-9), where primary adult rabbit cardiomyocytes and H9c2 cardiomyocytes were used as models. In this case, Ang-(1-9) successfully attenuated Ang II-induced hypertrophy in these cells, an effect that was abolished when using the AT_2R antagonist PD123,319 suggesting protective signalling via this receptor (Flores-Muñoz et al., 2011). Further studies showed that continuous infusion of Ang-(1-9) in the SHRSP rat model resulted in a significant reduction in cardiac fibrosis compared with control animals, an effect which was attenuated by

infusion with PD123,319 suggesting anti-fibrotic signalling via the AT_2R (Flores-Munoz et al., 2012b).

The link between the RAS and cardiac remodelling has been made clear by many studies which have targeted both the classical axis of the RAS and the counter-regulatory axis of the RAS, where reduced signalling via the classical axis and increased signalling via the counter-regulatory axis are associated with beneficial and protective effects in the cardiac setting. Although various studies have highlighted the protective benefits of Ang-(1-7) in CVD, the short half-life of this peptide in the circulation (Brosnihan et al., 1998, Yamada et al., 1998) means that its use in therapeutics is limited. Studies modelling CVD have focused on the use of adenoviral vectors for overexpression of this peptide (Flores-Munoz et al., 2012a) or continuous infusion via osmotic minipump (Kar et al., 2011, Zeng et al., 2009) with success in conferring protection. However, further methods of delivery remain to be identified which may have further potential for therapeutic use in humans in the future.

1.4 Introduction to Extracellular Vesicles

Extracellular vesicles (EVs) are membrane vesicles enclosed in a phospholipid bilayer containing cytosol and chemical messengers from the secreting parental cell. It has been found that EVs are released naturally from all prokaryotic and eukaryotic cell types, and furthermore it has been demonstrated that EVs may also be isolated from a wide variety of bodily fluids such as blood, saliva, cerebrospinal fluid and urine (Colombo et al., 2014). Over the past 20 years, it has become apparent that EVs are important mediators of intercellular communication. Previously thought to be cell debris of no importance, studies have found that EVs are involved in transmission of biological signals between cells and are of notable importance in the regulation of many biological processes (Lee et al., 2012). Furthermore, EVs have been implicated as having pathophysiological roles in a variety of disease settings such as in many cancers, cardiovascular disease, neurodegenerative disease and infectious disease. As a result, EVs have become the target of many therapeutic interventions with applications in disease biomarker studies and potential drug delivery (Lee et al., 2012). EVs have become an area of increasing interest in recent years and have since been split into various categories based on attributes such as their size,

morphology and origin. Arguably, the most notable category of EV generating the most interest are exosomes. The term exosome defines vesicles of approximately 30-100 nm in size which are of endosomal origin and are formed in multivesicular bodies (MVBs) and are released from cells as a consequence of the MVBs fusing with the plasma membrane (Johnstone et al., 1987). The second most notable category of EVs are microvesicles (also previously termed microparticles, or in some cases ectosomes). Microvesicles are noted to be approximately 150-1000 nm in size and are formed by budding directly from the plasma membrane of the parental cell (Trams et al., 1981). Although exosomes and microvesicles are two distinct classes of EV, defining EVs and placing them into these categories has been a subject of much debate. It has been suggested that due to the endosomal origin of exosomes, they should display markers of their MVB origin (where they originated as intraluminal vesicles) which would not be present in microvesicles (having formed by budding from the plasma membrane) (Colombo et al., 2014). Thus, it is suggested that the molecular composition of exosomes should be more similar to that of endosomes, while the molecular composition of microvesicles should be more similar to that of the plasma membrane. Furthermore, electron microscopy and nanoparticle tracking analysis have suggested that exosomes do not exceed a size of 150 nm, whereas microvesicles do not seem to exhibit any size restriction (Colombo et al., 2014). Although these criteria exist for the classification of EVs it has been found that there is often overlap; for example, any EV sample obtained from a supernatant or fluid will often include a mixed population of exosomes and microvesicles (Colombo et al., 2014).

Further categories of EVs include vesicular apoptotic bodies which are reported to be of approximately 50-2000 nm in size, however apoptotic bodies differ from microvesicles by definition that they are released specifically from dying cells. These vesicles may be found in high abundance under certain conditions (even more so than exosomes and microvesicles in some cases) and generally contain markers and proteins associated with apoptosis (Thery et al., 2001). It has also been found that membrane protrusions may generate larger EVs, in this case termed oncosomes, which range in size from approximately 1-10 μm and are generally associated with malignant cells (Di Vizio et al., 2012).

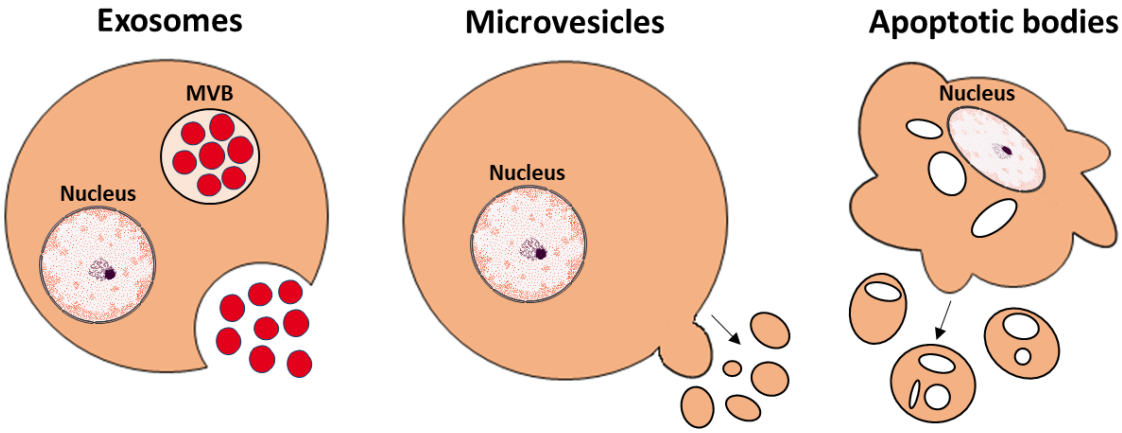

Figure 1-7 Formation of extracellular vesicles. Exosomes are formed within multivesicular bodies which are then released at the plasma membrane, while microvesicles are formed via budding directly from the plasma membrane itself. Apoptotic bodies may be formed as cells undergo apoptosis.

1.4.1 Exosomes: Formation and Transport

Exosome biogenesis occurs via the endosomal trafficking system within cells. Within MVBs, exosomes first begin as intraluminal vesicles (ILVs) which are part of a trafficking network involved in the exocytosis or degradation of various cellular components such as lipids, proteins and nucleic acids (Grant and Donaldson, 2009). Endosomal trafficking involves three types of endosome; early endosomes (precursors to late endosomes) which may fuse with clathrin-coated endocytic vesicles targeting the content for degradation, secretion or recycling; recycling endosomes where content is specifically destined for recycling; and late endosomes (Morelli et al., 2004). Any early endosomes which do not fuse with endocytic vesicles become late endosomes, and it is within the late endosomes that an accumulation of ILVs is observed as a result of inward budding from the endosomal membrane (Morelli et al., 2004). The inward budding of the endosomal membrane allows for the internalisation of lipids, proteins and nucleic acids within the ILVs. As late endosomes accumulate an abundance of ILVs they become known as MVBs which may either fuse with the plasma membrane, resulting in release of exosomes from the cell into the extracellular matrix, or they may fuse with lysosomal compartments in which case the content of the vesicles becomes destined for degradation (Grant and Donaldson, 2009).

It has been noted that during the formation of ILVs, the endosomal membrane becomes highly enriched with tetraspanins (a family of proteins with four transmembrane domains) thought to be critical for exosome formation, these include CD9 and CD63, two of the most commonly used markers for exosome-specific identification (Pols and Klumperman, 2009). Also found during ILV formation are the endosomal sorting complexes required for transport (ESCRT); a class of endosomal sorting complexes required for trafficking within the cell. Of the ESCRT complexes, it is thought that ESCRT I initiates intraluminal membrane budding by binding to ubiquitinated proteins found on the outside of the endosomal membrane which in turn allows for the activation of ESCRT II and recruitment of ESCRT III via ALIX, a cytoplasmic protein involved in the cell death pathway and in regulation of the endosomal/lysosomal system (Trioulier et al., 2004, Katzmann et al., 2001) which, as a result, is also a well characterised marker of exosome identification (Colombo et al., 2014). ALIX has

been shown to bind to tumour-susceptibility gene 101 (TSG-101) which is found on the ESCRT I complex allowing for interaction of ESCRT I and ESCRT III during the trafficking process. The involvement of TSG-101 in exosome formation and transport also allows for its use as an exosome identification and characterisation marker (Baietti et al., 2012, Colombo et al., 2014). Finally, deubiquitination enzymes are recruited to the complex allowing for the removal of the ubiquitin tag from the initial endosomal proteins which are then sorted into the ILVs (Katzmann et al., 2001). Although the ESCRT pathway has been highlighted as the most important driver of exosome biogenesis, it has also been shown that exosome biogenesis may still occur independently of this pathway (Stuffers et al., 2009). It was found that specific inactivation of each of the ESCRT complexes does not prevent the formation of MVBs in human epithelial (HEp-2) cells (Stuffers et al., 2009). Although morphological changes were observed in the components of the endocytic pathway when ESCRT complexes were depleted, early and late endosomes were still clearly observed and could be differentiated from one another. Further studies highlighted other important complexes with implications in exosome biogenesis; it was found that inward budding of the endosomal membrane to form ILVs required the lipid known as sphingolipid ceramide and that exosome formation could be somewhat inhibited by blocking neutral sphingomyelinase required for the production of sphingolipid ceramide (Trajkovic et al., 2008). As a result of these findings, neutral sphingomyelinase inhibitors are commonly used as blockers of exosome release (Wu et al., 2010).

Release of exosomes from the cell into the extracellular matrix is dependent on the fusion of MVBs with the plasma membrane. It has been found that there are several Rab GTPases which play an important role in exosome release, for example RAB11 and RAB35 are known to help facilitate the fusion of MVBs with the plasma membrane (Hsu et al., 2010). The involvement of RAB27A and RAB27B has also been demonstrated (Ostrowski et al., 2010); interestingly, it was observed that exosomes released via RAB27A/B are enriched with different proteins compared to those released via RAB11 and RAB35. Exosomes released via the RAB11 and RAB35 mechanism were enriched with cell specific proteins such as Wnt, PLP and flotillin (Laulagnier et al., 2004a) while exosomes released via the RAB27A/B mechanism were found to be enriched with late endosomal

proteins such as CD63 and ALIX (Ostrowski et al., 2010). These studies suggest that there are several mechanisms by which exosomes may be released from cells via different endosomal subtypes, and that cargo may vary depending on the mechanism of exosome biogenesis and release.

1.4.2 Microvesicles: Biogenesis and Release

Although biogenesis of exosomes has been studied in great detail, the biogenesis of microvesicles has not been as clearly defined. Several different mechanisms have been identified for the release of microvesicles from the plasma membrane using a variety of cell models, with the general consensus being that this class of EV is released via outward budding, or shedding, from the plasma membrane of the cell. Various studies have investigated the formation of microvesicles; it has been suggested that the contractile effects of the actin-myosin machinery may be involved in this process (Muralidharan-Chari et al., 2009). One study using a tumour cell model has shown that the activation of phospholipase D (PLD) via ADP-ribosylation factor 6 (ARF6) results in the recruitment of ERK to the plasma membrane where it is able to phosphorylate and cause activation of the myosin light chain kinase (MLCK). This kinase in turn activates the myosin light chain causing contraction and resulting in the release of microvesicles from the plasma membrane (Muralidharan-Chari et al., 2009). Analysis of these microvesicles showed that they were enriched with specific cargo proteins including ARF6, MHC-I and β1-integrin (Muralidharan-Chari et al., 2009). Further studies have shown that microvesicles may also be released via other means; it has been shown that the TSG-101 subunit of ESCRT-I may be recruited to the plasma membrane via interaction with Arrestin 1 domain-containing protein 1 (ARRDC1) and that microvesicles released from the plasma membrane, in this case, contain TSG-101 and ARRDC1 among other cellular proteins (Nabhan et al., 2012). It has also been suggested that sphingomyelinases may play a role in the release of microvesicles from the plasma membrane; it was shown that a lysosomal related sphingomyelinase, known as acid sphingomyelinase, promoted the release of large microvesicles from astrocytes in response to activation of the ATP receptor, P2X7 (Bianco et al., 2009). These studies suggest that microvesicles may contain a wide variety of protein content specific to the parental cell or origin pathway of the vesicles. Furthermore, the detection of TSG-101 (a common marker in exosome identification) in microvesicles as well as

involvement of sphingomyelinases (certain classes known to be involved in exosome release) suggests some overlap between exosome and microvesicle content and trafficking further adding to the complexity of distinguishing these EV populations.

Aside from internal cellular mechanisms promoting the release of microvesicles, studies have also shown that release may be induced by various external factors. One study showed that microvesicle release could be increased as a result of calcium influx. It was observed that in human erythrocytes, an increase in intracellular calcium concentration caused redistribution and scrambling of phospholipids along with increased shedding of microvesicles from the plasma membrane, however these pathways are thought to be independent of one another (Bucki et al., 1998). A second study also analysing the effect of calcium influx showed that microvesicle release from human platelets required the presence of elevated intracellular calcium in order to occur (Pasquet et al., 1996). Further studies have shown that microvesicle release may also be increased in response to external factors such as hypoxia. One study using human breast cancer cells showed that hypoxia may promote the release of microvesicles from the plasma membrane via expression of the GTPase RAB22A, and that this occurrence is dependent on hypoxia-inducible factors (HIFs) such as HIF-1 which seem to mediate this expression (Wang et al., 2014a). These studies strongly suggest that under certain external stressors, cells may be induced to release increased numbers of microvesicles.

1.4.3 Extracellular Vesicle Content

The content of EVs consists mainly of lipids, nucleic acids [primarily messenger ribonucleic acids (mRNA) and micro ribonucleic acids (miRNA)] and proteins derived from the parental cell. It has been shown that the lipid bilayer of exosomes, compared to that of the plasma membrane of the cell, is enriched with cholesterol, sphingomyelin and desaturated lipids (Laulagnier et al., 2004b, Llorente et al., 2013) suggesting that the exosome bilayer may have increased rigidity in comparison to the plasma membrane. This increased rigidity of exosomes suggests a level of resistance to degradation allowing for them to act as a stable carrier for cargo exchange between cells (Laulagnier et al., 2004b).

Many recent studies have shown that EVs are used as a method of RNA transport. It has been suggested that the RNAs transported by EVs are generally shorter than normal cellular RNA (often less than 200 nucleotides in length) (Huang et al., 2013) and that the most abundant species of exosomal RNA are miRNAs which, in one study, were demonstrated to make up 76% of all mappable deep sequencing reads in exosomes derived from human plasma (Huang et al., 2013). However, another study showed that in exosomes derived from human serum, miRNAs (along with transfer RNAs) made up only 15% of the overall RNA content while the majority consisted of long interspersed and short interspersed elements (making up approximately 50% of RNA content present) (Bellingham et al., 2012) suggesting variation which is possibly affected by the origin of the EV sample. Various studies have demonstrated that RNA may be packaged into EVs and transferred to recipient cells (Valadi et al., 2007) and that this transferred RNA retains functionality. One study showed via labelling of both EVs and their EV-RNA cargo with optical reporters and use of live-cell imaging technologies that EV uptake by cells and translation of their cargo RNA could occur within 1 hr of horizontal transfer between cells in a cancer cell model (Lai et al., 2015). Further studies have shown that miRNAs transported to cells via EVs can regulate the translation of target mRNAs in the recipient cells. For example, it was found that exosomes derived from T cells contained different miRNAs to that of their parental cells and that delivery of these specific miRNAs could regulate gene expression in recipient antigen presenting cells (Mittelbrunn et al., 2011). Specifically, it was found that exosomal miRNA-335 could be transferred to antigen presenting cells and cause significant downregulation of expression of its target gene SRY-Box 4 (SOX4) (Mittelbrunn et al., 2011).

It has also been demonstrated that EVs are involved in the transport of DNA as segments of DNA ranging from 100 bp to 2.5 kbp in length could be found enclosed within EVs (Thakur et al., 2014). A comparison of double-stranded DNA (dsDNA) content within intact EVs compared to EVs treated with DNase showed that treatment could deplete any DNA in the isolation fraction not enclosed within the EVs (Thakur et al., 2014). This study showed that DNase removed all dsDNA segments longer than 2.5 kbp, suggesting that these were not enclosed within the EV lipid bilayer, however the smaller fragments <2.5 kbp could still be found protected within the remaining EVs (Thakur et al., 2014). Sequencing

studies carried out in exosomes derived from human serum showed that DNA found within the isolated exosomes included sequences which spanned all chromosomes (Kahlert et al., 2014). In certain cases, it was found that DNA within exosomes matched that of the genomic DNA of the parental cells; for example in cell models of melanoma and pancreatic cancer it was found that mutations in BRAF, KRAS, p53 and EGFR were present within the EV-DNA fraction (Kahlert et al., 2014). Although there is generally less focus on DNA transfer in EVs compared with RNA and protein, some studies have shown that EVs may transfer functional DNA. One study showed that chromosomal DNA found within cardiomyocyte-derived EVs could be transferred into the cytosol and nuclei of target fibroblasts, resulting in 333 significant gene expression changes (Waldenström et al., 2012). It was also found that exposure of rat intestinal epithelial cells to EVs containing oncogenic H-ras DNA could cause transfer of full-length H-ras to the recipient cells (Lee et al., 2014). The transferred DNA remained there for extended periods of time (measured at up to 30 days post-treatment) and resulted in stimulation of proliferation (Lee et al., 2014).

Often, the protein composition of EVs reflects the mode of biogenesis by which the EVs were produced; as already mentioned exosomes are often enriched in tetraspanins due to their presence during the formation of ILVs (Pols and Klumperman, 2009) as well as ESCRT pathway proteins which partly determine trafficking and release (Baietti et al., 2012), while microvesicles may be enriched with integrins and glycoproteins due to their plasma membrane origin (Heijnen et al., 1999). Further studies have shown that EVs may also include other functional protein classes. For example, analysis of EVs derived from ovarian cancer cells showed enrichment of signalling kinases including MAPK and the ErbB (EGFR) family of receptor tyrosine kinases, which could account for the biological activity demonstrated by EVs (Liang et al., 2013). Studies have shown that EVs may be used in the transfer of receptors and transcription factors to recipient cells and that these proteins have a functional effect in recipient cells. Often, when EVs are derived from cells with a pathological phenotype, EV transfer may be able to induce this phenotype in recipient cells. For example, it was found that microvesicles derived from glioblastoma cells contained an oncogenic form of EGFR which was able to increase proliferation in recipient glioma cells via upregulation of the MAPK/Akt signalling pathway, contributing to

the tumorigenic phenotype (Al-Nedawi et al., 2008). Another study showed that in a model of nasopharyngeal cancer, HIF-1α was upregulated in released exosomes and that treatment of recipient cells with these exosomes resulted in HIF-1α dependent increase in proliferation and invasiveness (Aga et al., 2014).

Together these studies suggest that cargo such as nucleic acids and proteins are able to be packaged into EVs for transfer between cells, and that in many cases the functionality of these signalling molecules remains intact and can be assessed and observed in recipient cells.

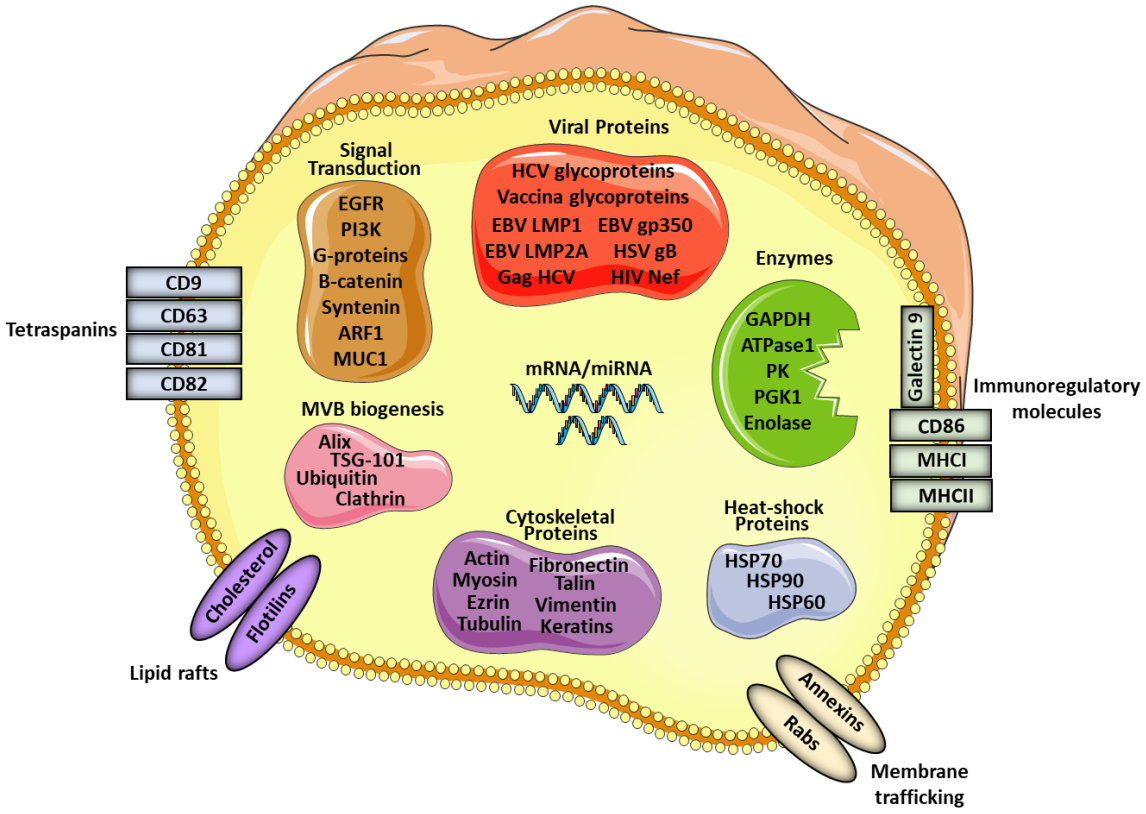

Figure 1-8 Content of extracellular vesicles. Extracellular vesicles have been shown to contain a variety of lipids, nucleic acids, proteins and other signalling molecules. These include viral, cytoskeletal, heat-shock and membrane trafficking proteins, as well as those involved in MVB biogenesis and signal transduction. Lipid rafts, immunoregulatory molecules, mRNA/miRNAs and a variety of enzymes have also been reported in abundance.

1.4.4 Extracellular Vesicles in Cell Communication: Uptake of EVs

Most evidence suggests that EVs are taken up by recipient cells via fusion with the plasma membrane or by various endocytotic processes such as clathrin- or caveolin-mediated endocytosis, phagocytosis, or lipid raft-mediated endocytosis (Mulcahy et al., 2014). It has been suggested that the mode of uptake of EVs by recipient cells may be dependent on the physiological state of the cell type, or for example, whether certain receptors are present on the cell surface that will recognise ligands on the EV surface. It has been shown that different mechanisms of uptake have been identified in different cell types. For example, it was found that both clathrin-dependent endocytosis and phagocytosis occurred in neurons (Morelli et al., 2004) while caveolin-mediated endocytosis occurs in epithelial cells (Nanbo et al., 2013). Furthermore, studies have shown that in certain tumour cells, the primary mechanism of EV uptake is via lipid raft-dependent endocytosis (Svensson et al., 2013). Research has suggested that uptake of EVs by recipient cells can be inhibited by blocking certain factors associated with the plasma membrane, suggesting that they are key players in uptake of EVs. For example, it was found that exosomes derived from glioblastoma cancer cells required association with heparan sulfate proteoglycans on the recipient cell plasma membrane in order for uptake to occur, as blocking with heparin significantly reduced the uptake of EVs *in vitro* (Christianson et al., 2013). Furthermore, it was also discovered that in cell types where exosome uptake is dependent on cholesterol enriched lipid rafts for entry to the cell, this process could be blocked by depletion of plasma membrane cholesterol. It was found that receptor blocking caused an activation in cholesterol efflux and prevented any influx and that this was associated with a reduction in exosome uptake (Plebanek et al., 2015).

The ability of EVs to interact and enter recipient cells is key for their functional effects. In some cases, EVs are able to trigger signalling cascades through interactions between their ligands and receptors found on the cell surface, where entry into the cytoplasm is not actually required. For example, in a study determining signalling mechanisms in neural stem precursor cells (NPCs), it was found that interferon gamma bound to the outside of EVs isolated from NPCs treated with pro-inflammatory cytokines could interact with interferon gamma receptor 1 (IFNGR1) found on the cell surface and initiate Stat-1 signalling within

the cell, promoting inflammatory responses (Cossetti et al., 2014). In other cases, it has been shown that in order for the contents of EVs to have a functional effect, direct entry into the cytoplasm is required either by fusion with the plasma membrane or via an endocytotic process (Montecalvo et al., 2012, Abrami et al., 2013). However, the process by which cargo passes through the endocytic pathway bypassing degradation and being released freely into the cell to elicit biological effects has not been fully elucidated. Although the exact process is unclear, internalisation of EVs into the cell cytosol has been visualised in several studies. In one case, fluorescent labelling of exosomes and their content allowed for visualisation of transfer between dendritic cells, where release of the exosome content was observed in the cytosol of the recipient cells (Montecalvo et al., 2012). Further studies showed that when exosomes were loaded with luciferin, detection of luciferase activity in the recipient cell cytosol was observed suggesting successful internalisation of the vesicles (Abrami et al., 2013).

1.4.5 Extracellular Vesicles in Drug Delivery

The ability for EVs to transfer biologically functional material between cells has generated interest in their potential use as vehicles for drug delivery. Although potential use for drug delivery is still being assessed and is in relatively early stages of research, several key attributes of EVs would suggest advantageous use in drug delivery; for example their robustness and stability in the circulation and their cell targeting properties (Colombo et al., 2014). Many recent studies have been concerned with the loading of EVs and various techniques have been established to do so. The first approach that has been described for the loading of EVs involves loading prior to isolation; in this case the parental cells underwent treatment or loading with therapeutics and EVs are derived afterwards. Studies have demonstrated success with transfection-based approaches for obtaining loaded EVs from cells. It was shown that HEK293 cells transfected with vectors for the expression of specific miRNAs (including miR-16, miR-21 and miR-143) caused over-expression of these miRNAs in the parental cells which further resulted in the production of EVs with increased expression of these miRNAs. It was also found that miR-143 was biologically active and could inhibit growth in a cancer cell model via gene silencing (Kosaka et al., 2012). In other studies, parental cells have been transfected directly with small

RNAs as opposed to using expression vectors. For example, it has been shown that transfection of THP-1 cells (a human monocytic leukaemia model) with miR-143 resulted in production of microvesicles from THP-1 macrophages which exhibited higher expression of miR-143 than controls (Akao et al., 2011). Although small RNAs are popular targets for therapeutic delivery in terms of EVs, other options have also been explored. It was found that incubation of mesenchymal stromal cells (MSCs) with high dose paclitaxel, a commonly used chemotherapeutic treatment, resulted in the production of exosomes containing paclitaxel that were able to inhibit tumour growth in an *in vitro* model via anti-proliferative pathways (Pascucci et al., 2014). Another similar study also showed that incubation of apoptotic tumour cells with the chemotherapeutic drugs doxorubicin or methotrexate resulted in the shedding of microvesicles containing these drugs, as determined by fluorescent tagging (Tang et al., 2012). Furthermore, it was found that the released microvesicles had a high-efficiency cytotoxic effect on tumour cells *in vitro* (Tang et al., 2012) suggesting that these particles are not only loaded with the chemotherapeutic drugs but that the drugs remain biologically active.

Further methods for the loading of EVs focus on loading post-isolation. In this case, EVs are first isolated from culture supernatant or other biological fluids and exogenously loaded with therapeutic molecules often via electroporation, sonification or treatment with detergents such as saponin. The phospholipid bilayer enclosing EVs provides a barrier for the passive loading of hydrophilic molecules such as small RNAs, however several studies have utilised electroporation for the loading of these molecules. Electroporation, based on the spontaneous formation of pores in the lipid bilayer as a response to electrical stimulation, has been shown to be a successful technique for the loading of EVs with small RNA molecules (Alvarez-Erviti et al., 2011). It was found that short-interfering RNA (siRNA) could be loaded into exosomes via electroporation, and furthermore, that these exosomes could exhibit a biological effect when introduced to the mouse brain via systemic intravenous injection. Results showed that siRNA delivery via electroporated exosomes reduced gene expression and protein expression of the BACE1 gene, a notable target in therapeutics for Alzheimer's disease (Alvarez-Erviti et al., 2011). Further studies also demonstrated that exosomes derived from human plasma could be loaded

via electroporation with siRNA specifically targeting the MAPK pathway. It was found that delivery of these exosomes to both monocytes and lymphocytes could successfully silence MAPK1 expression *in vitro*, inhibiting its proliferative effects (Wahlgren et al., 2012). Studies have also assessed other methods of exogenous loading of EVs. One study assessed several mechanisms of loading including room temperature incubation, freeze-thaw cycles, sonication and saponin treatment (Haney et al., 2015). When attempting to load exosomes with the antioxidant enzyme, catalase, it was found that loading efficiencies were highest when using sonication or treatment with saponin. Not only were exosomes successfully loaded via these means, it was also demonstrated that treatment of neurons with these exosomes protected against ROS production *in vitro* and decreased microglial activity in an *in vivo* mouse model of brain inflammation (Haney et al., 2015).

Although various successes have been demonstrated in terms of therapeutic loading of EVs both pre-isolation and post-isolation, most of these studies are still in the *in vitro* or *in vivo* stages of research and the most suitable methods of loading, doses, and targeting strategies for clinical application are still to be determined. However, the future outlook of EVs as therapeutic drug delivery vehicles remains promising.

1.4.6 Extracellular Vesicles and Cardiovascular Disease

Owing to the fact that EVs are released from almost all cell types, including those associated with the cardiovascular system such as endothelial cells, vascular smooth muscle cells, fibroblasts, cardiomyocytes and macrophages, as well as being found in most bodily fluids such as plasma, serum and urine (Colombo et al., 2014); EVs are being widely investigated as biomarkers for cardiovascular disease. In addition to this, research is also being carried out into their use as therapeutic delivery systems against cardiovascular disease. Cardiovascular diseases such as myocardial infarction, hypertension, coronary artery disease and the resultant cardiovascular remodelling are a common cause of mortality worldwide, and recently studies have begun to associate EVs with these diseases and cardiovascular events.

1.4.6.1 Extracellular Vesicles: Basic Research in CVD

EVs have been researched extensively in the cardiovascular system in terms of basic research strategies for therapeutics. One area undergoing extensive research is the use of EVs derived from mesenchymal stem cells (MSCs) for cardiac regenerative medicine. The traditional basis of this therapy involves injection of MSCs into the myocardium to prevent cardiac damage or allow for repair (Mangi et al., 2003) however it has been reported that MSC secreted factors may be more beneficial in terms of improving heart function than the MSCs themselves (Gnecchi et al., 2005, Ratajczak et al., 2012). Early studies investigating the effects of paracrine factors derived from MSCs showed that administration of conditioned media from cultured human-MSCs could reduce myocardial infarct size in a porcine model of ischaemia and reperfusion injury (Timmers et al., 2007), and had a similar effect in rat hearts after experimental-MI surgery *in vivo* (Gnecchi et al., 2006). More recent studies have highlighted the importance of the exosomal fraction in heart function improvement; it was shown in a mouse model of myocardial ischaemia/reperfusion injury that administration of exosomes derived from human MSCs was able to significantly reduce infarct size (Lai et al., 2010). Furthermore, a second study in a mouse model of ischaemia/reperfusion injury found that human MSC-derived exosomes not only reduced infarct size by 45% compared to control animals, but also decreased levels of oxidative stress and increased activation of the PI3K/Akt pathway almost immediately after reperfusion, overall enhancing cardiac function after ischaemia/reperfusion injury (Arslan et al., 2013). It has also been demonstrated that EVs derived from cardiomyocyte progenitor cells (CPC) may have potential therapeutic benefits in cardio-protection. It has been shown *in vitro* that EVs derived from CPCs are able to stimulate the migration of endothelial cells dependent on activation by matrix metalloproteinases (Vrijsen et al., 2010). Further *in vitro* studies showed that exosomes derived from mouse heart CPCs were able to protect H9c2 cardiomyoblasts against oxidative stress via inhibition of caspases. This study also demonstrated that in a mouse model of myocardial ischaemia/reperfusion injury, CPC-exosomes introduced to the heart via intramyocardial injection could reduce cardiomyocyte apoptosis by over 50%, highlighting their cardio-protective effect (Chen et al., 2013).

Clinical studies have suggested that patterns of miRNA expression change in response to cardiovascular disease (Ikeda et al., 2007) and as circulating EVs are known to contain selectively packaged miRNAs, EV and miRNA association has become a topic of interest in basic research. For example, it was revealed that miR-126, a well characterised regulator of angiogenesis and maintenance of vascular integrity (Fish et al., 2008), has increased expression in various EV populations including endothelial microvesicles and endothelial progenitor cells (Jansen et al., 2013, Ranghino et al., 2012). Not only were these EV populations found to be enriched with miR-126, but endothelial microvesicles could mediate transfer of biologically active miR-126 resulting in increased migration and proliferation of endothelial cells *in vitro* and acceleration of re-endothelialisation *in vivo* (Jansen et al., 2013). Endothelial progenitor cell-derived microvesicles enriched with miR-126 (known to regulate the response to VEGF in endothelial cells) were shown to improve regeneration and neovascularisation in a mouse model of hindlimb ischaemia via transfer of miR-126 along with another pro-angiogenic microRNA, miR-296 (Ranghino et al., 2012).

Along with the protective effects of EVs in the cardiovascular setting, it has also been shown in numerous studies that EVs obtained from cells or patients exhibiting pathological disease phenotypes are able to induce detrimental effects in recipient cells or animal models. For example, it was found that microvesicles isolated from human atherosclerotic plaques were able to induce endothelial monocyte adhesion *in vitro* and *ex vivo* by transfer and increase of ICAM-1 protein levels and subsequent ERK1/2 phosphorylation (Rautou et al., 2011). Furthermore, this effect was found to be more pronounced in EVs derived from plaques of symptomatic patients vs EVs from plaques of asymptomatic patients. The study concluded that EVs derived from atherosclerotic plaques were likely to promote atherosclerotic plaque progression (Rautou et al., 2011). Other studies found that EVs derived from the plasma of patients suffering from metabolic syndrome were able to induce vascular dysfunction when injected *ex vivo* into mouse aortas. It was found that these EVs enhanced expression of NADPH-oxidase and oxidative stress as well as increasing mRNA and protein levels of the inflammatory cytokine monocyte chemoattractant protein 1 (MCP-1) (Agouni et al., 2011). Earlier studies also found that circulating microvesicles

isolated from the plasma of patients with myocardial infarction were able to induce endothelial dysfunction in rat aortas *ex vivo*. Exposure of rat aortic rings with intact endothelium to EVs from myocardial infarction patients resulted in impairment of acetylcholine-induced endothelium-dependent relaxation, an effect not observed when treating with EVs from non-ischaemic patients (Boulanger et al., 2001). Furthermore, it was demonstrated that the effect of myocardial infarction EVs could be abolished by removal of the endothelium or by addition of a nitric oxide synthase inhibitor, suggesting that these EVs target and impair the endothelial nitric oxide transduction pathway (Boulanger et al., 2001).

1.4.6.2 Extracellular Vesicles and Cardiac Remodelling

Recent studies have demonstrated functions for EVs in communication between cardiac cell types and regulation of hypertrophy, apoptosis and fibrosis in cardiac remodelling. It has been shown that EVs may be involved in miRNA cross talk between cardiomyocytes and cardiac fibroblasts. Neonatal rat cardiac fibroblasts were found to secrete miRNA-enriched exosomes, specifically the presence of high levels of the miR-21 passenger strand (the strand generally degraded upon dicer processing of the pre-miRNA), miR-21*, was detected (Bang et al., 2014). This study identified a pathological role for exosomal miR-21* where it functioned to silence the gene targets, sorbin and SH3 domain-containing protein 2 (SORBS2) and PDZ and LIM domain protein 5 (PDLIM5), which in turn induced cardiomyocyte hypertrophy. The study confirmed the importance of miR-21* via pharmacological inhibition with a miR-21* antagomir, which successfully attenuated the pathological effects in a mouse model of Ang II-induced hypertrophy (Bang et al., 2014). EVs have also been implicated in cardiomyocyte survival and apoptosis. It was found that EVs released from CPCs were able to inhibit cardiomyocyte apoptosis after myocardial infarction (Barile et al., 2014). This study showed that cultured CPCs derived from human atrial appendage explants produced EVs that were able to inhibit apoptosis in mouse HL-1 cardiomyocytes, an effect that was abolished when EVs were depleted from conditioned media. Furthermore, it was found that these EVs were enriched for miR-210 which could successfully downregulate gene expression of its targets [ephrin A3 and protein-tyrosine phosphatase 1B (PTP1b)] resulting in inhibition of cardiomyocyte apoptosis (Barile et al., 2014). Investigation of these effects *in*

vivo (myocardial infarction induced in normotensive WKY rats) showed that infarcted hearts injected directly with CPC-EVs exhibited reduced cardiomyocyte apoptosis and improved left ventricular ejection fraction compared to control-injected animals (Barile et al., 2014). It was also found that exosomes derived from transgenic mouse cardiomyocytes overexpressing heat shock protein 20 (Hsp20) contained higher levels of Hsp20 along with phosphorylated Akt, survivin and superoxide dismutase 1 (SOD1) in comparison to exosomes derived from wildtype cardiomyocytes, all of which contributed to protection against hyperglycaemia-induced cardiomyocyte cell death *in vitro* (Wang et al., 2016). These exosomes were also discovered to protect against induced adverse cardiac remodelling in a diabetic mouse model, an effect which was abolished when exosome generation was blocked by the neutral sphingomyelinase 2 inhibitor, GW4869 (Wang et al., 2016).

Studies have also found that EVs may play a role in the progression of cardiac fibrosis associated mechanisms. It has been shown that heat shock protein 90 (Hsp90) is a key regulator of fibrotic signalling in cardiac fibroblasts, and that cardiomyocyte-derived exosomes containing Hsp90 [together with cardiomyocyte secretion of interleukin 6 (IL-6)] are able to activate Stat-3 signalling in cardiac fibroblasts resulting in excess collagen synthesis and contributing to the cardiac dysfunction present during cardiomyocyte hypertrophy (Datta et al., 2017). A second study found that exosomes released from cardiomyocytes (in this study termed “cardiosomes”) during exercise contained certain upregulated miRNAs including miR29b and miR455 (Chaturvedi et al., 2015). It was found that exercised diabetic mice released these cardiac exosomes and that miR29b and miR455 were significantly upregulated in the exosomes compared with those from control sedentary mice. Furthermore, these exosomes were able to bind to the 3’ untranslated region (UTR) of the matrix metallopeptidase 9 (MMP9) mRNA and reduce the expression in the diabetic heart, overall resulting in a decrease in cardiac fibrosis compared to control treatment (Chaturvedi et al., 2015).

Angiogenesis is an essential process that must occur during cardiac repair and regeneration after cardiovascular events such as myocardial injury, and EVs have been implicated as having pro-angiogenic properties in various studies. It was found that cardiomyocytes overexpressing Hsp20 released exosomes enriched

with Hsp20 which were able to promote proliferation and migration in human umbilical vein endothelial cells, an effect also observed when treating with recombinant human Hsp20 (Zhang et al., 2012). Furthermore, it was found that blockade of the vascular endothelial growth factor receptor 2 (VEGFR2) abolished these effects, suggesting a role for cardiomyocyte exosomal Hsp20 in the activation of VEGFR2 in regulation of myocardial angiogenesis (Zhang et al., 2012). Commonly, insufficient angiogenesis is associated with the diabetic heart often resulting in ischaemic cardiovascular events (Wang et al., 2014b). It was reported that cardiomyocytes isolated from Goto-Kakizaki rats (an established model of type 2 diabetes) produced exosomes that were able to exhibit anti-angiogenic effects (Wang et al., 2014b). Diabetic cardiomyocytes produced exosomes enriched with miR-320 which were able to inhibit proliferation, migration and tube formation in mouse cardiac endothelial cells, effects which could be blocked by inhibiting exosome transfer using GW4869. This study showed that the transferred miR-320 could successfully downregulate its target genes (Hsp20, ETS Proto-Oncogene 2 (Ets2) and insulin-like growth factor 1 (IGF-1)) in recipient mouse cardiac endothelial cells and that this in turn inhibited angiogenic processes, an effect that was prevented by knockdown of miR-320 (Wang et al., 2014b).

Taken together, studies thus far suggest an important role for EVs in relation to cardiac remodelling, with implications in both promotion and prevention of cardiomyocyte hypertrophy, cardiomyocyte apoptosis, fibrosis and angiogenesis, with effects often dependent on the cell of origin, the EV cargo, and the disease model of interest.

1.4.6.3 Extracellular Vesicles and the RAS

More recently, studies have begun to suggest a link between EVs and the RAS. Arguably, one of the most important discoveries in this area was that exosomes derived from HEK293T cells during membrane stretch, and mouse serum during cardiac pressure overload contain AT_1Rs which retain their function (Pironti et al., 2015). It was first noted that both membrane stretch *in vitro* and cardiac pressure overload *in vivo* increases the number of exosomes released compared to controls. Secondly, it was discovered that exosomes derived from cells under the stress of membrane stretch contained approximately 8-9 AT_1Rs per 100

exosomes while circulating exosomes from control animals contained <1 AT_1R per 100 exosomes, which increased to approximately 2 AT_1Rs per 100 exosomes under cardiac pressure overload, as determined by AT_1R radioligand binding assay (Pironti et al., 2015). Whether or not the AT_1Rs present on exosomes were transferred was determined by fluorescent tagging. AT_1R-YFP and Alix-mCherry (a fluorescent label for exosome visualisation) expressing cells produced exosomes that showed transfer of Alix-mCherry to the cytoplasm and AT_1R-YFP to the plasma membrane of recipient cells. It was then shown that transferred AT_1Rs could undergo internalisation following stimulation with Ang II and also increase ERK phosphorylation (Pironti et al., 2015). This study also showed that exosomes carrying functional AT_1Rs could modulate blood pressure *in vivo*. AT_1R-enriched exosomes were injected intravenously into AT_1R-KO mice infused with Ang II and showed a 30% increase in blood pressure compared with saline injected or control exosome injected mice. Furthermore, heart tissue levels of phospho-ERK were increased in AT_1R-exosome animals compared with controls which, together with the other data, suggests that exosomes can transfer functional AT_1Rs (Pironti et al., 2015).

Other studies have also highlighted an important link between exosomes and the RAS in the cardiac setting. It was found that treatment of neonatal rat cardiac fibroblasts (NRCFs) with exogenous Ang II caused a significant increase in exosome release from these cells via activation of the AT_1R and AT_2R, an effect which was not observed in treatment with other classical hypertrophic stimuli (Lyu et al., 2015). Neonatal rat cardiomyocytes (NRCMs) treated with NRCF-derived exosomes exhibited enhanced Ang II production with upregulation of key components of the classical RAS including renin, angiotensinogen, AT_1R and AT_2R, along with downregulation of ACE2. Cardiomyocyte hypertrophy and upregulation of the MAPK/Akt pathways were induced by NRCF-exosomes however this could be attenuated by use of AT_1R and AT_2R antagonists, or by inhibition of exosome release (Lyu et al., 2015). Furthermore, it was shown that Ang II induced exosome release from cardiac fibroblasts and cardiac hypertrophy could be significantly attenuated in Ang II infused mice by use of exosome inhibitor co-treatment, further highlighting the link between exosomes and the pathological actions of the RAS (Lyu et al., 2015).

A second study also found that exposure to Ang II upregulated the release of microvesicles. In order to investigate the link between the RAS, microvesicles and increased thrombotic risk, the effects of Ang II treatment were assessed in terms of generation of procoagulant microvesicles. When human mononuclear cells were exposed to Ang II, it was found that microvesicle release was significantly increased compared to control cells, as were intracellular calcium concentration and microvesicle-associated tissue factor levels (Cordazzo et al., 2013). It was also found that these effects could be inhibited by blockade of the AT_2R but not the AT_1R. This model suggests a link between RAS-mediated generation of procoagulant microvesicles and thrombosis (Cordazzo et al., 2013).

More recently, it has been shown that MSC-derived microvesicles are able to regulate the RAS with promising effects in pulmonary arterial hypertension (PAH). In a rat model of monocrotaline (MCT) induced PAH, animals were injected with either saline, MSC-microvesicles or MSC-microvesicles and the Mas antagonist A779 every two days for 5 weeks of MCT exposure (Liu et al., 2018). It was found that MSC-microvesicles were able to alleviate pulmonary arterial pressure and right ventricular hypertrophy index. Furthermore, ACE2 expression was found to be increased in the lungs and Ang-(1-7) plasma levels were also significantly increased compared to control PAH animals while, conversely, ACE and Ang II levels were decreased compared to control animals (Liu et al., 2018). In animals treated with MSC-microvesicles and the Mas receptor antagonist, A779, the protective effects were abolished, suggesting an important role for the counter-regulatory axis of the RAS in MSC-microvesicle induced protection in PAH (Liu et al., 2018).

Taken together, these studies suggest a relatively new link between EVs and regulation of the RAS and its downstream effects. Although this link has not been researched extensively, these key studies suggest that EVs may have implications in a variety of cardiovascular disease settings where aberrant RAS signalling is known to be involved.

1.5 Hypothesis and Aims

Components of the renin-angiotensin system (RAS) are altered in extracellular vesicles (EVs) under pathological cardiomyocyte hypertrophy. Cells of the heart release different components of the RAS within EVs depending on their physiological state. EVs carrying Ang II are able to exacerbate cardiomyocyte hypertrophy while those carrying Ang-(1-7) are able to attenuate cardiomyocyte hypertrophy.

- To characterise EVs released from different cardiac cell types; H9c2 cardiomyocytes and NRCF cells, as well as circulating EVs from normotensive and hypertensive rat models.

- To determine the effects of Ang II treatment on the release of EVs from cardiac cells and analyse the hypertrophic effects of these EVs on recipient cardiomyocytes.

- To determine the effects of Ang-(1-7) treatment on the release of EVs from cardiomyocytes and analyse the potential protective effects of these EVs on recipient cardiomyocytes under Ang II-induced hypertrophy.

- Exogenously load serum-EVs with Ang-(1-7) and determine any protective effects via intravenous delivery in an Ang II infused rat model.

- Analyse Ang II and Ang-(1-7) levels in circulating EVs derived from the serum of healthy subjects vs. coronary artery disease patients having undergone coronary artery bypass graft (CABG) surgery.

Chapter 2 Materials and Methods

2.1 Cells and suppliers

H9c2 cells are an immortalised cardiomyoblast cell line derived from BDIX embryonic rat heart tissue (Hescheler et al., 1991). All batches of H9c2(2-1) cells were purchased from Sigma Aldrich (Irvine, UK) where cultures are originally supplied by HPA Culture Collections (Salisbury, UK).

2.2 Antibodies and suppliers

Table 2-1 Primary antibodies for western immunoblot and ICC

Antigen	Manufacturer	Host Species	Concentration	Dilution	Buffer
CD63	Abcam ab108950	Mouse	1mg/mL	1:500	Blocking Buffer
TSG-101	Abcam ab125011	Rabbit	0.22mg/mL	1:1000	Blocking Buffer
HSP-70	Abcam ab2787	Mouse	1mg/mL	1:1000	Blocking Buffer

Table 2-2 Secondary antibodies for western immunoblot and ICC

Antigen	Secondary Antibody	Manufacturer	Concentration	Dilution	Buffer
CD63	Rabbit anti-mouse IgG Alexa Fluor 680	Thermo Fisher Scientific A21065	2mg/mL	1:15000	Blocking Buffer
HSP-70					
TSG-101	Goat anti-rabbit IgG Alexa Fluor 680	Thermo Fisher Scientific A21076	2mg/mL	1:15000	Blocking Buffer

2.3 qRT-PCR probes and suppliers

Table 2-3 Rat TaqMan Probes

Gene	Gene Name	Assay ID	Manufacturer	Label
GAPDH	Glyceraldehyde 3-phosphate dehydrogenase	Rn99999916_s1	Thermo Fisher Scientific	VIC-MGB
Nppb	Natriuretic Peptide Precursor B	Rn00580641_m1	Thermo Fisher Scientific	FAM-MGB
Agtr2	Angiotensin II Type 2 Receptor	Rn00560677_s1	Thermo Fisher Scientific	FAM-MGB
Agtr1	Angiotensin II Type 1 Receptor	Rn02758772_s1	Thermo Fisher Scientific	FAM-MGB
Mas1	Mas Receptor	Rn00562673_s1	Thermo Fisher Scientific	FAM-MGB

2.4 Standard solutions and buffers

10x Phosphate-buffered saline (PBS), pH 7.4: 1.37 M NaCl, 27 mM KCl, 100 mM Na_2HPO_4, 18 mM KH_2PO_4

10x Tris-buffered saline (TBS), pH 7.4: 1.369 M NaCl, 27 mM KCl, 247 mM Tris base

Western lysis buffer: 50 mM Tris-HCl pH7.4, 50 mM NaF, 1 mM $Na_4P_2O_7$, 1 mM EGTA, 1 mM Ethylenediaminetetraacetic acid (EDTA), 1 % (v/v) Triton-X 100, 1 mM DTT, 1 mM Na_3VO_4, 0.1 mM PMSF, 250 mM mannitol, 1 x complete mini protease inhibitor cocktail tablet (for 10 mL solution) (Roche, Burgess Hill, UK), 1 x phosSTOP phosphatase inhibitor cocktail tablet (for 10 mL solution) (Roche, Burgess Hill, UK)

Western transfer buffer: 192 mM Glycine, 25 mM Tris base, 0.01 % SDS, 200 mL Methanol/L

Western blocking buffer: 1x Tris-buffered saline (TBS) with 1.095g/mL Tween-20 1:1 (v/v) SEA BLOCK (ThermoFisher Scientific, Paisley, UK) pH 7.4

ICC blocking buffer: 1% normal goat serum blocking solution (Vector Laboratories, Peterborough, UK) in 1x Phosphate-buffered Saline (PBS) pH 7.4

ADS buffer, pH 7.35: 116 mM NaCl, 20 mM 4-(2-hydroxyethyl)-1-piperazineethanesulfonic acid (HEPES), 1 mM NaH_2PO_4, 5.5 mM Glucose, 5 mM KCl, 0.8 mM $MgSO_4$

1x Trypsin EDTA: 10% Trypsin-EDTA Solution 10X (0.5% trypsin, 0.2% EDTA, trypsin gamma irradiated by SER-TAIN Process, without phenol red, in saline) (Sigma Aldrich, Irvine, UK) in 1x Phosphate-buffered saline (PBS), pH 7.4

2.5 Cell culture procedures and plasticware

All cell culture was performed aseptically in sterile class II laminar flow hoods (Thermo Fisher, Paisley, UK) and cells were maintained in humidified incubators at 37ºC and 5% CO_2/95% O_2. All tissue culture reagents were purchased from Gibco (Thermo Fisher, Paisley, UK) unless otherwise indicated. All cell culture plasticware used was Corning Cell Culture Consumables brand (Sigma Aldrich, Irvine, UK) unless otherwise indicated.

2.5.1 Culture growth media for H9c2 cardiomyocytes

H9c2 cardiomyocytes were cultured either in Gibco Minimal Essential medium (MEM) supplemented with 10% (v/v) FCS, 2 mM L-glutamine and 100 IU/mL penicillin, 100 µg/mL streptomycin, 1 mM sodium pyruvate (Thermo Fisher, Paisley, UK) or in Dulbecco's Modified Eagle's Medium (DMEM) supplemented with 10% (v/v) FCS, 2 mM L-glutamine and 100 IU/mL penicillin, 100 µg/mL streptomycin, 1 mM sodium pyruvate.

2.5.2 Culture growth media for neonatal rat cardiac fibroblasts

Neonatal rat cardiac fibroblast (NRCF) cells were cultured in Dulbecco's Modified Eagle's Medium (DMEM) supplemented with 20% (v/v) FCS, 2 mM L-glutamine and 100 IU/mL penicillin, 100 µg/mL streptomycin (Thermo Fisher, Paisley, UK). When initially plated, cells were grown in plating media; Dulbecco's Modified Eagle's medium (DMEM) and M199 supplemented with 100 IU/mL penicillin, 100 µg/mL streptomycin, 10% horse serum and 5% FCS (Thermo Fisher, Paisley, UK).

2.5.3 Isolation of NRCF and NRCM from neonatal rat hearts

All animal surgical procedures were performed in accordance with the Animal Scientific Procedures Act (1986) and licensed by the UK Home Office (under the project licence held by Dr Delyth Graham, PPL 70/9021). This particular procedure was performed under Schedule 1 (Humane Killing of Animals) to the Animal Scientific Procedures Act (1986).

Primary cardiac fibroblasts and cardiomyocytes were isolated from neonatal rat hearts (1-5 days old) by enzymatic digestion and differential plating to separate fibroblasts and cardiomyocytes, where fibroblasts where plated onto poly-L-lysine coated 10 cm^2 culture dishes which cardiomyocytes could not adhere to.

Neonatal rats were killed by decapitation and hearts immediately removed by thoracotomy and stored in ice-cold ADS buffer. The hearts were then transferred into a sterile laminar flow hood where any remaining lung and surrounding connective tissue was removed. Whole hearts were cut into small pieces using fine scissors and placed into a sterile 100 mL Duran bottle in ADS buffer on ice using a sterile Pasteur pipette. The ADS was carefully removed to begin enzyme digestion of the heart tissue in 30 mg collagenase type 2 (310 U/mg) (Worthington Biochemical Corp, NJ, USA) and 30 mg porcine pancreatin (Sigma Aldrich, Irvine, UK) dissolved in ADS. Cells were isolated in cycles of digestions at 37ºC for 5, 20, 25, 25, 28, and 25 minutes with varying stroke speeds (6 digestions total) (detailed in Table 2-4).

For the initial enzyme digestion, 10 mL enzyme was added to the homogenised hearts and incubated in a 37ºC shaking waterbath set at 180 strokes/min for 5 minutes. This allows for the breakdown of any remaining connective tissue to then release the cells and so after the initial digestion the enzyme was removed and discarded. After each enzyme digestion, the enzyme supernatant containing cells was removed and added to 2 ml 100% (v/v) foetal calf serum (FCS) (Thermo Fisher, Paisley, UK), subjected to centrifugation at 500g for 5 minutes and resuspended in 4 mL 100% (v/v) FCS. The cell suspension was then stored in a humidified chamber at 37ºC in 5% CO_2/95% air. Resuspended cells were

combined and stored in the humidified chamber with the initial cells after each round of enzyme digestion.

After the final enzymatic digestion all cells were combined and subjected to centrifugation at 500g for 6 minutes and then resuspended in 24 mL plating media. Resuspended cells were split across 2 poly-L-lysine (Sigma Aldrich, Irvine, UK) coated 10 cm^2 culture dishes and incubated at 37ºC in 5% CO_2/95% air for 1.5 hr to allow for the adhesion of cardiac fibroblasts to the coated plates. Following fibroblast adherence, media containing primary NRCM was then siphoned off using a sterile Pasteur pipette. The NRCM were subjected to centrifugation at 500g for 5 minutes, resuspended in 4 mL plating media and counted using 10 µL of cell suspension with a haemocytometer (outlined in section 2.5.4). NRCM were then frozen in liquid nitrogen in 10% DMSO/ plating media at a density of $2x10^6$ cells per cryovial (outlined in section 2.5.5).

The adhered fibroblasts were cultured in plating media for 24 hr before cells were washed twice with 1x PBS (Thermo Fisher, Paisley, UK) and media was replaced with NRCF maintenance media (outlined section 2.5.2).

Table 2-4 Digestion steps for NRCF and NRCM isolation

Digest	Enzyme Volume (mL)	Time (min)	Strokes/min
1	10	5	180
2	10	20	160
3	8	25	150
4	8	25	150
5	6	28	160
6	6	25	150

2.5.4 Culture and passaging of H9c2 and NRCF cells

H9c2 cardiomyocytes and NRCF cells were cultured in a humidified chamber at 37ºC in 5% CO_2/95% air using the cell-specific media stated previously (sections 2.5.1 and 2.5.2). H9c2 cells were passaged by trypsin-ethylenediamine tetra-acetic acid (trypsin EDTA) when the culture reached 70% confluence, while NRCF cells were passaged when the culture reached 100% confluence. Briefly, cells were washed twice with sterile Dulbecco´s calcium and magnesium free PBS (Thermo

Fisher, Paisley, UK) and incubated with 2 mL of trypsin-EDTA at 37°C for approximately 3 minutes. Once the majority of the cells had detached the action of the trypsin-EDTA was blocked with 10 mL of the appropriate complete media. Cells were harvested by centrifugation at 500g and re-suspended in fresh media before seeding. NRCF were seeded into poly-L-lysine coated flasks, where flasks were treated with 2 mL poly-L-Lysine (Sigma Aldrich, Irvine, UK) for 5 minutes, this was then removed and flasks washed twice with sterile PBS. Generally H9c2 cells were passaged at 1:3 – 1:10 while NRCF were passaged at 1:2 – 1:3.

NRCM were seeded directly onto culture plates for experimental use after resurrection from cryostorage. Due to their lack of proliferation they were not passaged (Watkins et al., 2011).

When passaging and seeding cells for experimental procedures, they were first counted using a haemocytometer to ensure accurate and correct seeding densities of cells. After harvesting detached cells by centrifugation and re-suspending in fresh maintenance media, 10 µL of cell suspension was added to the haemocytometer and cells were counted within the 4 quadrants made up of 16 squares each to then determine the mean number of cells across the 4 quadrants. This was then used to calculate the number of cells per mL where cells/mL is equal to the mean of the 4 quadrants $x10^4$. The volume of cell suspension required to obtain the desired seeding density was calculated using the formula:

$$\boldsymbol{required\ volume\ (\mu L) = \frac{seeding\ density}{number\ of\ cells/\mu L}}$$

2.5.5 Cryopreservation of cells

For cryopreservation and long-term storage, cells were prepared as outlined in section 2.5.4. After centrifugation and removal of the supernatant, cells were re-suspended in an appropriate volume of complete cell culture media supplemented with 10% (v/v) dimethyl sulfoxide (DMSO) to achieve an approximate density of $1x10^6$ cells/mL. The resuspended cells were then aliquoted into 1 mL cryopreservation tubes which were placed into a freezing

container filled with 100% isopropanol and placed into a -80 ºC freezer for 24 hr to allow for a cooling rate of approximately -1ºC/minute to -80 ºC thus preventing cell rupture by rapid freezing. After 24 hr, frozen cells were transferred to liquid nitrogen storage tanks for long term storage.

2.5.6 Resurrection of frozen cell stocks from cryostorage

When resurrecting cells frozen down in liquid nitrogen the vials were initially stored on dry ice. Once ready to enter the sterile laminar flow hood, cells were thawed quickly in a 37ºC water bath. Cells were then resuspended gently by pipetting and transferred to a sterile 25 mL universal with 10 mL of the appropriate complete growth media. Next, cells were subjected to centrifugation at 500g for 5 minutes, the pellet resuspended in 1 mL complete growth media and transferred to a sterile vented T-75 cm^2 culture flask. After 24 hr, media was removed and replaced with fresh complete growth media to remove any dead cells.

2.5.7 H9c2 model of cardiomyocyte hypertrophy

Hypertrophy was performed as per a previously established protocol (Flores-Muñoz et al., 2011). Briefly, H9c2 cells were seeded onto 22x22mm^2 coverslips at a density of $3x10^4$ cells and maintained at 37ºC in a humidified chamber for 24 hr prior to experiments. Media was then changed to serum free for 24 hr followed by stimulation with 100 nM Ang II (Sigma Aldrich, Irvine, UK) (or untreated control) and incubated for 96 hr at 37ºC to stimulate hypertrophy. This model and protocol were used as the control for hypertrophy when testing EVs as possible inducers or inhibitors of hypertrophy.

2.5.7.1 Fluorescent staining of cells

Stimulated and control cells were washed twice with PBS and fixed with 4% (w/v) paraformaldehyde (PFA) (Sigma Aldrich, Irvine, UK) on ice for 15 minutes. Cells were washed twice and permeabilised with 0.1% Triton-x/PBS (Sigma Aldrich, Irvine, UK) for 10 minutes at room temperature. Cells were then washed twice and stained with 5 µg/mL phalloidin/fluorescein isothiocyanate (FITC) (Sigma Aldrich, Irvine, UK) in 1% bovine serum albumin (BSA)/PBS (Sigma Aldrich, Irvine, UK) for 1 hr. Stained cells were washed three times with PBS and

mounted using ProLong Gold Antifade Mountant with 4′,6-diamidino-2-phenylindole (DAPI) (Thermo Fisher, Paisley, UK). Slides were sealed after 24 hr and stored at 4ºC.

2.5.7.2 Imaging of cells by confocal microscopy and cell sizing

Images from 5 fields of view per coverslip were acquired using a Zeiss LSM 510 confocal microscope at a magnification of 25x with 0.7x zoom using the Argon/2 (488) and Diode405-30 lasers for the detection of FITC and DAPI, respectively. Cell area was then measured using ImageJ region of interest (ROI) manager and the average cell area was determined for each condition.

2.5.7.3 Treatment with Ang-(1-7)

As per the pre-established model of H9c2 cardiomyocyte hypertrophy (Flores-Muñoz et al., 2011), where stated, cells were pre-treated with 100 nM Ang-(1-7) (Phoenix Pharmaceuticals, CA, USA) 15 minutes before treatment with 100 nM Ang II as a control for the inhibition of Ang II-induced cellular hypertrophy. This model and protocol were used as the control for hypertrophy when testing EVs as possible inducers or inhibitors of hypertrophy.

2.5.7.4 Treatment with FAM-labelled Ang II

Where stated, 100 nM FAM-labelled Ang II (Cambridge Biosciences, Cambridge, UK) was used in place of unlabelled Ang II in the established model of hypertrophy as a control or while determining co-localisation of the peptide with PKH26-labelled EVs where parental cells were treated with 1 µM FAM-labelled Ang II.

2.5.7.5 Treatment with losartan and PD123,319

As per the pre-established model of H9c2 cardiomyocyte hypertrophy (Flores-Muñoz et al., 2011) where stated, cells were pre-treated with 10 µM losartan (AT_1R antagonist (Timmermans et al., 1993); Sigma Aldrich, Irvine, UK) or 10 µM PD123,319 (AT_2R antagonist (Timmermans et al., 1993); Sigma Aldrich, Irvine, UK) 30 minutes prior to treatment with 100 nM Ang II as a control for the possible abolishment of Ang II-induced hypertrophy via antagonising the AT_1R or

AT_2R. This model and protocol were used as controls when testing EV involvement with the AT_1R and AT_2R and induction of cellular hypertrophy.

2.5.8 Collection of conditioned culture medium

Parental H9c2 cells were cultured in vented T-150 cm^2 culture flasks to 70% confluence. NRCF were cultured to 100% confluence. Cells were treated with 1 µM Ang II or 1 µM Ang-(1-7) in serum-free media (supplemented only with 2 mM L-glutamine and 100 IU/mL penicillin, 100 µg/mL streptomycin) over a 48 hr period before conditioned culture media was collected and stored at 4ºC for up to two weeks. Where appropriate and stated, parental H9c2 cells were pre-treated with 10 µM losartan or 10 µM PD123,319 30 minutes prior to treatment with 1 µM Ang II, or where stated, 1 µM FAM-labelled Ang II.

2.6 Isolation of extracellular vesicles from conditioned culture medium

A workflow of an altered EV isolation procedure previously described (Théry et al., 2006) is outlined (Figure 2-1). The conditioned media removed from parental cells was subjected to centrifugation at 500g for 5 minutes to remove cell debris and then passed through a 0.22 µm sterile syringe filter to remove any further large particles >220nm in size. The media was transferred to Ultra-Clear, open-top thin-walled 16 x 102 mm ultracentrifuge tubes (Beckman Coulter, High Wycombe, UK) then underwent ultracentrifugation using a Beckman Coulter L-80XP ultracentrifuge with SW 32.1 Ti swinging-bucket rotor (Beckman Coulter, High Wycombe, UK) at 100,000g at 4ºC for 90 minutes. The supernatant was discarded and the pellet resuspended in 1 mL ice-cold 1x PBS. The tubes were then filled completely with PBS and the ultracentrifugation step was then repeated with EVs centrifuged in PBS at 100,000g at 4ºC for 90 minutes. Supernatant was discarded and the final pellet was resuspended in 100 µL PBS and EVs were stored at 4ºC for up to two weeks or -80ºC long term.

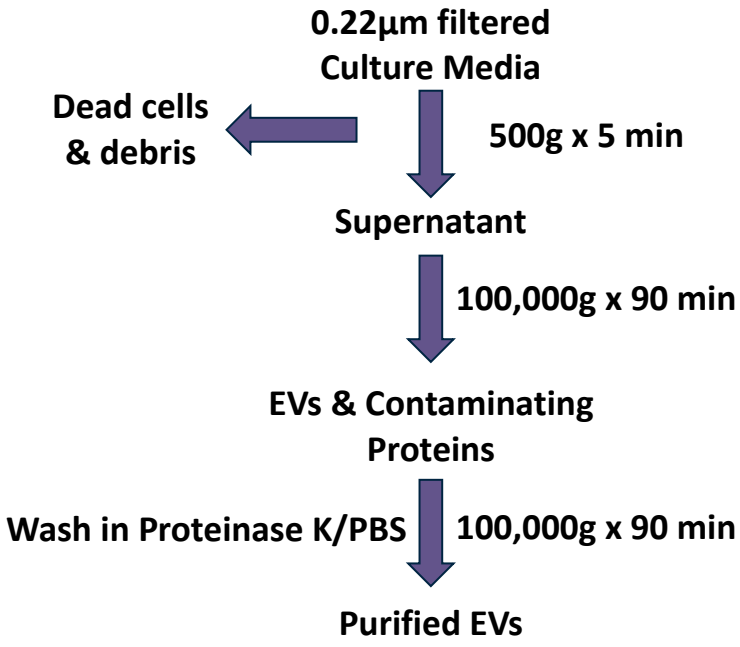

Figure 2-1 Workflow for extracellular vesicle isolation by ultracentrifugation. Culture media was passed through a 0.22 um filter to remove large particles before centrifugation at 500g for 5 min to pellet any further cell debris. Supernatant was then centrifuged at 100,000g for 90 min and the pellet treated with proteinase K before a repeat spin. Purified EVs were collected in PBS after the second spin (protocol information obtained from Thery et al., 2006 altered to include initial filtering of large particles).

2.6.1 Proteinase K treatment

To remove any excess peptide or contaminating proteins pelleted with EVs during ultracentrifugation, samples were treated with proteinase K. Proteinase K is a serine protease able to cleave a wide variety of proteins (Hilz et al., 1975) and in this case allows for the breakdown of proteins out with the vesicles while those contained within the vesicle membrane remain intact. Treatment with proteinase K was carried out after the first ultracentrifugation step where the EV pellet was resuspended in 500 µg/mL proteinase K (Sigma Aldrich, Irvine, UK) and incubated at 37ºC for 1 hr. Proteinase K was then inactivated by incubation in a heated water bath at 60ºC for 10 minutes. The ultracentrifugation protocol was then continued as described above.

2.6.2 PKH26-labelling of extracellular vesicles

EVs derived from H9c2 cardiomyocytes either pre-treated with 1 µM Ang II or control untreated were fluorescently labelled using the PKH26 Red Fluorescent Cell Linker Kit (Sigma Aldrich, Irvine, UK). Where appropriate and stated, 1 µM FAM-labelled Ang II was used to replace unlabelled Ang II. Briefly, previously isolated EVs were re-purified by ultracentrifugation at 100,000g for 90 minutes at 4ºC to remove the PBS suspension. The re-purified EV pellet (approximately 300 µg/mL EVs) was resuspended in 2.5 mL Diluent C while 10 µL PKH26 stain was added to a separate 2.5 mL Diluent C. Both suspensions were mixed together and incubated at room temperature for 5 minutes. The reaction was stopped by adding an equal volume of 5% BSA/PBS (Sigma Aldrich, Irvine, UK) for 1 minute at room temperature. Labelled EVs were then purified by ultracentrifugation at 100,000g for 90 minutes at 4ºC. The pellet was resuspended in 1 mL PBS and EVs underwent a second ultracentrifugation at 100,000g for 90 minutes at 4ºC. The final labelled EV pellet was resuspended in 250 µL PBS and stored at 4ºC for up to two weeks, or -80ºC long term.

2.7 Analysis of extracellular vesicles

EVs isolated from the conditioned culture media of H9c2 cardiomyocytes and NRCF were analysed and characterised via a set of gold standard methods

suggested by the International Society for Extracellular Vesicles (Van Deun et al., 2017).

2.7.1 Analysis of extracellular vesicles by Nanosight

Nanoparticle Tracking Analysis (NTA) by NanoSight (Malvern NanoSight LM10) measures the Brownian motion of particles in solution via light-scattering (Vestad et al., 2017). The system employs a focussed laser beam which is passed through a liquid sample allowing for illumination of the particles within that sample. The particles may be visualised microscopically utilizing the conventional microscope attached to the system with 20x magnification objective. The microscope is connected to a camera that allows for the capture of a video at 30 frames per second. Using the NTA software, particles in each frame of a 60 second video are tracked individually and simultaneously over time to allow generation of an average particle size distribution and concentration in the liquid sample. EVs isolated from conditioned culture media or serum were quantified by NTA. Briefly, 10 µL of isolated EV sample was diluted to 1:100 in 1 mL 1x PBS and loaded into the sample chamber of an LM10 NanoSight unit connected to an Andor DL-658-OEM-630 camera (Malvern Instruments, Malvern, UK) using a 1 mL syringe. Videos of 60 seconds in length were recorded in quintuplicate for each sample (across 5 different fields of view). Videos were then analysed using the accompanying NanoSight NTA 3.1 software set to detect particles between 0-1000 nm, and the gain and detection threshold adjusted accordingly to detect all particles in the field of view. Average particle size and concentration distribution plots were provided and the determined concentration was later adjusted for sample dilution.

2.7.2 Analysis of extracellular vesicles by transmission electron microscopy

Transmission electron microscopy (TEM) was performed by the Chemistry Department in the College of Science and Engineering, University of Glasgow, UK as described previously (Théry et al., 2006). Images were then provided for later analysis by Image J. Briefly, EVs were mixed with equal volumes of 4% paraformaldehyde. Next, 5 µL resuspended EVs were deposited onto Formvar-carbon coated EM grids and membranes were left to absorb for 20 min. Grids

were washed in 100 µL PBS droplets on parafilm before being transferred to 50 µL droplets of 1% glutaraldehyde for 5 min. Finally, grids were washed in 100 µL droplets of distilled water and incubated at room temperature for 2 min, this wash step was repeated 7 times. Multiple images of groups of EVs were generated for each condition and EVs were sized in length using the ImageJ straight line tool to compare average EV size across cell types and conditions.

2.7.3 Analysis of extracellular vesicles by western immunoblot

EVs isolated from H9c2 cardiomyocytes were analysed by western immunoblot for the detection of specific extracellular vesicle-related protein markers; CD31, TSG-101 and HSP-70. H9c2 cell lysates were used as a control for the presence of the markers.

2.7.3.1 Preparation of H9c2 cell lysates and protein extraction

Protein was extracted from H9c2 cell lysates to be used as a control for western immunoblotting of proteins associated with H9c2-derived EVs. Briefly, media was removed from cells and cells were washed once with ice cold sterile 1x PBS. Next, 500µL of western lysis buffer (section 2.4) was added per well of cells in a 6 well plate and cells were scraped off into the western lysis buffer using a plastic cell scraper (VWR International, Leicestershire, UK) and collected in a 1.5 mL Eppendorf tube. Cell lysates were placed on a rotator wheel and left spinning gently at 4ºC for 45 minutes. Lysates were then subjected to centrifugation at 13,000g for 10 minutes at 4ºC. The supernatant containing the proteins was removed and stored at -80ºC until use while the pellet was discarded.

2.7.3.2 Preparation of lysed extracellular vesicles

EV preparations isolated from H9c2 cardiomyocytes were lysed using western lysis buffer. EV samples were treated with 0.2x volumes of western lysis buffer, vortexed for 10 seconds and incubated on ice for 15 minutes. The samples were then vortexed a second time for 10 seconds and stored on ice until determination of protein concentration.

2.7.3.3 Determination of protein concentration

Protein concentration in H9c2 cell lysates and H9c2-derived EVs was determined by Bicinchoninic Acid (BCA) assay with the BCA Protein Assay Kit (Pierce, Illinois, USA) using colorimetric detection and quantification following the manufacturer's protocol. Briefly, a standard curve was generated using BSA (Pierce, Illinois, USA) serial dilutions (detailed Table 2-5). Next, 200 µL of working reagent was added to 25 µL of standard or sample in triplicate in a 96 well culture plate and incubated in the dark for 30 minutes at 37ºC. The plate was then analysed using a Victor X3 plate reader (Perkin Elmer, Massachusetts, USA) at 560 nm wavelength using the Perkin Elmer 2030 Workstation software. Results were then calculated according to the linear equation based on the standard curve generated.

Table 2-5 Standards for BCA protein assay

Standard	BSA concentration (µg/mL)
A	2000
B	1500
C	1000
D	750
E	500
F	250
G	125
H	25
I	0 = blank

2.7.3.4 SDS-polyacrylamide gel electrophoresis

Sodium dodecyl sulphate polyacrylamide gel electrophoresis (SDS-PAGE) and western blotting were used to detect specific proteins associated with EVs. Samples lysed in western lysis buffer were prepared at the appropriate concentration in 4x loading buffer containing 10% weight/volume (w/v) SDS, 30% (v/v) glycerol, 10% (v/v) Tris-HCl pH 6.8, 0.01% (w/v) bromophenol blue and 2% (v/v) ß-mercaptoethanol. Samples were heated to 95ºC for 5 minutes to denature proteins before being loaded into the wells. Samples were loaded into

NuPAGE 4-12% Bis-Tris Midi Protein 12+2-well gels (Thermo Fisher, Paisley, UK) and electrophoresed at 140V for 1.5 hr.

2.7.3.5 Electrophoretic transfer of proteins from gel to membrane

Protein was transferred to Hybond-P polyvinylidene difluoride membrane (Amersham Bioscience UK Limited, Buckingham, UK) at 200 mA for 2 hr in transfer buffer (0.025 M Tris, 0.2 M glycine, 20% (v/v) methanol, 0.01 M SDS) at 4ºC. The membrane was then blocked in 1:1 1xTBS-Tween/Seablock blocking buffer (Thermo Fisher, Paisley, UK) for 1 hr at room temperature before antibody detection was carried out.

2.7.3.6 Primary and secondary antibody detection

The membrane was incubated with the primary antibody diluted in blocking buffer at the manufacturer's recommended dilution overnight at 4ºC with shaking. Following primary antibody incubation, the membrane was washed three times with 1xTBS-Tween for 5 minutes with shaking at room temperature. This was followed by incubation with the appropriate LI-COR fluorescence secondary antibody (LI-COR Biosciences, Nebraska, USA) at the manufacturer's recommended dilution in blocking buffer for 1 hr at room temperature in the dark with shaking. The membrane was then washed three times with 1xTBS-Tween for 5 minutes with shaking at room temperature before being imaged on the LI-COR Odyssey CLx Imaging System (LI-COR Biosciences, Nebraska, USA). Images were optimised and analysed using the Image Studio Lite v5.2 software (LI-COR Biosciences, Nebraska, USA).

2.7.3.7 Stripping of nitrocellulose membranes

Blots were stripped by incubation with sodium hydroxide. Briefly, two sodium hydroxide pellets (Sigma Aldrich, Irvine, UK) were fully dissolved in 50 mL dH_2O. The sodium hydroxide solution was added to the blot and incubated at room temperature for 20 minutes with shaking before being washed twice with 1x PBS. Blots could then be blocked again in blocking buffer before re-probing with a second set of primary and secondary antibodies.

2.8 Gene expression analysis

Gene expression analysis was performed on H9c2 cardiomyocytes treated under specified experimental conditions to determine changes in expression of genes involved in the renin-angiotensin system; AT_1R, AT_2R and Mas1 as well as changes in the hypertrophy marker gene, brain natriuretic peptide (BNP) (Majalahti et al., 2007).

2.8.1 Preparation of cells for gene expression analysis

Cells were seeded at a density of $1x10^5$ per well into 6-well culture plates and treated appropriately under different experimental conditions over a 48 hr period. RNA was extracted using the miRNeasy Minikit (Qiagen, West Sussex, UK) according to the manufacturer's protocol. First, cells were lysed and homogenized in QIAzol lysis reagent (Qiagen, West Sussex, UK). Lysed cells could then be stored long term at -80ºC until RNA isolation was carried out.

2.8.2 RNA isolation

Homogenates frozen in QIAzol lysis reagent were thawed at room temperature and once completely thawed, incubated for a further 5 minutes at room temperature. Next, 140 µL chloroform (Sigma Aldrich, Irvine, UK) was added to the homogenate, shaken for 15 seconds and incubated at room temperature for 3 minutes. The homogenate was centrifuged at 12,000g for 15 minutes at 4ºC and the upper aqueous phase was transferred to a new collection tube with 1.5x volumes of 100% ethanol (Sigma Aldrich, Irvine, UK) and mixed thoroughly by pipetting. Subsequently, 700µL of sample was transferred to a RNeasy Mini spin column with collection tube and centrifuged at 8000g for 15 seconds at room temperature, flow through was then discarded. This step was repeated using 700 µL of Buffer RWT (Qiagen, West Sussex, UK), flow through was discarded and the step repeated again using 500 µL of Buffer RPE (Qiagen, West Sussex, UK). Flow through was discarded again and 500 µL of Buffer RPE was added and subjected to centrifugation at 8000g for 2 minutes. The RNeasy Mini spin column was transferred to a new collection tube and 50 µL of RNase-free water (Qiagen, West Sussex, UK) was added directly onto the spin column membrane. RNA was eluted by centrifugation at 8000g for 1 minute.

2.8.2.1 On-column DNase digest

Where appropriate, an on-column DNase digest was carried out during RNA isolation. RNase-free DNase (Qiagen, West Sussex, UK) treatment was carried out on RNA isolation samples to remove any contaminating DNA. Following the manufacturer's instructions, 350 µL of Buffer RWT was added to the spin column and subjected to centrifugation at 8000g for 15 seconds. Flow through was discarded; 10 µL DNase I stock solution with 70µL Buffer RDD (Qiagen, West Sussex, UK) was added to the column and incubated at room temperature for 15 minutes. Finally, 350 µL Buffer RWT was added to the column before centrifugation at 8000g for 15 seconds and then the flow through was discarded.

2.8.3 Determination of RNA concentration by Nanodrop

The RNA concentration in an isolated sample was quantified using a Nanodrop 1000 Spectrophotometer (ThermoFisher Scientific, Paisley, UK) which allows for the measurement of nucleic acid concentration in a sample volume of 1 µL (giving sample concentration in ng/µL). First, 1 µL of sample is applied to the pedestal area of the system which then forms a liquid column once the upper arm is lowered onto the sample. A xenon light then pulses a 260nm wavelength light through the liquid sample and the absorption is measured by the CCD detector in the bottom of the system. The concentration of the sample is then calculated by the system using a modified Beer-Lambert equation:

$$c = (A * \varepsilon)/b$$

where c is the nucleic acid concentration in ng/µL, A is the absorbance in absorbance units (AU) measured at 260 nm, ε is the wavelength-dependent extinction coefficient in ng-cm/µL and b is the path length in cm. For RNA, the wavelength-dependent extinction coefficient is 40ng-cm/µL and the path length is specific to the spectrophotometer used, in this case 0.2 mm and 1 mm for the Nanodrop 1000. RNA absorbs at 260 nm but not at 280 nm, and as a result the 260/280 ratio was used to determine the purity of the RNA samples, where a ratio of 1.8-2.2 was considered pure.

2.8.4 Synthesis of cDNA

After RNA quantification, cDNA was synthesised from the purified RNA samples by reverse transcription. mRNA isolated from cells was reverse transcribed into complementary DNA (cDNA) using the Reverse Transcription Kit (Applied Biosystems, Warrington, UK) according to the manufacturer's instructions. Next, 750 ng mRNA was reverse transcribed in a 40 µL total reaction unless otherwise stated. Cycling conditions were as follow: 25ºC for 10 minutes for pre-annealing, 48ºC for 30 minutes to enable reverse transcription and 95ºC for 5 minutes for reverse transcription inactivation. cDNA was then stored at -20ºC until used in qPCR procedures.

2.8.5 qPCR and analysis

QPCR was carried out in a 384-well PCR plate (ThermoFisher Scientific, Paisley, UK) in simplex using a 10 µL total reaction including 2x Taqman Gene Expression Mastermix (Applied Biosystems, Warrington, UK), FAM/VIC labelled probes (Thermo Fisher, Paisley, UK), RNase-free water (Qiagen, West Sussex, UK) and cDNA. The plate was sealed with an optical adhesive lid (ThermoFisher Scientific, Paisley, UK) and the thermal profile was as follows: 95ºC for 10 minutes followed by 40 cycles of 95ºC for 15 seconds and 60ºC for 1 minute. The plate was read using a QuantStudio 12K Flex Taqman machine (Applied Biosystems, Warrington, UK) with software v1.2.2 and data were collected when PCR amplification was in the exponential phase, which was subsequently analysed using the ΔΔCt method (Livak and Schmittgen, 2001) utilising Microsoft excel. The cycle threshold (Ct) of a sample is defined as the number of amplification cycles required for the fluorescence dye emissions to reach a specific threshold, specified by the manufacturer. In this case, Ct values of $\geq$36 were removed. The difference between the Ct value for the gene of interest and the Ct value of the housekeeper gene was then calculated (the value known as the ΔCt) to normalise the data. The mean ΔCt of the technical replicates was then calculated, followed by the mean ΔCt across biological replicates. The ΔΔCt is then calculated using the following equation:

$$\Delta\Delta Ct = \Delta Ct \text{ (treated samples)} - \Delta Ct \text{ (control samples)}$$

The fold change in mRNA expression between two groups, referred to as the relative quantification (RQ) was then calculated using the following equation:

$$RQ = 2^{-\Delta\Delta Ct}$$

The RQ of a specific mRNA is always given relative to the expression of the control group, where its expression is given as 1.

2.9 Isolation of extracellular vesicles from serum

EVs were isolated from animal (samples collected in accordance with the Animal Scientific Procedures Act [1986] and licensed by the UK Home Office [under the project licence held by Dr Delyth Graham, PPL 70/9021]) or human serum samples using the Invitrogen Total Exosome Isolation Kit (Thermo Fisher Scientific, Paisley, UK). Briefly, serum samples first underwent centrifugation at 2000g for 30 minutes to remove cells and debris. Next, 500 µL of serum supernatant was transferred to a new collection tube and mixed with 0.2 volumes of Total Exosome Isolation reagent (Thermo Fisher Scientific, Paisley, UK) by vortexing and incubated at 4ºC for 30 minutes. Samples then underwent centrifugation at 10,000g for 10 minutes at room temperature to pellet EVs. Supernatant was discarded and the EV pellet was resuspended in 250 µL PBS. EVs were stored at 4ºC short term and -80ºC long term.

2.10 Exogenous loading of extracellular vesicles via electroporation

EVs were electroporated using Sterile Red Cap Electroporation Cuvettes (Geneflow, Staffordshire, UK) with a Bio-Rad Micropulser (Bio-Rad Laboratories, California, USA). Briefly, EVs were diluted in 50 mM Trehalose/PBS (Sigma Aldrich, Irvine, UK) to 0.56 µg/µL. Soluble Ang II (Sigma Aldrich, Irvine, UK) or Ang-(1-7) peptide (Phoenix Pharmaceuticals, CA, USA) was also diluted to 0.56 µg/µL in 50mM Trehalose/PBS (equal volumes of untreated 50 mM Trehalose/PBS were used for the control naïve electroporation). The diluted EVs and diluted peptide were combined and incubated on ice for 45 minutes. Next, 125 µL of the mix was added to a cuvette (chilled at 4ºC overnight) and electroporated with a 15 ms pulse at 400 mV. Subsequently, 875 µL of ice cold 1% BSA (Sigma Aldrich,

Irvine, UK) was added immediately to the cuvette and mixed by pipetting; the total volume was transferred to a centrifuge tube on ice. The cuvette was discarded and the procedure was repeated until the full volume of EVs had been electroporated. Electroporated samples were then left to recover for 24 hr before re-purification in order to prevent proteinase K from entering the EVs and causing death of recipient cells in later experiments (Figure 2-2). Total electroporated samples underwent ultracentrifugation at 100,000g for 90 minutes at 4ºC. The supernatant was discarded and the pellet resuspended in 500 µg/mL proteinase K/PBS (Sigma Aldrich, Irvine, UK) and incubated at 37ºC for 1 hr, followed by inactivation at 60ºC for 10 minutes. The ultracentrifugation step was then repeated where proteinase K treated EVs were centrifuged in PBS for a second time at 100,000g for 90 minutes at 4ºC. The final pellet was resuspended in 100 µL PBS and electroporated EVs were stored at -80ºC.

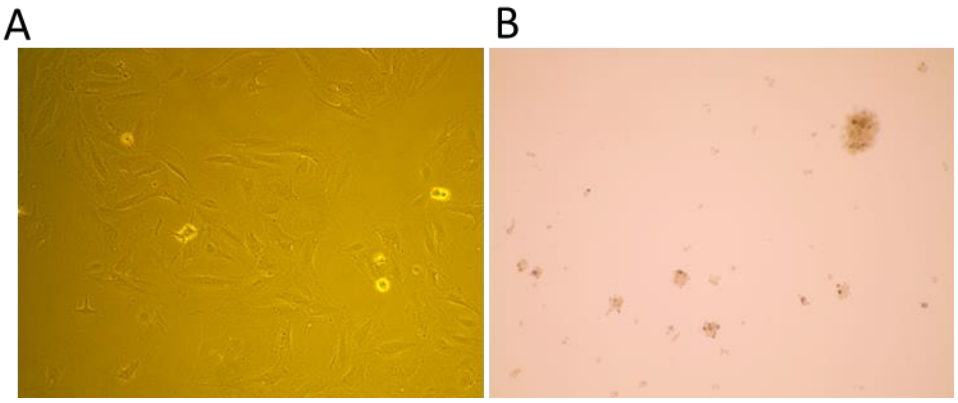

Figure 2-2 Live imaging of H9c2 cells by light microscopy after treatment with electroporated EVs. (A) Recipient H9c2 cells treated with electroporated EVs which underwent a 24 hr recovery period before re-purification and proteinase K treatment. (B) Recipient H9c2 cells treated with electroporated EVs which were not allowed to recover before re-purification and proteinase K treatment, resulting in EV-mediated delivery of proteinase K to the recipient cells.

2.11 Detection of Ang II within extracellular vesicles by ELISA

Ang II content of endogenously and exogenously loaded EVs was determined using an Ang II EIA-Kit (Bertin Pharma, Bordeaux, France) according to the manufacturer's protocol. Firstly, EV samples were lysed using western lysis buffer. 0.2 volumes of western lysis buffer was added to each EV sample, vortexed for 10 seconds and incubated on ice for 15 minutes before vortexing for a further 10 seconds. Samples were then briefly sonicated (5 second pulse at 20 Hz) before carrying out the ELISA. Briefly, 8 standards were prepared by serial dilution ranging from 0.98-125 pg/mL (detailed in Table 2-6) and 100 µL of each standard and purified lysed EVs were added to the pre-coated anti-Angiotensin II IgG plate in duplicate. Untreated wells served as negative controls while a quality control of known Ang II concentration (15 pg/mL) supplied with the assay served as positive control. The plate was incubated for 1 hr at room temperature with gentle shaking. Glutaraldehyde [0.5 % (v/v)] was prepared by the addition of 100 µL glutaraldehyde to 1x manufacturer's wash buffer and 50 µL of glutaraldehyde was added to each well and incubated with gentle agitation for 5 minutes. The glutaraldehyde was then neutralised with borane trimethylamine which was reconstituted in 5 mL 2 N HCl/Methanol (50/50, v/v), 50 µL was added to each well and incubated for 5 minutes with gentle shaking to inactivate the glutaraldehyde. The plate was washed five times with manufacturer's wash buffer and 100 µL anti-Angiotensin II IgG Tracer was added to each well. The plate was sealed and incubated overnight at 4ºC with shaking. The anti-Angiotensin II IgG Tracer was then removed and the plate was washed 5x prior to a 10 min incubation in 300 µL manufacturer's wash buffer. The plate was then washed a further five times. The plate was then developed by the addition of 200 µL Ellman's Reagent to each well and incubated at room temperature for 30 minutes in the dark with gentle agitation to allow for colour development. The absorbance was then measured at 405 nm using a Victor X3 plate reader with the Perkin Elmer 2030 Workstation software (Perkin Elmer, Massachusetts, USA). For the determination of sample concentration, the blanking value (Ellman's reagent only) was subtracted from all measurements and a standard curve with origin at x = 0 and a linear trendline was plotted. Using the linear equation, sample

concentration was calculated. For samples with a negative concentration (below the detection limit of the ELISA) as determined from the standard curve, Ang II concentration was assumed to be 0 pg/mL.

Table 2-6 Ang II standards for ELISA

Standard	Volume of Standard (µL)	Volume of Assay Buffer Diluent (µL)	Standard Concentration (pg/mL)
S1	1000	0	125
S2	500	500	62.5
S3	500	500	31.25
S4	500	500	15.63
S5	500	500	7.81
S6	500	500	3.91
S7	500	500	1.95
S8	500	500	0.98

2.12 Detection of Ang-(1-7) within extracellular vesicles by ELISA

Ang-(1-7) content of exogenously loaded EVs was determined using an Ang-(1-7) ELISA kit (Aviva Systems Biology, San Diego, California) according to the manufacturer's protocol. Firstly, EV samples were lysed using western lysis buffer. Next, 0.2 volumes of western lysis buffer was added to each EV sample, vortexed for 10 seconds and incubated on ice for 15 minutes before vortexing for a further 10 seconds. Samples were then briefly sonicated (5 second pulse at 20 Hz) before carrying out the ELISA. Briefly, 8 standards were prepared by serial dilution ranging from 7.8-500 pg/mL (detailed Table 2-7) and 50 µL of each standard and sample were added to the pre-coated anti-Angiotensin-(1-7) IgG microplate in duplicate. This was immediately followed by adding 50 µL 1X Angiotensin-(1-7)-Biotin Complex to each well (excluding absolute blanks) and incubated at 37ºC for 1 hr. The plate was washed three times with 200 µL of the manufacturer's 1X Wash Buffer before the addition of 100 µL 1X Avidin-HRP Conjugate to each well. The plate was then incubated for 45 minutes at 37ºC. The plate was washed a further three times with 200 µL 1X Wash Buffer before the addition of 90 µL TMB Substrate to each well. The plate was then incubated

at 37ºC for 30 minutes to allow for colour development. Next, 50 µL manufacturer's Stop Solution was added to each well to end the reaction. Absorbance was measured immediately at 450 nm using a Victor X3 plate reader and Perkin Elmer 2030 Workstation software (Perkin Elmer, Massachusetts, USA). For the determination of sample concentration, the blanking value (TMB substrate and Stop Solution only) was subtracted from all measurements which were then log-transformed and a standard curve with origin at x = 0 and a linear trendline was plotted. Using the linear equation, sample concentration was calculated. For samples with a negative concentration (below the detection limit of the ELISA) as determined from the standard curve, Ang-(1-7) concentration was assumed to be 0 pg/mL.

Table 2-7 Ang-(1-7) standards for ELISA

Standard	Standard to dilute	Volume of standard to dilute (µL)	Volume of diluent added (µL)	Final concentration (pg/mL)
1	500pg/mL	300	0	500
2	500pg/mL	300	300	250
3	250pg/mL	300	300	125
4	125pg/mL	300	300	62.5
5	62.5pg/mL	300	300	31.2
6	31.2pg/mL	300	300	15.6
7	15.6pg/mL	300	300	7.8
8	Blank	0	300	0.0 (Blank)

2.13 Rat model of Ang II infusion

All surgical procedures were performed in accordance with the Animal Scientific Procedures Act (1986) and licensed by the UK Home Office (under the project licence held by Dr Delyth Graham, PPL 70/9021). Male WKY rats were purchased from Envigo (Huntingdon, UK) at 10 weeks of age and housed in controlled 12 hr light/dark conditions with constant temperature (21±3˚C) with *ad libitum* access to water and standard diet (rat and mouse No. 1 maintenance diet, Special Diet Services). It was determined that a dose of 200 ng/kg/min Ang II infusion would be enough to exhibit a pressor effect in adult rats over a 14 day period (Kim-Mitsuyama et al., 2005, Osada-Oka et al., 2016) without any immediate lethal

effects. Power calculations were performed using Minitab 19 statistical software and determined that 8 animals per group would allow 80% power at $\alpha = 0.05$ to detect a difference in blood pressure readings of 25 mmHg between control and Ang II infused WKY rats (details described further in section 2.16.1).

2.13.1 Osmotic minipump preparation

Animals were randomly assigned in a blinded manner to treatment groups involving vehicle or 200 ng/kg/min Ang II infusion and weighed prior to preparation to ensure correct dosage calculations. To deliver Ang II under continuous infusion over a 14 day period, subcutaneously implanted Alzet model 2002 osmotic minipumps (Charles River, Tranent, UK) were used. The minipumps had a continuous flow rate of 0.47 µL/hr for 14 days, however after this time flow rate is unreliable (as stated in manufacturer's instructions). Preparations of Ang II solutions and minipumps were carried out under sterile conditions with sterile latex gloves worn at all times while handling the minipumps. A stock solution of 50 µg/µL Ang II was prepared using sterile RNase free H_2O. The minipumps used have a maximum reservoir volume of 200 µL and so to achieve complete filling of the minipump, Ang II stock was diluted to this volume in sterile RNase free H_2O. The dilution was calculated based on average animal weight and flow rate of the minipump to achieve the required dose of 200 ng/kg/min.

The minipump and flow moderator were removed from packaging under sterile conditions and placed in a sterile 5 mL container of known weight, the weight of the empty minipump was then recorded. A sterile blunt-tipped needle used as a filling tube (Charles River, Tranent, UK) was attached to a 1 mL syringe and used to carefully fill the minipump reservoir with 200 µL of appropriately diluted Ang II solution (or vehicle) by inserting the filling tube into the reservoir and slowly expelling the solution in an upright position ensuring no air bubbles. The flow moderator was then inserted into the reservoir and any excess solution wiped away. The minipumps were returned to the same sterile 5 mL container and re-weighed to give an indication of the volume of solution within the pump by comparing to the pre-weight. Filled minipumps were primed overnight at room temperature in a 0.9% sterile saline solution to ensure that upon implantation, delivery of Ang II begins immediately at the correct flow rate.

2.13.2 Anaesthetic procedure

Rats were anaesthetised where appropriate for surgical procedures and echocardiography using an induction box filled with 5% isoflurane in 1.5 L/min medical oxygen. Once anaesthetised, rats where placed in either the supine or prone position with nose and mouth inserted and secured in an anaesthetic mask. All rats were checked to be fully under anaesthesia before beginning any surgical procedures and isoflurane levels were adjusted depending on the procedure carried out.

2.13.3 Osmotic minipump implantation surgery

Minipump implantation surgery was carried out under sterile conditions with sterile surgical drapes covering the operating table and sterile gowns and gloves worn at all times. Surgical instruments were autoclaved prior to use. Animals were first anaesthetised with 5% isoflurane in 1.5 L/min oxygen and once fully unconscious, maintained at 2.5% isoflurane in 1.5 L/min oxygen. Rats were given 5 mg/kg Rymadil analgesic subcutaneously prior to beginning surgery. The surgery was carried out with animals in the prone position, where the animal was shaved between the shoulder blades and swabbed with povidone-iodine solution (Betadine®). Surgical scissors were used to create a superficial incision of approximately 2-3 cm in length in the skin, parallel to the shoulder blade. The skin was parted from the underlying muscular layer by gently opening and closing scissors within the incision to produce a subcutaneous pocket. The pocket was held open and the minipump removed from the saline solution using forceps and inserted subcutaneously with the flow moderator distal to the incision area. The incision was sutured using 4-0 gauge VICRYL RAPIDE® Ethicon sutures (NU-CARE, Bedfordshire, UK). Rats were placed in clean cages after surgery with well-being checked daily until sacrifice.

2.13.4 Femoral vein injection

Rats had previously been randomly assigned treatment groups; vehicle + PBS injection, 200 ng/kg/min Ang II + PBS injection, 200 ng/kg/min Ang II + naïve EV injection, and 200 ng/kg/min Ang II + Ang-(1-7) EV injection. EVs were prepared and loaded via electroporation as described in section 2.10 and diluted appropriately in sterile PBS. A dose of 30 µg EVs was administered to animals via

femoral vein injection under the same anaesthetic as minipump implantation, immediately after implantation. A second dose of 30 µg EVs was administered 7 days post-implantation into the femoral vein of the opposite leg. Animals were maintained under anaesthesia at 2.5% isoflurane in 1.5 L/min oxygen and the surgery was carried out in the supine position. The hind leg was extended and secured. The inner thigh was shaved and skin gently pulled up with forceps, a scalpel was used to create a small incision of approximately 1 cm in length in the skin directly above the femoral vein, running parallel to the vein. A sterile single-use hypodermic 1 mL insulin syringe with 28 gauge needle (BD Medical Technology, New Jersey, USA) was used to administer 30 µg EVs in a volume of 200 µL directly into the femoral vein. The incision was sutured using 4-0 gauge VICRYL RAPIDE® Ethicon sutures (NU-CARE, Bedfordshire, UK). Rats were placed in clean cages after surgery with well-being checked daily until sacrifice.

2.13.5 Tail cuff plethysmography

Tail cuff plethysmography was carried out using a Visitech BP-2000 Series II Blood Pressure Analysis System (Visitech Systems, North Carolina, USA). Blood pressure measurements were taken at day 0 and day 13 to provide start and end-point measurements for the study. Prior to obtaining the day 0 blood pressure reading, animals were trained and acclimatised to the machine system in order to reduce variability and improve result reproducibility. To obtain measurements, the system was pre-heated to 37ºC and assessed for leaks in pressure cuffs before animals were placed into a restraining chamber on the pre-heated surface to maintain body temperature, and the tail was fed through a cuff positioned at the proximal end of the chamber and secured. Four animals were measured in parallel with the system configured to carry out 10 preliminary recordings followed by 15 real recordings which would be used to obtain average systolic blood pressure values. The upper pressure limit was set to 230 mmHg with the standard time between measurements set at 2.5 seconds. Programmed statistical analysis allowed for the automatic removal of outliers due to such issues as excessive movement during a reading.

2.13.6 Transthoracic echocardiography

All echocardiography was performed and analysed by Dr Tamara Martin who remained blinded throughout the duration of the study. Echocardiography was performed at day 0 prior to any surgical procedures, and again at day 12 (representative of end-point echocardiography). Echocardiography was performed using an Acuson Sequoia c512 ultrasound system with a linear array transducer at a frequency of 15 MHz. Rats were fully anaesthetised and then maintained at 1.5% isoflurane in 1.5 L/min oxygen. Hair was removed from the chest using an electric shaver and the rats were placed in the supine position, with slight rotation onto their right side. Ultrasound gel pre-warmed to room temperature was applied to both the transducer and animal skin. The heart was imaged along the long-axis which provides visualisation of the left atrium and left ventricle and M-mode measurements were recorded for 6 cardiac cycles, repeated 3-4 times. Analysis of echocardiograph images was carried out using Image J software where distanced between waveform peaks and troughs were measured. These measures were used to calculate % fractional shortening via a defined formula:

$$\boldsymbol{Fractional\ shortening}\ (\%) = \frac{(\boldsymbol{EDD - ESD})}{\boldsymbol{EDD}}\ \boldsymbol{x\ 100}$$

EDD = End diastolic diameter

ESD = End systolic diameter

2.13.7 Humane killing procedure

Rats were fully anaesthetised at 5% isoflurane in 1.5 L/min medical oxygen and euthanised by cardiac puncture at 14 days Ang II/vehicle infusion. The thoracic cavity was exposed by making a transverse incision and the rib cage cut on either side to expose the beating heart. A 21-gauge needle attached to a 5 mL syringe was inserted into the apex of the heart through the left ventricle and 4-5 mL blood was slowly removed to prevent collapse of the heart.

Blood collected was transferred to heparin coated BD Vacutainer tubes (BD Medical Technologies, New Jersey, USA) or normal Eppendorf tubes to allow for later plasma isolation and serum isolation, respectively.

2.13.8 Serum and plasma isolation from blood

Blood was collected in heparin coated tubes following sacrifice for plasma isolation, or normal Eppendorf tubes for serum isolation. Plasma and serum were isolated by centrifugation of the blood at 2000g for 10 minutes at 4°C. Plasma and serum samples were then aliquoted and stored at -80°C.

2.13.9 Tissue collection

After sacrifice by cardiac puncture, the heart, aorta, liver, lung, kidneys, spleen and brain tissues were collected along with samples of adipose and skeletal muscle. Tissues were gently blotted clean on absorbent paper towel to remove any excess blood and whole organ weights were recorded. The heart was then processed to remove the right atria and ventricle, and the left ventricle was weighed before being cut in half transversely. The lower apex was placed in 4% PFA for histological analysis while the upper half was snap frozen in liquid nitrogen for future use in gene expression analysis. The aorta and spleen were both cut in half transversely with one half stored in 4% PFA and the other snap frozen. Renal fascia was removed and each kidney was cut in half and stored similarly. The brain was cut in half along the sagittal plane with one half stored in 4% PFA and the other snap frozen. Small portions of liver and lung were taken to be both fixed and snap frozen, while skeletal muscle and adipose tissues were only stored snap frozen.

2.14 Tissue processing and histology

Heart tissue was fixed in 4% PFA for 24-48 hr before being washed three times in PBS to remove traces of fixative and stored in 70% ethanol at 4°C. Hearts were then dehydrated and placed into Shandon Biopsy Cassettes (Thermo Scientific, Paisley, UK) before being placed into paraffin wax at 60°C in a Citadel 1000 Tissue Processor (Thermo Scientific, Paisley, UK) which exposed tissues to a time sequence of alcohol and xylene treatment at different concentrations (shown in Table 2-8). Tissues were then embedded in 60°C paraffin wax using a Shandon Histocentre 3 (Thermo Scientific, Paisley, UK) and left to cool. Tissue blocks were stored at -20°C in the 24 hr prior to being sectioned. Blocks were cut into 5 µm sections using a Leica RM2235 Microtome (Leica Biosystems, Milton Keynes,

UK). Sections were placed in 40°C water to allow for softening of the wax embedding before being transferred to a silane treated microscope slide. Slides were then baked dry in a 50°C oven overnight. Prior to staining, all sections were de-waxed and rehydrated at room temperature via timed Histo-Clear (Fisher Scientific, Loughborough, UK) treatment and treatment in gradients of ethanol (detailed in Table 2-9).

Table 2-8 Tissue processing conditions for fixed tissues

Solution	Incubation Time
70% Ethanol	15 min
85% Ethanol	15 min
90% Ethanol	25 min
95% Ethanol	25 min
100% Ethanol	15 min
100% Ethanol	15 min
100% Ethanol	15 min
Xylene	30 min
Xylene	30 min
Paraffin Wax	30 min
Paraffin Wax	30 min

Table 2-9 Sequence of re-hydration for fixed tissue

Solution	Incubation Time
Histoclear	7 min
Histoclear	7 min
100% Ethanol	7 min
90% Ethanol	7 min
70% Ethanol	7 min
Water	5 min

2.14.1 Picrosirius red staining

After re-hydration, section slides were placed into fresh Weigert's haematoxylin (Sigma Aldrich, Irvine, UK) for 10 minutes, made up in accordance with the manufacturer's instructions. Excess stain was then removed by washing under a running H_2O tap for a further 10 minutes. Slides were then stained in a 0.1% picrosirius red solution made using 0.1% w/v picrosirius red F3B (Sigma Aldrich, Irvine, UK) in dH_2O and incubated in the dark for 90 minutes. Slides were then washed twice for 5 minutes each time with 0.01 N HCl (acidified H_2O) to remove any excess picrosirius red stain. Excess moisture was removed and sections were dehydrated (detailed in Table 2-10) and mounted under coverslips in DPX mounting medium (Sigma Aldrich, Irvine, UK) before being left to try overnight at room temperature.

Table 2-10 Sequence of de-hydration for fixed tissue

Solution	Incubation Time
70% Ethanol	7 min
90% Ethanol	7 min
100% Ethanol	7 min
Histo-Clear	7 min
Histo-Clear	7 min
Water	5 min

2.14.2 Wheat Germ Agglutinin

Cut sections were de-waxed and re-hydrated as described previously (Table 2-8, Table 2-9) and this was followed by sodium citrate mediated antigen retrieval. Slides were boiled for 10 minutes in pre-heated sodium citrate solution to unfold the antigen masked by the paraformaldehyde fixation, and then allowed to cool for a further 20 minutes to allow the antigen to re-fold correctly. This was followed by rinsing in running tap H_2O for 5 minutes and then two 5-minute PBS washes. Next, sections were blocked in PBS with 1% BSA (Sigma Aldrich, Irvine, UK) and 5% goat serum (Vector Labs, Peterborough, UK) for 1 hr at room temperature. Sections were then incubated with 10 µg/mL Alexa Fluor 555 conjugated WGA (Thermo Scientific, Paisley, UK), prepared in the same blocking solution, for 1 hr. Following this, sections were washed twice with PBS for 5 minutes each time and coverslips mounted with ProLong Gold+DAPI (Thermo

Scientific, Paisley, UK). Slides were dried in the dark overnight at room temperature before epifluorescence imaging.

2.14.3 Imaging and Analysis

Sections stained for picrosirius red and wheat germ agglutinin were imaged on the EVOS FL Imaging System (Thermo Scientific, UK). Images of 5 fields of view per section were taken from around the entire myocardium. Picrosirius red staining was analysed using the Image-Pro Analyzer 7.0 programme (MediaCybernetics, Rockville, USA) where the scale was manually set using a predefined macro. The colour and intensity of stain was selected and specified, and stained area was expressed as a percentage of the total area. Wheat germ agglutinin staining was analysed in ImageJ. The scale was set manually using a predefined macro and single-cardiomyocyte cross-sectional area was measured using the region of interest tool. Per image, 25 cardiomyocytes were measured. Cardiomyocyte diameter was measured across the widest point of the cross-section of a cell, with 40 cardiomyocytes measured per image. Mean cell area and diameter was determined as the average of all measurements across all 5 images.

2.15 Human Serum Samples

Serum was isolated from blood samples obtained from patients undergoing elective CABG surgery at the Western Infirmary, Glasgow, UK with control subjects recruited via advertisement. Ethical permission was obtained from the West of Scotland Research Ethics Committee 1 (reference number: 06/S0703/110) and the investigation conformed to the principles outlined in the Declaration of Helsinki. Thank you to Professor Christian Delles at the University of Glasgow for providing access to these samples.

2.16 Statistical Analysis

Statistical analysis was performed using GraphPad Prism Version 4, 5 or 6 (GraphPad Software, CA, USA) and statistical significance was determined by Student’s t-test or one-way ANOVA with Tukey’s post-hoc analysis, depending on how many groups were being compared, for unpaired data following a normal

distribution. Data are expressed as mean ± standard error unless otherwise stated. Where samples were related or paired, a Wilcoxon signed-rank test was used to determine whether mean ranks differed significantly. A p-value of $p<0.05$ was considered to be statistically significant in all experiments. All assays were performed in triplicate in three independent experiments unless indicated in the figure legend.

Analysis of fluorescent co-localisation (described in section 4.4.2) was performed using Image J and determined by Pearson's correlation coefficient (Pearson's r), which was used to measure the linear correlation between red fluorescence and green fluorescence giving a value between -1 (negative correlation) and +1 (positive correlation), where a value of zero suggests no association. An output value of greater than 0.5 was considered to be a relatively strong positive correlation between red and green fluorescence (Mukaka, 2012). Co-localisation was also measured by Manders' overlap coefficients M1 and M2 to further determine the degree of co-localisation (Dunn et al., 2011). Manders' coefficient M1 was used to determine the ratio of the summed intensities of pixels from the green image for which the intensity in the red channel is above zero, to the total intensity in the green channel. Manders' coefficient M2 was used to determine the ratio of the summed intensities of pixels from the red image for which the intensity in the green channel is above zero, to the total intensity in the red channel (Dunn et al., 2011). Coefficient values generated for each biological condition where then analysed by Student's t-test to determine any statistically significant differences between the sample means.

In section 6.4.2, SPSS was used to perform Fisher's exact test for categorical analysis to determine statistical significance between the proportions of patient samples with detectable Ang II for healthy control subjects vs. CABG patients.

2.16.1 Power calculation for *in vivo* trial

Power calculations were performed using Minitab 19 statistical software and carried out based on blood pressure measured by tail cuff plethysmography. Based on the literature, normotensive blood pressure readings of approximately 130 mmHg were utilised with an estimated increase of 25 mmHg upon infusion with 200 ng/kg/min Ang II over 14 days (Mishra et al., 2019, Zhang et al., 2017b,

Cui et al., 1999). Therefore, an increase in systolic blood pressure to 155±15.0 mmHg (SD based on literature and accuracy of the technique) estimated that 8 animals per group would allow for 80% power at $\alpha = 0.05$ to detect differences of 25 mmHg.

Chapter 3 Analysis and characterisation of extracellular vesicles

3.1 Introduction

3.1.1 Extracellular vesicle characterisation: guidelines

As the field of EV research has grown rapidly over the past decade, the need for standardisation in research and publication has become a matter of importance. The sharp increase in publications detailing the physiological and pathological effects of EVs in disease, along with the morphological structure of the EVs themselves has led to the publishing of minimal study guidelines which have since been defined by the International Society for Extracellular Vesicles (ISEV) (Lotvall et al., 2014, Théry et al., 2018). The first guidelines produced in 2014 suggested the minimal experimental requirements for the definition of EVs (for example, experimental procedures which must be included to define a vesicle as either an exosome or a microvesicle) and their functions (Lotvall et al., 2014). These initial guidelines suggested that EVs should be characterised at both the population level and the single vesicle level. It was recommended that populations are characterised via use of EV-related protein markers chosen dependent on the origin of the vesicle (eg. MVB associated or plasma membrane associated), for example TSG-101, Alix or the tetraspanins (Pols and Klumperman, 2009, Trioulier et al., 2004) however overlap in protein expression between microvesicles and exosomes has caused difficulty in this area. It was also suggested that single vesicles are separately characterised by at least two complimentary techniques such as transmission electron microscopy and nanoparticle tracking analysis (NTA) (Lotvall et al., 2014). Furthermore, upon characterisation of the EVs themselves the guidelines also state the importance of proper use in functional studies. ISEV recommended that quantification of EV activity should include at least some dose-dependent studies, along with process controls to analyse the possibility of potential sample contaminants having an effect on results, which may then be misinterpreted as effects caused by the EVs (Lotvall et al., 2014). The guidelines also suggested the use of EV-labelling studies, for example to show localisation of EVs within a cell model and highlighted that it may be beneficial to show that any effects observed which were deemed to be associated with EVs, could be depleted by specific inhibition of the EVs or their activity, or by reducing the dose of the EVs (Lotvall et al., 2014).

In 2017, updated minimal requirements for EV studies were published (Witwer et al., 2017). Although the standardisation of research studies involving EVs has been determined to be an important requirement for future development in this subject area, the vast uncertainty in a field which is still considered to be relatively new and up and coming meant that some level of flexibility is still required within the set of suggested rigorous guidelines (Witwer et al., 2017). Issues arising such as scientists not being able to follow all of the suggested guidelines were solved by suggesting that discussion of why certain experiments could not be performed be included in prospective manuscripts. Early 2017 saw the publication of EV-TRACK, a consortium suggesting the need for more transparent reporting in EV research with the overall goal of encouraging researchers to put the suggested experimental guidelines into practice (Van Deun et al., 2017). EV-TRACK assessed the current practices in EV research to highlight the level of heterogeneity across this field. For example, their in-depth analysis of publications in the field found over 1000 unique protocols used to isolate EVs from biological fluids (Van Deun et al., 2017). Furthermore, they also discovered vast variation within common protocols, for example the most common isolation technique was observed to be via ultracentrifugation however nearly all experiments analysed reported using different g-forces and time durations (Van Deun et al., 2017). These are only a few examples of the heterogeneity discovered within publications in this field. The new EV-TRACK platform allows researchers to upload experimental protocols to an open-access online interface. Experiments are then assigned an EV-METRIC score based on the experimental parameters which assesses whether enough information has been provided in terms of interpretation and experimental reproducibility in line with the minimal suggested guidelines (Van Deun et al., 2017, Lotvall et al., 2014). It has been recommended that funding bodies, editors and reviewers implement the use of EV-TRACK and the EV-METRIC system in grant applications and manuscripts in order to reduce the level of heterogeneity in publication of EV research, particularly in relation to isolation, analysis, and characterisation of EVs (Van Deun et al., 2017).

At the end of 2018, due to advances in the field and development of collective knowledge associated with EV characterisation, the minimal guidelines for the study of EVs were updated once more (Théry et al., 2018). Although clearly

indicating that the original 2014 guidelines (Lotvall et al., 2014) were still valid, a larger group of researchers were consulted in order to reach consensus for the 2018 guidelines (Théry et al., 2018) to provide clearer requirements for EV research and publication. Evolution of the field meant that the new guidelines could provide more in-depth information on characterising EV populations where previous guidelines included grey areas. For example, they do not propose existence of protein markers purely specific to each EV class due to overlap, however do suggest named markers known to be enriched in exosomes or enriched in microvesicles which may help with classification (Théry et al., 2018). Although the original methods for characterisation of EVs are still valid, the new guidelines included assessment of newer techniques that had since been used in the EV field. For example, in terms of deducing particle release number, where previous analysis included mainly NTA and TEM, techniques such as flow cytometry, resistive pulse sensing, and surface plasmon resonance with atomic force microscopy are now also in common use (Théry et al., 2018).

3.1.2 Characterisation of cardiac cell-derived extracellular vesicles

Very few studies have characterised the EVs released from the cardiac cell types; the H9c2 cardiomyoblast cell line and neonatal rat cardiac fibroblasts (NRCF) or assessed the effects of Ang II on release of EV populations. It has been shown previously via TEM and NTA that more than 95% of EVs released from NRCF cells fell into the size range of 50-100 nm and that these vesicles may then be classified as exosomes (Lyu et al., 2015). Furthermore, they also highlighted that treatment of NRCF cells with Ang II stimulated increased release of exosomes from the cells compared with controls. This was shown via increased overall protein levels with proportional increase in levels of specific EV-related markers indicating that the total protein level of NRCF-derived exosomes reflects the number of exosomes following Ang II stimulation in parental cells (Lyu et al., 2015). Other studies including characterisation of exosomes derived from H9c2 cardiomyocytes, in this case in a model of ischaemia, found vesicles derived from H9c2 under normal conditions to be approximately 126 nm in diameter with release of approximately $9.32 \pm 0.35 \times 10^8$ particles/mL (with no significant change in size or particle release as a result of ischaemia stimulation) (Ribeiro-Rodrigues et al., 2017). A second study found that EVs derived from

H9c2 under control conditions were mainly found to be 50-100 nm in diameter as measured by both TEM and NTA (Wang et al., 2017a). A further study utilising both cell types has shown that both NRCF and H9c2-derived EVs fall into the size range of 100-170 nm in diameter, with similar TEM profiles, and again suggested that size could not be influenced by ischaemia (Borosch et al., 2017). When taking these studies together, it can be observed that there is some clear variation in terms of characterisation of EVs derived from H9c2 and NRCF cell types. Under certain stressors, it has been found that EV release is increased in these cell types (Lyu et al., 2015), while under others it seems to be unaffected (Borosch et al., 2017, Ribeiro-Rodrigues et al., 2017).

3.1.3 Characterisation of circulating extracellular vesicles

Along with cell culture supernatant, EVs may also be isolated from a diverse range of other biological fluids including blood plasma, blood serum, urine, semen, amniotic fluid, saliva and cerebrospinal fluid (Raposo and Stoorvogel, 2013). Many studies have focused on the isolation of circulating EVs from plasma or serum (in both animal studies and human patient studies) for strategies such as biomarker discovery or for functional assessment in animal or cell-based disease models. For example, it was found that circulating microvesicles derived from WKY rats (characterised, in this case, via flow cytometry analysis of EV markers) undergoing myocardial left anterior descending coronary artery ligation were able to reduce infarct size and cardiomyocyte apoptosis when administered intravenously in a model of ischaemia/reperfusion injury (Wang et al., 2017b) suggesting a protective role for these naturally occurring circulating vesicles. Further studies noted that exosomes derived from the serum of healthy human subjects (characterised by flow cytometry and western immunoblot analysis) could attenuate hydrogen peroxide-induced apoptosis in the H9c2 cardiomyocyte cell model and that this was associated with activation of ERK1/2 signalling (Li et al., 2018) further suggesting that they may be a useful therapeutic strategy in myocardial injury. Although some studies have carried out basic characterisation of circulating EVs, currently no direct comparison exists in terms of characterisation of EVs derived from the WKY rat vs. stroke-prone spontaneously hypertensive (SHRSP) rat models. The SHRSP is a well-established experimental model of essential hypertension, where it also exhibits other key characteristics of cardiovascular disease such as left ventricular hypertrophy and endothelial

dysfunction (Dominiczak et al., 1997, Graham et al., 2007). While the SHRSP has been shown to exhibit these clear phenotypes, a reference strain, the WKY rat, exhibits a contrasting phenotype and so is commonly used as a normotensive control in studies investigating pathological disease mechanisms in the SHRSP model (Dominiczak et al., 1997, Graham et al., 2007, Wynne et al., 2018). Owing to the fact that many studies suggest EV profiles to be altered under pathological disease conditions (Raposo and Stoorvogel, 2013), it is of interest to determine whether any differences are observed between the WKY and SHRSP rat models.

3.2 Aims

- Characterise EVs derived from H9c2 cardiomyocytes and assess effects of Ang II stimulation on EV release.

- Characterise EVs derived from NRCF cells and assess effects of Ang II stimulation on EV release, and comparison of NRCF-EV characteristics with H9c2-EVs.

- Comparative characterisation of EVs derived from WKY rat serum vs SHRSP rat serum.

3.3 Key Methods

Table 3-1 Chapter 3 key methods

EV isolation	Cell culture media Section 2.6
	Rat serum Section 2.9
EV characterisation	Nanosight Section 2.7.1
	Transmission Electron Microscopy Section 2.7.2
	Western Immunoblot Section 2.7.3
	Bicinchoninic Acid Assay Section 2.7.3.3

3.4 Results

3.4.1 Characterisation of H9c2-derived extracellular vesicles +/- Ang II-stimulation

H9c2 cardiomyocytes were either untreated or treated with 1 μM Ang II in serum-free media over a 48 hr period. EVs were then isolated from the conditioned media via ultracentrifugation with proteinase K treatment and EV sample populations were characterised in terms of size and particle release by NTA and transmission electron microscopy (TEM). Protein concentration was assessed via bicinchoninic acid (BCA) assay followed by detection of specific EV-related protein markers via western immunoblot.

Analysis of size and concentration of EVs released from H9c2 cardiomyocytes +/- Ang II via NanoSight NTA showed no significant differences between the two groups for either size or particles released per mL (Figure 3-1). A representative microscopic image and size/concentration track produced by the NanoSight is shown in Figure 3-1 A & B. The average size of control EVs was found to be 123.7±6.6 nm vs. 126.2±7.8 nm for EVs derived from Ang II stimulated cells (n=8 per group, p=0.81) (Figure 3-1 C). Concentration was also determined in terms of particles/mL. It was found that control untreated H9c2 cells released an average of $5.9x10^8 \pm 1.5x10^8$ particles/mL vs. $6.8x10^8 \pm 2.1x10^8$ particles/mL for H9c2 cells stimulated with Ang II (n=8 per group, p=0.75) (Figure 3-1 D).

Further size analysis via TEM images on isolated EVs also reported no significant differences in size between EVs derived from control H9c2 cardiomyocytes and EVs derived from Ang II-stimulated H9c2 cardiomyocytes (Figure 3-2 A-B). TEM image data analysis suggest that the average size of EVs released from control H9c2 cardiomyocytes was approximately 106.1±8.7 nm vs. 115.8± 2.7 nm for Ang II-stimulated H9c2 (n=15 per group, p=0.53) (Figure 3-2 B).

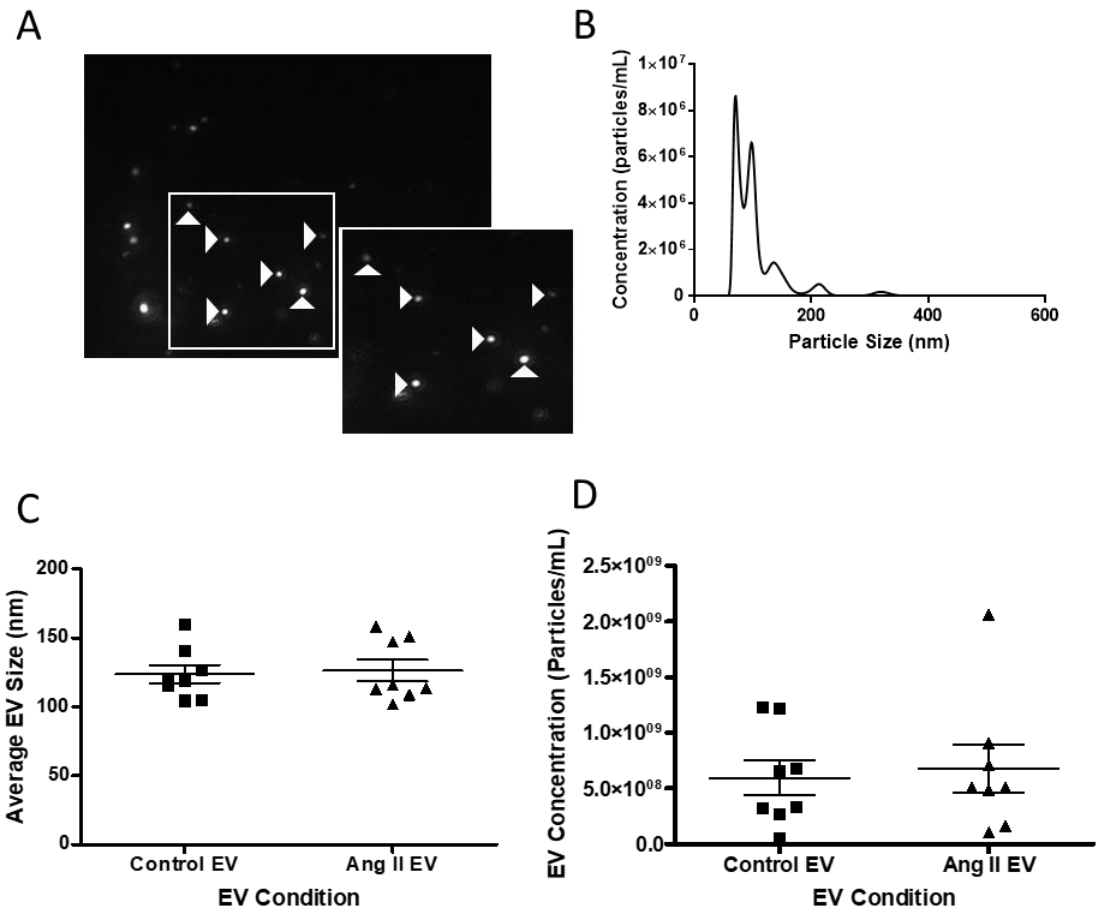

Figure 3-1 Characterisation of EVs derived from H9c2 cardiomyocytes +/- Ang II stimulation via NTA. (A) Representative microscopic image of EVs released from H9c2 cardiomyocytes. EVs indicated by white arrows. (B) Representative track produced by NanoSight showing example size and concentration data produced. (C) Size comparison of EVs derived from control H9c2 vs Ang II stimulated H9c2 (n=8, p=0.81, Student's t-test). (D) Particle concentration comparison of EVs derived from control H9c2 vs Ang II-stimulated H9c2 (n=8, p=0.75, Student's t-test).

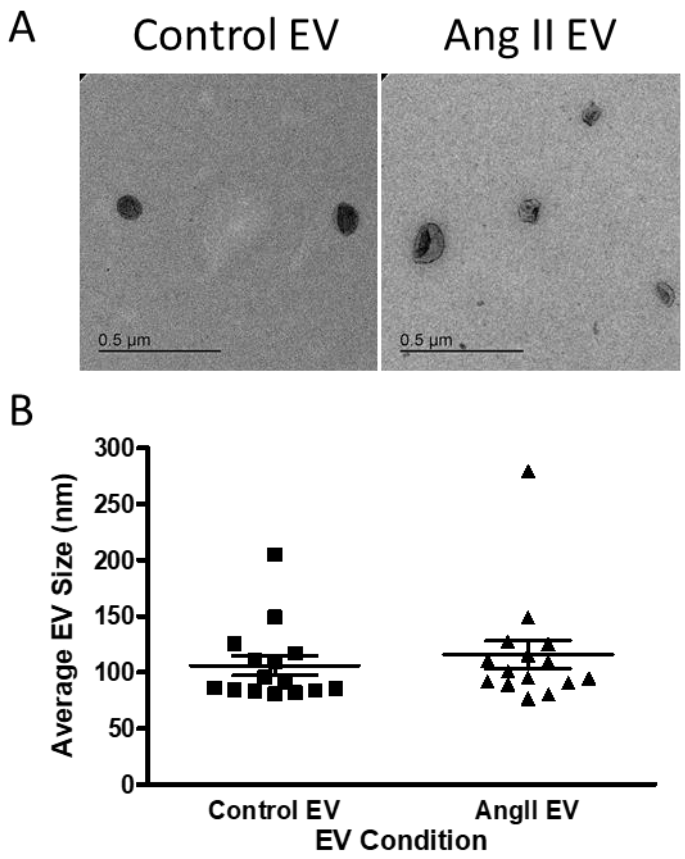

Figure 3-2 Characterisation of EVs derived from H9c2 cardiomyocytes +/- Ang II stimulation via TEM. (A) Representative images of EVs derived from control H9c2 cardiomyocytes vs Ang II-stimulated H9c2 cardiomyocytes. Scale bar: 0.5 µm. (B) Size comparison of diameter of EVs derived from control H9c2 vs Ang II-stimulated H9c2 (n=15, p=0.53, Student's t-test).

Protein concentration was determined by BCA assay for EVs derived from both control H9c2 and EVs derived from Ang II-stimulated H9c2 and no significant difference in protein concentration between the two groups was observed (Figure 3-3). Values obtained for protein concentration for both groups are shown in the table in Figure 3-3 A. The average protein concentration in EVs derived from control H9c2 was found to be approximately 34.1±9.9 µg/mL vs. 31.2±8.4 µg/mL from EVs derived from Ang II-stimulated cells (n=4 per group, p=0.83) (Figure 3-3 B).

EVs released from H9c2 cardiomyocytes under control conditions were also probed for three specific EV-related protein markers; TSG-101, CD63 and Hsp70 (Théry et al., 2006) (Figure 3-3 C). Both TSG-101 and CD63 were found to be present in the H9c2 control cell lysates and the EV fraction, however although Hsp70 was detectable in the H9c2 cell lysates, it was not present in the EV fraction (TSG-101; n=3, CD63; n=2, Hsp70; n=2) (Figure 3-3 C).

A

Sample	Concentration (µg/mL)
Control EVs	53.5 16.65 49.05 17.1
Ang II EVs	40.7 18.43 49.75 15.7

B

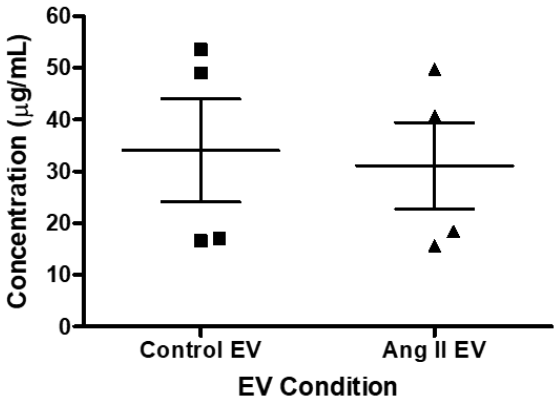

C

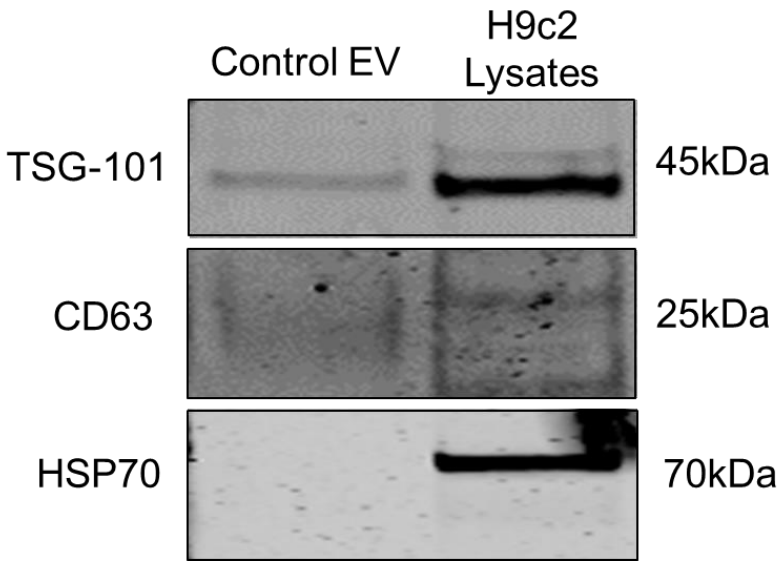

Figure 3-3 Analysis of H9c2-derived EV protein content by BCA assay and western immunoblot. (A) Protein concentration values for EVs derived from H9c2 +/- Ang II-stimulation as determined by BCA assay. (B) Protein concentration comparison of EVs released from H9c2 +/- Ang II-stimulation (n=4, p=0.83, Student's t-test). (C) Detection of EV markers; TSG-101, CD63 and Hsp70 in control EVs and control H9c2 cell lysates (TSG-101; n=3, CD63; n=2, Hsp70; n=2).

3.4.2 Characterisation of NRCF-derived extracellular vesicles +/- Ang II-stimulation

NRCF cells were isolated from neonatal rat hearts (< 5 days old) and were either untreated or treated with 1 μM Ang II in serum-free media over a 48 hr period. EVs were then isolated from NRCF cell conditioned media via ultracentrifugation with proteinase K treatment and EV sample populations were characterised in terms of size and particle release by NTA via NanoSight and TEM.

Analysis of size and concentration of EVs released from NRCF cells +/- Ang II-stimulation via NTA showed no significant differences between the two groups for either size or particles released per mL (Figure 3-4). A representative microscopic image and size/concentration track produced by NTA is shown (Figure 3-4 A & B). Data gathered showed that the average size of EVs released from NRCF cells under control conditions was approximately 200.0±8.6 nm vs. 200.6±6.9 nm for EVs derived from Ang II-stimulated cells (n=7, p=0.95) (Figure 3-4 C). NTA of the number of particles released per condition showed that on average, control NRCF cells release approximately $6.9x10^8 \pm 1.3x10^8$ particles/mL vs. $6.9x10^8 \pm 1.6x10^8$ particles/mL for Ang II-stimulated NRCF cells (n=7, p=0.95) (Figure 3-4 D).

Analysis of TEM images of NRCF-derived EVs +/- Ang II-stimulation provided further information on the size and diameter of EVs released under each condition, however again no significant differences were observed (Figure 3-5 A-B). Data obtained by sizing analysis suggest that the average diameter of EVs released from control NRCF cells is approximately 194.8±12.0 nm vs. 192.8±14.3 nm for Ang II-stimulated NRCF cells (n=16 per group, p=0.91) (Figure 3-5 B).

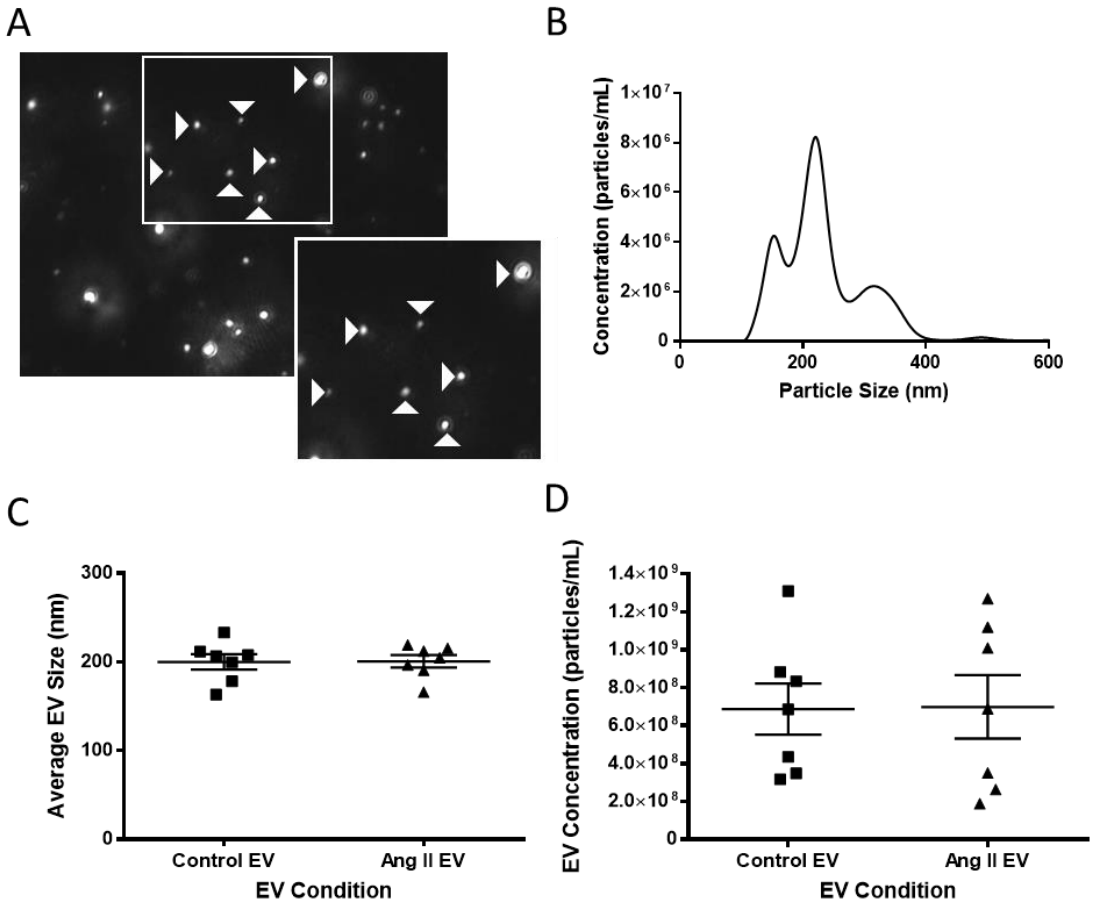

Figure 3-4 Characterisation of EVs derived from NRCF cells +/- Ang II stimulation via NTA. (A) Representative microscopic image of EVs released from NRCF cells. EVs are indicated by the white arrows. (B) Representative track produced by NanoSight showing example size and concentration data produced. (C) Size comparison of EVs derived from control NRCF vs Ang II stimulated NRCF (n=7, p=0.95, Student's t-test). (D) Particle concentration comparison of EVs derived from control NRCF vs Ang II-stimulated NRCF (n=7, p=0.95, Student's t-test).

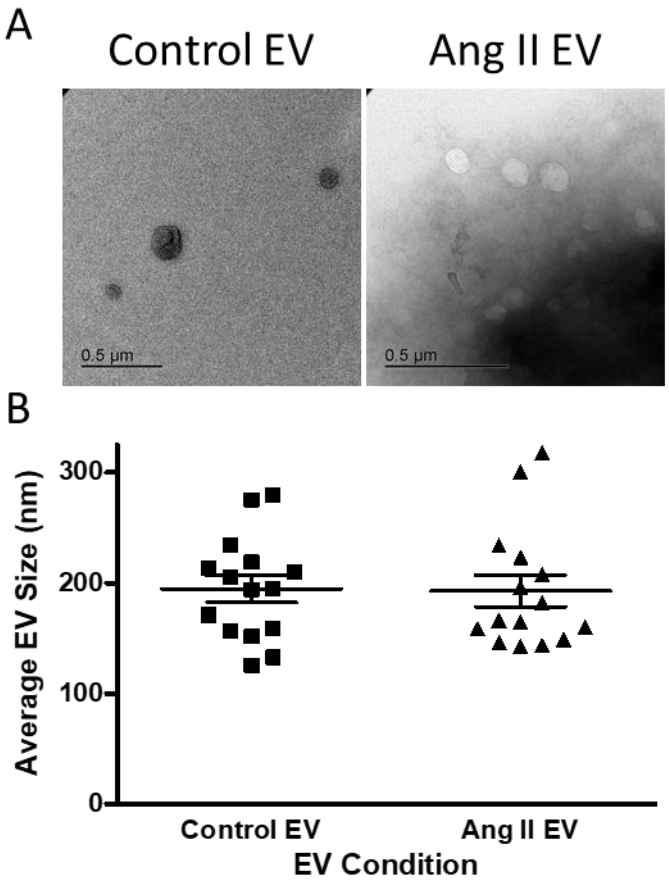

Figure 3-5 Characterisation of EVs derived from NRCF cells +/- Ang II stimulation via TEM. (A) Representative images of EVs derived from control NRCF cells vs. Ang II-stimulated NRCF cells. Scale bar: 0.5 µm. (B) Size comparison of diameter of EVs derived from control NRCF cells vs Ang II-stimulated NRCF cells (n=16, p=0.91, Student's t-test).

3.4.3 Size and concentration comparison of H9c2 and NRCF-derived extracellular vesicles

Following characterisation of EVs derived from both H9c2 cardiomyocytes and NRCF cells under control conditions and Ang II-stimulation, it was of interest to determine whether there were any significant differences in terms of size and concentration of EVs released between these two different cardiac cell types. Data obtained from NanoSight NTA and TEM image analysis was re-configured to compare sizing and concentration values obtained for the different cell types, EV data points were included regardless of whether they were obtained from control cells or Ang II stimulated as this caused no significant changes (Figure 3-6).

Analysing all data points together for NTA sizing showed that NRCF-derived EVs were significantly larger in diameter than H9c2-derived EVs. The average size of H9c2 EVs was 125.0±4.9 nm vs. 200.3±5.3 nm for NRCF cell-derived EVs (H9c2 EVs; n=16, NRCF EVs; n=14, $p<0.001$) (Figure 3-6 A). Although a significant difference in EV size was observed from the NTA data, there appeared to be no significant difference in particle concentration release between the two cell types. When comparing all data points, it was observed that the average number of particles released from H9c2 cardiomyocytes was $6.3x10^8 \pm 1.3x10^8$ particles/mL vs. $6.9x10^8 \pm 1.0x10^8$ from NRCF cells (H9c2 EVs; n=16, NRCF EVs; n=14, p=0.74) (Figure 3-6 B).

TEM image data was also re-analysed to determine any size differences between H9c2 EVs and NRCF EVs observed via this method. In similarity to the NTA data, a significant difference in EV size was found between those derived from H9c2 cardiomyocytes and those derived from NRCF cells. Representative TEM images are shown for EVs derived from each cell type in Figure 3-6 C. The data showed that when analysing all data points, the average size of EVs derived from H9c2 cardiomyocytes was approximately 104.3±5.0 nm vs. 193.9±8.6 nm for EVs derived from NRCF cells (H9c2 EVs; n=30, NRCF EVs; n=32, $p<0.001$) (Figure 3-6 D).

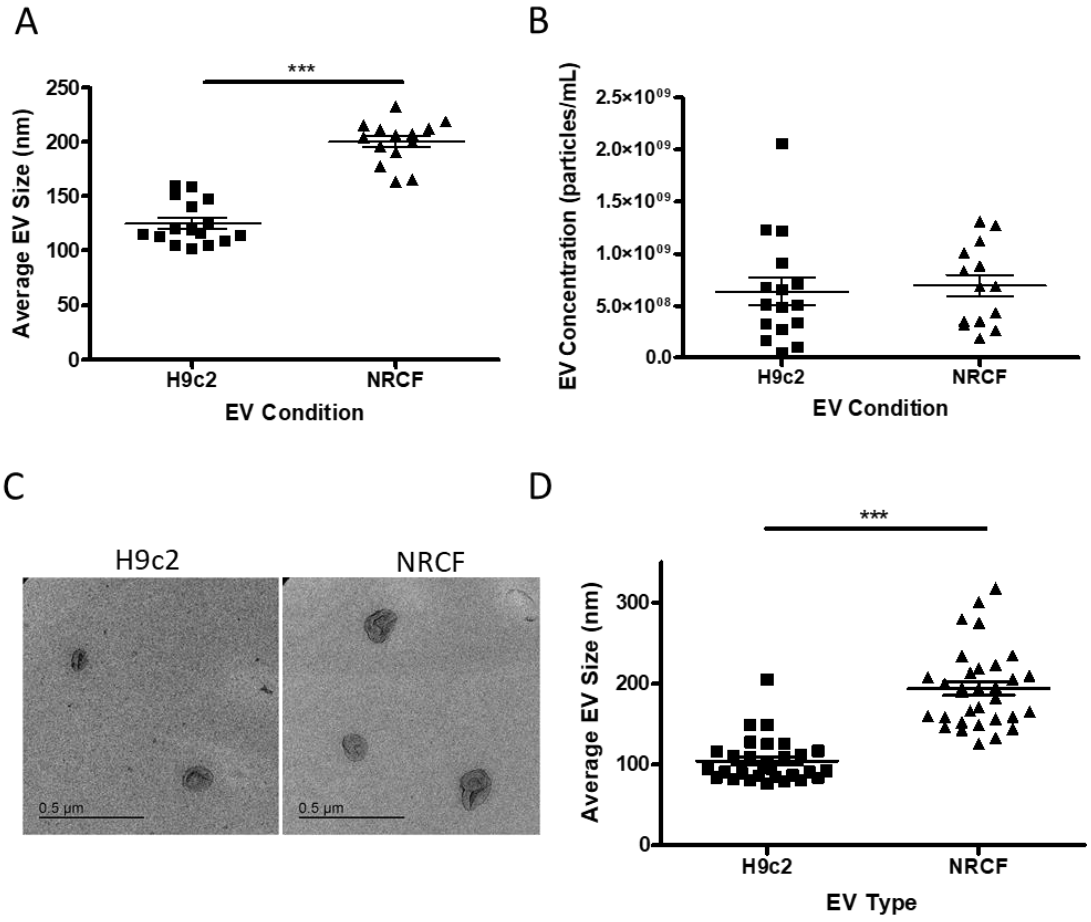

Figure 3-6 Comparison of EV size and concentration released from H9c2 cardiomyocytes and NRCF cells via NTA and TEM. (A) Comparison of size between H9c2-derived EVs and NRCF-derived EVs by NTA (H9c2; n=16, NRCF; n=14, ***p<0.001, Student's t-test). (B) Comparison of concentration between H9c2-derived EVs and NRCF-derived EVs by NTA (H9c2; n=16, NRCF; n=14, p=0.74). (C) Representative TEM images for EVs derived from each cell type. (D) TEM image analysis of EV size for H9c2-derived EVs vs. NRCF-derived EVs (H9c2 EVs; n=30, NRCF EVs; n=32, ***p<0.001, Student's t-test).

3.4.4 Characterisation and comparison of extracellular vesicles derived from WKY and SHRSP rat serum

Having determined whether EV profiles are changed in two different cardiac cell models using Ang II as a pathological stressor compared with controls, it was next established as to whether circulating EV profiles differed in an animal model of cardiovascular disease compared with control animals. In this study, EVs were isolated from 1 mL serum obtained from the blood of either WKY or SHRSP adult male rats. Isolated EVs were then analysed by NTA for average size and particle concentration, and by BCA assay for total protein concentration.

NanoSight NTA was used to show size and particle concentration ranges in the WKY samples, a representative microscopic image and size/concentration track produced by the NanoSight are shown in Figure 3-7 A & B. Analysis by NanoSight demonstrated that across the WKY samples, the EV size ranged from between approximately 95.1±1.5 nm and 172.7±3.8 nm while the particle concentration range was between $1.3x10^9±3.7x10^7$ and $4.9x10^9±4.7x10^8$ particles/mL (n=7) (Figure 3-7 C). Further analysis by BCA assay to determine total protein concentration in the samples showed that the range in protein concentration was between 1.67 µg/µL and 3.54 µg/µL (n=7) (Figure 3-7 D).

Similarly, EVs derived from SHRSP serum samples were also analysed to provide size and concentration ranges across the samples. A representative microscopic image and size/concentration track produced by the NTA are shown in Figure 3-8 A & B. NTA analysis showed that the EV size ranged from 84.0±1.7 nm to 106.7±2.6 nm across the samples analysed, the concentration was shown to be in the range of $1.6x10^9±4.3x10^7$ to $2.3x10^9±1.3x10^8$ particles/mL across the samples (n=8) (Figure 3-8 C). Analysis by BCA showed that the total protein concentration in the samples were in the range of 1.36 µg/µL to 2.89 µg/µL (n=8) (Figure 3-8 D).

A

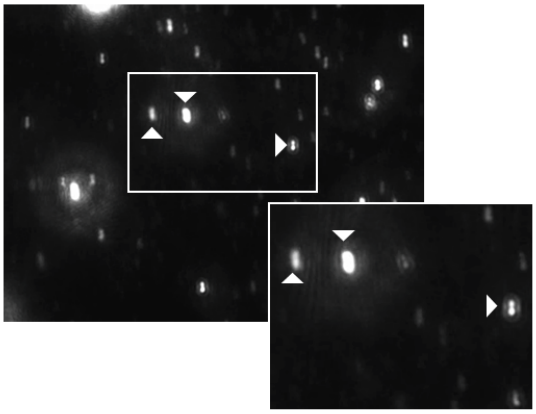

B

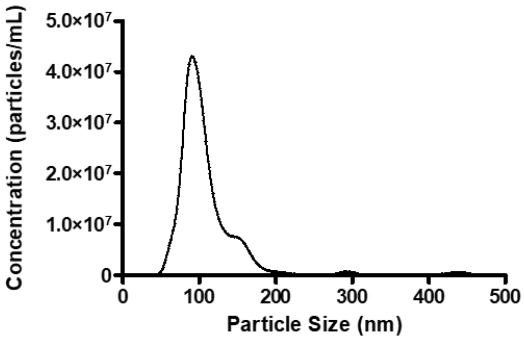

C

Sample	Size (nm)	Concentration (particles/mL)
A7021	170.4 +/- 1.1	2.80×10^9 +/- 9.65×10^7
A7238	172.7 +/- 3.8	2.46×10^9 +/- 1.15×10^8
A7022	134.6 +/- 3.8	4.87×10^9 +/- 4.65×10^8
A7241	95.1 +/- 1.5	2.75×10^9 +/- 2.09×10^8
A7240	107.8 +/- 1.7	1.40×10^9 +/- 7.85×10^7
A7257	118.9 +/- 2.5	1.43×10^9 +/- 1.00×10^8
A7264	126.5 +/- 0.7	1.30×10^9 +/- 3.80×10^7

D

Sample	Concentration (ug/uL)
A7021	2.7953
A7238	2.8530
A7022	1.6739
A7241	3.5150
A7240	3.5414
A7257	3.4093
A7264	3.2354

Figure 3-7 Characterisation of EVs derived from WKY rat serum. (A) Representative microscopic image of WKY serum EVs taken by NanoSight, EVs are indicated by the white arrows, with representative size/concentration track (B). (C) Tabulated size and concentration data obtained by NanoSight (n=7). (D) Tabulated protein concentration data obtained by BCA assay (n=7).

A

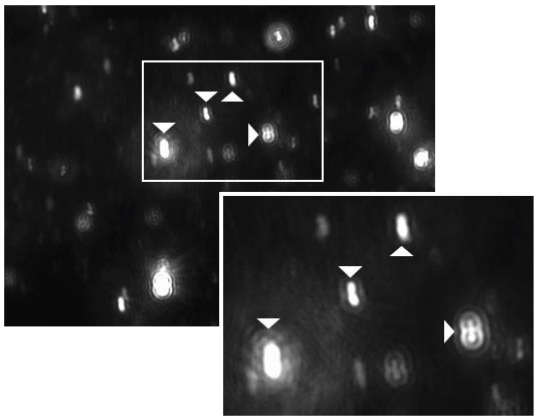

B

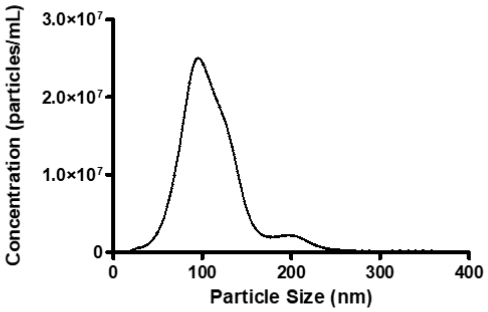

C

Sample	Size (nm)	Concentration (particles/mL)
C0271	84.0 +/- 1.7	2.30×10^9 +/- 1.27×10^8
C0283	103.4 +/- 1.9	2.26×10^9 +/- 1.34×10^8
C0305	106.7 +/- 2.6	1.73×10^9 +/- 6.52×10^7
C0308	98.4 +/- 1.5	2.15×10^9 +/- 9.57×10^7
C0380	97.4 +/- 2.3	1.56×10^9 +/- 4.32×10^7
C0381	89.4 +/- 2.5	1.77×10^9 +/- 1.85×10^8
C0368	88.5 +/- 0.7	1.58×10^9 +/- 4.14×10^7
C0367	85.8 +/- 1.0	1.95×10^9 +/- 1.11×10^8

D

Sample	Concentration (ug/uL)
C0271	2.8971
C0283	1.6978
C0305	1.8011
C0308	2.1585
C0380	1.5967
C0381	1.3668
C0368	1.9026
C0367	2.1905

Figure 3-8 Characterisation of EVs derived from SHRSP rat serum. (A) Representative microscopic image of SHRSP serum EVs taken by NanoSight, EVs are indicated by the white arrows, with representative size/concentration track (B). (C) Tabulated size and concentration data obtained by NanoSight (n=8). (D) Tabulated protein concentration data obtained by BCA assay (n=8).

Following separate characterisation of EVs derived from WKY rat serum and SHRSP rat serum under normal control conditions, it was of interest to determine whether there were any significant differences in size, particle release or total protein concentration of circulating EVs released between these two animal models. Data obtained from NTA for size and concentration, and protein concentration determined by BCA, was combined to allow for comparison between the two EV populations.

Analysis of the EV sizing data showed that WKY serum-derived EVs were significantly larger in diameter than SHRSP serum-derived EVs. The average size of EVs derived from WKY serum was approximately 132.3±11.2 nm vs. 94.2±2.9 nm for SHRSP serum derived EVs (WKY EVs; n=7, SHRSP EVs; n=8, $p<0.01$) (Figure 3-9 A). Particle concentration as determined by NTA showed the average concentration of WKY EVs to be $2.4x10^9±4.8x10^8$ particles/mL vs. $1.9x10^9±1.1x10^8$ particles/mL for EVs derived from SHRSP serum, however this difference was not significant (WKY EVs; n=7, SHRSP EVs; n=8, $p=0.27$) (Figure 3-9 B). Although no significant difference was found in terms of particle concentration determined by NTA, a significant difference in total protein concentration was observed between the two groups when BCA data was compared. It was found that average total protein concentration in WKY serum-derived EVs was 3.0±0.2 µg/µL vs. 1.9±0.1 µg/µL for SHRSP serum-derived EVs (WKY EVs; n=7, SHRSP EVs; n=8, $p<0.01$) (Figure 3-9 C).

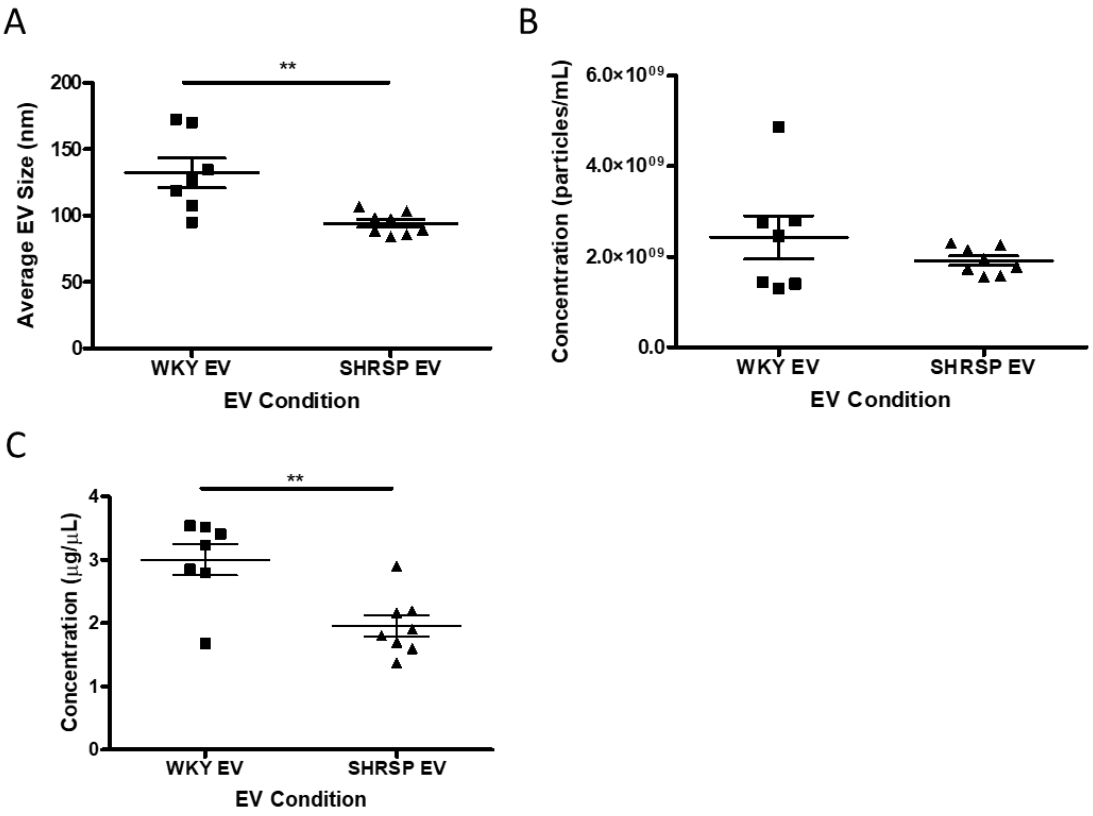

Figure 3-9 Comparative characterisation of EVs derived from WKY and SHRSP rat serum. (A) Comparison of EV size between WKY and SHRSP serum-derived EVs as determined by NTA (WKY EVs; n=7, SHRSP EVs; n=8, **p<0.01, Student's t-test). (B) Comparison of particle concentration between WKY and SHRSP serum-derived EVs as determined by NTA (WKY EVs; n=7, SHRSP EVs; n=8, p=0.27, Student's t-test). (C) Comparison of total protein concentration between WKY and SHRSP EVs as determined by BCA assay (WKY EVs; n=7, SHRSP EVs; n=8, **p<0.01, Student's t-test).

3.5 Discussion

Following the introduction of the minimal guidelines for EV research in 2014, inclusion of methods of vesicle characterisation prior to any functional studies, or other use, have become an important factor in EV research (Lotvall et al., 2014). In this study, EVs were isolated from the conditioned culture medium of two cardiac cell types; H9c2 and NRCF, and from serum samples obtained from two rat strains; WKY and SHRSP. A selection of standard methods recommended by the International Society for Extracellular Vesicles (ISEV) were used in the characterisation of these vesicles including NTA, BCA, TEM and western immunoblotting (Lotvall et al., 2014). Briefly, it was found that NRCF cells release significantly larger EVs in comparison to H9c2 cells, and that treatment of parental cells with Ang II did not affect EV size or release in either cell model. It was also found that EVs derived from WKY serum were significantly larger than those derived from SHRSP serum and also exhibited higher protein content.

Although, commonly, vesicles are characterised with the end goal of specific categorisation into EV sub-populations such as exosomes, microvesicles or apoptotic bodies, the ultimate determinant which allows for this is the tracing of the cellular origin of the vesicle population (Colombo et al., 2014). Generally, techniques such as cryo-electron microscopy allow for visualisation of EVs in their most native state and it is possible, although difficult, to image evidence such as the fusion of MVBs with the plasma membrane which would then suggest a sub-population of exosomes present in a given sample. Similarly, it may be possible to image microvesicles budding directly from the plasma membrane (Colombo et al., 2014, Théry et al., 2018). Due to the fact that criteria such as these are difficult to obtain on a routine basis, complexity regarding the correct nomenclature is reduced in this study by always referring to vesicles isolated using the blanket term “extracellular vesicles” or “EVs” rather than assuming presence of a sub-class of vesicles. Characterisation carried out during this study was used primarily to confirm presence and purity of EV samples used in further functional studies, as well as to confirm effects on EVs and their release under modelled pathological disease conditions.

This study found that EVs were released in abundance from the cardiac cell types, H9c2 and NRCF, as expected owing to the fact that it has been reported

and critically discussed in a number of comprehensive reviews that all cell types release and use EVs as a method of cellular communication (Yáñez-Mó et al., 2015, Raposo and Stoorvogel, 2013, Colombo et al., 2014). It has also been reported in various studies ranging from those in the field of cardiovascular research to those in cancer, immunology and neuroscience, that EV profiles may change under pathological disease conditions, with particular emphasis on changes in the concentration of particles released compared to control conditions (Colombo et al., 2014). In this study, H9c2 cardiomyocytes were treated with Ang II in order to induce cellular hypertrophy (Flores-Muñoz et al., 2011) prior to EV isolation however it was observed that Ang II treatment did not significantly alter the EV profile in terms of size or concentration of particles released. Interestingly, it has previously been reported that treatment of parental cells with Ang II significantly increased particle release compared to basal conditions (Lyu et al., 2015) however this observation was made in NRCF cells and so cell-type specificity could be playing a role in this phenomena. Intriguingly, this study also analysed the effects of Ang II treatment on EV release in NRCF cells and, similarly to the observations made in H9c2 cardiomyocytes, there was no significant difference found in either size or concentration of particles released from NRCF cells compared to control conditions. There is no clear answer as to why one study found a significant increase in EV release following Ang II stimulation where this study did not, however it should be noted that particle release was measured only in terms of total protein concentration (Lyu et al., 2015) whereas in this study both total protein concentration and NTA were assessed; in either study it may be a matter of questioning sample purity to account for differences in protein levels found. Furthermore, it should also be noted that one other study reported an increase in microvesicle release following Ang II stimulation (Cordazzo et al., 2013). In this case, it was found that Ang II stimulation of human mononuclear cells resulted in upregulation of microvesicle shedding from the cells, dependent on AT_2R signalling. However, this study analysed only the presence of phosphatidyl serine (a marker of coagulation) positive microvesicles after Ang II stimulation and measured particle concentration via an indirect method. In this case, microvesicles were measured by nanomolar phosphatidyl serine levels present (Cordazzo et al., 2013) as opposed to a direct EV analysis method such as NTA or

TEM which could potentially give rise to the presence of phosphatidyl serine-positive cellular contaminants.

Various studies have described other stressors that are able to increase the production of EVs. For example, it has been found that rat renal proximal tubular cells under hypoxic challenge produce significantly more exosomes compared with control cells, though it is also reported that size remains unchanged between the two conditions (Zhang et al., 2017a). It was also shown in an ovarian cancer cell model that cells exposed to hypoxia significantly increase their exosome release compared to control cells (Dorayappan et al., 2018). Further studies have shown that EV release may be increased by such stressors as photo-oxidative blue light stimulation in retinal cells (Zhang et al., 2019), treatment of mammalian cells with plant polyphenols (Soleti et al., 2018), and antibiotic treatment such as ciprofloxacin (Nemeth et al., 2017). Although many different stressors across a variety of research fields have been shown to increase EV release, solid evidence suggesting that Ang II has the same effect has not been fully established.

A comparative analysis of EVs derived from H9c2 and NRCF cells was also included in this study. Although no difference in concentration of particles released was observed, a clear difference in the size of particles released was found via both analysis methods whereby it was shown that NRCF cells release significantly larger EVs compared to those released by H9c2 cells. Various techniques are used to quantify vesicle size, with the most common being NTA and TEM (Lotvall et al., 2014). One other study has also directly compared EV size between H9c2 and NRCF-derived EVs and it was reported that both populations fell into a size range of 100-170 nm with a modal size of 150 nm for both (Borosch et al., 2017). In this case, EV sizes were analysed via tuneable resistive pulse sensing (TRPS), a relatively new method in EV analysis which involves passing single particles through a size-tuneable nanopore where passage is determined by adjusting pore size (Weatherall et al., 2016, Borosch et al., 2017). It is possible that clear differences in EV sizes observed between studies could be a result of utilizing different analysis techniques, or the accuracy and robustness of the chosen techniques. A second study focusing only on NRCF-derived EVs suggested that almost all EVs isolated fell into a size range of 50-100

nm, and in this case analysis was carried out via NTA (Lyu et al., 2015). This difference could be due to variation in analysis technique, or natural variability in the cell type. Furthermore, both studies reported that isolation of NRCF cells was carried out in-house, which also holds true for the studies presented here. It is therefore possible that differences observed in EV characteristics could be occurring due to parental cell isolation purity, or a number of other variables associated with primary cell isolation, rat strain for example. Other studies that have characterised EVs derived from H9c2 cardiomyocytes, have reported released EVs to be approximately 126 nm in diameter (Ribeiro-Rodrigues et al., 2017) under control conditions, however other studies have reported a size range of 50-100 nm (Wang et al., 2017a). Again, it is possible that differences in EV characteristics observed are related to the condition of the parental cell, for example in terms of cell passage number, or in terms of phenotypic morphology which is known to vary and change easily in H9c2 cardiomyocytes (Watkins et al., 2011).

As described, various studies suggest that disease pathology may change EV profiles. In these studies, profiles of circulating EVs were analysed and compared between two different rat models; the hypertensive SHRSP rat and its normotensive counterpart, the WKY rat. Significant differences were observed between the two in terms of EV size, where WKY EVs were found to be larger than SHRSP EVs, and in terms of total protein concentration, where WKY EVs where found to have a higher protein concentration than SHRSP EVs. Very few studies have characterised circulating EVs derived from these rat models; one study carried out basic characterisation of circulating microvesicles derived from the WKY rat under sham and ischaemic conditions (Wang et al., 2017b). This study only included characterisation via flow cytometry to determine the origin of most vesicles to be endothelial- or platelet-derived, however it also reported that under ischaemic conditions the concentration of both types of vesicle were significantly increased compared with the sham group (Wang et al., 2017b). Another study detailed basic characterisation of exosomes derived from the plasma of WKY and spontaneously hypertensive (SHR) rats for their research (Otani et al., 2018). In this case, exosomes were characterised via TRPS and the study reported that vesicles derived from WKY and SHR plasma were approximately 90-100 nm in diameter with no significant differences between

the two; they also reported no significant differences in concentration of particles released, however noticed a modest trend for WKY plasma to contain more (Otani et al., 2018). The findings detailed in the present study suggest a difference in size profile between circulating EVs from WKY and SHRSP rats, however owing to the initial availability of samples, this study analysed EVs from serum as opposed to plasma and therefore there is a likelihood that the EV origin may differ between the two studies and so some differences in EV profile may be expected. A further study aiming to characterise exosomes from blood plasma via NTA also reported an average population size of <100 nm in vesicles derived from WKY rat plasma (Baranyai et al., 2015), a finding in agreement with the aforementioned study (Otani et al., 2018). Although some studies mentioned here have carried out basic characterisation of circulating EVs from WKY rats, there is very little evidence for characterisation of SHRSP-derived circulating EVs and minimal published data detailing comparison of EV profiles between the two models (van Kralingen et al., 2019).

3.5.1 Study limitations

EVs were isolated from both H9c2 cardiomyocytes and NRCF cells and characterised via several methods which allowed for comparison between the two cell types. However, characterisation was limited by a number of factors, for example characterisation of H9c2 EVs via western immunoblot and BCA assay were completed with only low n numbers. NRCF EVs were not characterised via these methods at all meaning comparison between the two cell types was limited to only TEM and Nanosight analysis, as such, further characterisation would have been beneficial. EVs were also isolated from both WKY and SHRSP rat serum for characterisation and comparison, however in this case only via Nanosight and BCA assay, where continuity of methods (eg. analysis via TEM) may have been more apt.

3.6 Summary

EVs are released in abundance from the two cardiac cell types; H9c2 cardiomyocytes and NRCF cells. The data suggest that treatment of parental H9c2 or NRCF cells with Ang II does not affect the profile of EVs released from the cells in terms of either size or particle concentration. Furthermore, comparative analysis of H9c2 and NRCF-derived EVs showed that size profiles significantly differ between the two vesicle types, suggesting that they may be releasing different EV sub-populations. Comparative analysis of serum-derived EVs from WKY and SHRSP rats showed different size profiles between the two, as well as differences in total protein concentration. These observations suggest that EV profiles may change under pathological disease conditions, with relevance to chronic hypertension and cardiac dysfunction.

Chapter 4 The role of extracellular vesicles in the H9c2 cardiomyocyte model of Ang II-induced hypertrophy

4.1 Introduction

4.1.1 Modelling cardiomyocyte hypertrophy in cells

Cardiac hypertrophy involves the thickening of the ventricles of the heart and generally occurs as an adaptive response to chronically increased workload by the heart (Ruilope and Schmieder, 2008). As a response to increased mechanical load cardiomyocytes enlarge in order to both increase mass and reduce wall stress. Although the response is initially adaptive and reversible; over time it may become maladaptive leading to cardiomyocyte apoptosis and, ultimately, heart failure (Hunter and Chien, 1999). Due to the risks associated with the development of cardiac hypertrophy, the need for established disease models is crucial. Commonly, cultured cardiomyocytes are used to investigate the signalling mechanisms and cellular changes associated with the hypertrophic response and these cells are most often obtained from neonatal rat hearts (Bogoyevitch et al., 1995). Neonatal rat cardiomyocytes (NRCMs) have been established as a useful model for studying hypertrophic mechanisms in the cardiac setting; they have been shown to exhibit many cellular and molecular changes associated with hypertrophy such as cell size increase, actin filament reorganisation, increased collagen synthesis and upregulation of hypertrophy associated genes (Bogoyevitch et al., 1995). Despite this, there are various drawbacks to using NRCMs as a cell model; for example, the use requires the need for high numbers of animals in order to isolate cells; the cells have very low percentage viability after isolation; and the cells do not proliferate meaning new batches must be used in every experiment (Watkins et al., 2011). Similarly, adult rat ventricular myocytes (ARVMs) are also used in cell models of cardiovascular disease. ARVMs are also known to respond to hypertrophic stimuli and also express foetal hypertrophy marker genes upon stimulus with Ang II (Peter et al., 2016). These cells share the most similarities in terms of structural morphology (rod shaped, binucleated, and with a sarcomeric structure) and behaviour (contract under electrical stimulus) to cardiomyocytes in intact tissue and therefore present as an ideal model for cardiomyocyte-based research. However, when in culture, the ARVM phenotype changes over time and so most studies must be completed in the first 24 hours after isolation, which poses as a major limitation (Peter et al., 2016).

Due to the difficulties associated with the use of primary cardiomyocytes for cell hypertrophy models, a small number of cardiomyocyte cell lines have been established and have since been used extensively as alternatives for cell research in this area. One such cell line is the HL-1 line. HL-1 cells are a cardiac muscle cell line derived from mouse atrial tumours which, unlike primary cardiomyocytes, can be serially passaged (Claycomb et al., 1998). Despite this, it was found that these cells maintain their ability to contract as well as the phenotypic characteristics associated with adult cardiomyocytes such as morphological and biochemical properties, and gene expression profiles (Claycomb et al., 1998). Since being established, these cells have been used successfully in various studies of atrial fibrillation involving atrial cardiomyocyte hypertrophy (Hao et al., 2018, Kim et al., 2018b, Bloch et al., 2016).

4.1.2 The H9c2 cell model of cardiomyocyte hypertrophy

The second established cardiac cell line used for modelling cardiomyocyte hypertrophy is the H9c2 cell line, specifically H9c2(2-1) (Kimes and Brandt, 1976). These cells were initially derived from the embryonic heart tissue of the BDIX rat strain, and in contrast to HL-1 cells, they were derived from ventricular tissue (Kimes and Brandt, 1976) making them a more appropriate model for certain types of cardiac hypertrophy, such as hypertrophy caused by chronic hypertension which more commonly affects the ventricular muscles of the heart (Watkins et al., 2011). When initially establishing this cell line, several important observations regarding upkeep where made. It was found that H9c2 cells retained initial morphology for four months (approximately 20 passages) however after this time, multinucleated myotube-like cells began to present in cultures (Kimes and Brandt, 1976). It was also found that H9c2 cells propagate normally as a mononucleated myoblast, however upon reaching full confluence, the cells again begin to show quick overgrowth and formation of multinucleated tubular structures; conversely, growth inhibition occurred when H9c2 cells were plated at a low seeding density ($<5x10^4$ cells/dish) (Kimes and Brandt, 1976). As a result of these initial observations, all of these factors are generally taken into account when culturing H9c2 cardiomyocytes in order to maintain the cardiomyocyte phenotype.

Although H9c2 cardiomyocytes are no longer able to beat (a classical phenotype of NRCMs) they have been shown to exhibit many similarities to primary cardiomyocytes in terms of morphology, G-protein expression and electrophysiology (Hescheler et al., 1991, Sipido and Marban, 1991). It was found via lectin-binding studies that H9c2 cells exhibit a similar surface sugar residue profile to primary cardiomyocytes, and that transient potassium and calcium currents behaved similarly to characteristic cardiac currents (Hescheler et al., 1991, Sipido and Marban, 1991). Furthermore, signal-transducing G-proteins located in the cell membrane such as Gs alpha-subunits and Gi alpha-subunits characteristic of cardiomyocytes were also found to be expressed (Hescheler et al., 1991). Not only have H9c2 cells been shown to exhibit similar morphological, physiological and biochemical properties to primary cardiomyocytes, but it has also been shown that they respond in a similar manner when exposed to hypertrophic agents. For example, Transforming Growth Factor ß (TGF-ß) has been associated with the onset of hypertrophy in cardiomyocytes (Gray et al., 1998, Huang et al., 2004). It was found that stimulation of H9c2 cells with TGF-ß resulted in characteristic features of cardiomyocyte hypertrophy such as increase in cell size coinciding with rearrangement of actin filaments, and upregulation of atrial natriuretic peptide (ANP) expression, a common gene expression marker for hypertrophy (Huang et al., 2004). Similarly, it was shown that phenotypes associated with cellular hypertrophy could be induced in H9c2 cells by hydrogen peroxide stimulation (Zhou et al., 2007). Furthermore, it was found that overexpression of Myocyte Stress 1 (MS1) (an actin-binding protein upregulated in the early stages of left ventricular hypertrophy) could significantly increase cell size and reduce apoptosis in H9c2 cardiomyocytes (Koekemoer et al., 2009).

4.1.3 The Ang II-induced hypertrophy model

As described, cardiomyocytes are known to respond characteristically to a range of hypertrophic stimuli. Ang II is an important mediator of CVD pathophysiology with potent effects on hypertrophy, fibrosis and inflammation mainly via signalling through the AT_1R (Brilla et al., 1997, Bunkenburg et al., 1992). It has been previously reported across a variety of studies that stimulation of cardiomyocytes with Ang II results in a hypertrophic response. It was found that in cultured NRCMs, overexpression of the AT_1R via an adenoviral vector followed

by Ang II stimulation resulted in a characteristic hypertrophic response (Thomas et al., 2002, D'Amore et al., 2005). In this case, Ang II stimulation was reported to cause an increase in cell size accompanied by elevated expression of ANP associated with MAPK signalling (Thomas et al., 2002). It was also found that stimulation of NRCMs with Ang II resulted in cellular hypertrophy associated with increased signalling of ERK1/2, PLC Beta 3 and G alpha q/11 (Bai et al., 2004). Further studies have reinforced the hypertrophic effects of Ang II in cardiomyocytes. It was shown that stimulation of NRCMs with 1 μM Ang II significantly increased cell size over a 48 hr time period, along with 4-fold increase of beta-myosin heavy chain expression (ß-MHC) (another characteristic gene expression hypertrophy marker) and superoxide generation (Laskowski et al., 2006). Increased cardiac B-type Natriuretic Peptide (BNP) expression is also associated with cardiac hypertrophy where an *in vivo* study showed that stimulation of cardiac hypertrophy via Ang II infusion resulted in characteristic increased expression of BNP (Majalahti et al., 2007).

The Ang II hypertrophy model has been readily established in H9c2 cells and is often used as a control stimulus for induction of cellular hypertrophy. Commonly, Ang II is used as a control hypertrophic stimulus in studies investigating possible inhibitory molecules against cardiac hypertrophy. It has been shown that while investigating inhibition of hypertrophy with simvastatin, treatment with 100 nm Ang II over a 24 hr period results in H9c2 cell hypertrophy, as measured by protein expression of ANP and ERK1/2 (Guo et al., 2010). Studies involving antagonization of pro-hypertrophic signalling with Ang-(1-9) in H9c2 cells showed that Ang II stimulation resulted in a 1.2-fold increase in cell size along with upregulation of the hypertrophy markers; ANP, BNP and ß-MHC over a 96 hr period; these observations were also made using primary adult rabbit cardiomyocytes (Flores-Muñoz et al., 2011). Further studies investigating the protective role of VEGFB-VEGFR1 in cardiomyocyte hypertrophy showed that stimulation of H9c2 cells with 1 μM Ang II resulted in increased gene and protein expression of ß-MHC, BNP and ANP along with characteristic increase in cell size over a 48 hr period (Shen et al., 2018). Autophagy studies investigating the inhibitory effects of WenxinKeli (WXKL) in Ang II-induced hypertrophy showed significant increase in length and width of cells following stimulation of H9c2 cells with 10 M Ang II over a 24 hr period (Li et al., 2017) Furthermore, while

studying the protective role of Stat-3, a significant increase in cell size was observed following stimulation with 5 μM Ang II over 12, 24 and 48 hr periods (Chen et al., 2017).

The studies briefly described above are only a few of those using Ang II as a pro-hypertrophic stimulus in H9c2 cells. Taken together it has been shown that a range of Ang II concentrations across varying time points are able to induce cellular hypertrophy in H9c2 cardiomyocytes, with as little as 100 nM treatment over 24 hr (Guo et al., 2010) to 10 M treatment over 24 hr (Li et al., 2017) generating characteristic changes in cell size, hypertrophy marker gene expression and hypertrophy marker protein expression.

4.1.4 Extracellular vesicle signalling in cardiomyocyte hypertrophy

More recently, studies have begun to report the effects of EVs on cardiomyocyte hypertrophy. One study investigating cell:cell communication in the heart found that cardiac fibroblasts release EVs enriched with miRNAs which potently induce cardiomyocyte hypertrophy (Bang et al., 2014). This study found that NRCF cells release exosomes enriched with miR-21, a previously described inducer of cardiomyocyte hypertrophy (Thum et al., 2007, Thum et al., 2008, Bang et al., 2014), which are able to elicit hypertrophic effects in NRCMs. Fluorescent labelling of exosomes showed transfer between NRCFs and NRCMs, and following incubation, a significant increase in cardiomyocyte cell size was observed (Bang et al., 2014) suggesting a role for EVs in hypertrophic signalling between cardiac cells. Furthermore, it was also shown that after inflammatory stimulation by TNF-α, NRCF cells secreted miRNA-enriched exosomes which may then be incorporated by H9c2 cardiomyocytes (Tian et al., 2018). This incorporation resulted in upregulation of the hypertrophy markers ANP and ß-MHC in an Nrf2 (nuclear factor erythroid 2-related factor 2) dependent manner, a signalling molecule closely linked to oxidative stress-mediated cardiac remodelling (Tian et al., 2018). Further studies showed that exposure of NRCF cells to Ang II resulted in increased production of EVs which are then able to elicit characteristic hypertrophic effects in NRCMs, including increased cell size, increased ^{3}H-leucine uptake, and increased gene expression of the hypertrophy markers ANP, BNP and ß-MHC (Lyu et al., 2015), effects which seemed to mirror

those of exogenous Ang II treatment. Other detrimental effects in the cardiac setting have also been observed in relation to EV signalling. It was found that cultured adult rat cardiomyocytes under hypoxic challenge released exosomes containing Hsp60 which were able to elicit inflammatory responses in cardiomyocytes, as well as increase cardiomyocyte apoptosis (Gupta and Knowlton, 2007), similar findings were observed in the H9c2 cardiomyocyte cell line (Tian et al., 2013). Further studies in this area showed that EV secretion in cardiomyocytes is linked to their particular microenvironment at the time, for example whether cells were under stress or not, such as hypoxic vs. normoxic conditions, and that the EVs released under each condition could elicit different effects in recipient cells (Malik et al., 2013, Ribeiro-Rodrigues et al., 2017).

Together, these studies suggest an important role for EVs in terms of hypertrophic signalling in the heart. Studies suggest involvement of EVs in communication between cardiac fibroblasts and cardiomyocytes, and between cardiomyocytes and cardiomyocytes not only in terms of hypertrophic signalling but also other pathological outcomes such as cardiomyocyte apoptosis and oxidative stress, however the involvement of the RAS here remains to be investigated.

4.2 Aims

- To determine Ang II levels within EVs isolated from H9c2 cardiomyocytes +/- Ang II treatment.

- To assess the ability of proteinase K to remove any contaminating Ang II not enclosed within EVs.

- To assess the effects of EVs isolated from Ang II stimulated H9c2 cardiomyocytes on the hypertrophy of recipient H9c2 cardiomyocytes.

- To determine the effects of EVs isolated from Ang II stimulated NRCF cells on the hypertrophy of H9c2 cardiomyocytes.

4.3 Key Methods

Table 4-1 Chapter 4 key methods

EV isolation	Cell culture media Section 2.6
	Proteinase k treatment Section 2.6.1
Ang II detection within EVs	Co-localisation analysis Section 2.6.2
	Ang II ELISA Section 2.11
Assessment of H9c2 hypertrophy	Hypertrophy assay Section 2.5.7
	Gene expression analysis Section 2.8

4.3.1 Cell work methodology schematic

A schematic representation of the work flow plan for the altered H9c2 hypertrophy model (Flores-Muñoz et al., 2012) used in section 4.4.4 to determine the effects of Ang II EVs on cellular hypertrophy is shown in Figure 4-1. The full protocols are described in section 2.5.7.

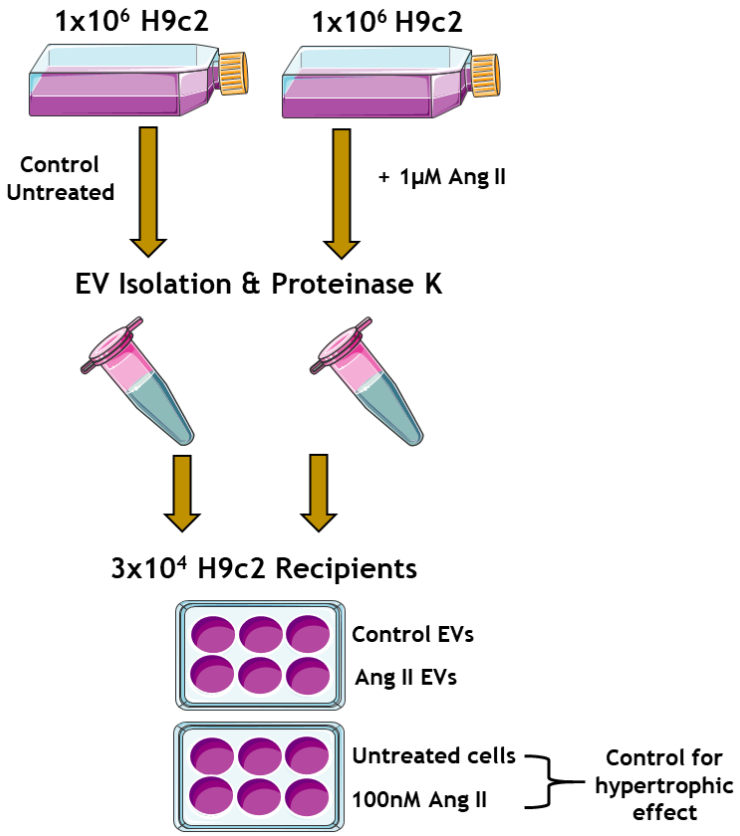

Figure 4-1 Schematic representation of the work flow plan for investigating the effects of Ang II signalling via EVs in the H9c2 model of cardiomyocyte hypertrophy.

4.4 Results

4.4.1 Localisation of extracellular vesicles in H9c2 cells

In order to determine successful uptake of EVs into H9c2 cells, fluorescent labelling techniques were utilised. H9c2 cardiomyocytes were either untreated or treated with 1 μM Ang II in serum-free media over a 48 hr period and EVs were isolated (control EVs or Ang II EVs, respectively) from the resulting conditioned media. Isolated EVs were then stained with PKH26 (red) before being placed onto recipient H9c2 cardiomyocytes. After 1 hr of incubation, recipient cells were fixed and stained to observe localisation of EVs within the cells.

Image analysis showed that PKH26-stained control EVs derived from H9c2 cells localised to the recipient cell nucleus after 1 hr of incubation (Figure 4-2 A). Similarly, Ang II EVs stained with PKH26 were also found to be associated with the recipient cell nucleus after 1 hr (Figure 4-2 B). It was observed that PKH26-stained EVs localise to most, but not all, of the cell nuclei imaged for each condition at this time point (Figure 4-2).

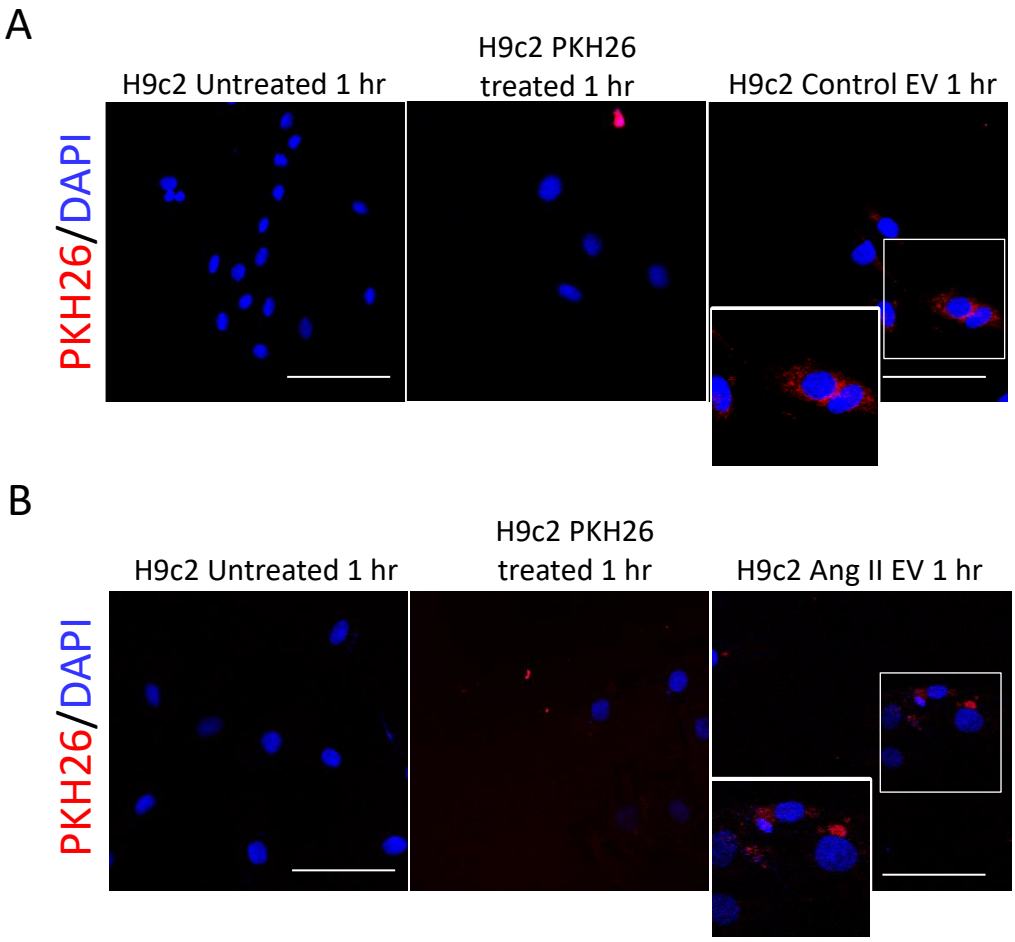

Figure 4-2 EVs derived from H9c2 +/- Ang II treatment localise to the recipient cell nucleus. (A) Localisation of PKH26-stained control EVs in recipient H9c2 cardiomyocytes. (B) Localisation of PKH26-stained Ang II EVs in recipient H9c2 cardiomyocytes (scale bar: 100 μm). Representative images of n=3.

4.4.2 Detection of Ang II within extracellular vesicles

To determine whether Ang II was detectable within EVs, co-localisation analysis of the peptide and EVs was carried out. H9c2 cardiomyocytes were either untreated or treated with 1 μM FAM-labelled Ang II (green). EVs isolated from the conditioned media were then stained with PKH26 (red) and placed onto recipient H9c2 cardiomyocytes. The recipient H9c2 were then fixed and stained to determine localisation of the two labels within the cell.

Following a 1 hr incubation, EVs were visibly associated with the recipient cell and co-localisation of FAM and PKH26 could be detected in the H9c2 cardiomyocytes treated with EVs derived from FAM-Ang II stimulated H9c2 cells (Figure 4-3 A), while in recipient cells treated with control EVs, only PKH26 was detected (Figure 4-3 B). Co-localisation analysis and comparison of the control and FAM-Ang II images were carried out via Pearson's coefficient R which showed significant overlap of FAM and PKH26 in the FAM-Ang II EV treated cells compared to the control EV treated cells, where the FAM signal was not present (control 0.003 ± 0.002 vs. Ang II 0.605 ± 0.177, $p<0.05$) (Figure 4-3 C). Further co-localisation analysis was carried out using Mander's coefficient M1 which again showed significant co-localisation of FAM-Ang II and PKH26-labelled EVs (control 0.0004 ± 0.0003 vs. Ang II 0.612 ± 0.135, $p<0.05$) (Figure 4-3 D) and Mander's coefficient M2 which showed similar results (control 0.033 ± 0.027 vs. Ang II 0.618 ± 0.199, $p<0.05$) (Figure 4-3 E).

Ang II levels within EVs were also detected by ELISA (Figure 4-4). EVs derived from H9c2 cardiomyocytes +/- 1 μM Ang II treatment were lysed and Ang II content was determined by high-sensitivity Ang II ELISA. It was found that Ang II could be detected at low levels within EVs derived from control cells; approximately 10.51 ± 6.29 pg/mL Ang II detected. However, when parental cells had been stimulated with Ang II this level increased to approximately 27.50 ± 11.45 pg/mL ($n=7$, $p=0.015$; Wilcoxon matched pairs test) (Figure 4-4).

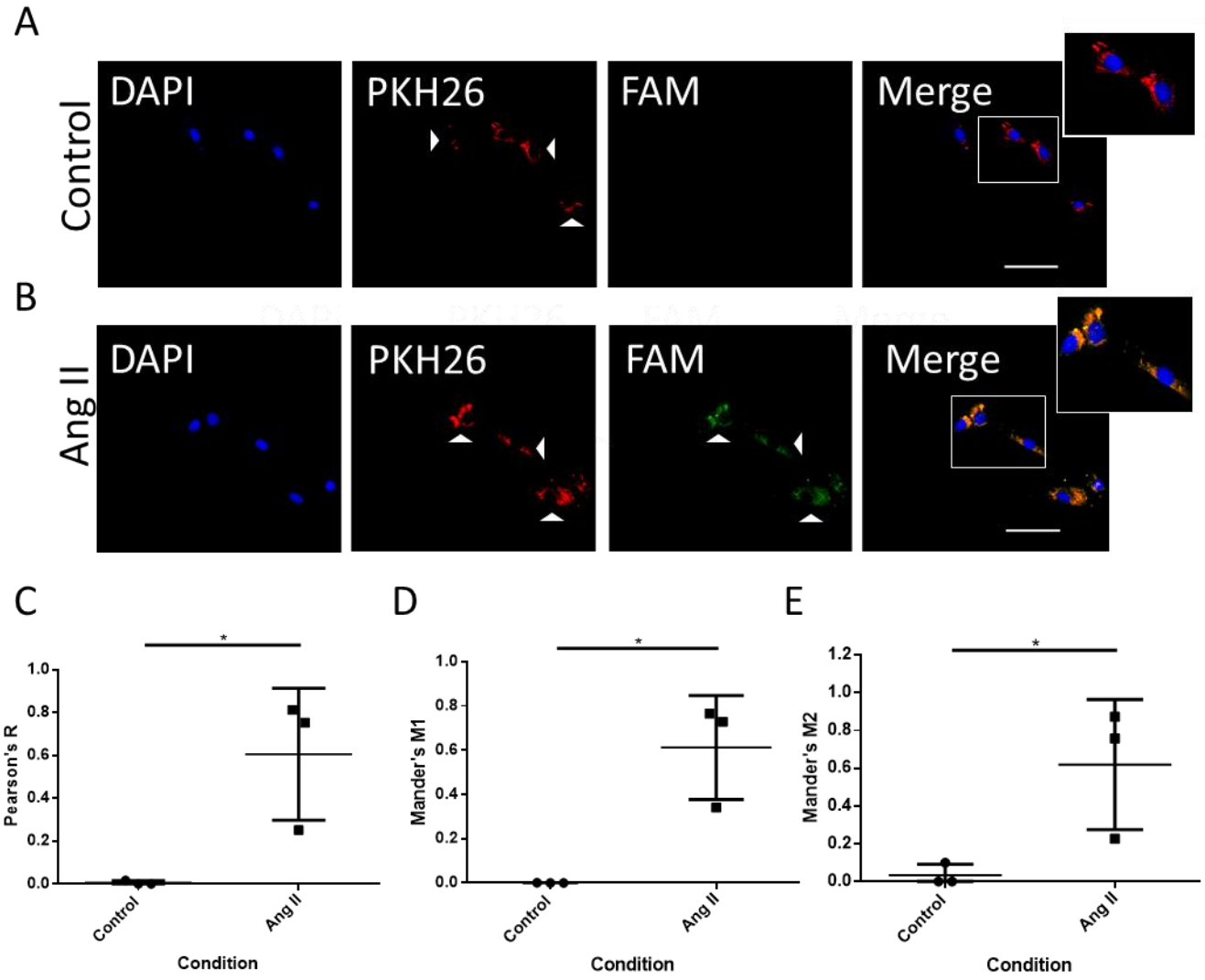

Figure 4-3 Co-localisation of FAM-labelled Ang II and PKH26-labelled EVs. (A) Representative panel of localisation of control EVs to the recipient cell nucleus (scale bar: 100 µm). (B) Representative panel of co-localisation of FAM-Ang II and PKH26-EVs to the recipient cell nucleus. (C) Co-localisation analysis by Pearson's coefficient R (n=3, *p<0.05, Student's t-test). (D) Co-localisation analysis by Mander's coeffiecients M1 (n=3, *p<0.05, Student's t-test) and (E) M2 (n=3, *p<0.05, Student's t-test).

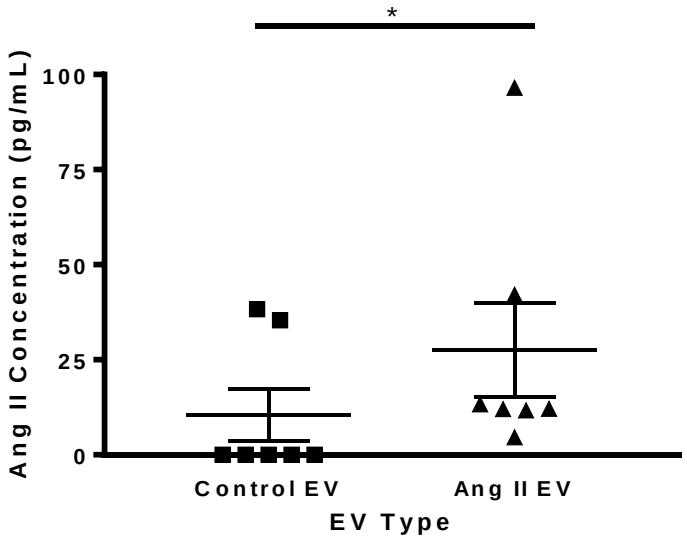

Figure 4-4 Detection of Ang II within H9c2-EVs by ELISA. Detection of Ang II levels within control EVs and Ang II EVs by high-sensitivity ELISA (n=7, *p<0.05; Wilcoxon matched pairs test).

4.4.3 Proteinase K treatment depletes soluble Ang II

In order to prevent the effects of any contaminating exogenous Ang II peptide, proteinase K treatment was utilised to deplete any excess from EV isolations. Initially, Ang II stocks were treated with proteinase K to determine whether or not proteinase K could effectively digest this peptide. Next, the concentration that remained was tested to determine whether it could initiate a hypertrophic response in H9c2 cardiomyocytes.

Ang II stocks of 1 μM concentration were either untreated or digested with proteinase K and Ang II levels for both conditions were determined by high-sensitivity Ang II ELISA. Data showed that the concentration of undigested Ang II was 137.4±0.7 pg/mL compared with 2.8±0.9 pg/mL for exogenous Ang II treated with proteinase K, suggesting successful digestion of the peptide ($n=3$, $p<0.001$) (Figure 4-5 B). The remaining concentration of Ang II post-digestion with proteinase K; 2.8±0.9 pg/mL, was calculated to be the equivalent of approximately 0.0013 nM Ang II.

Upon the observation that proteinase K digestion depletes soluble Ang II stocks to a concentration of approximately 0.0013 nM, treatment with this concentration was investigated in H9c2 cardiomyocytes to determine whether it was sufficient to elicit a hypertrophic response (Figure 4-5 A & C). H9c2 cardiomyocytes were left untreated or treated with 0.0013 nM soluble Ang II or 100 nM Ang II (+ve control) and cells were imaged for sizing analysis. Representative images of H9c2 cardiomyocytes for each group are shown in Figure 4-5 A. The data showed the average size of control H9c2 cardiomyocytes to be 3234.0±41.6 μm^2 vs. 6071.0±93.9 μm^2 for 100 nM Ang II treated and 3255.0±32.7 μm^2 for 0.0013 nM Ang II treated (Figure 4-5 C). There was no significant difference in cell size between control cells and 0.0013 nM Ang II treated cells, however stimulation with 100 nM Ang II significantly increased cell size compared to control cells and 0.0013 nM Ang II treated cells ($n=3$ per group, $p<0.001$) (Figure 4-5 C).

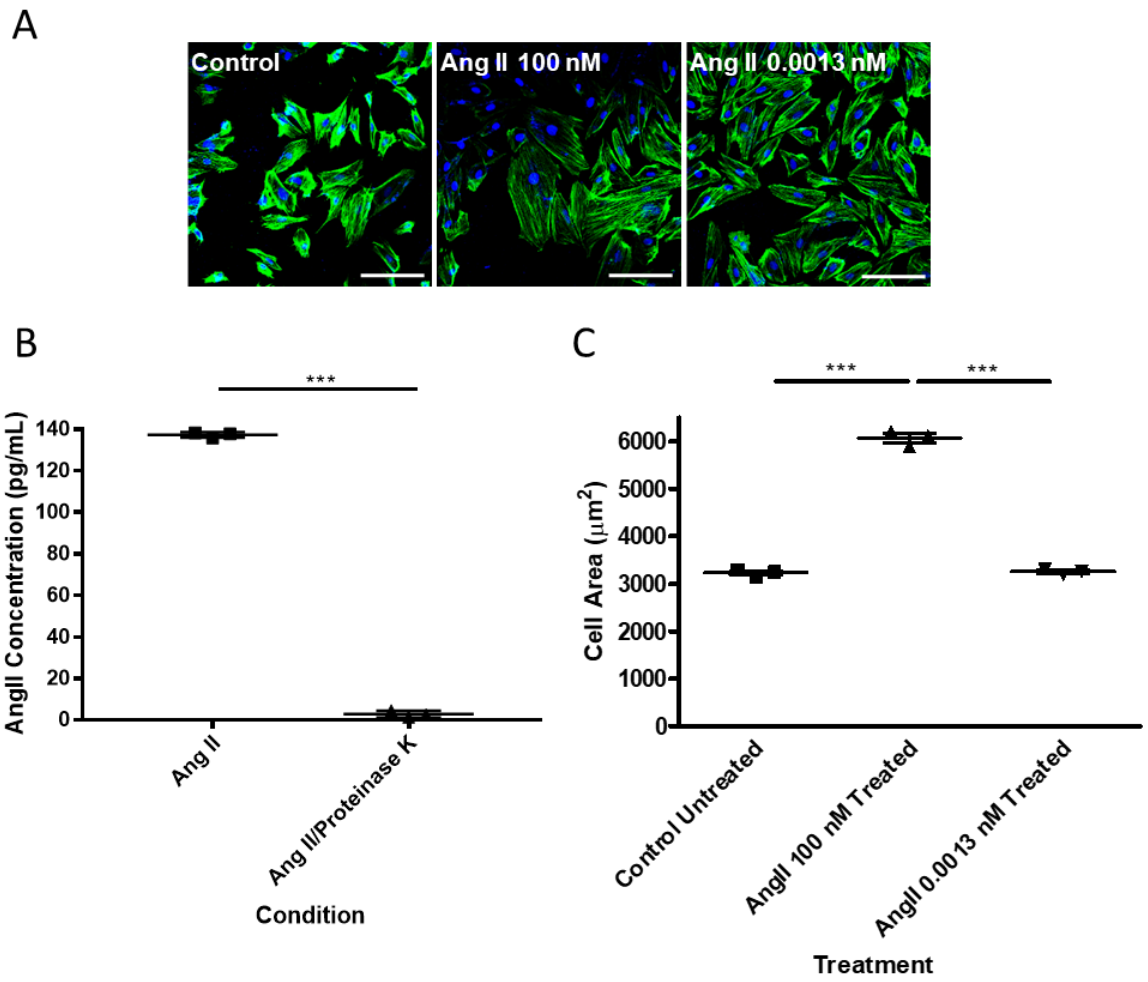

Figure 4-5 Proteinase K digestion efficiently depletes soluble Ang II. (A) Representative images of H9c2 cardiomyocytes under each condition (Scale: 100 μm). (B) ELISA detecting Ang II levels +/- proteinase K treatment (n=3, ***p<0.001, Student's t-test). (C) Assessment of cell size in H9c2 cardiomyocytes under each condition (n=3, ***p<0.001, one-way ANOVA).

4.4.4 Assessment of hypertrophy in H9c2 cardiomyocytes treated with H9c2-derived extracellular vesicles

H9c2 cardiomyocytes were either untreated or treated with 1 μM Ang II over a 48 hr period, EVs were then isolated from the resulting conditioned media, treated with proteinase K, and placed onto recipient H9c2 cardiomyocytes; untreated cells and 100 nM Ang II stimulated cells were used as controls for the hypertrophic response. Cells were then either imaged in order to determine any changes in cell size or used for gene expression analysis to determine changes in hypertrophy marker expression (Figure 4-6).

The data showed that stimulation with 100 nM Ang II induced a significant hypertrophic response in terms of cell size compared with controls. Representative images for each treatment group are shown in Figure 4-6 A. Control untreated cells were found to have an area of 3710.0±200.9 μm^2 vs. 6475.0±123.6 μm^2 for 100 nM Ang II stimulated cells (n=3, $p<0.001$) (Figure 4-6 B). No significant difference was observed between control untreated cells and control EV treated cells, however Ang II EV treatment significantly increased cell area compared with both controls (control untreated; 3710.0±200.9 μm^2 and control EV treated; 3368.2±84.0 μm^2 vs. Ang II EV treated; 6202.2±97.7 μm^2 (n=3, $p<0.001$)) (Figure 4-6 B) suggesting that the EVs are able to elicit a hypertrophic response in H9c2 cardiomyocytes.

The hypertrophic response was further investigated by gene expression analysis for the established hypertrophy marker BNP. It was found that in the controls for hypertrophic response, treatment with 100 nM Ang II significantly increased BNP gene expression compared with control untreated cells, with a 5.3-fold increase in expression observed (n=4, $p<0.05$) (Figure 4-6 C). It was also observed that treatment of H9c2 cardiomyocytes with Ang II EVs significantly increased the expression of BNP compared to cells treated with control EVs, with a 3.6-fold increase in expression observed (n=4, $p<0.05$) (Figure 4-6 C) again suggesting that EVs derived from Ang II stimulated H9c2 cardiomyocytes are able to elicit a hypertrophic response in recipient H9c2 cardiomyocytes.

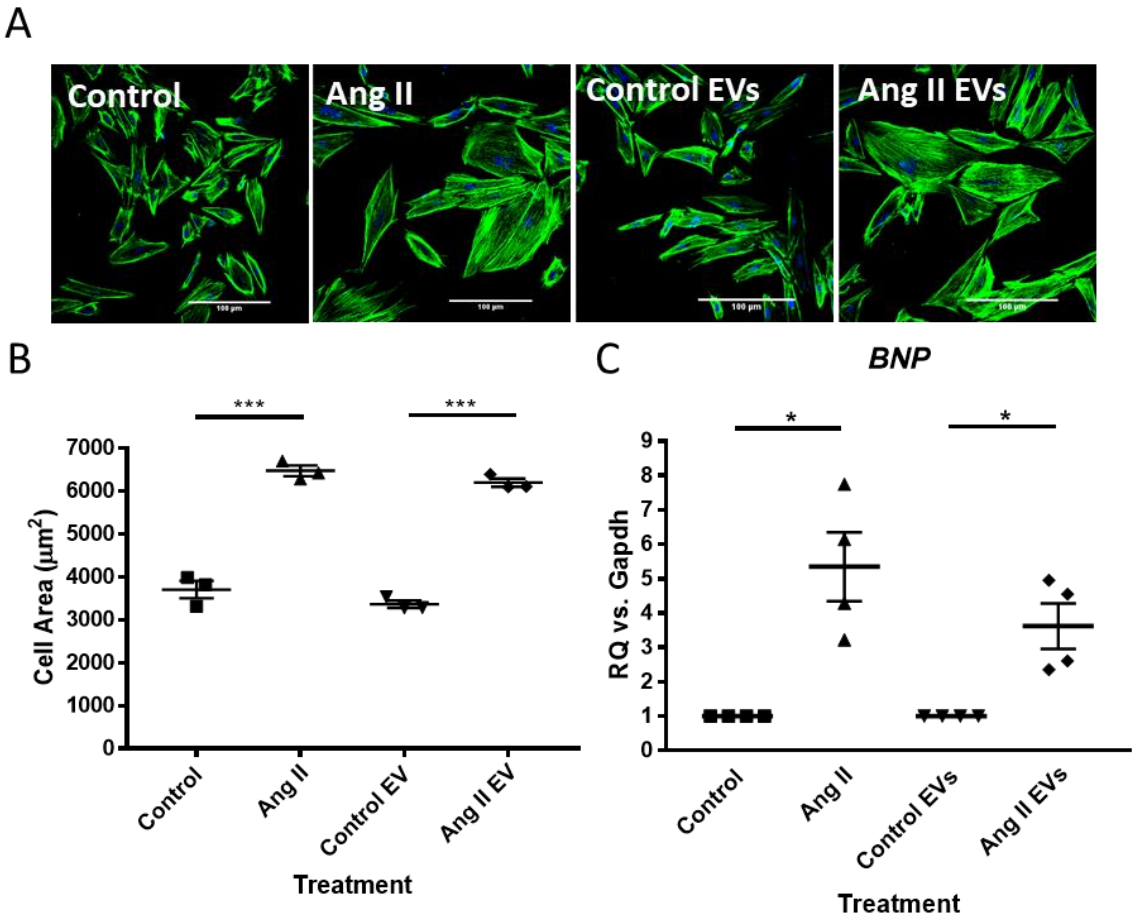

Figure 4-6 Assessment of cellular hypertrophy in H9c2 cardiomyocytes treated with H9c2-derived EVs. (A) Representative confocal images of H9c2 cardiomyocytes in each treatment group (Scale: 100 μm). (B) Analysis of H9c2 cardiomyocyte cell size under each condition (n=3, ***p<0.001, one-way ANOVA). (C) Analysis of BNP gene expression in H9c2 cardiomyocytes under each condition (n=3, *p<0.05, one-way ANOVA).

4.4.5 Effect of extracellular vesicles derived from H9c2 +/- Ang II on RAS gene expression

As EVs derived from Ang II-stimulated H9c2 cardiomyocytes were able to induce hypertrophy in recipient H9c2 cardiomyocytes, and Ang II was detectable within these EVs, it was of interest to determine whether treatment of H9c2 cardiomyocytes with Ang II EVs would drive any changes in expression of RAS-related genes. H9c2 cardiomyocytes were either untreated, treated with 100 nM Ang II, treated with control EVs, or treated with Ang II EVs over 48 hr. Expression of the genes AT_1R, AT_2R, and MAS were then analysed in the recipient cells.

When normalised to control untreated cells, it was found that treatment with Ang II did not significantly alter the expression of either the AT_1R, AT_2R, or MAS genes (MAS; n=4, AT_1R; n=5, AT_2R; n=5) (Figure 4-7 A, B & C). Similarly, it was found that treatment with control EVs or Ang II EVs did not significantly change the expression of the AT_1R, AT_2R, or MAS genes (MAS; n=4, AT_1R; n=5, AT_2R; n=5) (Figure 4-7 A, B & C). Data was also analysed to compare control EV treatment with Ang II EV treatment (Figure 4-7 D, E & F) for each of the genes of interest. It was found that Ang II EV treatment did not significantly change the expression of either the AT_1R, AT_2R, or MAS genes when normalised to control EV treated H9c2 cardiomyocytes (MAS; n=4, AT_1R; n=5, AT_2R; n=5) (Figure 4-7 D, E & F).

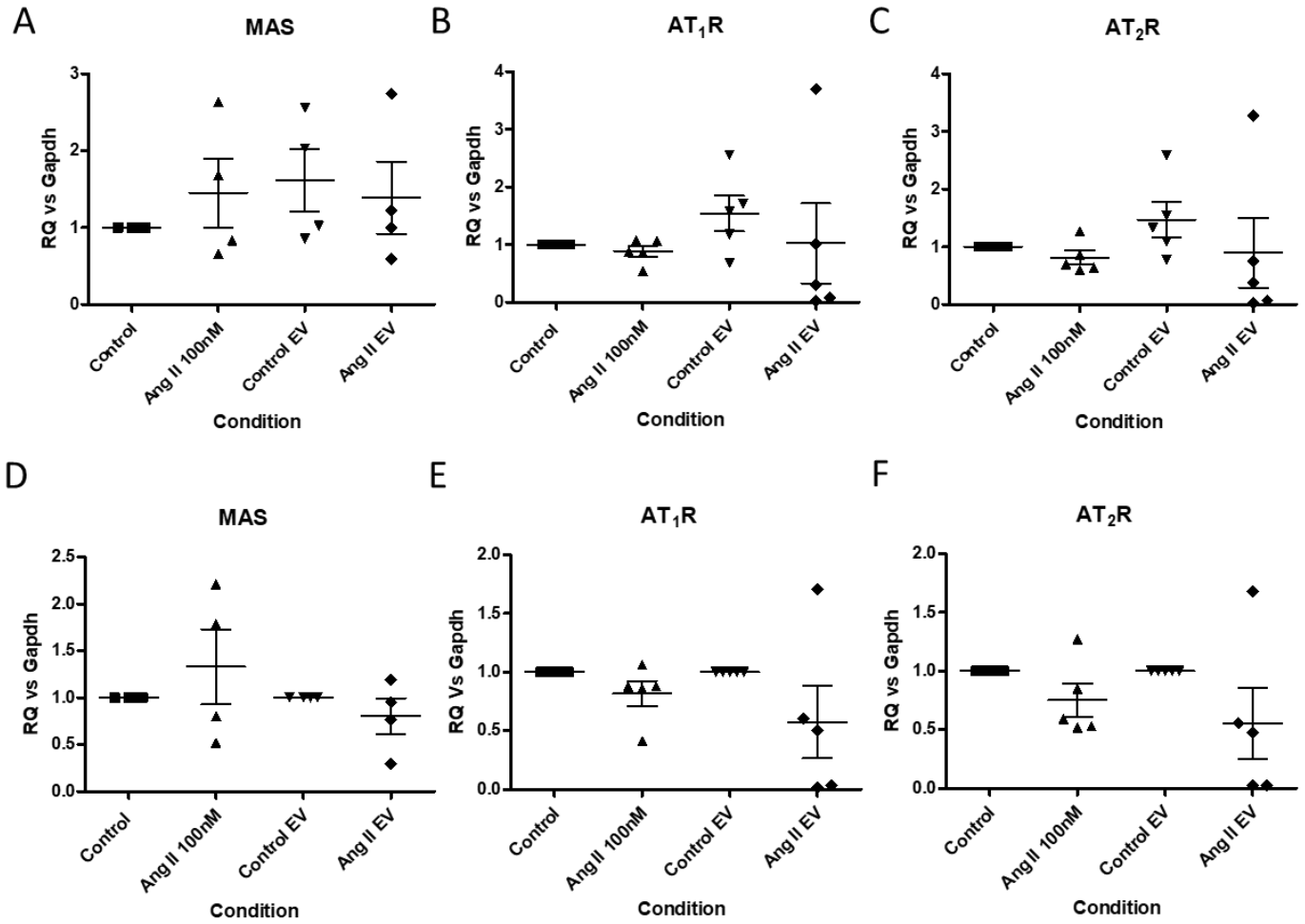

Figure 4-7 Analysis of RAS gene expression in H9c2 cardiomyocytes treated with EVs. (A) MAS, (B) AT_1R and (C) AT_2R gene expression analysis with treatment groups normalised to control untreated H9c2 cardiomyocytes. (D) MAS, (E) AT_1R and (F) AT_2R gene expression analysis with Ang II EV treated normalised to control EV treated H9c2 cardiomyocytes (MAS; n=4, AT_1R; n=5, AT_2R; n=5).

4.4.6 Investigating the role of the AT_1R: pre-blocking of parental H9c2 cardiomyocytes with losartan

To determine any involvement of the AT_1R in Ang II EV-induced hypertrophy, the effects of pre-blocking with losartan were investigated. Parental H9c2 cells were treated with 10 μM losartan (Flores-Muñoz et al., 2011) prior to stimulation with 1 μM Ang II. EVs were isolated from the resulting conditioned media and analysed by NTA to determine whether pre-blocking of parental cells with losartan would affect the size or concentration of particles released by the cells. EVs were then placed onto recipient H9c2 cardiomyocytes to determine effects on Ang II EV-induced hypertrophy.

Representative size and concentration NTA tracks for control EVs, Ang II EVs, control/losartan EVs and Ang II/losartan EVs are shown in Figure 4-8 A, B, C & D. NTA analysis showed no significant differences in EV size when parental H9c2 cardiomyocytes were pre-blocked with losartan for either control or Ang II stimulated cells (control EVs; 172.1±1.7 nm, Ang II EVs; 171.1±1.4 nm, control/losartan EVs; 172.1±2.5 nm, Ang II/losartan EVs; 174.7±0.9 nm) (n=6, p=0.52) (Figure 4-8 E). In this experiment, analysis of particle concentration showed a significant increase in Ang II stimulated cells vs. control cells (control untreated; $4.5x10^8±3.04x10^7$ particles/mL vs. Ang II stimulated; $7.3x10^8±6.5x10^7$ particles/mL) (n=6, $p<0.01$) (Figure 4-8 F). Similarly, a significant difference in particles released was observed between control/losartan EVs and Ang II/losartan EVs (control/losartan EVs; $4.9x10^8±4.1x10^7$ particles/mL vs. Ang II/losartan EVs; $8.9x10^8±3.2x10^7$ particles/mL) (n=6, $p<0.001$) (Figure 4-8 F). However, no significant difference was observed between control EVs vs. control/losartan EVs or Ang II EVs vs. Ang II/losartan EVs suggesting the effect observed is not related to the pre-blocking of parental cells.

The effects of these EVs on H9c2 cardiomyocyte hypertrophy were investigated via cell sizing analysis. Representative images for each condition are shown in Figure 4-9 A. It was found in the hypertrophy stimulus controls that 100 nM Ang II stimulation caused a significant increase in cell size compared with control untreated cells (control untreated; 2936.0±198.2 μm^2 vs. 100 nM Ang II treated; 5680.0±126.2 μm^2) (n=3, $p<0.001$). It was also shown that co-treatment with 100 nM Ang II and 10 μM losartan prevented this hypertrophic response (100 nM Ang II

treated; 5680.0±126.2 μm^2 vs. 100 nM Ang II/10 μM losartan treated; 3302.0±251.2 μm^2) (n=3, p<0.001). As shown previously, treatment with Ang II EVs significantly increased cell size compared to treatment with control EVs (control EV treated; 3031.0±236.2 μm^2 vs. Ang II EV treated; 5514.0±98.06 μm^2) (n=3, p<0.001). Interestingly, it was found that pre-treating parental H9c2 cardiomyocytes with losartan abolished the pro-hypertrophic effects observed with treatment of Ang II EVs, where the increase in cell size was significantly attenuated (Ang II EV treated; 5514.0±98.06 μm^2 vs. Ang II/losartan EV treated; 3223.0±299.9 μm^2) (n=3, p<0.01). There were also no significant differences observed between control/losartan EV treated cells and Ang II/losartan EV treated cells (control/losartan EV treated; 2959±179.1 μm^2 vs. Ang II/losartan EV treated; 3223.0±299.9 μm^2) (n=3, p=0.49) (Figure 4-9 B).

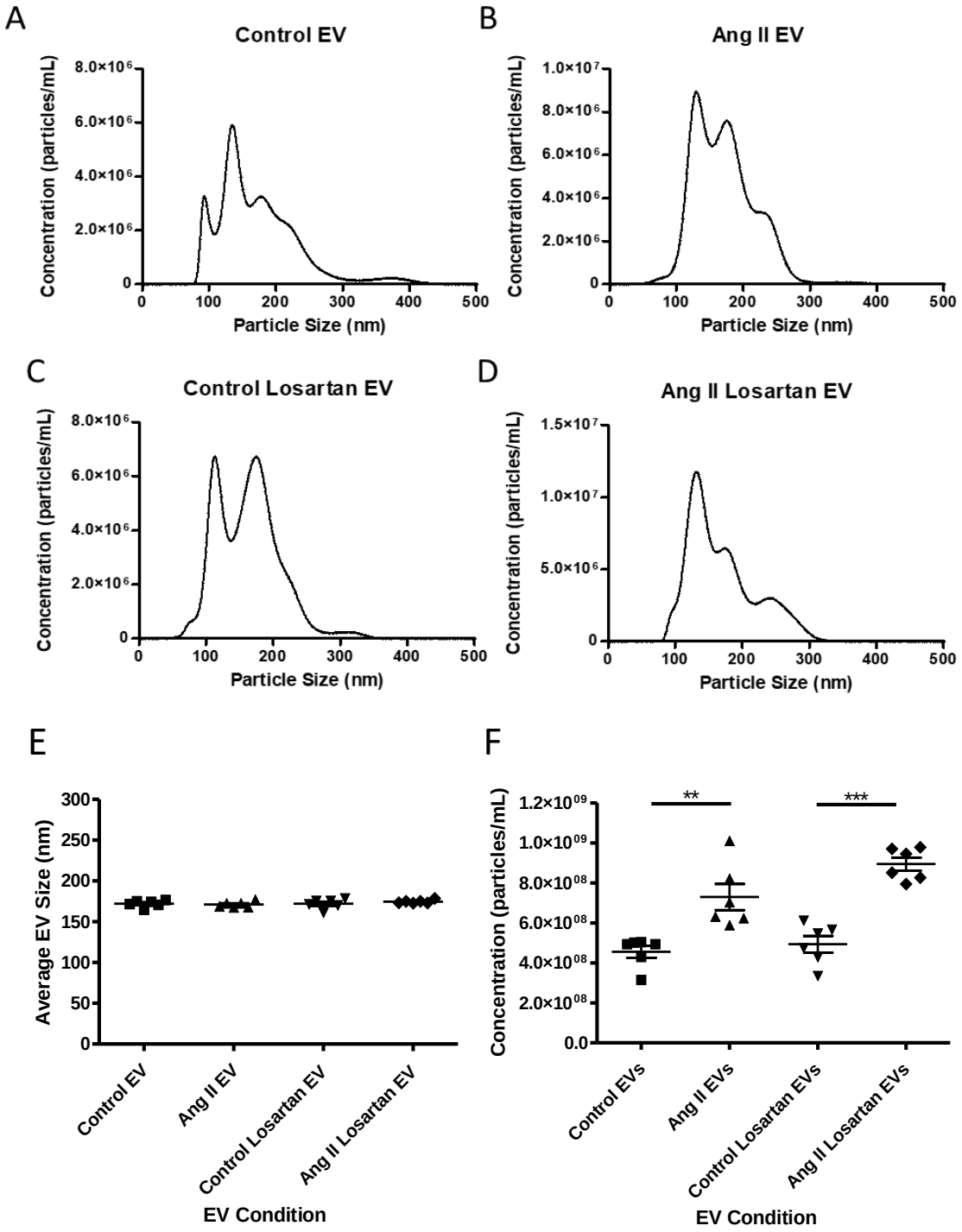

Figure 4-8 Analysis of losartan pre-blocking on EV size and release from H9c2 cardiomyocytes. (A) Representative size and concentration NTA tracks for control EVs, (B) Ang II EVs, (C) control/losartan EVs and (D) Ang II/losartan EVs. (E) Nanosight NTA comparison of EV size between conditions (n=6). (F) Nanosight NTA comparison of particle concentration between conditions (n=6, **p<0.01, ***p<0.001, one-way ANOVA).

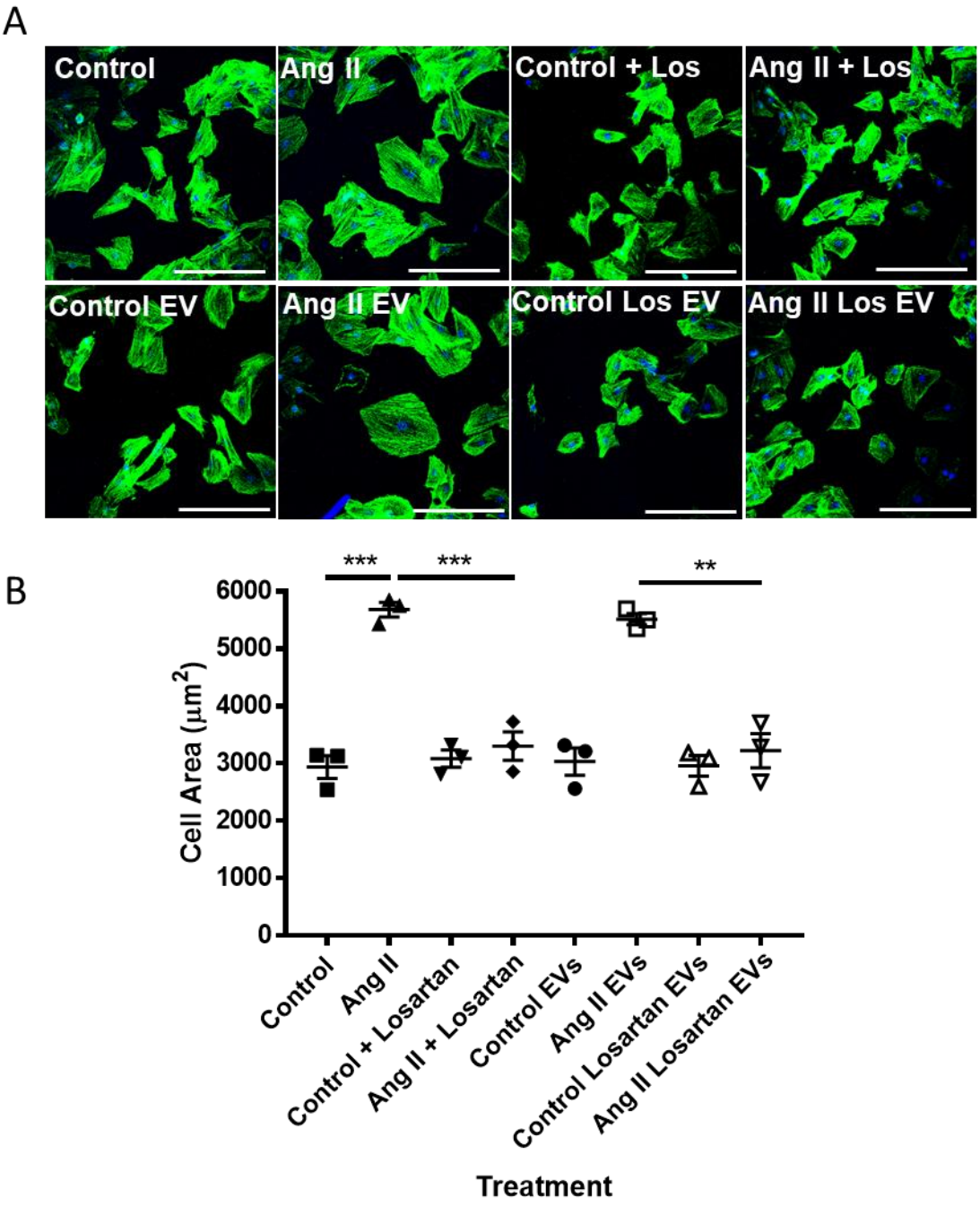

Figure 4-9 Analysis of cell size in H9c2 cardiomyocytes treated with EVs derived from losartan pre-blocked cells. (A) Representative confocal images of H9c2 cardiomyocytes under each treatment condition (Scale: 100 μm). (B) Analysis of H9c2 cardiomyocyte cell size under each condition (n=3, **p<0.01, ***p<0.001, one-way ANOVA).

4.4.7 Investigating the role of the AT_2R: pre-blocking of parental H9c2 cardiomyocytes with PD123,319

Next, in order to investigate the involvement of the AT_2R in the hypertrophic response induced by Ang II EVs, pre-blocking with PD123,319 was performed. Parental H9c2 cardiomyocytes were treated with 10 μM PD123,319 (Flores-Muñoz et al., 2011) prior to stimulation with 1 μM Ang II. Conditioned media was then collected and isolated EVs were analysed by NTA to first determine whether pre-blocking parental cells with PD123,319 would affect the size or concentration of particles released by the cells. EVs were then placed onto recipient H9c2 cardiomyocytes to deduce any effects on the previously established hypertrophic response.

Isolated EVs were analysed by NanoSight NTA and representative size and concentration tracks for control EVs, Ang II EVs, control/PD123,319 EVs and Ang II/PD123,319 EVs are shown in Figure 4-10 A, B, C & D. Analysis by Nanosight showed no significant differences in EV size when parental H9c2 cardiomyocytes were pre-blocked with PD123,319 for either control or Ang II-stimulated cells (control EVs; 161.2±3.9 nm, Ang II EVs; 159.7±5.5 nm, control/PD123,319 EVs; 180.2±4.1 nm, Ang II/PD123,319 EVs; 166.1±4.9 nm) (n=6, p=0.82) (Figure 4-10 E). Similarly, no significant differences in concentration of particles released were observed between groups when parental cells were pre-blocked with PD123,319 (control EVs; $3.8x10^8±3.6x10^7$ particles/mL, Ang II EVs; $3.6x10^8±2.9x10^7$ particles/mL, control/PD123,319 EVs; $3.6x10^8±6.2x10^6$ particles/mL, Ang II/PD123,319 EVs; $3.8x10^8±3.6x10^7$ particles/mL) (n=6, p=0.90) (Figure 4-10 F). These data suggest that pre-blocking of parental cells with PD123,319 does not affect size or concentration of particles released.

The effects of EVs released from PD123,319 pre-blocked H9c2 cardiomyocytes were then investigated via cell sizing analysis in recipient cells. Representative images for each condition are shown in Figure 4-11 A. As expected, it was observed in the hypertrophy stimulus controls that 100 nM Ang II stimulation caused a significant increase in cell area compared with control untreated cells (control untreated; 3230.0±263.1 μm^2 vs. 100 nM Ang II treated; 5882.0±211.9 μm^2) (n=3, p<0.001) (Figure 4-11 B). It was observed that co-treatment with 100 nM Ang II and 10 μM PD123,319 caused no significant difference in cell area when

compared to stimulation with 100 nM Ang II (100 nM Ang II treated; 5882.0±211.9 μm^2 vs. 100 nM Ang II/10 μM PD123,319 treated 6008.0±231.1 μm^2) (n=3, p=0.70) suggesting that PD123,319 could not prevent the hypertrophic response caused by soluble Ang II stimulation (Figure 4-11 B). Treatment with Ang II EVs effectively and significantly increased cell area compared to treatment with control EVs, as observed in previous experiments (control EVs; 3367.0±270.1 μm^2 vs. Ang II EVs; 5314.0±224.0 μm^2) (n=3, $p<0.001$). The data also showed that pre-blocking parental H9c2 cardiomyocytes with PD123,319 did not affect the ability for Ang II EVs to induce a hypertrophic response in recipient cells, where no significant difference was observed in cell size between Ang II EV treated and Ang II/PD123,319 EV treated cells (Ang II EVs; 5314.0±224.0 μm^2 vs. Ang II/PD123,319 EVs; 5022±269.1 μm^2) (n=3, p=0.45). Ang II/PD123,319 EVs also significantly increased cell size compared to control/PD123,319 EVs (control/PD123,319 EVs; 3331.0±199.7 μm^2 vs. Ang II/PD123,319 EVs; 5022±269.1 μm^2) (n=3, $p<0.01$) (Figure 4-11 B). Together, these data suggest that when pre-blocking parental H9c2 cardiomyocytes with PD123,319, EVs derived from Ang II stimulated cells are still able to initiate a hypertrophic response in recipient H9c2 cardiomyocytes.

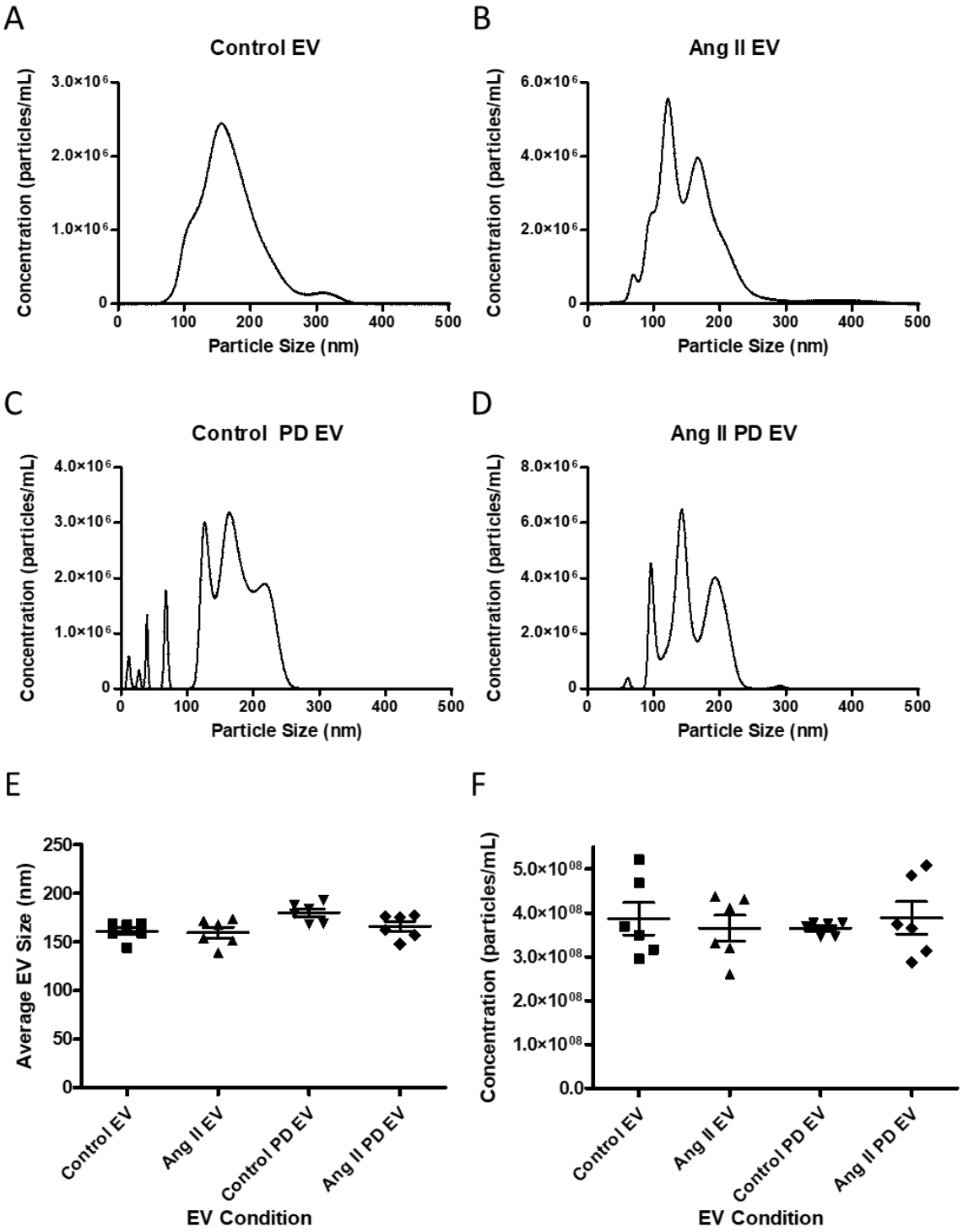

Figure 4-10 Analysis of PD123319 pre-blocking on EV size and release from H9c2 cardiomyocytes. (A) Representative size and concentration NTA tracks for control EVs, (B) Ang II EVs, (C) control/PD123319 EVs and (D) Ang II/PD123319 EVs. (E) Nanosight NTA comparison of EV size between conditions (n=6). (F) Nanosight NTA comparison of particle concentration between conditions (n=6).

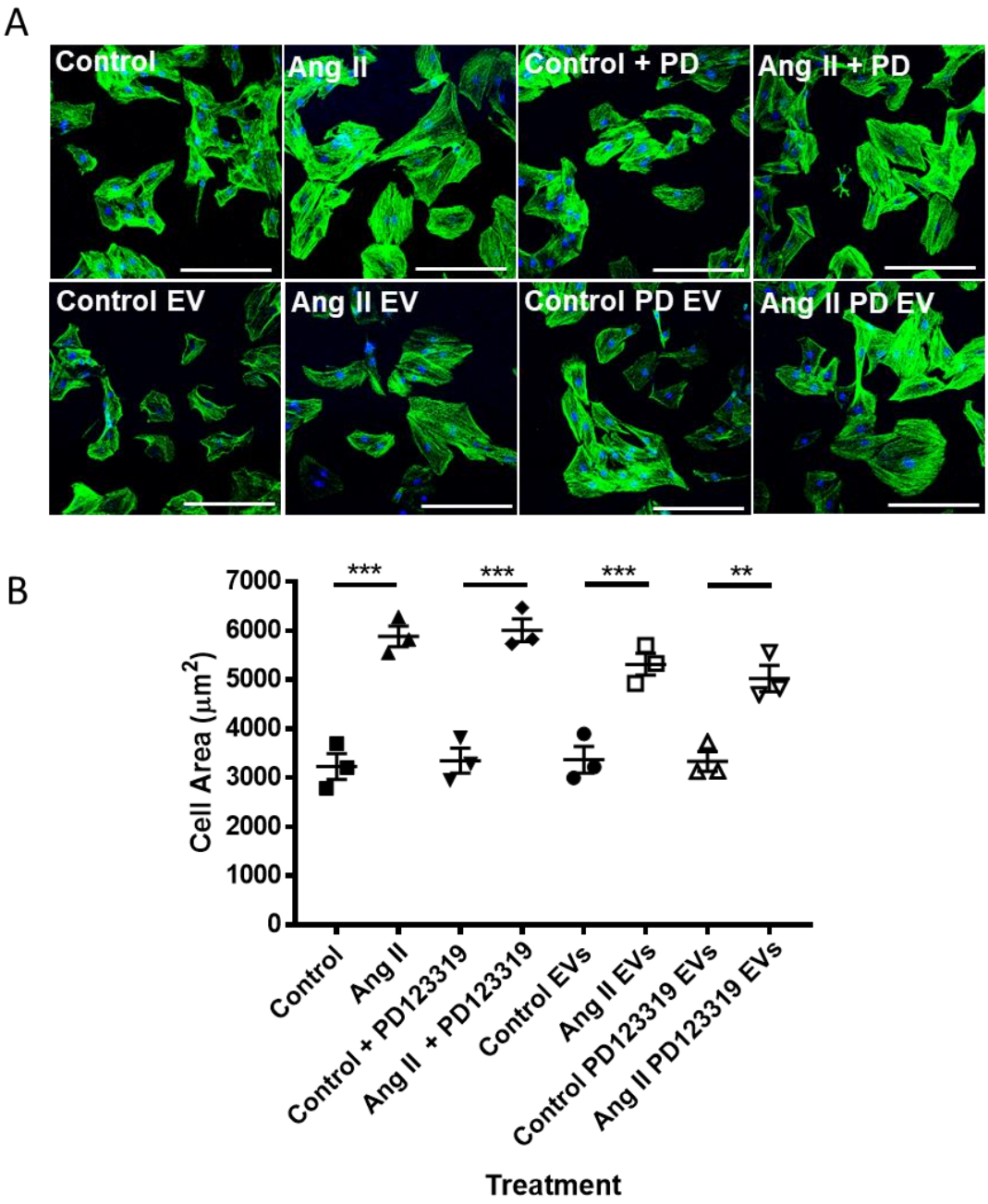

Figure 4-11 Analysis of cell size in H9c2 cardiomyocytes treated with EVs derived from PD123319 pre-blocked cells. (A) Representative confocal images of H9c2 cardiomyocytes under each treatment condition (Scale: 100 μm). (B) Analysis of H9c2 cardiomyocyte cell size under each condition (n=3, **p<0.01, ***p<0.001, one-way ANOVA).

4.4.8 Assessment of hypertrophy in H9c2 cardiomyocytes treated with NRCF-derived extracellular vesicles

After establishing cardiomyocyte: cardiomyocyte hypertrophic signalling via EVs, it was of interest to determine whether this effect could also occur via EV signalling between cardiac fibroblasts and cardiomyocytes. NRCF cells were either untreated or treated with 1 μM Ang II over a 48 hr period, EVs were then isolated from the resulting conditioned media and placed onto H9c2 cardiomyocytes; untreated cells and 100 nM Ang II stimulated cells were used as controls for the hypertrophic response. Cells were then imaged in order to determine any changes in cell size (Figure 4-12).

Representative images for each condition are shown in Figure 4-12 A. As expected for the hypertrophic stimulus controls, it was observed that treatment with 100 nM Ang II significantly increased cell size compared with controls (control untreated; 3494.0±159.1 μm^2 vs. 100 nM Ang II treated; 6233.0±20.70 μm^2) (n=3, $p<0.001$). No significant difference was observed between control untreated cells and control EV treated cells, suggesting that these EVs are not able to induce hypertrophy in H9c2 cardiomyocytes. However, it was observed that treatment with NRCF-derived Ang II EVs significantly increased H9c2 cell size compared to both control untreated cells and control EV treated cells (control untreated; 3494.0±159.1 μm^2 and control EV treated; 3356.0±62.1 μm^2 vs. Ang II EV treated; 6074.0±175.6 μm^2) (n=3, $p<0.001$) (Figure 4-12 B). These data suggest that NRCF-derived Ang II EVs are able to induce a hypertrophic response in H9c2 cardiomyocytes.

Next, Ang II levels within NRCF-derived EVs were analysed by ELISA (Figure 4-13). EVs derived from NRCF cells +/- 1 μM Ang II treatment were lysed and Ang II content in each group was determined by high-sensitivity Ang II ELISA. It was observed that Ang II could be detected at low levels within EVs derived from control untreated NRCF cells, where 4.81±4.80 pg/mL Ang II was detected. When parental NRCF cells had been stimulated with 1 μM Ang II, this level increased to 73.3±30.1 pg/mL Ang II (n=7, p=0.0156) (Figure 4-13).

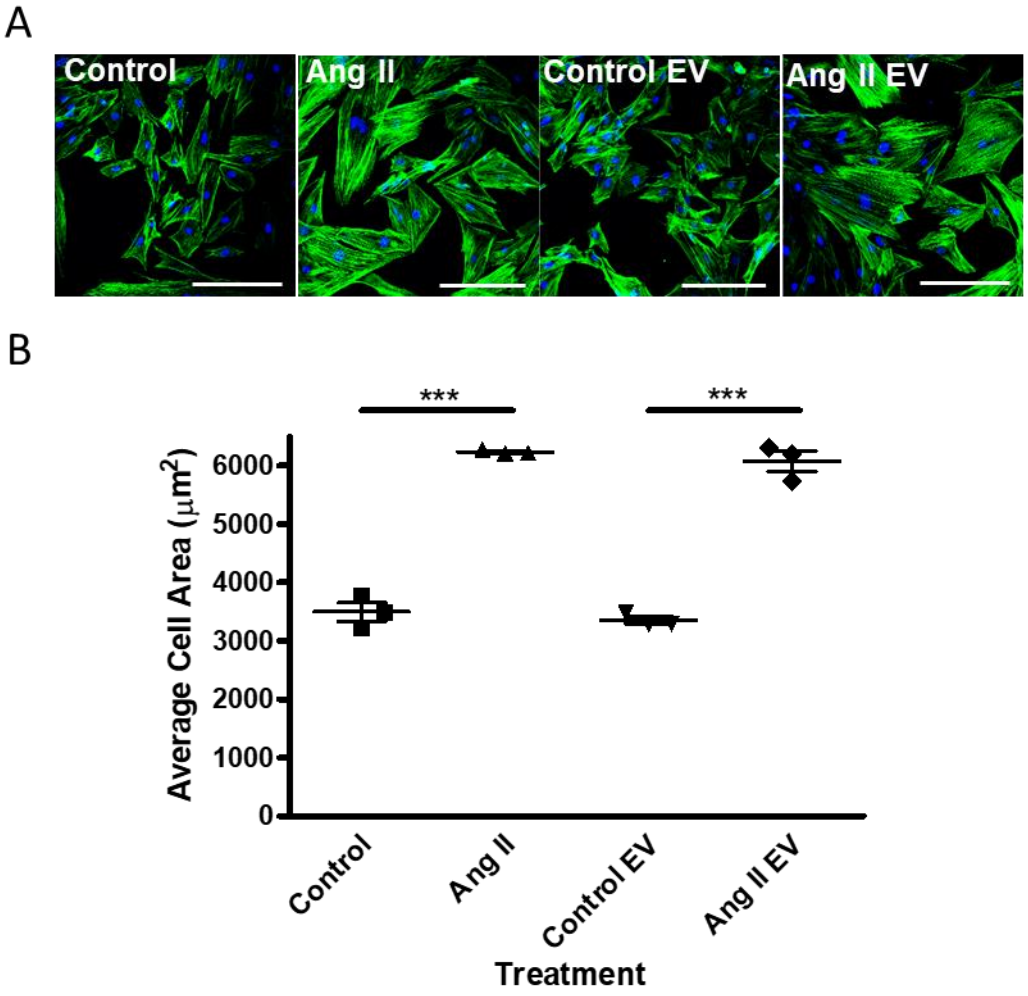

Figure 4-12 Assessment of cellular hypertrophy in H9c2 cardiomyocytes treated with NRCF-derived EVs. (A) Representative confocal images of H9c2 cardiomyocytes in each treatment group (Scale: 100 μm). (B) Analysis of H9c2 cardiomyocyte cell size under each condition (n=3, ***p<0.001, one-way ANOVA).

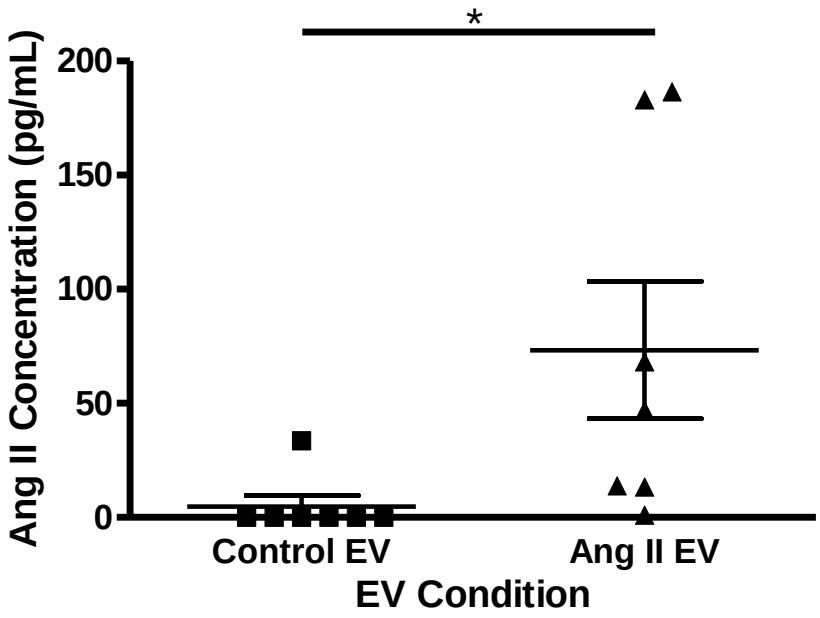

Figure 4-13 Detection of Ang II within NRCF-EVs by ELISA. Detection of Ang II levels within control EVs and Ang II EVs by high-sensitivity ELISA (n=7, *p<0.05; Wilcoxon matched pairs test).

4.5 Discussion

In this study, it was shown that EVs released from Ang II-stimulated H9c2 cardiomyocytes were able to induce a hypertrophic response in recipient H9c2 cardiomyocytes. Due to significant co-localisation of labelled Ang II with labelled EVs, along with detection of Ang II within EVs, it is possible that this response could be occurring via transfer between cells of Ang II enclosed within the EVs.

Induction of hypertrophy in cardiomyocytes by soluble Ang II stimulation is a widely accepted model, and although a variety of different concentrations and time points have been used across studies it is generally accepted that a 100 nM Ang II concentration may evoke a hypertrophic response over a time period of 24 to 96 hr (Guo et al., 2010, Flores-Muñoz et al., 2011). Due to previous Ang II-induced hypertrophy studies in H9c2 cardiomyocytes showing significant increases in cell size and hypertrophy marker gene expression at 96 hr, the 100 nM Ang II over 96 hr model (Flores-Muñoz et al., 2011) was chosen for these studies. Although initial experiments of co-localisation analysis showed EVs to be associated with the cell nucleus after 1 hr incubation, parameters were kept the same for all groups and so incubation occurred over a 96 hr period to match the conditions used for the 100nM Ang II hypertrophy stimulus control.

Observations made regarding cell size increase and upregulation of hypertrophy marker gene expression suggest that EVs derived from Ang II treated H9c2 cardiomyocytes are able to have as potent an effect on hypertrophy induction as soluble Ang II peptide (at a concentration of 100 nM) does in recipient cells. Similar effects were also observed when treating H9c2 cardiomyocytes with NRCF-derived EVs. These findings match similar observations reported in other studies, one of which, highlights many key findings relating to the present study (Lyu et al., 2015). It was found that treatment of NRCM cells with 50 µg/mL NRCF-derived Ang II EVs (EVs obtained from 1 µM Ang II treated cells after 48 hr) over a 48 hr period caused a significant increase in cell size and upregulation of BNP gene expression (as well as ANP, αMHC and ßMHC gene expression) to a level matching that of treatment with 1 µM Ang II, or seemingly surpassing (Lyu et al., 2015). The data in the present study, as well as reports from the literature, suggest a potent hypertrophic effect driven by EVs derived from Ang II-stimulated cells. This study also reported the Ang II content of EVs derived

from NRCF cells by Ang II ELISA (Lyu et al., 2015). In the present study, it was noted that Ang II could be detected within control EVs at low levels, but significantly higher in EVs derived from both Ang II treated H9c2 cardiomyocytes and Ang II treated NRCF. Reports in the literature were unable to detect Ang II within either control EVs or Ang II EVs, however in this case ELISA sensitivity is questionable. The ELISA used had a detection limit of 21.19 pg/mL (Lyu et al., 2015), whereas the present study made use of a high-sensitivity Ang II ELISA where the detection limit is listed as 0.98 pg/mL. Considering many readings detected in the present study were below 21.19 pg/mL it is possible that inefficient sensitivity accounts for the differences between the two sets of studies. Lyu et al. 2015 also reported EV effects on AT_1R and AT_2R gene expression and studied their involvement in EV signalling. In their studies, it was found that NRCF-Ang II EVs significantly increased AT_1R and AT_2R gene expression compared to treatment with NRCF-control EVs. In the present study, these observations were not made and although the answer as to why is not clear, gene expression analysis was only carried out in recipient cells treated with H9c2-EVs rather than NRCF-EVs and so the effects could possibly be related to parental cell-specificity. Furthermore, they also suggested that treatment with PD123,319 and Telmisartan (AT_2R and AT_1R antagonists, respectively) significantly reduced exosome release from NRCF cells (Lyu et al., 2015) whereas the present study did not record any inhibition of EV release when treating parental H9c2 cardiomyocytes with PD123,319 or losartan. However, particle release was measured differently between studies; total protein concentration (Lyu et al., 2015) vs. NTA in the present study and again, EVs of different cell types were being investigated.

A further observation made in the present studies showed that in certain experiments, treatment of parental cells with Ang II caused a significant increase in EV release from H9c2 cardiomyocytes, an observation not made in the initial EV characterisation described in Chapter 3. It is unclear as to why this result was observed in only one experiment but due to the lack of consistency it could be attributed to some natural difference between cell batches in how they respond to stress, or another unknown artefact which remains unclear.

Although in this study Ang II was detected within EVs derived from Ang II-stimulated parental cells (both H9c2 and NRCF), the levels detected were extremely low. For example, levels detected within H9c2-derived Ang II EVs were equivalent to approximately 27.5 picomolar, a vastly lower concentration than the suggested hypertrophic stimulus of 100 nanomolar, yet data showed a significant hypertrophic response in terms of increased cell size and upregulation of BNP gene expression. As a result, these data ask the question of whether the hypertrophic response is occurring due to low levels of Ang II within the EVs, or whether other signalling mechanisms are at play. Although the exact mechanisms are not known, studies have repeatedly reported the potential for creating pathological stress in parental cells which results in the production (or over-production) of EVs which then have the potential to transfer the pathological phenotype to recipient cells. This phenomenon has been particularly well described in models of hypoxia where EVs produced under hypoxic conditions have the potential to elicit pathological effects in cell models of disease (Dorayappan et al., 2018, Wang et al., 2014a). Based on the detected concentration of Ang II, it would be beneficial in future studies to profile the exact contents of the EVs to determine whether the hypertrophic effects are caused by the Ang II present, or by Ang II and some other components involved in hypertrophic signalling.

4.5.1 Study limitations

The key cell model utilised in this study was the H9c2 model of cardiomyocyte hypertrophy and, although a commonly used and well-established model, it comes with certain limitations. Due to its immature phenotype, it is more commonly used as a model for NRCMs (despite lacking spontaneous beating) as opposed to ARVMs and therefore may provide less information in relation to CVD in the adult heart. However, analysis of hypertrophy in either of these primary cells (NRCMs or ARVMs) may have provided more information about cell behaviour in intact tissue and could be beneficial for future studies.

4.6 Summary

EVs released from Ang II stimulated H9c2 cardiomyocytes are able to induce a hypertrophic response in recipient H9c2 cardiomyocytes. The co-localisation and ELISA data suggest that EVs may be transferring active Ang II peptide to recipient cells, which respond with F-actin rearrangement, increased cell size and increased expression of hypertrophy markers. Treatment of EVs with proteinase K during isolation efficiently depletes any contaminating Ang II which may have remained in the conditioned media and thus passed through the isolation protocol. Furthermore, analysis of the effects of pre-blocking in parental cells with AT_1R or AT_2R blockers showed that blocking the AT_1R with losartan abolished the Ang II EV-induced hypertrophic effect, while blocking the AT_2R with PD123,319 did not. This suggests a possible role for Ang II/AT_1R signalling in the parental cells, where disruption of this pathway affects their ability to release EVs that elicit pathological effects in recipient cells. This study also showed that EVs released from Ang II stimulated NRCF cells are similarly capable of inducing a hypertrophic response in H9c2 cardiomyocytes. Taken together, these observations highlight a potential role for EVs in RAS signalling in relation to cellular hypertrophy.

Chapter 5 Investigating the therapeutic potential of angiotensin-(1-7) loaded extracellular vesicles

5.1 Introduction

5.1.1 Angiotensin-(1-7) in cardio-protection

The counter-regulatory axis of the RAS has been well described as having opposing effects to the classical RAS axis, where the main effector peptide, Ang-(1-7), has been shown to elicit cardio-protective effects via interaction with the Mas receptor (Santos et al., 2003). The effects of Ang-(1-7) in the heart have been well documented and reported across a large number of studies. The confirmation of the presence of ACE2 in cardiomyocytes (Zisman et al., 2003) suggests a mechanism for the local formation of Ang-(1-7) in the heart, which may contribute to its potent protective effects in this organ. It has been found that Ang-(1-7) induces vasodilation in the coronary vessels of various animal models including dogs (Brosnihan et al., 1996), pigs (Porsti et al., 1994) and rodents (Souza et al., 2013) where commonly, increased Ang-(1-7)/Mas receptor signalling results in increased NO synthesis promoting vasodilation (Souza et al., 2013). Further to this, it has also been demonstrated in adult mouse ventricular cardiomyocytes that acute exposure to Ang-(1-7) results in stimulation of eNOS, producing an increase in NO synthesis and release (Dias-Peixoto et al., 2008). Initial studies investigating the cardio-protective effects of Ang-(1-7) showed that low concentrations could reduce cardiac arrhythmias associated with ischaemia/reperfusion in rat hearts (Neves et al., 1997), however this effect was opposed when using 10-fold higher concentrations suggesting that a fine balance may be required in relation to Ang-(1-7) signalling in order to prevent deleterious effects from occurring (Neves et al., 1997). As well as having demonstratable effects on heart rhythm, many studies have also reported the anti-remodelling effects of Ang-(1-7) in the heart. Initially it was found that expression of a fusion protein producing Ang-(1-7) could attenuate cardiac fibrosis induced by isoproterenol treatment in a transgenic rat line (Botelho-Santos et al., 2007). Further studies went on to show that stimulation of cardiomyocyte apoptosis by hypoxia could be attenuated by Ang-(1-7)/Mas signalling (Chang et al., 2016) and that adenoviral delivery of Ang-(1-7) could inhibit Ang II-induced cardiomyocyte hypertrophy via Mas receptor signalling (Flores-Muñoz et al., 2011). Similar anti-remodelling effects were also reported in other disease models; it was found that chronic infusion of Ang-(1-7) via osmotic minipump prevented the development of cardiac fibrosis in the

deoxycorticosterone acetate (DOCA)-salt model of hypertension (Grobe et al., 2006). A further study demonstrated that bolus injection of Ang-(1-7) could prevent left ventricular remodelling and general heart dysfunction caused by renal dysfunction in 5/6 nephrectomy mice, an experimental model of chronic renal failure (Li et al., 2009). Together, these studies highlight an important role for Ang-(1-7) in prevention of aberrant remodelling in the heart under various disease settings, where a variety of delivery mechanisms have been used to increase the levels of Ang-(1-7) for therapeutic benefit.

5.1.2 The angiotensin II-infusion model of hypertension

A commonly used experimental model of hypertension is continuous infusion of Ang II via osmotic minipump. As the major vasoactive peptide in the RAS, Ang II has been documented to have effects on cell proliferation, hypertrophy and inflammation *in vitro* (Mehta and Griendling, 2007), while *in vivo* studies support its effects on sustained blood pressure elevation, enhanced inflammation and increased thickening of vessels (Fyhrquist et al., 1995). Aside from the classic observation of sustained blood pressure increase, Ang II infusion in rodent models has also been reported to result in cardiac and vascular hypertrophy, fibrosis and cardiac dysfunction (Zhang et al., 2017b) allowing it to be used effectively as a disease model for therapeutic interventions involving the heart. Various studies have reported the use of Ang II infusion in myocardial remodelling, where a multitude of different doses and exposure times have been used in rodent models to induce hypertension and cardiac remodelling. One study aiming to target 5' adenosine monophosphate-activated protein kinase (AMPK)-ACE2 signalling demonstrated that a dose of 200 ng/kg/min over 4 weeks was able to induce cardiac fibrosis, myocardial hypertrophy and heart dysfunction in Sprague-Dawley rats (Zhang et al., 2017b) while another using the same dose and time point also reported Ang II-induced cardiac dysfunction and hypertrophy (Yan et al., 2019). A third study using this dose of Ang II continually infused in Sprague-Dawley rats over just 1 week found increased cardiac weight, collagen deposition and fibrosis in the heart (Cui et al., 1999). Research carried out in Wistar rats also showed that a lower Ang II dose of 120 ng/kg/min over 4 weeks caused an increase in blood pressure, vascular reactivity, ventricular hypertrophy and cardiac fibrosis (Mishra et al., 2019). Further studies have shown that continuous infusion of Ang II at a dose of 3.2 mg/kg/day over 2 weeks

in male C57BL/6 mice induced cardiac dysfunction, increased blood pressure, and cardiac remodelling (Izumiya et al., 2012), also highlighting mice as viable rodent models for Ang II infusion in cardiovascular disease. Taken together, these studies highlight the potential for the use of Ang II-infusion models in investigating cardiovascular disease, where a variety of effective doses, exposure times and rodent models have been reported.

5.1.3 Loading of extracellular vesicles

The ability of EVs to cross barriers such as the blood/brain barrier or simply the cytoplasmic membrane, has made them a relatively new, but potentially exciting target for use as therapeutic delivery molecules (Liu and Su, 2019). Their stability in the circulation as well as their natural transportation properties has led to the engineering of EVs to contain and potentially deliver therapeutic molecules in disease models. Recent studies have highlighted various mechanisms for loading EVs with therapeutic molecules such as proteins or nucleic acids. One study focusing on Parkinson's Disease models showed that the antioxidant enzyme, catalase, could be loaded into exosomes via permeabilization with either saponin, sonication or extrusion (Haney et al., 2015). Catalase remained functionally active once exosomes were taken up by neuronal cells, with significant neuroprotective effects observed *in vitro* and *in vivo* as a result of treatment (Haney et al., 2015). Further studies showed that transfection could be used to load short-interfering RNA (siRNA) molecules into exosomes; it was found that exosomes isolated from HeLa cells could be transfected with specific siRNA molecules using lipofectamine (Shtam et al., 2013). In addition, the transfected siRNA could later be detected in recipient cells after exosomal transfer (Shtam et al., 2013). Currently the most common method for extracellular vesicle loading is via electroporation, whereby this technique is generally used to load miRNA or siRNA molecules. One study utilised an Atto655-fluorescently labelled siRNA which was loaded into HEK-293 derived exosomes via electroporation, with excess siRNA molecules removed by gel filtration (Faruqu et al., 2018). Fluorescence imaging showed the labelled siRNA to be present within recipient cells 24 hr after treatment with the loaded exosomes highlighting electroporation to be a viable method for loading EVs with siRNAs (Faruqu et al., 2018). Another study showed that electroporation could be used to load miRNAs into EVs; in this case, exosomes were isolated from

endothelial progenitor cells and loaded with miR-126, a miRNA shown to be involved in vascular protection (Sun et al., 2018a). This study showed that the miR-126-loaded exosomes could transfer biologically active miR-126 in both *in vitro* and *in vivo* models of deep vein thrombosis where it was found to promote thrombus resolution (Sun et al., 2018a). Although reported less frequently, electroporation has also been used to exogenously load DNA into EVs. One study exploring the potential for DNA loading found that loading efficiency and capacity were dependent on DNA size, where dsDNA molecules of no more than 1000 bp in length were most effectively electroporated (Lamichhane et al., 2015). Furthermore, it was confirmed that the loaded EVs could transfer this dsDNA to recipient cells, however when attempting to then transfer electroporated plasmid DNA via EVs, recipient cells did not show any measurable DNA transfer or protein expression suggesting functional DNA transfer was not achieved (Lamichhane et al., 2015). These studies highlight the potential for electroporation as a mechanism for loading EVs with therapeutic molecules. However, in some cases, potential problems arise surrounding the structural integrity of the vesicles after electroporation, and the biological activity of their cargo (Lamichhane et al., 2015, Liu and Su, 2019), both of which must be taken into account when utilising this method. Furthermore, although use of electroporation has been well documented for loading siRNA and miRNA molecules into EVs, loading of peptides via this method has not yet been reported.

5.1.4 Extracellular vesicle delivery in rodent models

Although currently in the spotlight as potential delivery vehicles for therapeutic molecules, potential limitations arise surrounding the targeting of EVs to specific organs in disease models. Currently, most methods of delivery in *in vivo* models involve repeat bolus injections of EVs into the circulation, however in some cases more direct injection methods are used such is intramyocardial for delivery to the heart (Shi et al., 2019) or intranasal for delivery to the brain (Narbute et al., 2019). Regardless of method used, many studies have found success with bolus injection of EVs in rodent models, whether by direct tissue delivery or simply by intravenous administration. One study reported that exosomes derived from human MSCs were able to promote the differentiation of fibroblasts to myofibroblasts and provide cardioprotective effects when injected

directly into the hearts of Sprague-Dawley rats via the myocardial route (Shi et al., 2019). Similarly, it was found that in a mouse model of myocardial ischaemia-reperfusion injury, exosomes derived from mesenchymal stromal cells injected directly into the peri-infarct site were able to regulate macrophage polarization and attenuate injury (Zhao et al., 2019). Other studies have shown the potential for delivery via the intranasal route, which is commonly used when targeting EVs to the brain. A study investigating the potential use of human stem cell-derived EVs in Parkinson's Disease utilised intranasal injection to target the brains of male Wistar rats with medial forebrain bundle lesion to model the disease (Narbute et al., 2019). The study suggested that EVs injected via this route were able to reach the brain with the result that gait impairment was suppressed, and motor function improved compared with controls (Narbute et al., 2019). Due to the more complex nature of these delivery methods, many studies have utilised intravenous injections to introduce EVs into the circulation without specific targeting to a particular organ. It was found that exosomes derived from MSCs could attenuate the progression of atherosclerosis in $ApoE^{-/-}$ mice when injected via the tail vein (Li et al., 2019). Once injected into the circulation, it was found that the MSC-exosomes migrated to the atherosclerotic plaques where they decreased plaque area and macrophage infiltration compared with control mice (Li et al., 2019). Another study found that tail vein injection of MSC-derived exosomes could improve cardiac function and reduce cardiomyocyte apoptosis in a mouse model of dilated cardiomyopathy (Sun et al., 2018b). Finally, it has been demonstrated that tail vein injection of mesenchymal stromal cell-derived EVs improves functional stroke recovery and promotes neurovascular plasticity in Wistar rats subjected to transient middle cerebral artery occlusion (Xin et al., 2013). Taken together, the studies highlighted here suggest that bolus injection of EVs, whether directly administered to a particular organ or intravenously, is a viable therapeutic delivery strategy in rodent disease models, with particular relevance to cardiovascular disease.

5.2 Aims

- To assess the effects of EVs isolated from Ang-(1-7) stimulated H9c2 cardiomyocytes on Ang II-induced hypertrophy in recipient H9c2 cardiomyocytes.

- To investigate the potential use of electroporation for the loading of RAS peptides into EVs.

- To determine the effects of EVs electroporated with Ang-(1-7) in cardio-protection in an *in vitro* model of Ang II-induced cardiomyocyte hypertrophy.

- To determine the effects of EVs electroporated with Ang-(1-7) in cardiovascular protection in an *in vivo* model of Ang II-induced hypertension.

5.3 Key Methods

Table 5-1 Chapter 5 key methods

EV isolation	Cell culture media Section 2.6
	Rat serum Section 2.9
	Proteinase k treatment Section 2.6.1
Exogenous loading of EVs	Electroporation Section 2.10
	Ang-(1-7) ELISA Section 2.12
Assessment of H9c2 hypertrophy	Hypertrophy assay Section 2.5.7
in vivo surgical procedures	Osmotic minipump implantation Section 2.13.3
	Femoral vein injection Section 2.13.4
in vivo analysis	Tail cuff plethysmography Section 2.13.5
	Transthoracic echocardiography Section 2.13.6
	Picrosirius red analysis Section 2.14.1
	Wheat germ agglutinin Section 2.14.2

5.3.1 Cell work methodology

A schematic representation of the work flow plan for the altered H9c2 hypertrophy model (Flores-Muñoz et al., 2012) used in section 5.4.1 to determine the effects of Ang-(1-7) EVs on cellular hypertrophy is shown in Figure 5-1. The full protocols are described in section 2.5.7.

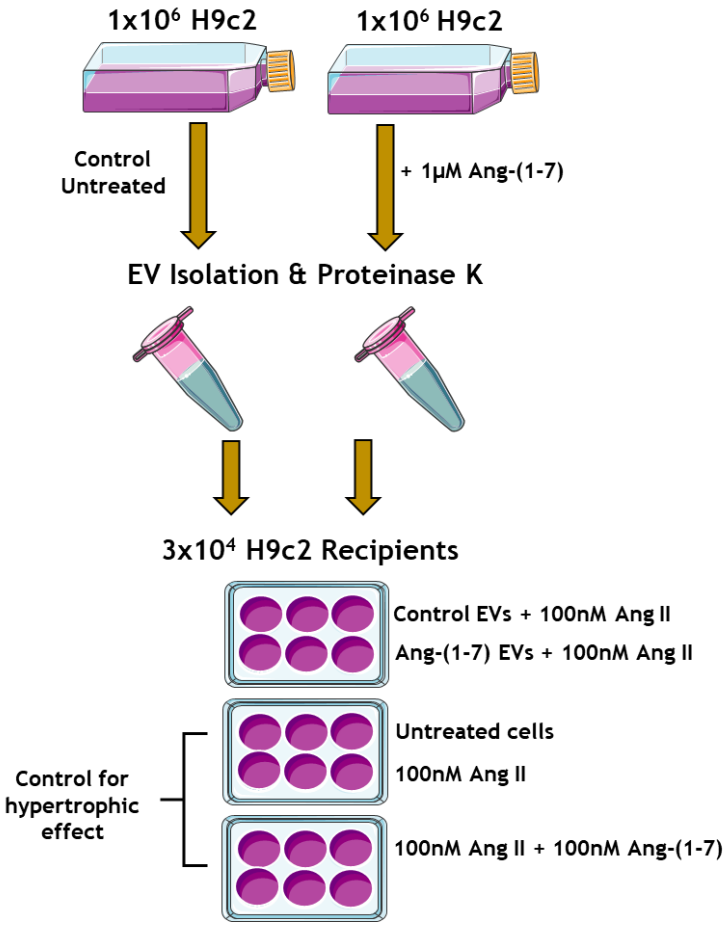

Figure 5-1 Schematic representation of the work flow plan for investigating the effects of Ang-(1-7) signalling via EVs in the H9c2 model of cardiomyocyte hypertrophy.

5.3.2 Work flow for EV electroporation

A schematic representation of the work flow plan for the electroporation of EVs to exogenously load either Ang II or Ang-(1-7) and determine their effects on cellular hypertrophy is shown in Figure 5-2. The full protocols are detail in sections 2.5.7 and 2.10.

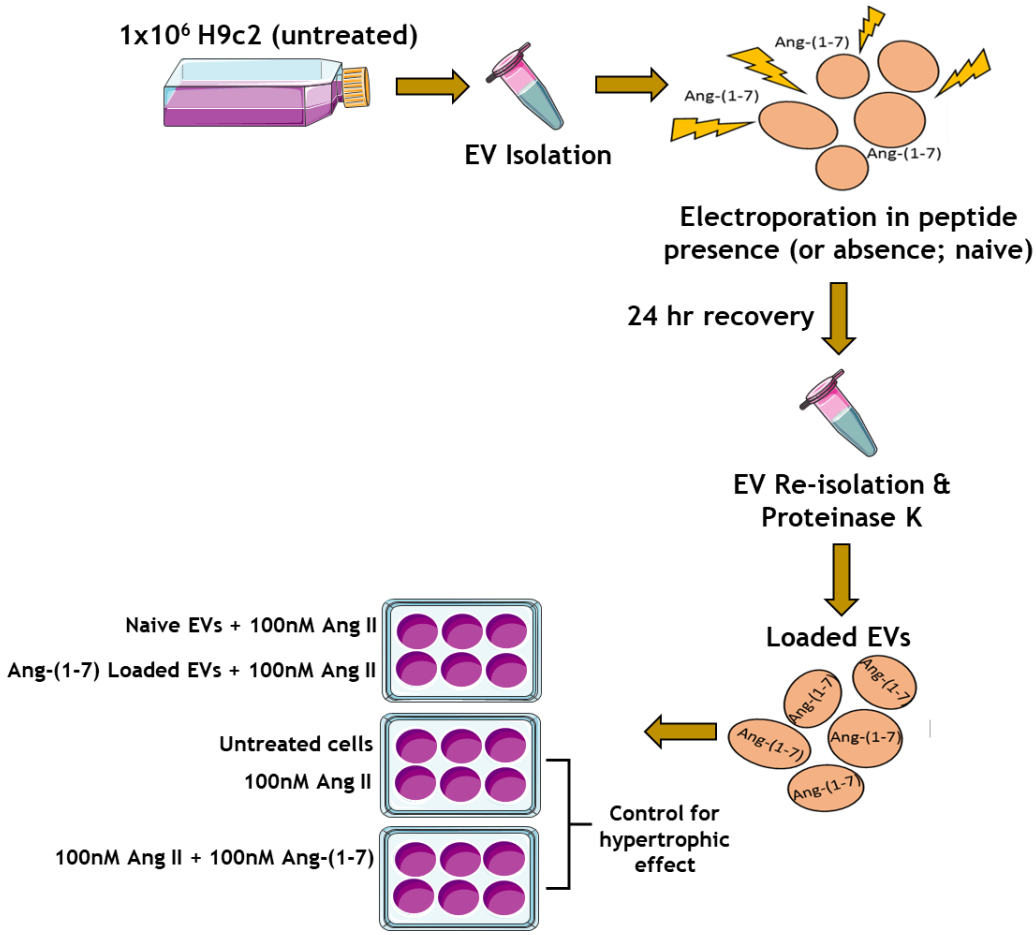

Figure 5-2 Schematic representation of the work flow plan for the electroporation of EVs for exogenous loading and delivery of angiotensin peptides in the H9c2 model of cardiomyocyte hypertrophy.

5.4 Results

5.4.1 Assessment of hypertrophy in Ang II-stimulated H9c2 cardiomyocytes co-treated with extracellular vesicles derived from Ang-(1-7) treated H9c2 cardiomyocytes

In order to prevent the effects of any contaminating exogenous Ang-(1-7) peptide, proteinase K treatment was utilised to deplete any excess from EV isolations as described previously. Initially, Ang-(1-7) stocks were treated with proteinase K to determine whether or not proteinase K could effectively digest this peptide. Ang-(1-7) stocks of 1 μM concentration were either untreated or digested with proteinase K and Ang-(1-7) levels for both conditions were then determined by Ang-(1-7) ELISA. Data showed that the average concentration of undigested Ang-(1-7) was 223.9±3.6 pg/mL compared with 4.9±1.4 pg/mL for exogenous Ang-(1-7) treated with proteinase K, suggesting that the peptide had been successfully digested ($n=3$, $p<0.001$) (Figure 5-3).

Next, H9c2 cardiomyocytes were either untreated or treated with 1 μM Ang-(1-7) over a 48 hr period. EVs were then isolated from the resulting conditioned media, treated with proteinase K, and placed onto recipient H9c2 cardiomyocytes in varying amounts, along with co-stimulation with 100 nM Ang II. Untreated cells and cells treated with 100 nM Ang II only were used as controls for the hypertrophic response. Cells were then imaged in order to determine any changes in cell size (Figure 5-4). The cell sizing data showed that stimulation with 100 nM Ang II induced a significant hypertrophic response in terms of cell size and F-actin rearrangement compared with controls as observed previously. Representative images for each treatment group are shown in Figure 5-4 A. Control untreated cells were found to have an area of 3231.0±62.0 μm^2 vs. 6133.0±25.7 μm^2 for 100 nM Ang II stimulated cells, while co-stimulation with 100 nM Ang II and 100 nM Ang-(1-7) did not cause a significant increase in cell size, with the average area being 3319.0±117.6 μm^2 ($n=3$, $p<0.001$) (Figure 5-4 B). It was found that treatment with Ang II and control EVs still significantly increased cell size compared with control cells (control untreated; 3231.0±62.0 μm^2 vs. Ang II+control EV treated; 6108.0±48.4 μm^2) and exhibited classical F-actin rearrangement characteristic of Ang II stimulation. Treatment with low (L) amounts Ang-(1-7) EVs also did not prevent Ang II-induced increase in cell size

(100 nM Ang II stimulated; 6133.0±25.7 μm^2 vs. Ang II+Ang-(1-7) EV (L); 5972.0±79.9 μm^2, n=3), however treatment with medium (M) and high (H) amounts of Ang-(1-7) EVs significantly inhibited the hypertrophic effects of Ang II (100 nM Ang II stimulated; 6133.0±25.7 μm^2 vs. Ang II+Ang-(1-7) EV (M); 5148.0±266.8 μm^2 vs. Ang II+Ang-(1-7) EV (H); 3412.0±105.3 μm^2 (n=3, $p<0.01$, $p<0.001$, respectively)) (Figure 5-4 B). These data suggest that at higher amounts, EVs derived from Ang-(1-7) treated H9c2 cardiomyocytes are able to inhibit Ang II-induced hypertrophy in recipient H9c2 cardiomyocytes.

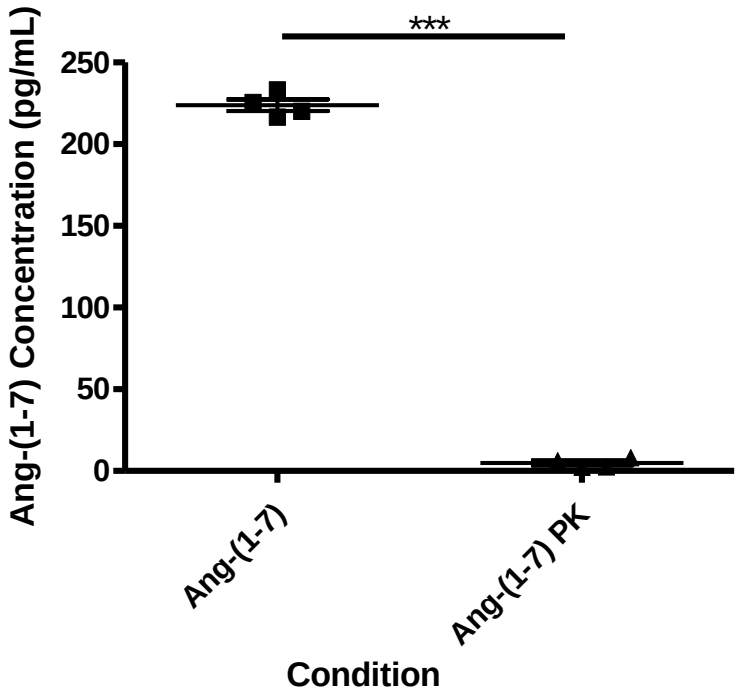

Figure 5-3 Proteinase K digestion efficiently depletes soluble Ang-(1-7). Ang-(1-7) stocks of 1 μM concentration either untreated or treated with 500 pg/mL proteinase K over a 1 hr time period, after which remaining peptide levels in each group were determined by Ang-(1-7) ELISA (n=3, ***p<0.001, Student's t-test).

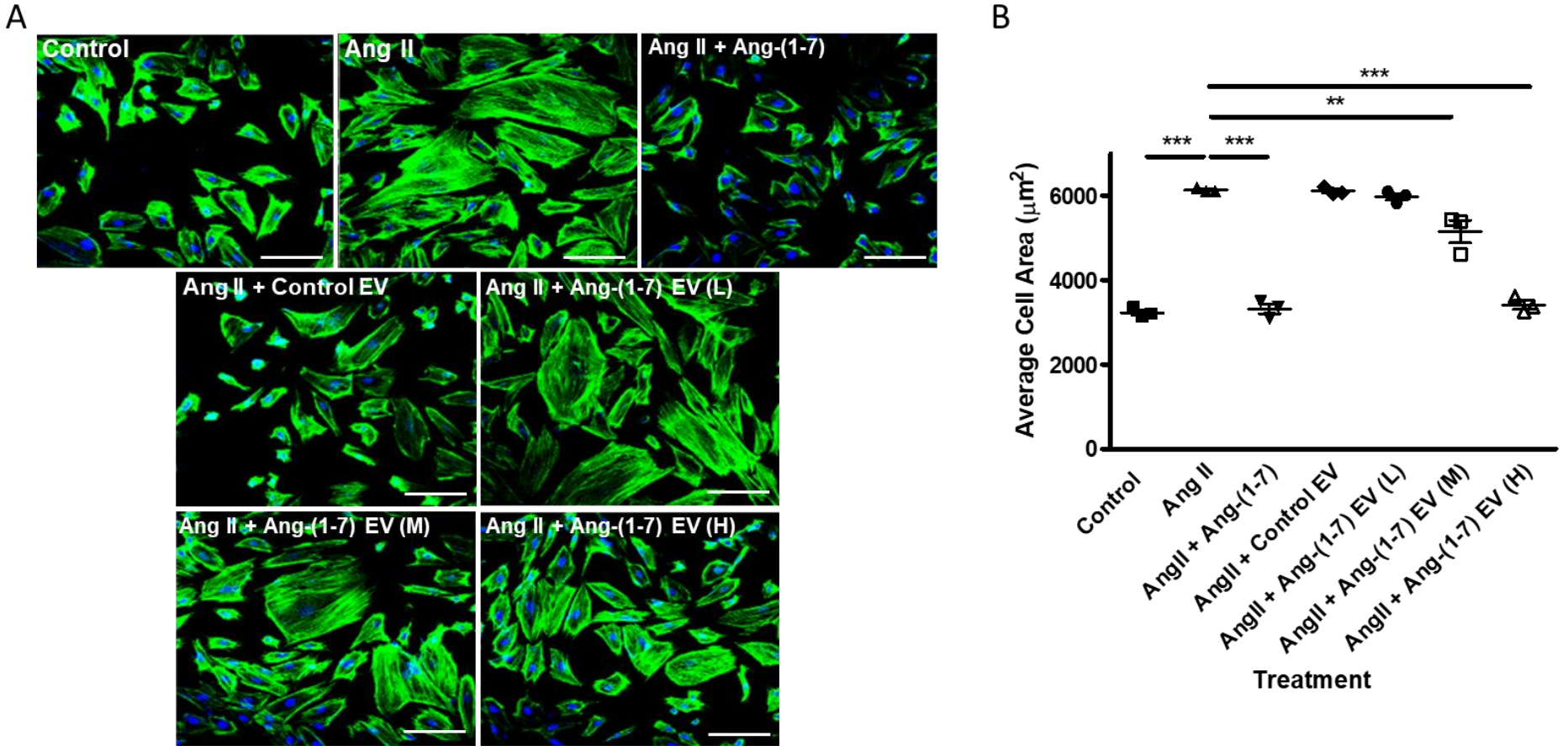

Figure 5-4 Assessment of cellular hypertrophy in H9c2 cardiomyocytes co-treated with soluble Ang II and EVs derived from Ang-(1-7) treated H9c2 cardiomyocytes. (A) Representative confocal images of H9c2 cardiomyocytes in each treatment group (Scale: 100 μm). (B) Analysis of H9c2 cardiomyocyte cell size under each condition (n=3, **p<0.01, ***p<0.001, one-way ANOVA).

5.4.2 Optimisation of electroporation: exogenous loading of Ang II and Ang-(1-7) into H9c2 derived extracellular vesicles

To determine whether EVs could be used more efficiently to deliver small peptides, electroporation was used to exogenously load naïve vesicles derived from H9c2 cardiomyocytes. EVs were isolated from the conditioned media of untreated H9c2 cardiomyocytes after 48 hr. EVs were then naively electroporated or electroporated in the presence of Ang II and treated with proteinase K to remove any excess peptide from the sample. EVs were then analysed by NTA to ensure structural integrity and then analysed for Ang II content by ELISA (Figure 5-5). Similarly, EVs underwent electroporation in the presence of Ang-(1-7) (or were naively electroporated) and analysed by both NTA and Ang-(1-7) ELISA (Figure 5-6).

NTA data confirmed the presence of EVs after naïve electroporation or electroporation with Ang II and re-isolation. Representative microscopic images and size/concentration tracks produced by the NanoSight for naïve electroporated EVs and Ang II electroporated EVs are shown (Figure 5-5 A, B, C & D). The ELISA data showed that electroporation in the presence of Ang II caused EVs to be loaded with significantly more Ang II than naively electroporated EVs (naïve electroporated EV; 9.7±7.1 pg/mL vs. Ang II electroporated EV; 183.4±14.6 pg/mL, n=5, $p<0.001$) (Figure 5-5 E). Due to the upper detection limits of the standard curve for the ELISA kit used, Ang II electroporated EVs were then diluted to varying degrees to determine whether Ang II levels may initially have been off the scale of the standard curve. Ang II electroporated EVs were diluted 1/100, 1/500 and 1/1000. ELISA analysis confirmed this as undiluted EVs were found to contain 199.4±10.2 pg/mL vs. 195.1±8.1 pg/mL for the 1/100 dilution, 114.3±9.5 pg/mL for the 1/500 dilution and 58.2±5.9 pg/mL for the 1/1000 dilution (n=5) (Figure 5-5 F). These data suggest that Ang II may be exogenously loaded into EVs efficiently via electroporation.

Similarly, EVs electroporated in the presence of Ang-(1-7) were also analysed by NTA and ELISA. Representative microscopic images and size/concentration tracks produced by the NanoSight for naïve electroporated EVs and Ang II electroporated EVs are shown (Figure 5-6 A, B, C & D). Analysis by Ang-(1-7) ELISA found that EVs electroporated in the presence of Ang-(1-7) contained

significantly higher levels of the peptide than naively electroporated EVs (naïve electroporated EV; 9.8±1.3 pg/mL vs. Ang-(1-7) electroporated EV; 501.3±1.3 pg/mL, n=3, $p<0.001$) (Figure 5-6 E). A 1/500 dilution of Ang-(1-7) electroporated EVs was also included to determine whether Ang-(1-7) content was above the upper limit of the ELISA standard curve in the initial sample, which the data suggested to be the case; (Ang-(1-7) electroporated EV; 501.3±1.3 pg/mL vs 1/500 Ang-(1-7) electroporated EV; 2.331±0.2, n=3, $p<0.001$) (Figure 5-6 F).

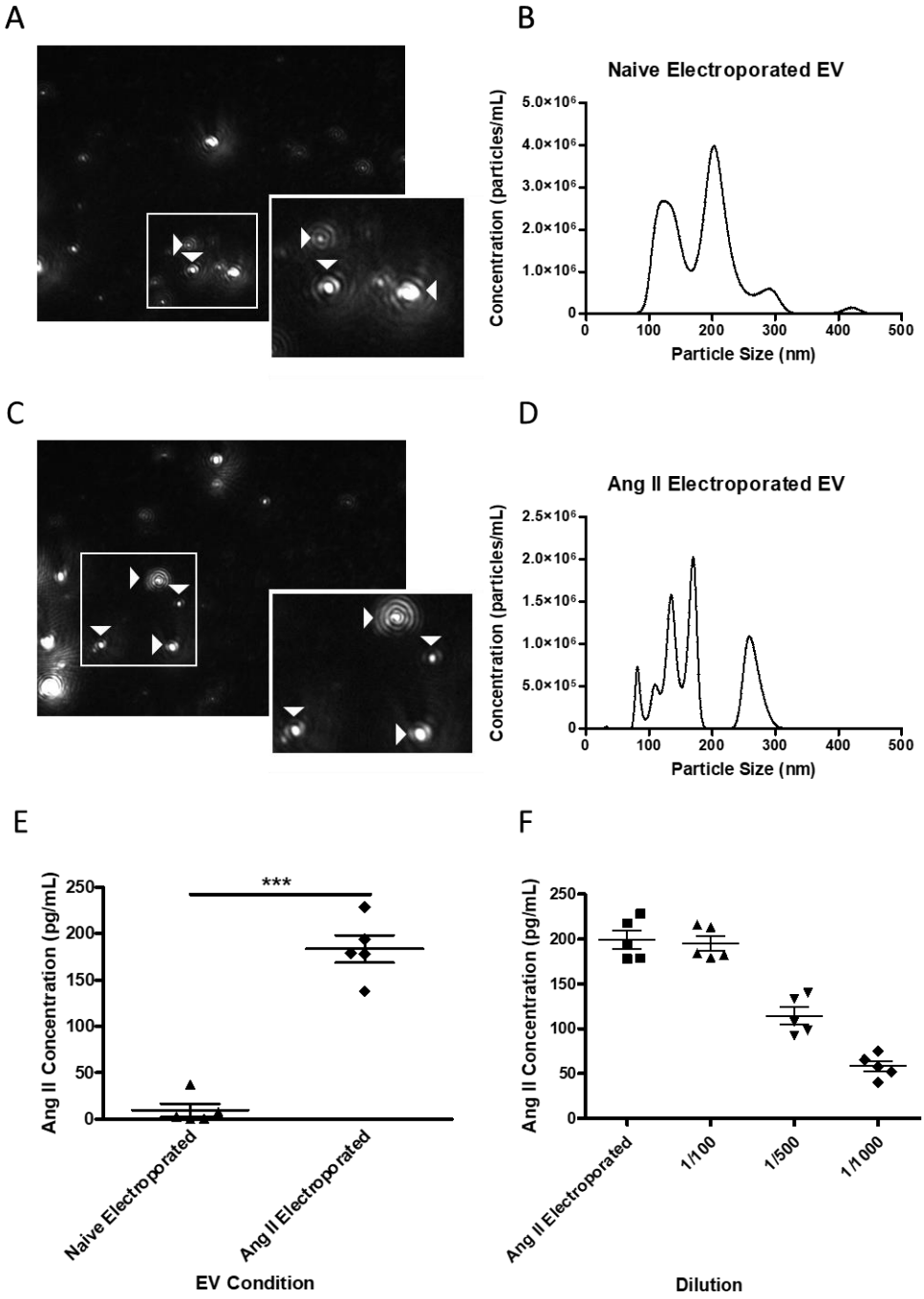

Figure 5-5 Optimisation of electroporation of EVs with Ang II. (A) Representative NTA microscopic image of naïve electroporated EVs (marked by white arrows) and (B) representative size/concentration track. (C) Representative NTA microscopic image of Ang II electroporated EVs (marked by white arrows) and (D) representative size/concentration track. (E) ELISA comparison of Ang II content between naïve electroporated EVs and Ang II electroporated EVs (n=5, ***p<0.001, Student's t-test). (F) ELISA analysis of diluted Ang II electroporated EVs (n=5).

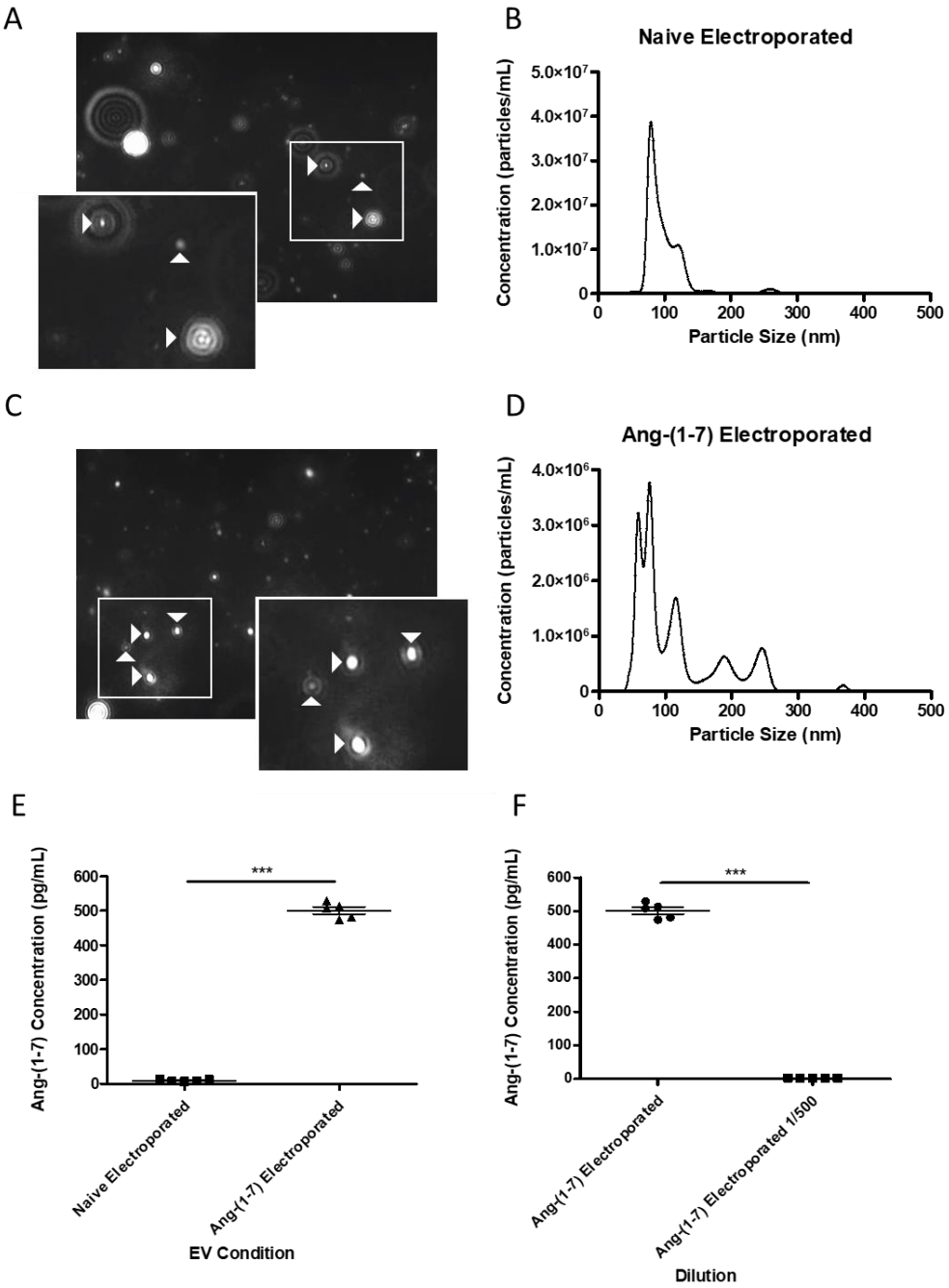

Figure 5-6 Optimisation of electroporation of EVs with Ang-(1-7). (A) Representative NTA microscopic image of naïve electroporated EVs (marked by white arrows) and (B) representative size/concentration track. (C) Representative NTA microscopic image of Ang-(1-7) electroporated EVs (marked by white arrows) and (D) representative size/concentration track. (E) ELISA comparison of Ang-(1-7) content between naïve electroporated EVs and Ang-(1-7) electroporated EVs. (F) ELISA analysis of diluted Ang-(1-7) electroporated EVs (n=5, ***p<0.001, Student's t-test).

5.4.3 Effect of Ang-(1-7) electroporated H9c2-derived extracellular vesicles on Ang II-induced hypertrophy in recipient H9c2 cardiomyocytes

EVs were isolated from the conditioned media of untreated H9c2 cardiomyocytes after 48 hr. EVs were then electroporated naively or in the presence of Ang-(1-7) and treated with proteinase K to digest any remaining contaminating peptide. Electroporated EVs were then placed onto recipient H9c2 cardiomyocytes in amounts of 1 µg, 5 µg and 10 µg, along with co-stimulation with 100 nM Ang II. Untreated cells and cells treated with 100 nM Ang II only were used as controls for the hypertrophic response. Cells were then imaged in order to determine any changes in cell size (Figure 5-7).

Representative images for each treatment group are shown (Figure 5-7 A). The cell sizing data showed that stimulation with 100 nM Ang II induced a significant hypertrophic response in terms of cell size and F-actin rearrangement compared with controls, while co-stimulation with 100 nM Ang II and 100 nM Ang-(1-7) did not induce a hypertrophic response (control untreated; 2577.0±79.2 μm^2 vs. 100 nM Ang II stimulated; 4789.0±51.2 μm^2 vs. 100 nM Ang II+100 nM Ang-(1-7) stimulated; 2563.0±70.5 μm^2, n=3, $p<0.001$) (Figure 5-7 B). It was also observed that treatment with naïve electroporated EVs at each of the three amounts did not inhibit Ang II-induced cellular hypertrophy (100 nM Ang II stimulated; 4789.0±51.2 μm^2 vs. Ang II+1 µg naïve EVs; 4649.0±70.7 μm^2 vs. Ang II+5 µg naïve EVs; 4646.0±83.3 μm^2 vs. Ang II+10 µg naïve EVs; 4723.0±46.8 μm^2, n=3) (Figure 5-7 B). Similarly, the lower amounts (1 µg and 5 µg) of Ang-(1-7) electroporated EVs did not inhibit Ang II-induced hypertrophy, however treatment with 10 µg Ang-(1-7) electroporated EVs caused significant inhibition of the Ang II-induced increase in cell size and F-actin rearrangement (100 nM Ang II stimulated; 4789.0±51.2 μm^2 vs. Ang II+1 µg Ang-(1-7) EVs; 4583.0±49.0 μm^2 vs. Ang II+5 µg Ang-(1-7) EVs; 3995.0±318.5 μm^2 vs. Ang II+10 µg Ang-(1-7) EVs; 2752.0±26.1 μm^2, n=3, $p<0.001$) (Figure 5-7 B). Together these data suggest that EVs electroporated in the presence of Ang-(1-7) are able to inhibit Ang II-induced cellular hypertrophy in H9c2 cardiomyocytes when given at a dose of at least 10 µg.

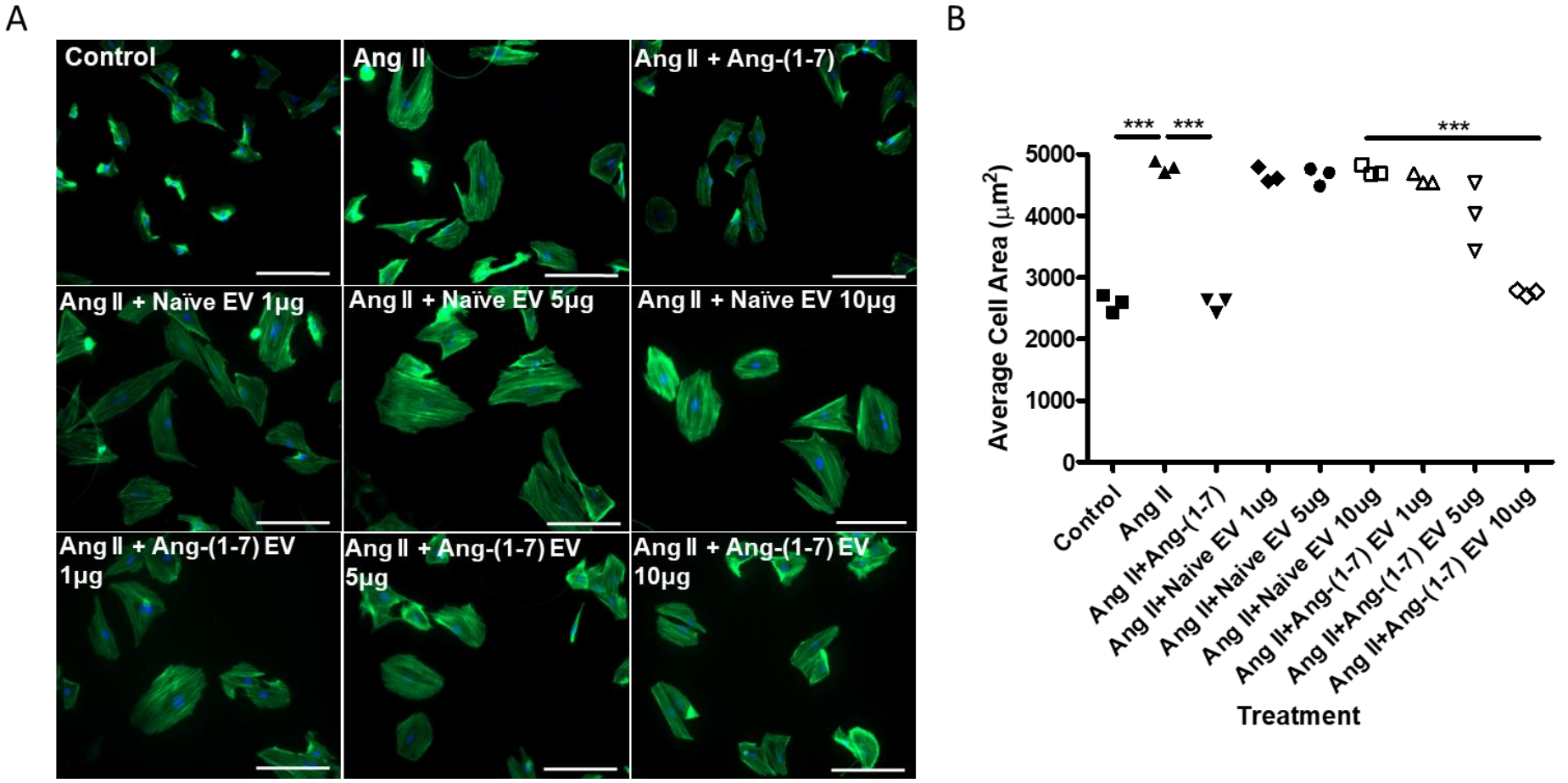

Figure 5-7 Assessment of cellular hypertrophy in H9c2 cardiomyocytes co-treated with soluble Ang II and Ang-(1-7) electroporated EVs. (A) Representative confocal images of H9c2 cardiomyocytes in each treatment group (Scale: 100 µm). (B) Analysis of H9c2 cardiomyocyte cell size under each condition (n=3, ***p<0.001, one-way ANOVA).

5.4.4 Exogenous loading of rat serum-derived extracellular vesicles with Ang-(1-7) via electroporation

Next, exogenous loading with Ang-(1-7) via electroporation was explored in serum-derived EVs to determine whether they could be used as a method of delivery *in vivo* as well as *in vitro*. EVs were isolated from the serum of healthy WKY rats and either naively electroporated or electroporated in the presence of Ang-(1-7). It was found that WKY serum-EVs electroporated in the presence of Ang-(1-7) contained significantly higher levels of peptide than naively electroporated EVs (naïve electroporated EV; 40.1±9.2 pg/mL vs. Ang-(1-7) electroporated EV; 153.1±26.7 pg/mL, n=8, $p<0.01$) (Figure 5-8 A). Interestingly, it was also observed that naïve EVs contain a higher baseline level of Ang-(1-7) than previously observed in EVs derived from cell culture media (Figure 5-6 E). Diluting Ang-(1-7) electroporated EVs significantly reduced detection levels, however not by the expected magnitude for a 1/500 dilution, suggesting that EVs may be more efficiently loaded than the ELISA kit used is able to detect accurately (Figure 5-8 B). Together, these data suggest that a low baseline level of Ang-(1-7) is present in WKY serum-derived EVs, however the Ang-(1-7) content may be significantly increased via electroporation in the presence of the peptide.

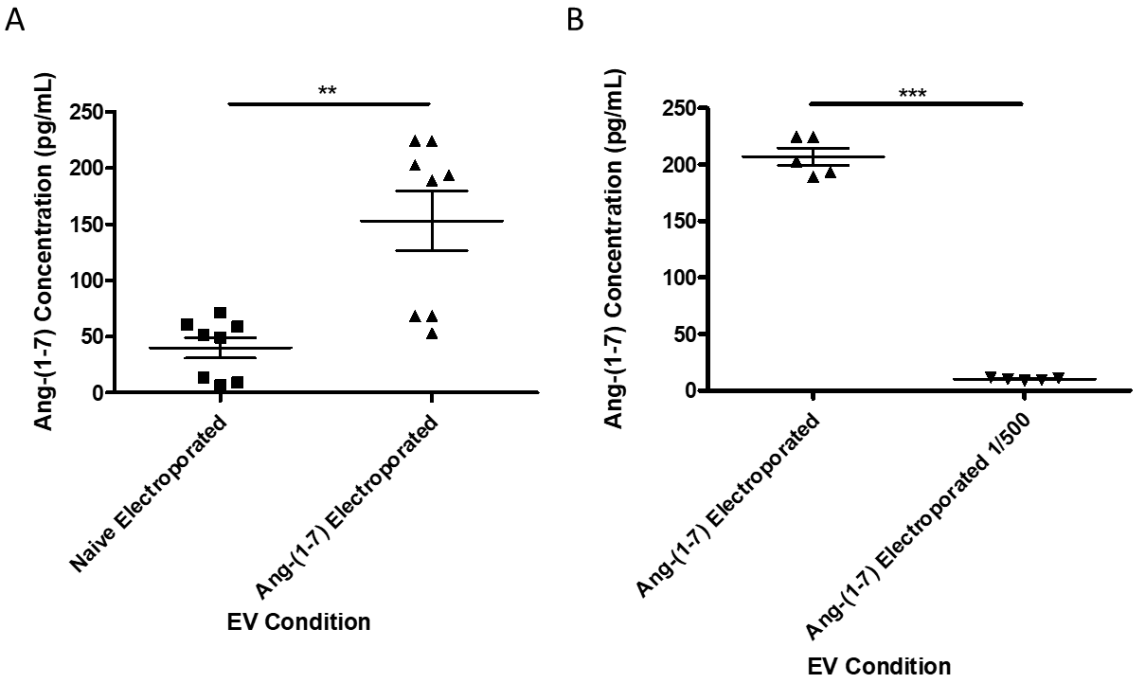

Figure 5-8 Assessment of electroporation efficiency in WKY serum-derived EVs by ELISA. (A) Analysis of Ang-(1-7) content in naïve electroporated EVs vs. Ang-(1-7) electroporated EVs by ELISA (n=8, **p<0.01). (B) ELISA analysis of diluted Ang-(1-7) electroporated EVs (n=5, ***p<0.001, Student's t-test).

5.4.5 Effect of Ang-(1-7) loaded serum extracellular vesicles on Ang II-induced hypertrophy in H9c2 cardiomyocytes

Having established that WKY serum-derived EVs are able to be efficiently loaded with Ang-(1-7) via electroporation, it was next of interest to determine whether these EVs could inhibit Ang II-induced hypertrophy in the H9c2 cardiomyocyte model. EVs isolated from WKY serum were naively electroporated or electroporated in the presence of Ang-(1-7), treated with proteinase K and then placed onto H9c2 cardiomyocytes at a dose of 10 µg. Cells were co-stimulated with 100 nM Ang II. Untreated cells and cells treated with 100 nM Ang II only were used as controls for the hypertrophic response. Cells were then imaged in order to determine any changes in cell size (Figure 5-9).

Representative images for each treatment group are shown in Figure 5-9 A. It was confirmed that stimulation with 100 nM Ang II induced a significant increase in cell size with observation of F-actin rearrangement, compared with control untreated cells, while co-stimulation with 100 nM Ang II and 100 nM Ang-(1-7) did not induce cellular hypertrophy (control untreated; 3495.0±44.7 μm^2 vs. 100 nM Ang II stimulated; 5837.0± 19.6 μm^2 vs. 100 nM Ang II+100 nM Ang-(1-7) stimulated; 3512.0±46.0 μm^2, n=3, $p<0.001$) (Figure 5-9 B). Interestingly, it was found that treatment with naïvely electroporated serum EVs at a dose of 10 µg was also able to significantly blunt Ang II-induced cellular hypertrophy (Ang II stimulated; 5837.0± 19.6 μm^2 vs. Ang II+10 µg naïve EVs; 4127.0±62.0 μm^2 vs. Ang II+10 µg Ang-(1-7) EVs; 3564.0±148.2 μm^2, n=3, $p<0.01$, $p<0.001$) (Figure 5-9 B). Together these data suggest that WKY serum-derived EVs electroporated in the presence of Ang-(1-7) are able to inhibit Ang II-induced cellular hypertrophy in H9c2 cardiomyocytes. Interestingly, a protective effect is also observed after treatment with the control EVs, a result which could be attributed to the baseline levels of Ang-(1-7) found within these vesicles (Figure 5-8 A).

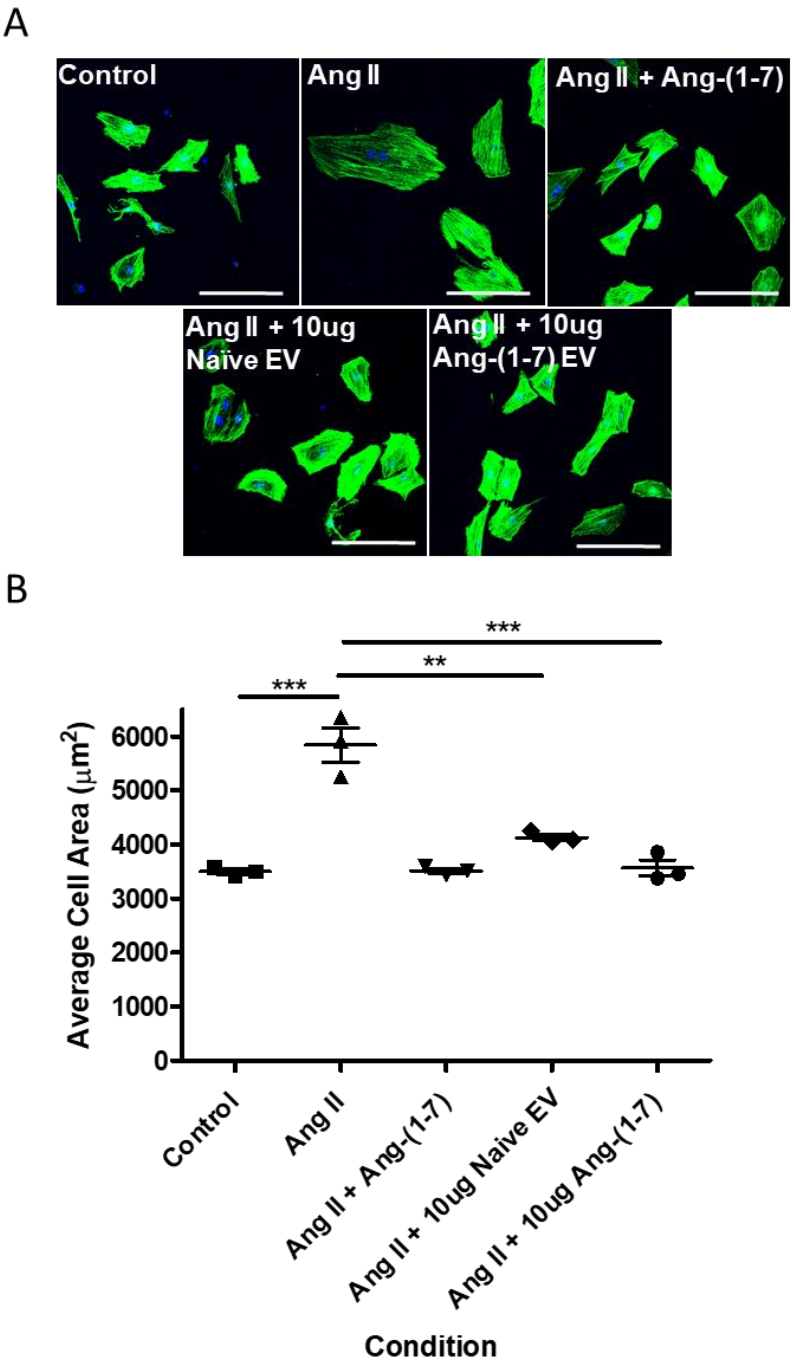

Figure 5-9 Assessment of cellular hypertrophy in H9c2 cardiomyocytes co-treated with soluble Ang II and electroporated serum-derived EVs. (A) Representative confocal images of H9c2 cardiomyocytes in each treatment group (Scale: 100 μm). (B) Analysis of H9c2 cardiomyocyte cell size under each condition (n=3, **p<0.01, ***p<0.001, one-way ANOVA).

5.4.6 Effect of Ang-(1-7) loaded serum extracellular vesicles on blood pressure in Ang II-infused Wistar Kyoto rats

Having established a cardio-protective effect for Ang-(1-7) loaded EVs *in vitro*, the protective capabilities were next assessed *in vivo*. EVs isolated from WKY serum were naively electroporated or electroporated in the presence of Ang-(1-7). Next, 11-week-old male WKY rats were either vehicle infused or continuously infused with Ang II at a dose of 200 ng/kg/min over 14 days. At day 0 and day 7 a bolus injection of 30 µg naïve EVs, Ang-(1-7) EVs or PBS control was introduced via the femoral vein. Systolic blood pressure was measured via tail cuff plethysmography at day 0 prior to surgery and day 14 as an endpoint measure (Figure 5-10).

Day 0 systolic blood pressure measurements showed animals across all groups to be in the range of approximately 130-140 mm Hg (control+PBS; 139.3±4.1 mm Hg, Ang II+PBS; 134.8±4.4 mm Hg, Ang II+Naïve EV; 136.9±4.6 mm Hg, Ang II+Ang-(1-7) EV; 141.2±2.2 mm Hg, n=8 per group) (Figure 5-10 A). At day 14 systolic blood pressure had risen variably across all groups ranging from approximately 140-160 mm Hg (control+PBS; 141.8±6.4 mm Hg, Ang II+PBS; 158.0±11.4 mm Hg, Ang II+Naïve EV; 146.0±5.0 mm Hg, Ang II+Ang-(1-7) EV; 148.6±7.0 mm Hg, n=8 per group) (Figure 5-10 B).

Analysis of change in systolic blood pressure between day 0 and day 14 showed a variable increase across the groups. Control+PBS animals showed little change across the 14 day period (0.8±9.6 mm Hg, n=8 per group) while Ang II+PBS animals appeared to exhibit a larger increase in systolic blood pressure over this time (22.1±12.9 mm Hg, n=8 per group) however this change was not significant. The data suggests that blood pressure raised slightly for both the naïve EV treatment group and Ang-(1-7) EV treatment group (Ang II+Naïve EV; 6.9±7.9 mm Hg, Ang II+Ang-(1-7) EV; 9.7±4.8 mm Hg, n=8 per group) however these changes did not reach statistical significance (Figure 5-10 C).

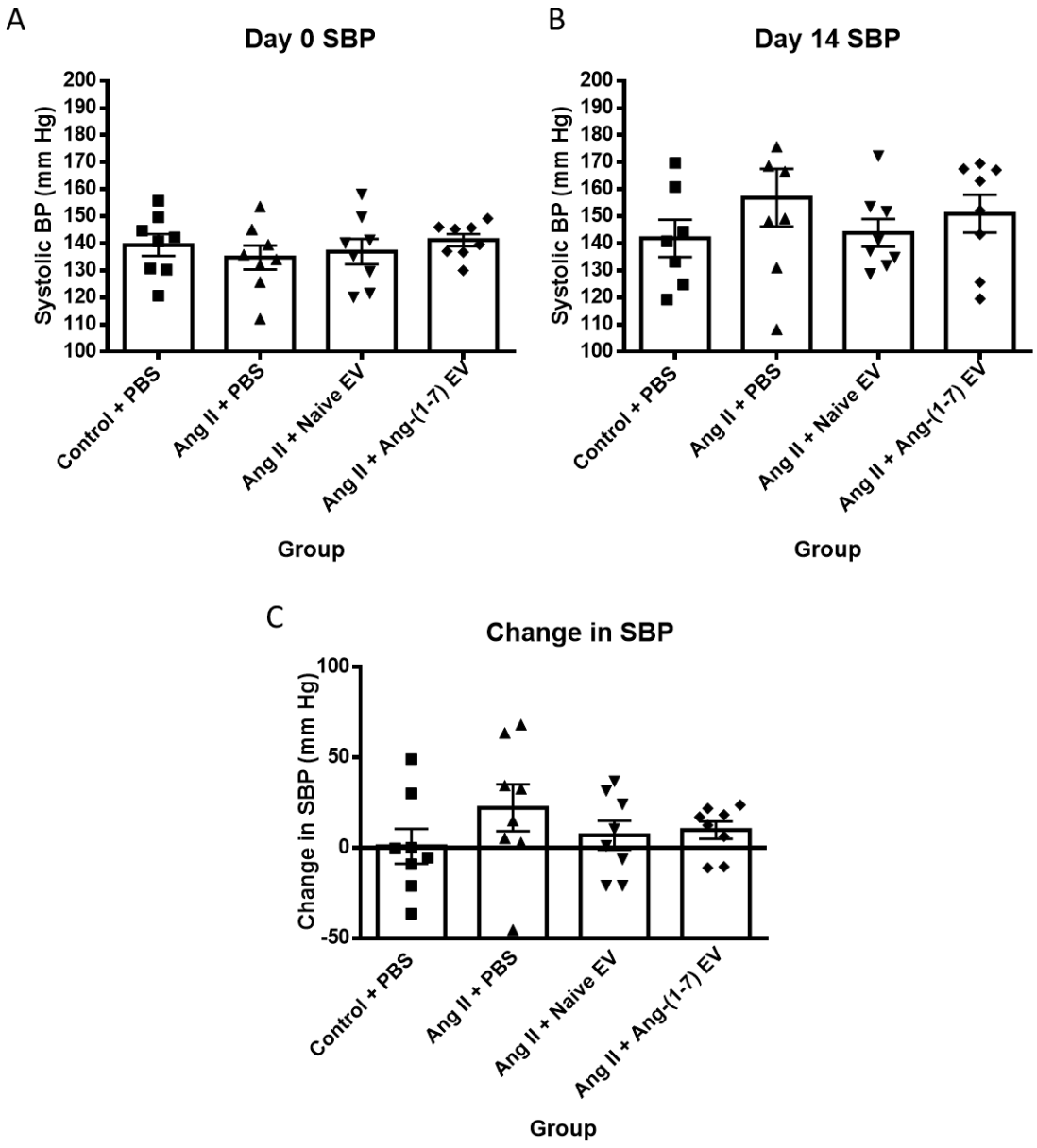

Figure 5-10 Analysis of systolic blood pressure by tail cuff plethysmography between day 0 and day 14. (A) Average day 0 systolic blood pressure across each treatment group. (B) Average day 14 systolic blood pressure across each treatment group. (C) Change in blood pressure between day 0 and day 14 for each treatment group (n=8 per group, p=0.44).

5.4.7 Effect of Ang-(1-7) loaded serum extracellular vesicles on cardiac dysfunction in Ang II-infused Wistar Kyoto rats

The effect of Ang-(1-7) loaded EVs on cardiac function was assessed next via transthoracic echocardiography in each of the 4 treatment groups (control+PBS, Ang II+PBS, AngII+naïve EVs, Ang II+Ang-(1-7) EVs). Data was displayed as change in percentage fractional shortening between day 0 and day 14 (Figure 5-11).

The day 0 data showed that all groups had fractional shortening in the range of 53-57 % (control+PBS; 54.3±2.0 %, Ang II+PBS; 55.7±2.3 %, AngII+naïve EVs; 53.9±3.4 %, Ang II+Ang-(1-7) EVs; 56.2±1.6 %, n=8 per group) (Figure 5-11). The day 14 data showed no significant differences in fractional shortening for any of the groups when compared to their respective day 0 measurements (control+PBS; 53.3±1.7 %, Ang II+PBS; 53.8±3.2 %, Ang II+Ang-(1-7) EVs; 55.1±1.7 %, AngII+naïve EVs 54.8±3.6 %, n=8 per group). As these data did not reach statistical significance, it shows that no differences in cardiac function were revealed during this study (Figure 5-11).

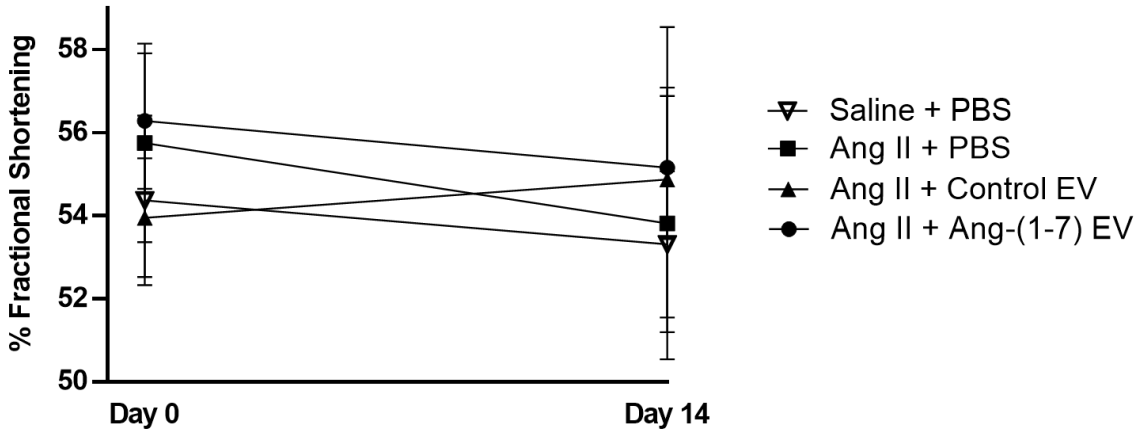

Figure 5-11 Analysis of cardiac dysfunction via transthoracic echocardiography between day 0 and day 14. Change in average % fractional shortening for each treatment group between day 0 and day 14 (n=8 per group, p=0.35).

5.4.8 Effect of Ang-(1-7) loaded serum extracellular vesicles on fibrosis in the hearts of Ang II-infused Wistar Kyoto rats

At day 14, all animals were humanely killed, and heart tissue was collected and fixed for histological analysis. Sections were stained with picrosirius red to analyse the extent of fibrosis in the heart across each of the 4 treatment groups; control+PBS, Ang II+PBS, AngII+naïve EVs, and Ang II+Ang-(1-7) EVs (Figure 5-12). Representative images for each treatment group are shown (Figure 5-12 A). Analysis of percentage fibrosis across each group showed that picrosirius red staining could be detected in both the vehicle-infused and the Ang II-infused animals, however there was no significant difference in percentage fibrosis between the two groups (Figure 5-12 B). The data did not reveal any significant differences in percentage fibrosis between any of the groups analysed (Ang II+PBS; 7.0±2.3 %, Ang II+naïve EVs; 10.7±3.2 %, Ang II+Ang-(1-7) EVs; 4.2±1.0 %, n=8 per group). Although it appeared that there was a slight reduction in percentage fibrosis under treatment with Ang-(1-7) loaded EVs, this data did not reach statistical significance (Figure 5-12 B).

A

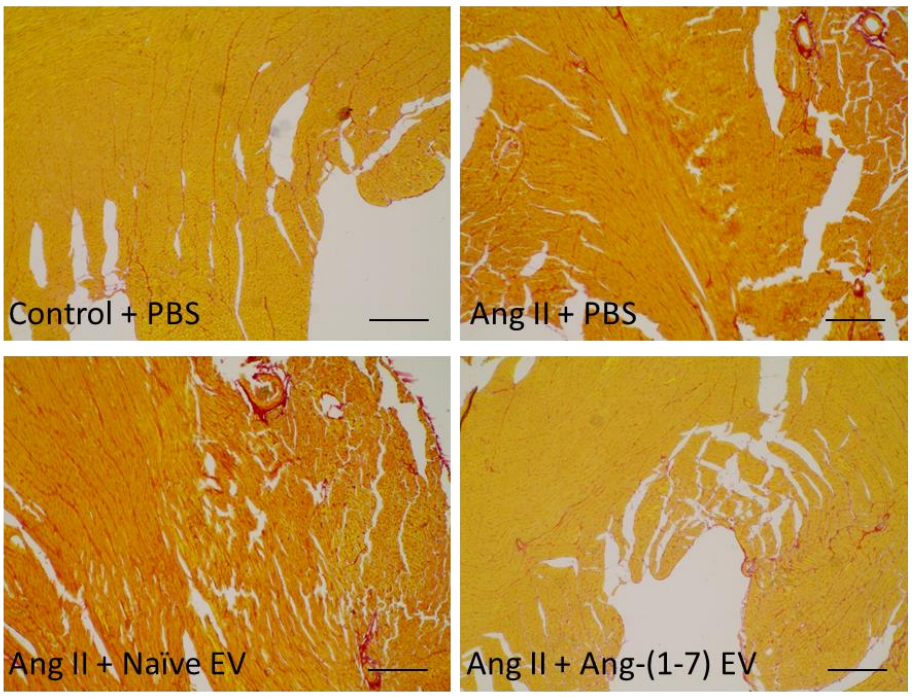

B

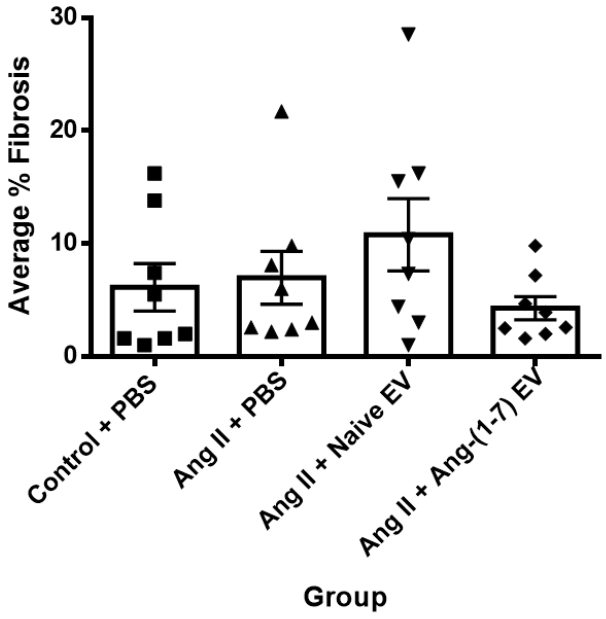

Figure 5-12 Analysis of percentage fibrosis in the heart via picrosirius red staining across each treatment group. (A) Representative images of picrosirius red stained heart sections for each treatment group (images obtained from median animal of each group) (10x Magnification, scale: 100 μm). (B) Analysis of percentage fibrosis in each treatment group (n=8 per group, p=0.25).

5.4.9 Effect of Ang-(1-7) loaded serum extracellular vesicles on cardiac hypertrophy in Ang II-infused Wistar Kyoto rats

Further parameters used to assess the cardio-protective potential of Ang-(1-7) loaded EVs were heart weight to tibia length ratio to assess cardiac hypertrophy along with further histological analysis utilising wheat germ agglutinin staining to determine the extent of cardiomyocyte hypertrophy across the 4 treatment groups; control+PBS, Ang II+PBS, AngII+naïve EVs, and Ang II+Ang-(1-7) EVs (Figures 5-13 & 5-14). The HW/BW data suggests that continuous infusion with Ang II slightly increases the ratio compared with vehicle infused animals, while treatment with Ang-(1-7) EVs inhibits this increase in cardiac hypertrophy, where naïve EVs do not (control+PBS; 0.0031±0.0011, Ang II+PBS; 0.0034±0.0012, AngII+naïve EVs; 0.0034± 0.0012, Ang II+Ang-(1-7) EVs; 0.0032±0.0011, n=8 per group), however these differences were not found to be significant (Figure 5-13 A). Similarly, assessment of cardiac hypertrophy via LV/TL ratio suggests a slight increase in hypertrophy in Ang II infused animals compared with vehicle infused animals, while again Ang-(1-7) EVs show a potential protective effect where naïve EVs do not, however no significant differences were observed (Figure 5-13 B).

Cardiomyocyte hypertrophy was also determined via wheat germ agglutinin staining across the 4 treatment groups. Sections were imaged and cell size was determined by both measurement of cell area and measurement of Feret's maximum diameter (Pertl et al., 2013) (Figure 5-14). Representative images for each treatment group are shown (Figure 5-14 A). Analysis of average cell area suggested that continuous Ang II infusion stimulated cardiomyocyte hypertrophy compared with vehicle infusion, while treatment with Ang-(1-7) loaded EVs, but not naïve EVs, slightly dampened this effect (control+PBS; 1409±104 μm^2 vs. Ang II+PBS; 1707±118 μm^2 vs. Ang II+naïve EVs; 1714±112 μm^2 vs. Ang II+Ang-(1-7) EVs; 1521±104 μm^2, n=8 per group) however the changes were not statistically significant (Figure 5-14 B). Analysis of cell diameter showed a similar result (control+PBS; 53.9±2.0 µm vs. Ang II+PBS; 60.4±2.7 µm vs. Ang II+naïve EVs; 61.1±2.1 µm vs. Ang II+Ang-(1-7) EVs; 56.6±2.5 µm, n=8 per group) (Figure 5-14 B) however, again data did not reach statistical significance.

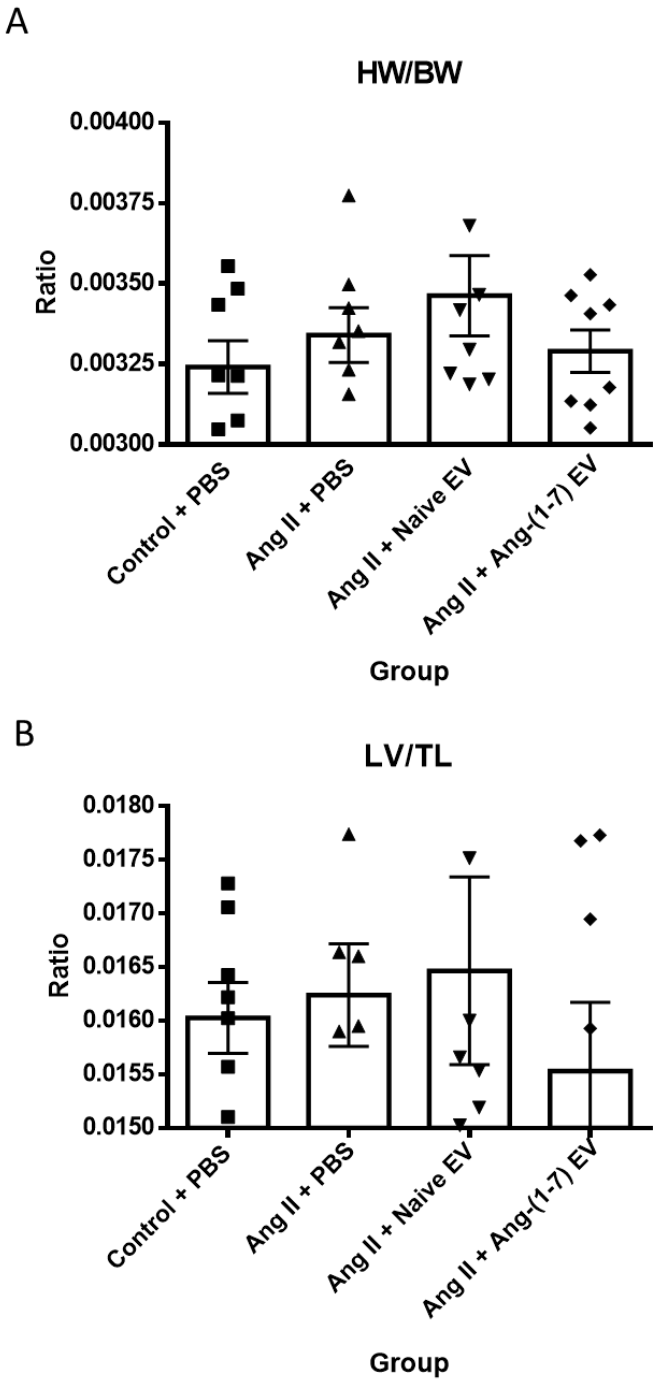

Figure 5-13 Analysis of cardiac hypertrophy via HW/BW and LV/TL ratios. (A) Analysis of HW/BW ratios across the 4 treatment groups (n=8 per group, p=0.30). (B) Analysis of LV/TL ratios across the 4 treatment groups (n=8 per group, p=0.47).

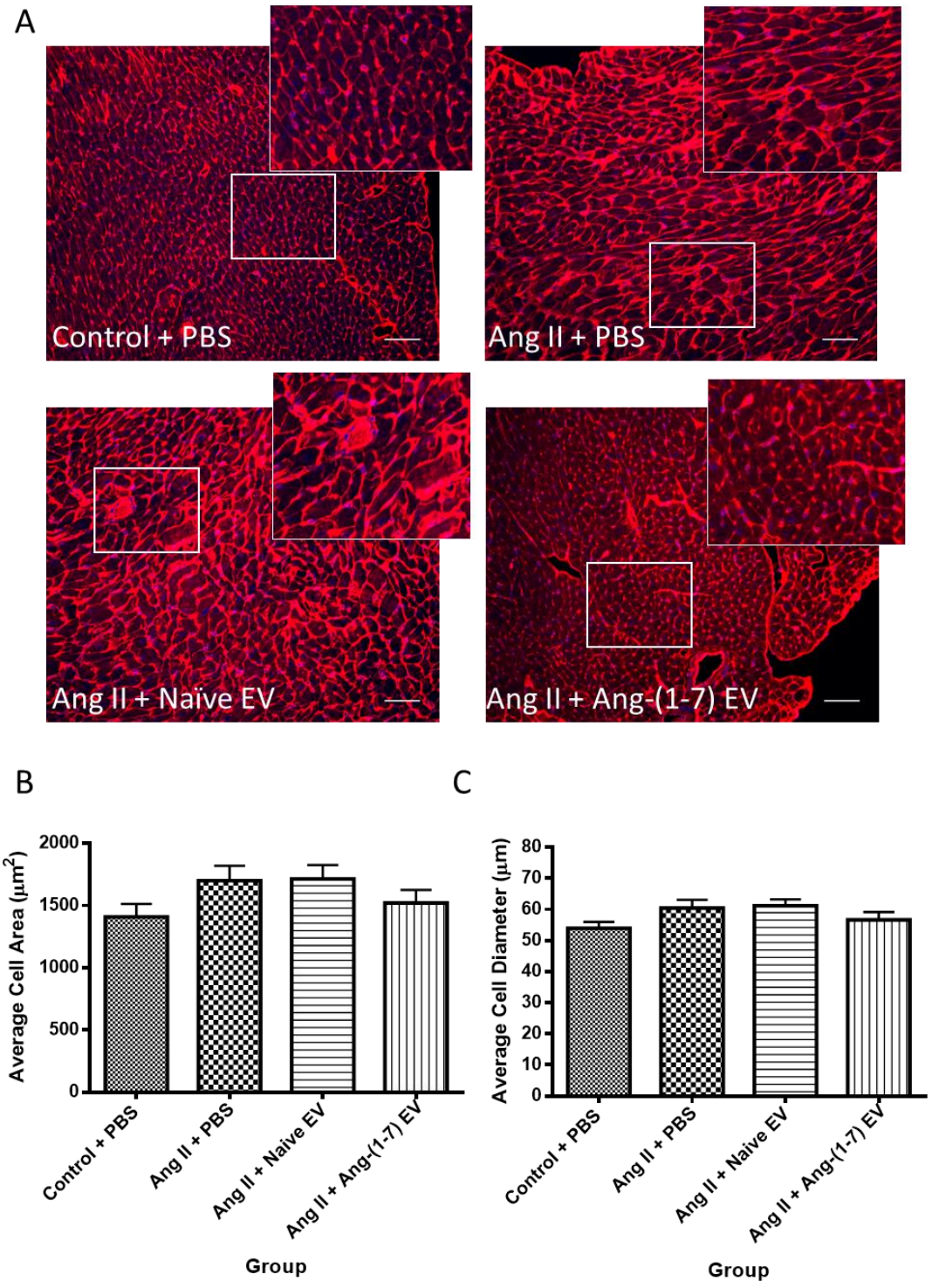

Figure 5-14 Analysis of cardiomyocyte hypertrophy via wheat germ agglutinin staining across each treatment group. (A) Representative images of wheat germ agglutinin and DAPI stained heart sections for each treatment group (images obtained from median animal of each group) (20x Magnification, scale: 100 µm). (B) Analysis of average cell area and (C) diameter in each treatment group (n=8 per group, area; p=0.16, diameter; p=0.13).

5.5 Discussion

In this study, *in vitro* investigations showed that EVs released from Ang-(1-7)-stimulated H9c2 cardiomyocytes were able to inhibit cellular hypertrophy induced by co-treatment with Ang II, which suggested Ang-(1-7) was also present within the EVs released from stimulated parental cells (as described for Ang II in Chapter 4). In terms of use as a therapeutic delivery vehicle, it was of interest to investigate the possibility of increasing peptide levels within EVs via exogenous loading for delivery in both *in vitro* and *in vivo* models of hypertrophy. Electroporation of EVs in the presence of Ang II or Ang-(1-7) significantly increased levels of peptide within the vesicles highlighting the potential for this loading method.

Investigation of cardiomyocyte hypertrophy commonly utilises Ang II stimulation models for induction of the response (Flores-Muñoz et al., 2011). Various studies have shown that treatment with Ang-(1-7) negates the pathological effects of Ang II and provides protection in the cardiovascular setting. It has been demonstrated that co-treatment of H9c2 cardiomyocytes with soluble 100 nM Ang II and 100 nM Ang-(1-7) peptide prevents the characteristic increase in cell size and F-actin rearrangement normally observed under treatment with Ang II over 96 hr (Flores-Muñoz et al., 2011). A similar observation was made when using adenoviral delivery of Ang-(1-7) in the same model of Ang II-induced cardiomyocyte hypertrophy (Flores-Munoz et al., 2012a). As such, this model (Flores-Muñoz et al., 2011) was used in the present study to control for the hypertrophic effects of Ang II stimulation, and the anti-hypertrophic effects of co-stimulation with Ang-(1-7). Further studies also report the antagonising effects of Ang-(1-7) against Ang II. A study utilising NRCMs found that treatment with Ang II significantly increased the surface area of the cardiomyocytes as well as increased protein synthesis and expression of hypertrophy markers, all of which could be blunted by co-treatment with Ang-(1-7) (Lin et al., 2016). *In vivo* studies found that continuous infusion of Ang II and Ang-(1-7) at equal doses in Sprague-Dawley rats reduced cardiomyocyte cross-sectional area, interstitial fibrosis, and expression of hypertrophy markers normally observed under Ang II infusion alone (McCollum et al., 2012). A similar study also performed in normotensive Sprague-Dawley rats found that continuous infusion of both peptides attenuated the cardiac hypertrophy and perivascular fibrosis

phenotypes observed when animals were infused with Ang II alone (Guo et al., 2017). Taken together, these studies highlight the therapeutic potential for Ang-(1-7) demonstrated both *in vitro* and *in vivo*. However, in these studies, delivery is reliant on continuous infusion by subcutaneous osmotic minipump implantation, a method only viable in animal studies. This highlights the importance of exploring other delivery avenues for Ang-(1-7), for example use of EVs in the present study.

In this study, it was demonstrated that EVs derived from either control H9c2 cardiomyocytes or the serum of healthy normotensive animals could be exogenously loaded with Ang-(1-7) via electroporation. Furthermore, it was found that the EV loaded Ang-(1-7) retained its functionality, providing protective effects when delivered in an *in vitro* model of Ang II-induced cardiomyocyte hypertrophy. Although electroporation has become a commonly used method for loading EVs, it has primarily been utilised in the transfer of nucleic acids such as miRNA, siRNA and DNA (Liu and Su, 2019) as opposed to delivery of peptides or proteins. However, although a seemingly promising method some studies have reported the occurrence of adverse effects to the EVs themselves as a result of electroporation (Johnsen et al., 2014), which may hinder their ability to deliver therapeutic cargo. One study investigating the efficiency of siRNA loading by electroporation reported that the protocol itself resulted in siRNA aggregates which could not actually be retained within the exosomes and initially gave false positive results in fluorescent co-localisation studies (Kooijmans et al., 2013). Several others demonstrated that the exosomes themselves could also aggregate (Hood et al., 2014, Johnsen et al., 2016). These studies also reported that use of a trehalose-based pulse media could diminish exosome aggregation while still permitting efficient loading, providing a viable method of maintaining the structural integrity of the delivery vehicles (Hood et al., 2014, Johnsen et al., 2016). The results reported in these studies provided key information for the design of the present study, which utilised both trehalose buffer to minimize EV aggregates, and proteinase K treatment to digest any excess peptide or peptide aggregates which may remain in the EV solution after electroporation. Although this study investigated the loading of peptides into EVs as opposed to nucleic acids, the data gathered using the

aforementioned techniques and analysis by ELISA suggests successful and efficient loading into EVs via this method.

The present studies also demonstrated that Ang-(1-7) exogenously loaded into EVs could mediate a protective effect. It was found that EVs loaded with Ang-(1-7) could protect H9c2 cardiomyocytes from hypertrophy induced by Ang II. The effect of Ang-(1-7)-EVs was comparable to that reported with soluble Ang-(1-7) peptide (Flores-Muñoz et al., 2011). Other studies using electroporated vesicles also found their cargo to remain functional once delivered. It was found that MSC-derived exosomes could be loaded with miR-132 via electroporation and that these exosomes were then able to increase target gene expression in endothelial cells, resulting in increased angiogenic ability (Ma et al., 2018). It was then demonstrated that these miR-132-loaded exosomes could promote angiogenesis *in vivo* in a mouse model of myocardial infarction (Ma et al., 2018). Again, although focused on nucleic acid loading, this research highlights the potential for loaded EVs as a delivery vehicle for functional molecules in cardiovascular disease.

The final part of the present studies aimed to establish the effects of the Ang-(1-7) loaded EVs in an *in vivo* model of cardiovascular disease. The present study attempted to use continuous Ang II infusion as a stimulus to induce adverse cardiovascular effects such as hypertension, cardiac hypertrophy and cardiac fibrosis in order to investigate the potential for EVs to deliver functionally protective Ang-(1-7). Generally, the Ang II dose and exposure time used to elicit adverse cardiovascular effects in rodents is variable across different research studies. The present study utilised a dose of 200 ng/kg/min across 14 days, which prior studies have reported to be effective (Cui et al., 1999, Yan et al., 2019). Although data for the parameters investigated here suggest a potential response to Ang II, Ang II infusion did not actually significantly increase blood pressure, cardiac fibrosis or cardiac hypertrophy compared with vehicle infused animals. In terms of systolic blood pressure, measurements were obtained via tail cuff plethysmography and although the data suggests there may be an increase in systolic blood pressure on Ang II infusion, variability and error in the readings prevented statistical significance. This could suggest that the Ang II dose and exposure period is correct, however a more accurate method of

measuring blood pressure may need to be utilised in future studies. It has been found in investigations across several species (including mice and rats) that direct methods of measuring blood pressure, such as via radiotelemetric recording, is more accurate than indirect methods such as tail cuff (Kurtz et al., 2005). The inaccuracies found with the indirect tail cuff method have been attributed to restraint stress, where large differences in systolic blood pressure readings have been observed in rodents even when they have been thoroughly pre-conditioned to the system (Gross and Luft, 2003, Popovic, 1988, Irvine et al., 1997). Due to the fact that implantable radiotelemetry allows for continuous and direct measurements of systolic blood pressure in rats without the need for restraint (Kramer and Kinter, 2003), it may be a more viable and reliable option for future studies. Aside from systolic blood pressure measurements, the current study also investigated fibrosis and cardiac hypertrophy as parameters to measure the effects of Ang II infusion, both of which are known to increase upon continuous infusion in rodents (Zhang et al., 2017b, Yan et al., 2019). Again, no statistically significant increase in percentage fibrosis or cardiomyocyte hypertrophy in response to Ang II infusion were detected. Due to the fact that both fibrosis and cardiomyocyte hypertrophy are driven by chronic increase in blood pressure (Tokuda et al., 2004, Dominiczak et al., 1997, Kagiyama et al., 2002), this could explain why no significant effects were observed in these parameters, as no significant blood pressure effects were observed throughout the present study. Variability in the animals' response to Ang II in the present study could suggest that either a higher dose or longer exposure time is required and may provide a more consistent response, which is needed to then fully and reliably assess the effects of loaded EVs in this model. Studies have shown that Ang II doses of 200 ng/kg/min (Zhang et al., 2017b) and 120 ng/kg/min (Izumiya et al., 2012) both over 4 weeks have significantly altered these cardiac parameters. This could suggest that an extension of the present study from 2 weeks to 4 weeks could allow for significant effects of Ang II infusion to take place. Furthermore, studies have shown that higher doses of Ang II, for example 400 ng/kg/min over a 4 week period (Guo et al., 2017) or 500ng/kg/min over a 4 week period (Bai et al., 2016) can induce a significant increase in blood pressure with associated cardiac pathology. Such approaches would mean the present study design would likely require addition of more bolus EV injections, or higher amounts of EVs across the extended time period.

Although statistical significance was not reached in terms of the effects of Ang II infusion, it is possible that Ang-(1-7) loaded EVs still have potential to elicit a protective effect in comparison to naïve electroporated EVs having observed promising effects *in vitro*. Due to the fact that a significant increase in blood pressure under Ang II infusion was not observed, downstream consequences such as fibrosis and hypertrophy may not be expected. As such, the protective effects of Ang-(1-7) delivery via EVs cannot be ascertained. These data suggest potential for EVs as a delivery mechanism for Ang-(1-7) in future studies after further optimisation. For example, perhaps a higher dose of EVs or more frequent injections in an optimised Ang II infusion model may elicit a stronger response than that observed in the present study. Furthermore, EVs were introduced via femoral vein injection to the circulation which, although has been shown in other cardiovascular disease-related studies to be an effective delivery method (Li et al., 2019, Sun et al., 2018b, Xin et al., 2013), is indirect and does not allow for targeting to the heart. It may be beneficial to investigate intramyocardial injection of EVs, which has been successfully demonstrated in other studies (Shi et al., 2019, Zhao et al., 2019), to ensure direct delivery to the heart. It has also been reported recently that exosomes engineered to express a cardiac tissue-targeting peptide show increased delivery to the heart, albeit by only 15%, compared to untargeted exosomes (Kim et al., 2018a). This method may help to bypass the invasiveness of intramyocardial injection and could therefore be worth exploration in future studies to ensure more efficient delivery of Ang-(1-7) loaded EVs to the heart. Lastly, it may be of interest in future studies to investigate the potential protective effects of these EVs in other models of CVD; for example it has been reported that exosomes derived from human cardiosphere-derived cells are able to aid in the recovery of the ischaemic myocardium in a rat model of myocardial infarction (Saha et al., 2019). It has also been reported that human MSC-derived exosomes are able to increase myocardial repair in rat acute myocardial infarction models via regulation of the TGF-β signalling pathway (Wang et al., 2018). These reports highlight the therapeutic potential for EVs in models of myocardial infarction, which may be an interesting avenue to explore in future studies. Furthermore, the use of EVs to deliver cardioprotective peptides to the heart with direct manipulation of the local RAS and therefore, RAS-induced hypertrophy, may be beneficial to areas of CVD such as HF-pEF for which there is urgent clinical need.

5.5.1 Study limitations

A key aim of this study was to analyse the effects of Ang-(1-7) loaded EVs in an *in vivo* model of Ang II-induced hypertension and subsequent cardiac hypertrophy. The interpretation of results was limited by the fact that the Ang II dose used did not significantly increase blood pressure and, as such, it is unlikely that any downstream effects of hypertension, such as hypertrophy, fibrosis or cardiac dysfunction would occur. It is possible that 14 days was not a long enough time period for the induction of blood pressure increase as well as observation of downstream effects in control animals and therefore adjustment of this would benefit future studies.

5.6 Summary

EVs released from Ang-(1-7) stimulated H9c2 cardiomyocytes are able to inhibit hypertrophy induced by co-stimulation with Ang II in recipient H9c2 cardiomyocytes. The ELISA data suggests that EVs released from H9c2 cardiomyocytes can be exogenously loaded with Ang II or Ang-(1-7) via electroporation with high efficiency. Furthermore, cell sizing data suggests that Ang-(1-7) loaded EVs are able to inhibit Ang II-induced hypertrophy. Similarly, it was found that EVs derived from WKY serum and loaded with Ang-(1-7) could also inhibit Ang II-induced hypertrophy *in vitro* and interestingly, this inhibitory effect was also observed following treatment with control serum-derived EVs.

Analysis of the effects of Ang-(1-7) loaded EVs *in vivo* showed no statistically significant findings across any of the parameters investigated. However, with further optimisation, delivery of Ang-(1-7) via EVs may prove to be a beneficial therapeutic approach against hypertension and downstream cardiac hypertrophy.

Chapter 6 Analysis of EVs derived from the serum of coronary artery bypass patients vs. control healthy subjects

6.1 Introduction

6.1.1 Coronary artery disease

Coronary artery disease (CAD), also known as ischaemic heart disease is a common cause of death in the UK (and the most common cause of premature death), killing over 66,000 people per year, and commonly occurs as a response to chronic hypertension (Mendis and Norrving, 2011). CAD manifests as a reduction of blood flow to the heart muscle due to development of atherosclerotic plaques in the coronary arteries and often results in adverse cardiac events including angina, myocardial infarction and sudden cardiac death (Wong, 2014). In the most severe cases of the disease, surgical procedures such as angioplasty and stent insertion to open narrowed or blocked vessels, or CABG surgery are used to improve life expectancy and reduce the risk of myocardial infarction (Rezende et al., 2015).

Vascular remodelling is generally characterised by changes in the size and composition of blood vessels in response to changes in blood flow, for example increased blood pressure (Ross, 1999). Damage or injury to the vessel wall causes wearing to the endothelial cell layer which in turn increases the occurrence of thrombosis and inflammation at the site of injury (Ross, 1999, West et al., 2001). This environment promotes the growth and migration of VSMCs as well as degradation of the extracellular matrix (Galis and Khatri, 2002, West et al., 2001) both of which are characteristic of pathological vascular remodelling. Various studies have highlighted the importance of the RAS in terms of vascular remodelling. Altered RAS signalling is a key contributor to the remodelling of the vasculature where pathology is generally mediated by Ang II signalling via the AT_1R (Hunyady and Catt, 2006), confirmed by use of ACEi and ARBs. It has been shown in various animal models that use of ACEi may reduce atherosclerosis (Charpiot et al., 1993, Hayek et al., 1999) while use of ARBs has been shown to reduce atherosclerotic lesion size (Daugherty et al., 2004). Conversely, it has been demonstrated that the counter-regulatory axis of the RAS protects against pathological outcomes by inhibiting the actions of Ang II. For example, overexpression of ACE2 via adenoviral gene transfer was found to reduce the inflammatory response in a rabbit model of atherosclerosis (Dong et al., 2009). Furthermore, the effects observed were associated with reduced

levels of Ang II and increased levels of Ang-(1-7) (Dong et al., 2009). *In vitro* studies have also highlighted the importance of Ang-(1-7) in the vasculature where signalling via the Mas receptor has been found to inhibit MAPK/ERK1/2 signalling resulting in reduced proliferation and migration of VSMCs, contrasting the effects of Ang II (Zhang et al., 2010).

6.1.2 Extracellular vesicles as circulating biomarkers in CVD

Analysis of EVs from human serum or plasma samples is still in the preliminary stages of research, however various studies have reported differences in EV populations released from CVD patients vs. healthy control subjects. Atherosclerosis involves the formation of plaque within the arteries where continual build-up over time results in narrowing of the arteries and continuous damage to the vascular endothelium (Libby et al., 2002). Development generally begins with early endothelial dysfunction occurring secondary to other factors such as hypertension or diabetes mellitus (Libby et al., 2002). Initially, low-density lipoproteins (LDL) accumulate within the vascular wall and once oxidised (Wilensky and Hamamdzic, 2007) release bioactive phospholipids which activate endothelial cells. This in turn upregulates cell surface integrin receptors allowing for interaction with adhesion molecules, such as ICAM-1 and VCAM-1, and thus facilitating the entry of inflammatory immune cells into the vessel wall intima (Amberger et al., 1997). Immune cells such as macrophages, T lymphocytes and mast cells have been found to produce pro-atherogenic mediators which further regulate cell recruitment, migration, proliferation and death, along with production of extracellular matrix, contributing to the progression of atherosclerotic plaques (Amberger et al., 1997, Wilensky and Hamamdzic, 2007).

It has been found that endothelial injury results in increased production of EVs from endothelial cells. Studies have shown that in diabetes mellitus patients suffering from diseases such as atherosclerosis, where there is extensive damage to the endothelium, increased levels of circulating EVs derived from endothelial cells are observed, confirmed by the presence of endothelial cell specific marker CD144 (VE-cadherin) on the EV surface (Koga et al., 2005). This study showed that endothelial-derived plasma EV levels were significantly higher in diabetes patients compared to those without diabetes, and that the elevated levels of

endothelial EVs were significantly associated with risk of coronary artery disease, more so than traditional risk factors such as high LDL-cholesterol and low HDL-cholesterol (Koga et al., 2005). Furthermore, this study presented endothelial-derived EVs as circulating biomarkers for identifying diabetes patients with risk of coronary artery disease development (Koga et al., 2005).

EVs have also been studied in patients with severe hypertension (defined as having diastolic blood pressure greater than 120 mm Hg and/or systolic blood pressure greater than 220 mm Hg). It was shown that both endothelial-derived and platelet-derived circulating microvesicles were increased in severely hypertensive patients (who were untreated at the time) compared to patients with mild hypertension (defined as having diastolic blood pressure greater than 95 mm Hg but less than 100 mm Hg) and normotensive patients (defined as having blood pressure readings of less than 140/90 mm Hg) (Preston et al., 2003). The significant correlation observed between increased microvesicle number and increasing severity of hypertension suggest that they may be used as specific markers for endothelial activation and platelet activation in severe uncontrolled hypertension (Preston et al., 2003). These studies suggest the potential for EVs to be used as biomarkers in CVD, where differing populations may be distinguishable between healthy subjects and those suffering from CVD.

6.1.3 The Vascular Function in Coronary Artery Bypass study

The Vascular Function in Coronary Artery Bypass (VASCAB) study aimed to assess the state of the blood, heart and blood vessels of patients with severe coronary artery disease (n=163) in comparison to age-matched healthy subjects (n=63) in order to identify key factors and signs involved in the development of coronary heart disease (Taurino et al., 2010). Key parts of this study involved gene expression profiling in whole blood samples which identified differentially expressed miRNAs associated with coronary artery disease (Taurino et al., 2010) and analysis of urine samples via proteomics to determine the presence of polypeptides specific to coronary artery disease patients (Delles et al., 2010). Access to serum samples (see Appendix) from patients and healthy subjects (matched as far as possible to adjust for age and sex as confounding variables) involved in this study allowed for a comparison of serum-derived EVs from each group to be performed.

6.2 Aims

- To analyse the size and concentration of EVs released from coronary artery bypass patients vs. healthy control subjects.

- To analyse the Ang II content of EVs released from coronary artery bypass patients vs. healthy control subjects.

- To analyse the Ang-(1-7) content of EVs released from coronary artery bypass patients vs. healthy control subjects.

6.3 Key Methods

Table 6-1 Chapter 6 key methods

EV isolation	Human serum Section 2.9, 2.15
EV characterisation	Nanosight Section 2.7.1
Ang II detection within EVs	Ang II ELISA Section 2.11
Ang-(1-7) detection within EVs	Ang-(1-7) ELISA Section 2.12

6.4 Results

6.4.1 Characterisation of extracellular vesicles released from CABG patients vs. healthy control subjects via NTA

EVs were first isolated from 50 µL of serum per patient using a Total Exosome Isolation (from Serum) kit. The EVs were then characterised by NTA to assess differences in size and concentration between the CABG patient group and the healthy control subject group (Figure 6-1 and Figure 6-2).

Analysis of the size of EVs found in human serum samples showed that EVs were significantly smaller in CABG patients compared with EVs from healthy control subjects (control subjects; 149.6±3.6 nm vs. CABG patients; 136.5±5.4 nm, n=43 per group, $p<0.05$) (Figure 6-1). Although a small difference, this data may suggest differing populations released under disease conditions compared with healthy conditions.

NTA was also used to analyse the concentration of particles released in the serum samples of control healthy subjects vs. CABG patients. It was found that EVs from CABG patients were released at significantly lower concentrations than those found in the serum of healthy subjects (control subjects; $0.27\pm0.015x10^{13}$ particles/mL vs. CABG patients; $0.18\pm0.008x10^{13}$ particles/mL, n=40-42, $p<0.001$) (Figure 6-2). Again, these data suggest the potential for different EV populations to be released under disease conditions compared with healthy conditions.

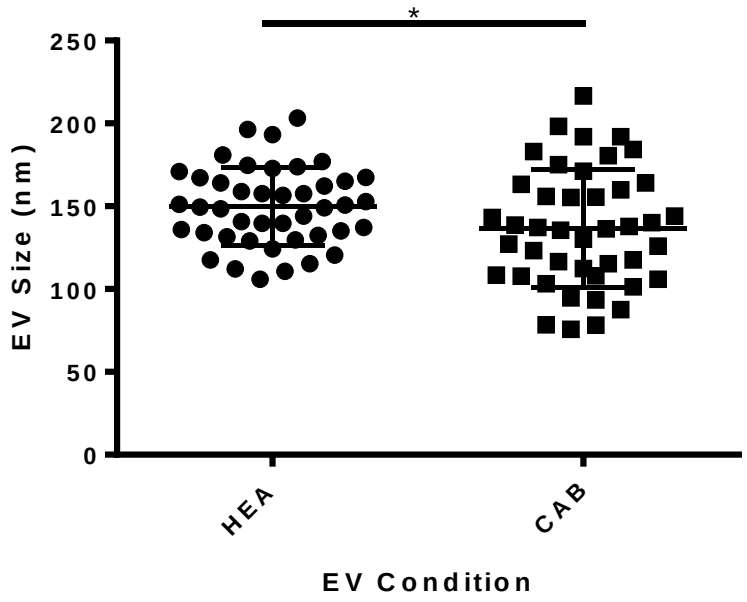

Figure 6-1 Characterisation of EV size in samples isolated from human serum. Overall size comparison of EVs derived from control healthy subjects (HEA) vs. CABG patients (CAB). EVs were isolated from 50 µL serum samples obtained from either CABG patients or healthy control subjects and analysed by NTA to determine average particle size across patient samples in each group. Each sample was analysed 5 times to give an average particle size for that patient which was then plotted for comparison (n=43 per group, *$p<0.05$, Student's t-test).

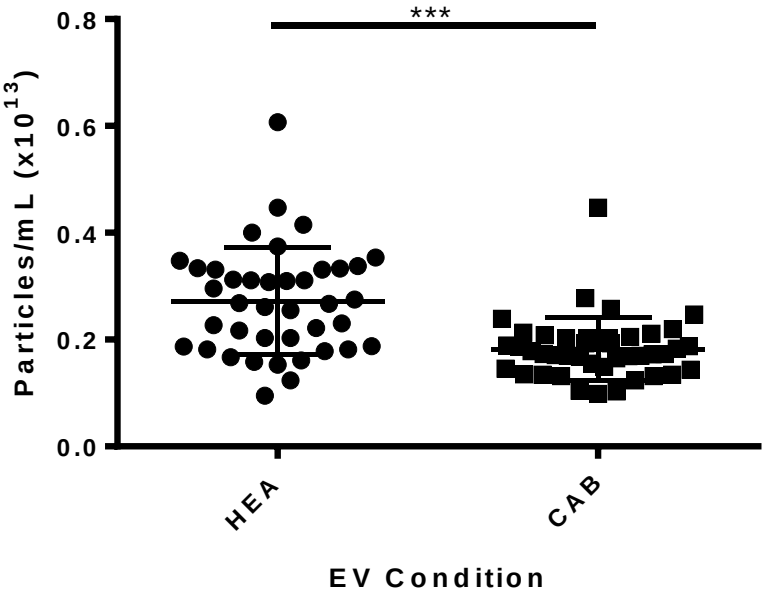

Figure 6-2 Characterisation of EV concentration in samples isolated from human serum. Overall concentration comparison of EVs derived from control healthy subjects (HEA) vs. CABG patients (CAB). EVs were isolated from 50 µL serum samples obtained from either CABG patients or healthy control subjects and analysed by NTA to determine average particle concentration across patient samples in each group. Each sample was analysed 5 times to give an average particle concentration for that patient which was then plotted for comparison (n=40-42 per group, ***p<0.001, Student's t-test).

6.4.2 Analysis of Ang II content in human serum-derived EVs by Ang II ELISA

To determine any potential differences in Ang II content of EVs derived from human serum samples between the two groups; control healthy subjects and CABG patients, isolated EVs were lysed and analysed by high-sensitivity Ang II ELISA to determine Ang II content (Figure 6-3).

It was found that Ang II could be detected at low levels within EVs derived from the serum of certain healthy control patients, where on average 2.4±0.72 pg/mL Ang II was detected (n=33), although it was undetectable in a large number of these subjects (n=14). It was also found that Ang II could be detected at significantly higher levels in CABG patients compared with the healthy controls, where on average CABG patient EVs contained 9.1±1.37 pg/mL and here, Ang II was only undetectable in one patient sample (n=36, $p<0.001$) (Figure 6-3). Data was also analysed by Fisher's exact test to determine statistical significance between the proportion of samples with detectable Ang II for healthy (detected in 18/33 samples) vs. CABG patient (detected in 35/36 samples) EVs ($p<0.001$). These data show that the EVs derived from CABG patients contain higher levels of Ang II compared to healthy control subjects.

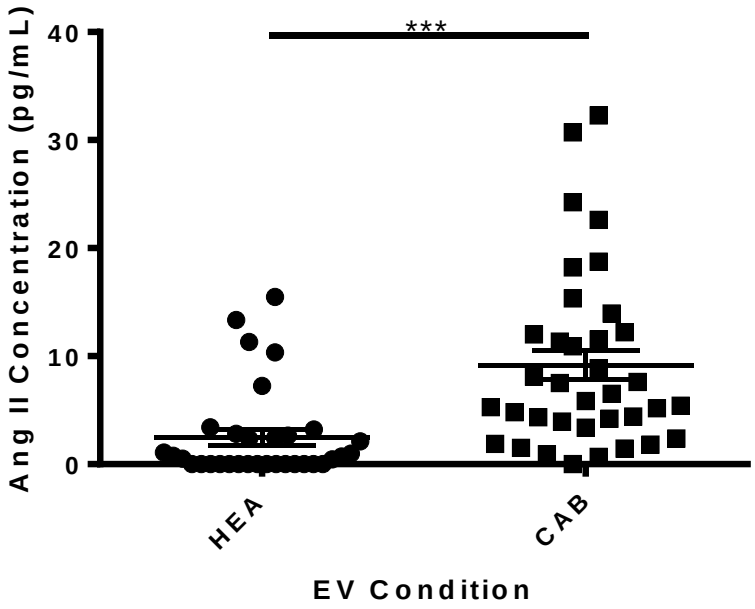

Figure 6-3 Analysis of Ang II content in EV samples isolated from human serum. Comparison of the Ang II levels found within serum-derived EVs from control healthy subjects (HEA) vs. CABG patients (CAB). 10 µg EVs isolated from the serum of CABG patients or healthy control subjects were lysed in RIPA buffer and Ang II content was then measured via high-sensitivity Ang II ELISA. Each EV sample was measured in duplicate to give the average Ang II level present for each patient or control subject (n=33-36 per group, ***p<0.001, Student's t-test; p<0.001, Fisher's exact test).

6.4.3 Analysis of Ang-(1-7) content in human serum-derived EVs by Ang-(1-7) ELISA

Having established a significant difference in Ang II levels between control healthy subject EVs and CABG patient EVs, it was next of interest to determine any potential differences in Ang-(1-7) content of the EVs between the two groups. Isolated EVs were lysed and analysed by Ang-(1-7) ELISA to determine Ang-(1-7) content (Figure 6-4).

It was found that Ang-(1-7) could be detected at low levels within both healthy control subjects and CABG patients, however the data suggested that lower levels of Ang-(1-7) may be present in CABG patient EVs vs. the control healthy subject EV group. Ang-(1-7) levels were found to be 5.3±0.75 pg/mL in control healthy subject EVs (n=38) compared with 3.4±0.58 pg/mL in CABG patient EVs (n=37) (Figure 6-4), however, this data did not reach statistical significance.

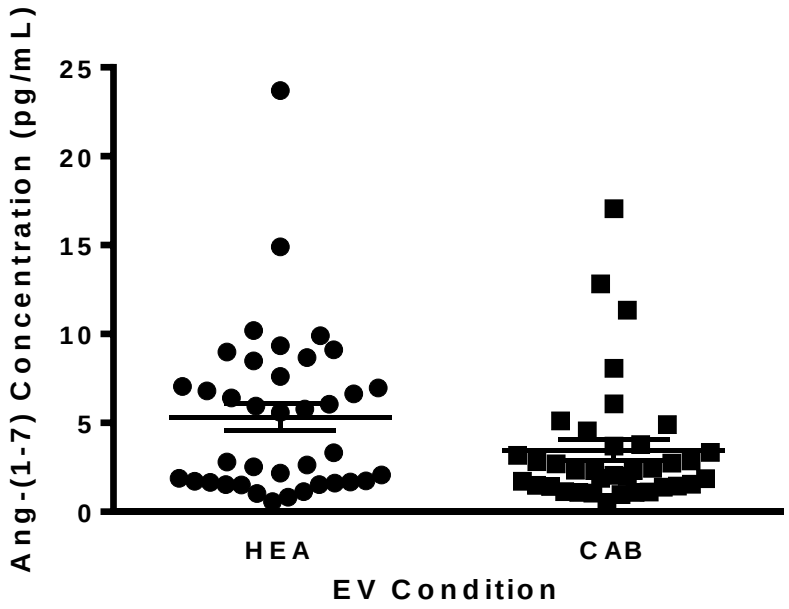

Figure 6-4 Analysis of Ang-(1-7) content in EV samples isolated from human serum. Comparison of the Ang-(1-7) levels found within serum-derived EVs from control healthy subjects (HEA) vs. CABG patients (CAB). 10 µg EVs isolated from the serum of CABG patients or healthy control subjects were lysed in RIPA buffer and Ang-(1-7) content was then measured via high-sensitivity Ang II ELISA. Each EV sample was measured in duplicate to give the average Ang-(1-7) level present for each patient or control subject (n=37-38 per group, p=0.057, Student's t-test).

6.4.4 Normalisation of peptide concentration to particle concentration

Differences in peptide level were initially established between CABG patients and healthy control subjects via Ang II or Ang-(1-7) ELISA, while particle concentration was determined by Nanosight NTA. It was next of interest to use this data to determine the concentration of Ang II and Ang-(1-7) per particle in CABG patients vs. healthy control subjects to further deduce any differences between the two. Peptide concentration was normalised to particle concentration by dividing the peptide concentration given in pg/mL by the particle concentration given in particles/mL (Figure 6-5).

Normalisation of the data showed that Ang II levels were significantly higher per EV particle in CABG patients vs healthy control subjects (healthy control EVs; 11.9±3.9 [$x10^{-12}$] pg/particle vs. CABG patient EVs; 53.5±8.2 [$x10^{-12}$] pg/particle, n=34-35, $p<0.001$) (Figure 6-5 A). Analysis of Ang-(1-7) concentration per particle showed no significant differences between healthy control subject and CABG patient EVs (healthy control EVs; 23.9±3.7 [$x10^{-12}$] pg/particle vs. CABG patient EVs; 18.7±3.2 [$x10^{-12}$] pg/particle, n=34-35, $p=0.29$) (Figure 6-5 B). These data show that the EVs derived from CABG patients contain higher levels of Ang II per particle compared to healthy control subjects, though no significant differences were observed for Ang-(1-7) levels between groups.

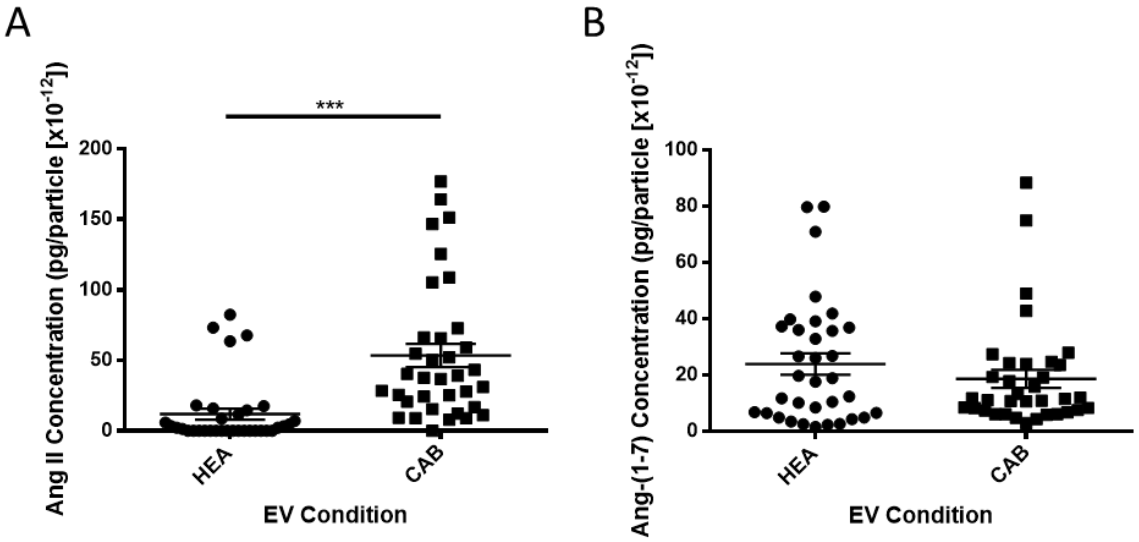

Figure 6-5 Normalisation of angiotensin peptide concentrations to EV particles/mL. (A) Concentration of Ang II per particle in healthy control subject (HEA) EVs vs. CABG patient (CAB) EVs (***p<0.001, Student's t-test). (B) Concentration of Ang-(1-7) per particle in CABG patient EVs and healthy control subject EVs (p=0.29, Student's t-test).

6.5 Discussion

In this small clinical study, it was observed that EVs isolated from human serum samples may differ depending on the disease condition of the patient. Significant differences were reported in size and concentration of EVs released between control healthy subjects and CABG patients, while a significant difference in Ang II levels within the EVs was also noted, whereby there were increased Ang II levels in the CABG patients. Although no significant differences in Ang-(1-7) levels were found, the data suggest that levels may be lower in CABG patient EVs.

The use of EVs as biomarkers for disease, including CVD, is a growing field where studies report significant differences in EV populations released under different disease states (Raposo and Stoorvogel, 2013). Generally, EV populations may be isolated from either plasma or serum samples for research into circulating microvesicles (Boulanger et al., 2006, Loyer et al., 2014) however, only serum samples were utilised in the present study, chosen primarily for availability and continuity across studies included within this thesis, despite most patient EV studies in the literature utilising plasma (as described in the following pages). The current study reported a small but significant difference in size and concentration, as measured by NTA, between EVs derived from the serum of control healthy subjects and CABG patients. It was found that EVs derived from CABG patients were significantly smaller and released at a significantly lower concentration than those from healthy control subjects, highlighting the potential for the release of different EV populations under disease conditions. Although size analysis is less commonly used, various studies have reported differences in particle concentration, though it is more commonly suggested that under cardiovascular disease conditions particle release increases, which contrasts the present study. For example, the Framingham Heart Study found association between increased circulating endothelial microvesicles and cardiometabolic risk factors (Amabile et al., 2014). This study (looking at individuals with no history of CVD) determined that risk factors such as hypertension, elevated triglycerides and metabolic syndrome were all significantly associated with the increased presence of circulating (CD144+) endothelial microvesicles (Amabile et al., 2014). This study also found circulating microvesicles to be associated with peripartum cardiomyopathy

(PPCM), a rare dilated cardiomyopathy with systolic dysfunction that occurs in late pregnancy or early postpartum (Honigberg and Givertz, 2019). The study reported an elevation in circulating endothelial-derived microvesicles in patients suffering from PPCM compared to control groups, along with a significant elevation compared to patients with coronary artery disease and ischaemic cardiomyopathy (Amabile et al., 2014). Similarly, it was found that in platelet-free plasma taken from patients with end-stage renal failure, there was a significant increase in levels of circulating annexin V-positive microvesicles compared to healthy control subjects, where endothelial-derived microvesicles correlated highly with arterial dysfunction (Amabile et al., 2005). Although these studies generally suggest higher levels of circulating microvesicles correlating with advanced disease state, they involved plasma-based EV analysis where the present study investigated serum-derived EVs which could partly account for the contrasting trends observed. Therefore, it may be of interest in future to investigate EV populations derived from plasma samples obtained from CABG patients and healthy control subjects. Furthermore, the present study utilising samples obtained from the VASCAB study, is one of the first to directly analyse EV populations in CABG patients vs healthy controls, the other reporting the converse to this study; that EV concentration is significantly higher in coronary patients (prior to surgery) than in healthy controls as quantified by flow cytometry (Valencia-Nunez et al., 2017). Other less direct studies related to CABG surgery research have also suggested important roles for EVs. It has been reported that remote ischaemic preconditioning increases EV particle concentrations in the serum of CABG patients, and that the EVs have altered miRNA expression associated with myocardial protection (Frey et al., 2019). A second study found that increased circulating microvesicles in CABG surgery patients were associated with increased risk for the requirement of blood transfusion (Jy et al., 2015).

Currently, the present study is the first to report Ang II and Ang-(1-7) levels within circulating EVs from healthy control subjects and CABG patients. Previous studies have analysed circulating Ang II and Ang-(1-7) levels in patients with CVD, with data being obtained from whole plasma samples. A study analysing circulating RAS components primarily in haemodialysis patients with CVD reported that circulating Ang II levels are increased in the plasma samples of

CVD patients compared to healthy controls (Yang et al., 2017) while Ang-(1-7) levels are decreased in CVD patients (Yang et al., 2017). A second study investigating RAS activity in heart failure patients showed that plasma Ang II levels were higher in patients with heart failure while Ang-(1-7) levels were lower, however treatment with ACEi suppressed plasma Ang II and elevated plasma Ang-(1-7) (Basu et al., 2017). Interestingly, one of these studies reported considerably higher levels of these peptides in general than the present study (Yang et al., 2017), while the second reported comparable levels (Basu et al., 2017) despite both investigating whole plasma samples. The data reported in the present study suggests higher levels of Ang II to be present in the EVs of CABG patient serum while lower levels are found in healthy control subject EVs. Conversely, this study suggests that Ang-(1-7) levels are lower in CABG patient EVs and higher in healthy subject EVs, although these data did not reach statistical significance across the patient samples used. Although differences between patient groups are small, this study analysed EVs derived only from serum samples and so it may also be beneficial in future to analyse EVs derived from plasma samples or even those of tissue specific origin, as recently it has been reported that EVs may be isolated directly from heart tissue (Loyer et al., 2018), in order to fully elucidate differences.

The actions of the RAS are diverse throughout the human body, and locally acting tissue-specific RAS are present in almost all tissues of the body which may be stimulated under certain conditions. For example, Ang II signalling via the AT_1R induces hypertension through vasoconstriction and sodium retention (van Kats et al., 1997, Timmermans et al., 1993), however hypertension also activates the tissue-specific RAS through mechanical stretch, as shown in cardiomyocytes (Baker et al., 1990), mesangial cells (Becker et al., 1998) and skeletal muscle myoblasts (Johnston et al., 2011). Activation of the tissue specific RAS under stress may be a potential explanation for the presence of RAS related peptides within EVs as reported in this thesis. One potential theory could involve the packaging of peptides generated within the cells in tissues allowing for later release in EVs. Many studies mentioned previously have reported the use of flow cytometry to determine the cellular origin of circulating EVs utilising cell type-specific markers to identify the source (Amabile et al., 2014, Amabile et al., 2005, Boulanger et al., 2006, Valencia-Nunez et al., 2017, Gorgens et al.,

2019) which could be utilised here in future. Owing to the short half-life of these peptides in their soluble form in the circulation (Al-Merani et al., 1978, Vilas-Boas et al., 2009), it could be hypothesised that packaging and transfer via EVs may attribute to longer lasting effects, however further investigation would be required to fully elucidate the role of the RAS and circulating EVs in CVD patients.

6.5.1 Study limitations

In this chapter, EVs were isolated from the serum of healthy control subjects or CABG patients in order for comparison via NanoSight and angiotensin peptide content. Although NanoSight analysis allowed for the comparison of concentration and particle size, further characterisation of these particles via TEM or western immunoblot would provide a more robust picture of the differences between the two. Furthermore, analysing plasma-derived EVs alongside serum-derived EVs may have provided a fuller picture of circulating particles and their differences between these groups. As collection of serum results in the rupture of platelet cells (and removal of other cell types from the fluid) the primary EV content may be attributed to apoptotic platelet cells, while plasma EVs have been attributed to platelets, endothelial cells, monocytes, leucocytes and erythrocytes (Colombo et al., 2014).

6.6 Summary

EVs isolated from the serum of CABG patients are significantly smaller in size compared with those derived from the serum of healthy control subjects. Furthermore, EVs are significantly less abundant in CABG patient serum compared with healthy control subject serum. The ELISA data suggests that EVs derived from CABG patient serum contain significantly higher levels of Ang II compared to EVs derived from control subject serum. Ang-(1-7) levels did not significantly differ between the two groups, however data may suggest levels to be lower in CABG patient EVs. Taken together, these observations highlight a potential difference in EV populations found in the circulation under CVD conditions compared to healthy conditions and these phenomena warrant further investigation in the future.

Chapter 7 General Discussion

7.1 Overall Summary

Pathological cardiac hypertrophy as a result of chronic hypertension is a serious condition which may further contribute to adverse cardiovascular events such as myocardial infarction, pathological remodelling or heart failure. For these reasons, ventricular hypertrophy is commonly used as a predictor of cardiovascular morbidity and mortality (Samak et al., 2016). Owing to its involvement in development of heart failure and ultimately death, there is a continual need for therapeutic interventions against pathological hypertrophy. The primary aims of the work presented in this thesis were to investigate whether EVs, specifically with a focus on RAS signalling, could contribute to cardiomyocyte hypertrophy and, furthermore, whether they could be harnessed for therapeutic delivery of the cardio-protective peptide Ang-(1-7) against cardiomyocyte hypertrophy.

Initially, the potential for isolation of EVs from cardiac cells and their signalling roles were assessed in an *in vitro* model of cardiomyocyte hypertrophy. It was found that EVs were released in abundance naturally from both cardiomyocyte and cardiac fibroblasts. Furthermore, it was shown that treatment of the parental cells with Ang II allowed them to produce EVs containing Ang II, which could further elicit pathological effects in recipient cardiomyocytes in terms of the hypertrophic response. Although Ang II treatment did not appear to alter the size, morphology or concentration of EVs released from parental cardiomyocytes and cardiac fibroblasts in this study, a clear functional response could be observed in recipient cells. A similar study reported the pathological effects of these Ang II EVs on recipient cells and suggested that Ang II treatment did in fact stimulate increased EV release from parental cells (Lyu et al., 2015), an observation not made here. It is possible that this phenomenon is a result of cell type or batch specificity as, for example, one experiment in the present study did suggest significant increase in EV release as a response to Ang II stimulation, however all other experiments did not show this result. Due to the ability of Ang II to signal via both the AT_1R and the AT_2R (Timmermans et al., 1993), the current study also investigated whether blockade of these receptors in the parental cells could affect the pathological function of the EVs produced. This study found that pre-blocking parental cardiomyocytes with the AT_2R antagonist, PD123,319 (Widdop et al., 1992), did not prevent the released Ang II EVs from

eliciting a hypertrophic response in recipient cardiomyocytes. However, it was noted that pre-blocking Ang II-stimulated parental cardiomyocytes with the AT_1R antagonist, losartan (Timmermans et al., 1993), resulted in the production of EVs which were unable to induce a hypertrophic response in recipient cells. This finding suggests the potential involvement of the AT_1R, but not the AT_2R, in Ang II signalling within the parental cells prior to release of EVs.

Following initial studies investigating the role of EVs in the endogenous packaging and delivery of Ang II, it was next determined as to whether the protective peptide Ang-(1-7) could be transferred within EVs, or cause cells to produce EVs with protective function. Ang-(1-7) has been established as having protective effects in various models of cardiomyocyte hypertrophy (Santos et al., 2003, Flores-Munoz et al., 2012a) however, owing to its short half-life in the circulation (Vilas-Boas et al., 2009) its use as a therapeutic agent is limited. The present study first investigated whether or not treatment of parental cardiomyocytes with Ang-(1-7) could produce EVs which could evoke a protective effect, after showing that Ang II treatment produced EVs which evoked a pathological effect. It was shown that at high doses, EVs produced by Ang-(1-7) stimulated cardiomyocytes could inhibit Ang II-induced hypertrophy in recipient cardiomyocytes. Although an interesting finding in itself, the question must be asked as to whether or not cells could endogenously load enough Ang-(1-7) into the EVs they produce for it to have a protective effect in other models, such as *in vivo* models. To ensure the most efficient loading of EVs, the potential use of electroporation for exogenous peptide loading was also investigated. Although electroporation has been used previously to load EVs (Faruqu et al., 2018, Ma et al., 2018, Hood et al., 2014, Lamichhane et al., 2015), these studies generally focus on nucleic acid loading while the present studies investigated peptide loading. It was demonstrated that electroporation could be used to efficiently load either Ang II or Ang-(1-7) into the EVs released from control untreated cells. Furthermore, it was found that the Ang-(1-7) electroporated EVs evoke protection against Ang II-induced hypertrophy in recipient cardiomyocytes.

Although successful loading of cell-derived EVs with delivery *in vitro* was established, the generation of enough EVs from culture media (Colombo et al., 2014) to load and deliver in an *in vivo* model remained potentially problematic.

As such, the next step was to investigate isolation of EVs from blood serum, as reports suggest increased EV output from bodily fluids such as serum, plasma and urine, in comparison to output from cell culture media (Raposo and Stoorvogel, 2013). The present study found that EVs isolated from SHRSP animals were significantly smaller than those from healthy WKY animals and that protein concentration was significantly lower in SHRSP serum EVs, which may suggest altered EV populations under disease conditions (Raposo and Stoorvogel, 2013). WKY serum-derived EVs were next utilised as delivery vehicles in the *in vitro* model of cardiomyocyte hypertrophy. Serum EVs electroporated with Ang-(1-7) were found to contain high levels of the peptide which could protect against Ang II-induced hypertrophy in cardiomyocytes. Interestingly, higher baseline levels of Ang-(1-7) were found within naïve serum EVs than seen previously in control cell-derived EVs. Furthermore, naïve serum EVs were also able to attenuate Ang II-induced hypertrophy *in vitro*, possibly due to the baseline levels of Ang-(1-7) reported here. This result suggests that EVs isolated from the serum of a healthy animal may already contain enough Ang-(1-7) to protect against cardiomyocyte hypertrophy at least *in vitro*, a point which should be considered when investigating a model of exogenous peptide loading into EVs.

Next, the use of Ang-(1-7) loaded EVs as a therapeutic intervention was investigated in an *in vivo* model of cardiac impairment. This involved bolus injection of loaded EVs into the circulation of Ang II infused animals to determine whether the EVs could provide protection against the reported detrimental effects of continuous Ang II infusion (Kagiyama et al., 2002, Mehta and Griendling, 2007, Yan et al., 2019). Preliminary evidence suggested that Ang-(1-7) loaded EVs may be conferring therapeutic effects against Ang II infusion in terms of reduction in systolic blood pressure, cardiac fibrosis and cardiac hypertrophy, however data obtained across the parameters measured did not reach statistical significance. As a result, further studies are required to fully determine the protective effects of Ang-(1-7) loaded EVs, perhaps utilising higher doses of Ang II or longer exposure times to ensure the observation of full effects in controls before analysing EV protection potential. Dose dependent studies may also be of interest to determine the most effective EV dose or number of injections required to confer protection.

Finally, EV populations derived from healthy control subjects and CABG patients were characterised and compared in terms of size, concentration, Ang II content and Ang-(1-7) content. The data gathered suggests that under coronary artery disease conditions, serum-derived EVs are smaller in size and released in lower numbers compared with healthy control subjects. Analysis of EV content by Ang II and Ang-(1-7) ELISA also suggested differences between the two populations, where Ang II levels were observed to be significantly higher in patient samples compared with healthy controls, however no significant differences in Ang-(1-7) levels were observed.

7.2 Future Perspectives

The initial aims of this thesis first involved the characterisation of EVs released from cardiac cell types and from normotensive rat serum, as these would later be used in functional studies of cardiac hypertrophy. In this thesis, characterisation mainly involved use of NTA, analysis of protein concentration by BCA and imaging by TEM, all of which are considered standard methods for EV characterisation (Lotvall et al., 2014, Théry et al., 2018). Characterisation data also included analysis of specific EV protein markers by western immunoblot to an extent, however this data set is incomplete, particularly with the updated EV study guidelines (Théry et al., 2018). These suggest the use of 3-5 categories of positive EV markers along with a single negative EV marker for full characterisation (Théry et al., 2018) and therefore future studies would benefit from including further characterisation via this method. The variability across the literature in terms of number of protein markers successfully shown via western immunoblot highlights potential difficulties with this technique in this field (Van Deun et al., 2017). As a result, another common technique used for characterisation of EV protein markers involves flow cytometry analysis of EVs attached to beads, which is widely accepted assuming the inclusion of appropriate controls such as antibody-only controls and isotype controls (Théry et al., 2006). If further characterisation is required, it may then be of interest to investigate these methods in future studies.

The established cell model utilised within this thesis allows for investigation of cardiomyocyte hypertrophy, primarily in terms of phenotypic changes such as observation of F-actin rearrangement and increase in cell area, as well as

increased gene expression of hypertrophy markers. The H9c2 cardiomyoblast cell line used was originally derived from the ventricular tissue of embryonic rats (Kimes and Brandt, 1976), which benefits their use as a model for cardiac hypertrophy as hypertrophy resulting from chronic hypertension generally occurs in the ventricular muscle of the heart. Although this cell line has been shown to convey many similar properties to primary cardiomyocytes, such as membrane morphology, G-protein expression and response to hypertrophic stimuli (Hescheler et al., 1991, Huang et al., 2004), it is not without limitations. The value of H9c2 cardiomyoblasts as model for cardiomyocyte hypertrophy has been questioned due to their ability to proliferate continuously and the fact that they do not beat, two traits which are strongly in contrast to primary cardiomyocytes (Watkins et al., 2011). As such, it may be of interest in future to investigate the effects of EV signalling and the RAS in primary cardiomyocytes, utilising either neonatal or adult rat cardiomyocytes as a model. However, as previously discussed, these come with their own study limitations due to the fact that they do not proliferate, and a high percentage of cell death is observed upon isolation (Vandergriff et al., 2015). Even so, it is likely that primary cells will have a more natural morphology and maintain many of the important markers and functions observed *in vivo* and therefore investigation of EV signalling in these cells is an important step which should definitely be considered for evaluation in future.

As stated, most parameters measured in terms cardiomyocyte hypertrophy in this model were phenotypic observations such as F-actin rearrangement, increased cell size and increase in gene expression of a specific hypertrophy marker. As the RAS is a key point of interest in these studies, where the effects of Ang II signalling via EVs has been investigated and shown to stimulate cellular hypertrophy; it would be of interest to determine whether any downstream signalling pathways related to Ang II signalling are affected in recipient cells. For example, it is known that Ang II signalling via the AT_1R upregulates signalling pathways such as MAPK/ERK1/2 and JNK/P38MAPK (Ocaranza and Jalil, 2012, Schluter and Wenzel, 2008) resulting in the classical pathological effects observed in cardiomyocytes. Therefore, it may be of interest to evaluate these outputs in recipient cells receiving EVs derived from Ang II stimulated parental cells, or EVs exogenously loaded with Ang II. It could be speculated that due to the level of cellular hypertrophy caused by Ang II EVs observed in the present

study, that the recipient cells may exhibit increased protein expression of JNK, ERK or any other downstream signalling molecule associated with Ang II/AT_1R stimulation (Mehta and Griendling, 2007). As such, future studies may benefit from investigating these outputs to further reinforce the link between EV signalling and the RAS. Similarly, the present study also investigated the protective effects of Ang-(1-7) EVs in this cell model – observing the effects from both endogenous and exogenous EV loading. Conversely to Ang II/AT_1R signalling, Ang-(1-7)/Mas signalling has been shown to downregulate MAPK/ERK1/2 pathways while also upregulating NO and cGMP signalling (Li et al., 2012), resulting in the reported protective effects in the cardiovascular system (Gomes et al., 2012). As a result, these signalling pathways could also be investigated in relation to increased Ang-(1-7) signalling via EVs, where downregulation of MAPK/ERK1/2 or upregulation of NO and cGMP pathways in recipient cells could be measurable parameters. As above, these further studies could help elucidate the mechanism by which loaded EVs affect cardiomyocyte hypertrophy in terms of the RAS. These cell-based studies found that Ang II EVs could induce hypertrophy in recipient cells, while Ang-(1-7) EVs could inhibit Ang II-induced hypertrophy in recipient cells, however these effects were investigated separately. It may be of interest to investigate cellular response when treating with both Ang II EVs and Ang-(1-7) EVs to determine whether Ang II signalling via EVs can be blocked with Ang-(1-7) delivery, also via EVs, as one signal is likely to be more powerful than the other.

The present study investigated potential changes in expression of RAS-related genes in recipient cells treated with Ang II EVs. Although Ang II was found to be present at higher levels within EVs released from Ang II stimulated cells compared with control cells, recipient cells did not exhibit an increase in expression of either the AT_1R or the AT_2R upon treatment with Ang II EVs. However, previous studies have shown that the exosomes themselves released from Ang II stimulated cells contain functional AT_1Rs (Pironti et al., 2015) therefore it may be beneficial to investigate the expression of these receptors within EVs released from cardiomyocytes +/- Ang II treatment. The potential for these EVs to transfer functional Ang II and AT_1Rs could provide further mechanistic information in this model of cardiomyocyte hypertrophy and so should be investigated in future. Similarly, investigation of Mas levels within

Ang-(1-7) EVs may confer further information on the mechanistic aspects of protective signalling in this model.

These studies also analysed the protective effects of Ang-(1-7) loaded EVs *in vivo*. Although thus far, no significant changes were observed across the various parameters investigated, this could be attributed to a number of reasons which could be further investigated in future studies. In order to assess the protective effects of Ang-(1-7) loaded EVs *in vivo*, this involved utilising an Ang II infusion model (Cui et al., 1999, Yan et al., 2019), where vehicle infusion was used to control for normal physiological responses and Ang II infusion was used to control for aberrant cardiovascular physiology. The key issue with these studies was that Ang II infusion failed to significantly induce deleterious effects such as increased blood pressure, cardiac fibrosis and cardiac hypertrophy compared to the vehicle control. As a result, the effects of either naïve EV delivery or Ang-(1-7) EV delivery could not be fully or reliably elucidated due to the lack of successful controls for comparison. Although no statistically significant changes were observed, the success of *in vitro* studies suggest it may be beneficial to redesign the *in vivo* study for future investigations, taking into account various parts of the initial design which could be optimised. For example, systolic blood pressure data suggested that the Ang II group responded variably to the dose used. Although the dose used has been described in the literature (Yan et al., 2019), it is more commonly utilised over a longer period of time and therefore extending the study length to 4 weeks may allow for more consistent development of cardiovascular pathophysiology across the animals (Zhang et al., 2017b, Izumiya et al., 2012). Aside from the Ang II group alone, the blood pressure data also suggested that the method used may be inaccurate in general. The present study utilised tail cuff plethysmography, an indirect blood pressuring technique which involves animal restraint (Popovic, 1988). It has been suggested that even when animals have been fully acclimatised to the procedure prior to measurements, they may still exhibit extreme restraint stress resulting in large and variable increases in blood pressure readings across one procedure (Popovic, 1988, Irvine et al., 1997). The day 0 systolic blood pressure data reported in the present study suggests that this may be the case. It appeared that some normotensive animals exhibited a hypertensive systolic blood pressure prior to the study beginning, despite acclimatisation procedures being followed. As a result, for

future studies it may be more beneficial to utilise a direct method of measuring blood pressure, such as via radiotelemetry which allows for continuous measurements while animals may move freely without restraint (Kramer and Kinter, 2003). Furthermore, as well as Ang II dose optimisation, any future studies would also likely benefit from dose exploration in terms of the EVs. Although data gathered in the present study suggest that the dose used may be conferring some protective effects, it would be of interest to determine an optimal bolus dose and therefore future studies should include groups treated with doses increasing by various folds. Furthermore, if the length of the study was altered there would be a requirement for an increase in the number of bolus injections administered across the time period as it has been found that EVs may be cleared from the circulation in as little as 24-48 hr after intravenous injection (Morishita et al., 2017). Increasing the number of bolus injections may help to ensure that any protective effects conferred by the EVs are prolonged throughout the duration of the study and will allow for them to be fully elucidated.

The results obtained from the analysis of human serum EVs suggest differing EV populations released under disease conditions compared with normal healthy conditions, albeit NanoSight data generally contrasts the current literature which suggests higher numbers released under disease conditions (Valencia-Nunez et al., 2017, Jy et al., 2015, Amabile et al., 2014). This contrast could potentially be attributed to the fact that the aforementioned studies analysed plasma-derived EVs while the present study investigated serum-derived EVs where natural differences in EV populations may occur. It may therefore be interesting to analyse plasma EV samples obtained from these patients for comparison between both the serum EV results and the current literature. Although these previous studies investigated size and concentration differences, the present study also directly compared Ang II and Ang-(1-7) levels within serum EVs from CABG patients versus healthy control subjects. The findings suggest higher levels of Ang II within patient EVs and lower levels of Ang-(1-7), however the latter did not reach statistical significance. Due to the natural variation expected when working with human samples, it may be of interest in future to analyse more samples from these cohorts as only a small pool was initially taken for this study.

7.3 Conclusions

In summary, the data within this thesis has provided evidence for the ability of EVs to transfer functional peptides associated with the RAS. For the first time, it was shown that EVs could be exogenously loaded via electroporation with Ang-(1-7) peptide which could then negate the pathological effects of Ang II *in vitro*, with promising effects *in vivo* in terms of cardiac hypertrophy. This new avenue for the delivery of functional Ang-(1-7) under pathological conditions will be valuable in future therapeutic investigations involving the RAS and cardiovascular disease.

Appendix

Participant Information (Chapter 6)

ID	CAD_Stat	sex	age	Aspirin	ACEI_ARB	CCB	Beta	Diur	Statin	Antiplt	Antidiab	Insulin	Nitrate	metfomin	giltazone	sulphonylurea
153	1	1	63	1	1	0	1	0	1	0	1	1	0	1	0	1
163	1	1	66	1	1	0	1	1	1	0	1	0	0	0	0	1
168	1	1	78	1	1	1	1	0	1	0	0	0	0			
175	1	1	49	0	1	0	1	1	1	0	1	1	0	1	0	0
186	1	1	50	0	0	1	1	0	1	0	0	0	1			
187	1	1	59	1	0	1	0	0	1	0	0	0	1			
188	1	1	77	0	0	0	1	0	1	0	0	0	0			
190	1	1	75	1	0	0	1	0	1	0	0	0	1			
193	1	1	49	1	1	0	0	0	1	0	1	0	1	1	1	1
195	1	1	70	1	1	0	1	0	1	0	1	0	1	1	0	0
202	1	1	60	1	1	0	1	0	1	0	0	1	1			
207	1	1	70	1	1	0	1	0	0	0	0	0	0			
210	1	1	45	1	1	1	1	0	1	0	0	0	0			
211	1	1	49	1	1	0	1	0	1	1	0	0	0			
218	1	1	47	1	0	0	1	0	1	1	0	0	1			
230	1	1	53	1	1	1	1	1	1	0	1	0	1	1	1	0
232	1	1	47	1	1	0	1	0	1	1	0	0	1			
150	1	1	71	1	1	1	0	0	1	0	0	0	1			
236	1	1	56	1	1	0	1	1	1	1	0	0	1			
286	1	1	59	1	0	1	1	0	1	1	0	0	1			
300	1	1	62	1	1	0	1	0	1	0	0	0	0			
320	1	1	76	1	0	1	1	0	1	0	0	0	1			
256	1	0	58	1	1	1	0	0	1	0	0	0	1			
295	1	1	54	1	0	0	1	0	0	0	0	0	1			
251	1	1	63	1	1	1	1	1	1	0	0	0	1			
253	1	1	49	1	1	0	0	0	1	0	0	0	1			

Participant Information (Chapter 6)

ID	CAD_Stat	sex	age	Aspirin	ACEI_ARB	CCB	Beta	Diur	Statin	Antiplt	Antidiab	Insulin	Nitrate	metfomin	giltazone	sulphonylurea
261	1	1	59	1	1	0	1	0	1	1	0	0	0			
312	1	1	53													
314	1	1	59	1	0	0	1	0	1	0	0	0	1			
307	1	1	80	1	0	0	1	0	1	0	0	0	0			
313	1	1	72	1	0	1	1	0	1	0	0	0	1			
325	1	1	57	1	1	0	1	1	1	0	0	0	0			
237	1	1	74	1	0	1	1	0	0	0	0	0	0			
284	1	1	66	1	0	0	1	1	1	1	0	0	1			
296	1	1	81	1	0	0	1	0	1	0	0	0	0			
275	1	1	59	1	0	0	1	0	0	1	0	0	0			
289	1	1	58	1	1	0	1	0	1	1	0	0	0			
318	1	0	68	1	1	1	1	0	1	1	0	0	1			
201	1	1	64	1	1	1	1	0	1	0	1	1	0	0	0	1
2017	0	1	55	0	0	0	1	1	0	0	0	0	0			
2004	0	1	70	1	0	0	0	0	0	0	0	0	0			
2010	0	0	84	1	0	0	1	0	0	0	0	0	0			
2016	0	1	66	0	0	0	0	0	0	0	0	0	0			
2024	0	1	63	0	1	0	0	1	1	0	0	0	0			
2025	0	0	68	0	0	0	0	0	0	0	0	0	0			
2034	0	1	61	0	0	0	0	0	0	0	0	0	0			
2039	0	1	74	1	0	0	0	0	0	0	0	0	0			
2041	0	1	63	0	0	0	0	0	0	0	0	0	0			
2042	0	1	67	0	0	0	0	0	0	0	0	0	0			
2044	0	1	54	0	0	0	0	0	0	0	0	0	0			
2049	0	1	50	0	0	0	0	0	0	0	0	0	0			
2052	0	1	50	0	0	0	0	0	0	0	0	0	0			

Participant Information (Chapter 6)

ID	CAD_Stat	sex	age	Aspirin	ACEI_ARB	CCB	Beta	Diur	Statin	Antiplt	Antidiab	Insulin	Nitrate	metfomin	giltazone	sulphonylurea
2056	0	1	71	0	0	0	0	0	0	0	0	0	0			
2057	0	1	53	1	0	0	0	0	0	0	0	0	0			
2061	0	1	55	0	0	0	0	0	0	0	0	0	0			
2062	0	0	57	0	0	0	0	0	0	0	0	0	0			
2066	0	1	60	0	0	0	0	0	0	0	0	0	0			
2075	0	1	52	0	0	0	0	0	0	0	0	0	0			
2074	0	1	57	0	0	0	0	0	0	0	0	0	0			
2065	0	1	68	0	0	0	0	0	0	0	0	0	0			
2071	0	1	54	0	0	0	0	0	0	0	0	0	0			
2013	0	0	69	0	0	0	0	0	0	0	0	0	0			
2046	0	0	60	0	1	0	1	0	0	0	0	0	0			
2050	0	1	57	0	1	0	0	1	0	0	0	0	0			
2053	0	0	55	0	0	0	0	0	0	0	0	0	0			
2043	0	0	59	0	0	0	0	0	0	0	0	0	0			
2051	0	0	54	0	0	0	0	0	0	0	0	0	0			
2055	0	0	52	0	0	0	0	0	0	0	0	0	0			
2067	0	1	54	0	0	0	1	0	0	0	0	0	0			
2015	0	0	67	0	0	0	0	0	0	0	0	0	0			
2068	0	1	50	0	0	0	0	0	0	0	0	0	0			
2022	0	0	66	0	0	0	0	0	1	0	0	0	0			
2023	0	0	67	0	0	0	0	0	0	0	0	0	0			
2027	0	0	61	0	0	0	0	0	0	0	0	0	0			
2029	0	0	66	0	0	0	0	0	0	0	0	0	0			
2031	0	0	67	0	0	0	0	0	0	0	0	0	0			
2018	0	0	57	0	0	0	0	0	0	0	0	0	0			
2021	0	0	63	0	0	1	0	0	0	0	0	0	0			
2058	0	0	64	0	0	0	0	0	0	0	0	0	0			

List of References

ABRAMI, L., BRANDI, L., MOAYERI, M., BROWN, M. J., KRANTZ, B. A., LEPPLA, S. H. & VAN DER GOOT, F. G. 2013. Hijacking multivesicular bodies enables long-term and exosome-mediated long-distance action of anthrax toxin. *Cell Rep,* 5**,** 986-96.

AGA, M., BENTZ, G. L., RAFFA, S., TORRISI, M. R., KONDO, S., WAKISAKA, N., YOSHIZAKI, T., PAGANO, J. S. & SHACKELFORD, J. 2014. Exosomal HIF1alpha supports invasive potential of nasopharyngeal carcinoma-associated LMP1-positive exosomes. *Oncogene,* 33**,** 4613-22.

AGABITI-ROSEI, E., MUIESAN, M. L. & SALVETTI, M. 2006. Evaluation of Subclinical Target Organ Damage for Risk Assessment and Treatment in the Hypertensive Patients: Left Ventricular Hypertrophy. *Journal of the American Society of Nephrology,* 17**,** S104-S108.

AGOUNI, A., DUCLUZEAU, P. H., BENAMEUR, T., FAURE, S., SLADKOVA, M., DULUC, L., LEFTHERIOTIS, G., PECHANOVA, O., DELIBEGOVIC, M., MARTINEZ, M. C. & ANDRIANTSITOHAINA, R. 2011. Microparticles from patients with metabolic syndrome induce vascular hypo-reactivity via Fas/Fas-ligand pathway in mice. *PLoS One,* 6**,** e27809.

AKAO, Y., IIO, A., ITOH, T., NOGUCHI, S., ITOH, Y., OHTSUKI, Y. & NAOE, T. 2011. Microvesicle-mediated RNA molecule delivery system using monocytes/macrophages. *Mol Ther,* 19**,** 395-9.

AL-MERANI, S. A., BROOKS, D. P., CHAPMAN, B. J. & MUNDAY, K. A. 1978. The half-lives of angiotensin II, angiotensin II-amide, angiotensin III, Sar1-Ala8-angiotensin II and renin in the circulatory system of the rat. *J Physiol,* 278**,** 471-90.

AL-NEDAWI, K., MEEHAN, B., MICALLEF, J., LHOTAK, V., MAY, L., GUHA, A. & RAK, J. 2008. Intercellular transfer of the oncogenic receptor EGFRvIII by microvesicles derived from tumour cells. *Nat Cell Biol,* 10**,** 619-24.

ALGHAMRI, M. S., WEIR, N. M., ANSTADT, M. P., ELASED, K. M., GURLEY, S. B. & MORRIS, M. 2013. Enhanced angiotensin II-induced cardiac and aortic remodeling in ACE2 knockout mice. *J Cardiovasc Pharmacol Ther,* 18**,** 138-51.

ALLEN, R. T., KRUEGER, K. D., DHUME, A. & AGRAWAL, D. K. 2005. Sustained Akt/PKB activation and transient attenuation of c-jun N-terminal kinase in the inhibition of apoptosis by IGF-1 in vascular smooth muscle cells. *Apoptosis,* 10**,** 525-35.

ALVAREZ-ERVITI, L., SEOW, Y., YIN, H., BETTS, C., LAKHAL, S. & WOOD, M. J. A. 2011. Delivery of siRNA to the mouse brain by systemic injection of targeted exosomes. *Nature Biotechnology,* 29**,** 341.

AMABILE, N., CHENG, S., RENARD, J. M., LARSON, M. G., GHORBANI, A., MCCABE, E., GRIFFIN, G., GUERIN, C., HO, J. E., SHAW, S. Y., COHEN, K. S., VASAN, R. S., TEDGUI, A., BOULANGER, C. M. & WANG, T. J. 2014. Association of circulating endothelial microparticles with cardiometabolic risk factors in the Framingham Heart Study. *Eur Heart J,* 35**,** 2972-9.

AMABILE, N., GUERIN, A. P., LEROYER, A., MALLAT, Z., NGUYEN, C., BODDAERT, J., LONDON, G. M., TEDGUI, A. & BOULANGER, C. M. 2005. Circulating endothelial microparticles are associated with vascular dysfunction in patients with end-stage renal failure. *J Am Soc Nephrol,* 16**,** 3381-8.

AMBERGER, A., MACZEK, C., JURGENS, G., MICHAELIS, D., SCHETT, G., TRIEB, K., EBERL, T., JINDAL, S., XU, Q. & WICK, G. 1997. Co-expression of ICAM-1, VCAM-1, ELAM-1 and Hsp60 in human arterial and venous endothelial

cells in response to cytokines and oxidized low-density lipoproteins. *Cell Stress Chaperones,* 2**,** 94-103.

AMBROSE, J. A. & SINGH, M. 2015. Pathophysiology of coronary artery disease leading to acute coronary syndromes. *F1000prime reports,* 7**,** 08-08.

ARSLAN, F., LAI, R. C., SMEETS, M. B., AKEROYD, L., CHOO, A., AGUOR, E. N., TIMMERS, L., VAN RIJEN, H. V., DOEVENDANS, P. A., PASTERKAMP, G., LIM, S. K. & DE KLEIJN, D. P. 2013. Mesenchymal stem cell-derived exosomes increase ATP levels, decrease oxidative stress and activate PI3K/Akt pathway to enhance myocardial viability and prevent adverse remodeling after myocardial ischemia/reperfusion injury. *Stem Cell Res,* 10**,** 301-12.

AUDOLY, L. P., OLIVERIO, M. I. & COFFMAN, T. M. 2000. Insights into the functions of type 1 (AT1) angiotensin II receptors provided by gene targeting. *Trends Endocrinol Metab,* 11**,** 263-9.

AVERILL, D. B., ISHIYAMA, Y., CHAPPELL, M. C. & FERRARIO, C. M. 2003. Cardiac angiotensin-(1-7) in ischemic cardiomyopathy. *Circulation,* 108**,** 2141-6.

BAI, F., PANG, X. F., ZHANG, L. H., WANG, N. P., MCKALLIP, R. J., GARNER, R. E. & ZHAO, Z. Q. 2016. Angiotensin II AT1 receptor alters ACE2 activity, eNOS expression and CD44-hyaluronan interaction in rats with hypertension and myocardial fibrosis. *Life Sci,* 153**,** 141-52.

BAI, H., WU, L. L., XING, D. Q., LIU, J. & ZHAO, Y. L. 2004. Angiotensin II induced upregulation of G alpha q/11, phospholipase C beta 3 and extracellular signal-regulated kinase 1/2 via angiotensin II type 1 receptor. *Chin Med J (Engl),* 117**,** 88-93.

BAIETTI, M. F., ZHANG, Z., MORTIER, E., MELCHIOR, A., DEGEEST, G., GEERAERTS, A., IVARSSON, Y., DEPOORTERE, F., COOMANS, C., VERMEIREN, E., ZIMMERMANN, P. & DAVID, G. 2012. Syndecan-syntenin-ALIX regulates the biogenesis of exosomes. *Nat Cell Biol,* 14**,** 677-85.

BAKER, K. M., CHERNIN, M. I., WIXSON, S. K. & ACETO, J. F. 1990. Renin-angiotensin system involvement in pressure-overload cardiac hypertrophy in rats. *Am J Physiol,* 259**,** H324-32.

BANG, C., BATKAI, S., DANGWAL, S., GUPTA, S. K., FOINQUINOS, A., HOLZMANN, A., JUST, A., REMKE, J., ZIMMER, K., ZEUG, A., PONIMASKIN, E., SCHMIEDL, A., YIN, X., MAYR, M., HALDER, R., FISCHER, A., ENGELHARDT, S., WEI, Y., SCHOBER, A., FIEDLER, J. & THUM, T. 2014. Cardiac fibroblast-derived microRNA passenger strand-enriched exosomes mediate cardiomyocyte hypertrophy. *J Clin Invest,* 124**,** 2136-46.

BANOS, M., ARELLANO-MENDOZA, M. G., VARGAS-ROBLES, H., AVILA-CASADO, M. C., SOTO, V., ROMO, E., RIOS, A., HERNANDEZ-ZAVALA, A., DE LA PENA-DIAZ, A. & ESCALANTE, B. 2011. Relationship between angiotensin II receptor expression and cardiovascular risk factors in Mexican patients with coronary occlusive disease. *Exp Mol Pathol,* 91**,** 478-83.

BARANYAI, T., HERCZEG, K., ONODI, Z., VOSZKA, I., MODOS, K., MARTON, N., NAGY, G., MAGER, I., WOOD, M. J., EL ANDALOUSSI, S., PALINKAS, Z., KUMAR, V., NAGY, P., KITTEL, A., BUZAS, E. I., FERDINANDY, P. & GIRICZ, Z. 2015. Isolation of Exosomes from Blood Plasma: Qualitative and Quantitative Comparison of Ultracentrifugation and Size Exclusion Chromatography Methods. *PLoS One,* 10**,** e0145686.

BARILE, L., LIONETTI, V., CERVIO, E., MATTEUCCI, M., GHERGHICEANU, M., POPESCU, L. M., TORRE, T., SICLARI, F., MOCCETTI, T. & VASSALLI, G. 2014. Extracellular vesicles from human cardiac progenitor cells inhibit

cardiomyocyte apoptosis and improve cardiac function after myocardial infarction. *Cardiovasc Res,* 103**,** 530-41.

BASU, R., POGLITSCH, M., YOGASUNDARAM, H., THOMAS, J., ROWE, B. H. & OUDIT, G. Y. 2017. Roles of Angiotensin Peptides and Recombinant Human ACE2 in Heart Failure. *J Am Coll Cardiol,* 69**,** 805-819.

BECKER, B. N., YASUDA, T., KONDO, S., VAIKUNTH, S., HOMMA, T. & HARRIS, R. C. 1998. Mechanical stretch/relaxation stimulates a cellular renin-angiotensin system in cultured rat mesangial cells. *Exp Nephrol,* 6**,** 57-66.

BELL, P. D., LAPOINTE, J. Y., SABIROV, R., HAYASHI, S., PETI-PETERDI, J., MANABE, K., KOVACS, G. & OKADA, Y. 2003. Macula densa cell signaling involves ATP release through a maxi anion channel. *Proc Natl Acad Sci U S A,* 100**,** 4322-7.

BELLINGHAM, S. A., COLEMAN, B. M. & HILL, A. F. 2012. Small RNA deep sequencing reveals a distinct miRNA signature released in exosomes from prion-infected neuronal cells. *Nucleic Acids Res,* 40**,** 10937-49.

BIANCO, F., PERROTTA, C., NOVELLINO, L., FRANCOLINI, M., RIGANTI, L., MENNA, E., SAGLIETTI, L., SCHUCHMAN, E. H., FURLAN, R., CLEMENTI, E., MATTEOLI, M. & VERDERIO, C. 2009. Acid sphingomyelinase activity triggers microparticle release from glial cells. *Embo j,* 28**,** 1043-54.

BLOCH, L., NDONGSON-DONGMO, B., KUSCH, A., DRAGUN, D., HELLER, R. & HUBER, O. 2016. Real-time monitoring of hypertrophy in HL-1 cardiomyocytes by impedance measurements reveals different modes of growth. *Cytotechnology,* 68**,** 1897-1907.

BOCK, H. A., HERMLE, M., BRUNNER, F. P. & THIEL, G. 1992. Pressure dependent modulation of renin release in isolated perfused glomeruli. *Kidney Int,* 41**,** 275-80.

BOGOYEVITCH, M. A., CLERK, A. & SUGDEN, P. H. 1995. Activation of the mitogen-activated protein kinase cascade by pertussis toxin-sensitive and -insensitive pathways in cultured ventricular cardiomyocytes. *The Biochemical journal,* 309 (Pt 2)**,** 437-443.

BOOZ, G. W. & BAKER, K. M. 1996. Role of type 1 and type 2 angiotensin receptors in angiotensin II-induced cardiomyocyte hypertrophy. *Hypertension,* 28**,** 635-40.

BOROSCH, S., DAHMEN, E., BECKERS, C., STOPPE, C., BUHL, E. M., DENECKE, B., GOETZENICH, A. & KRAEMER, S. 2017. Characterization of extracellular vesicles derived from cardiac cells in an in vitro model of preconditioning. *Journal of Extracellular Vesicles,* 6**,** 1390391.

BOTELHO-SANTOS, G. A., BADER, M., ALENINA, N. & SANTOS, R. A. 2012. Altered regional blood flow distribution in Mas-deficient mice. *Ther Adv Cardiovasc Dis,* 6**,** 201-11.

BOTELHO-SANTOS, G. A., SAMPAIO, W. O., REUDELHUBER, T. L., BADER, M., CAMPAGNOLE-SANTOS, M. J. & SOUZA DOS SANTOS, R. A. 2007. Expression of an angiotensin-(1-7)-producing fusion protein in rats induced marked changes in regional vascular resistance. *Am J Physiol Heart Circ Physiol,* 292**,** H2485-90.

BOULANGER, C. M., AMABILE, N. & TEDGUI, A. 2006. Circulating microparticles: a potential prognostic marker for atherosclerotic vascular disease. *Hypertension,* 48**,** 180-6.

BOULANGER, C. M., SCOAZEC, A., EBRAHIMIAN, T., HENRY, P., MATHIEU, E., TEDGUI, A. & MALLAT, Z. 2001. Circulating microparticles from patients with myocardial infarction cause endothelial dysfunction. *Circulation,* 104**,** 2649-52.

BRAUN-MENENDEZ, E., FASCIOLO, J. C., LELOIR, L. F. & MUNOZ, J. M. 1940. The substance causing renal hypertension. *J Physiol,* 98**,** 283-98.

BRIGHT, R. 1836. Tabular view of the morbid appearances in 100 cases connected with albuminous urine. *Guy's Hospital reports.,* 1.

BRILLA, C. G., SCHEER, C. & RUPP, H. 1997. Renin-angiotensin system and myocardial collagen matrix: modulation of cardiac fibroblast function by angiotensin II type 1 receptor antagonism. *J Hypertens Suppl,* 15**,** S13-9.

BROSNIHAN, K. B., LI, P. & FERRARIO, C. M. 1996. Angiotensin-(1-7) dilates canine coronary arteries through kinins and nitric oxide. *Hypertension,* 27**,** 523-8.

BROSNIHAN, K. B., LI, P., TALLANT, E. A. & FERRARIO, C. M. 1998. Angiotensin-(1-7): a novel vasodilator of the coronary circulation. *Biol Res,* 31**,** 227-34.

BUCKI, R., BACHELOT-LOZA, C., ZACHOWSKI, A., GIRAUD, F. & SULPICE, J. C. 1998. Calcium induces phospholipid redistribution and microvesicle release in human erythrocyte membranes by independent pathways. *Biochemistry,* 37**,** 15383-91.

BUNKENBURG, B., VAN AMELSVOORT, T., ROGG, H. & WOOD, J. M. 1992. Receptor-mediated effects of angiotensin II on growth of vascular smooth muscle cells from spontaneously hypertensive rats. *Hypertension,* 20**,** 746-54.

BURGHI, V., ECHEVERRIA, E. B., SOSA, M. H., QUIROGA, D. T., MUNOZ, M. C., DAVIO, C., MONCZOR, F., FERNANDEZ, N. C. & DOMINICI, F. P. 2019. Participation of Galphai-Adenylate Cyclase and ERK1/2 in Mas Receptor Signaling Pathways. *Front Pharmacol,* 10**,** 146.

CASTRO, C. H., SANTOS, R. A., FERREIRA, A. J., BADER, M., ALENINA, N. & ALMEIDA, A. P. 2005. Evidence for a functional interaction of the angiotensin-(1-7) receptor Mas with AT1 and AT2 receptors in the mouse heart. *Hypertension,* 46**,** 937-42.

CHALMERS, J., MACMAHON, S., MANCIA, G., WHITWORTH, J., BEILIN, L., HANSSON, L., NEAL, B., RODGERS, A., NI MHURCHU, C. & CLARK, T. 1999. 1999 World Health Organization-International Society of Hypertension Guidelines for the management of hypertension. Guidelines sub-committee of the World Health Organization. *Clin Exp Hypertens,* 21**,** 1009-60.

CHANG, R. L., LIN, J. W., KUO, W. W., HSIEH, D. J., YEH, Y. L., SHEN, C. Y., DAY, C. H., HO, T. J., VISWANADHA, V. P. & HUANG, C. Y. 2016. Angiotensin-(1-7) attenuated long-term hypoxia-stimulated cardiomyocyte apoptosis by inhibiting HIF-1alpha nuclear translocation via Mas receptor regulation. *Growth Factors,* 34**,** 11-8.

CHARPIOT, P., ROLLAND, P. H., FRIGGI, A., PIQUET, P., SCALBERT, E., BODARD, H., BARLATIER, A., LATRILLE, V., TRANIER, P., MERCIER, C. & ET AL. 1993. ACE inhibition with perindopril and atherogenesis-induced structural and functional changes in minipig arteries. *Arterioscler Thromb,* 13**,** 1125-38.

CHATURVEDI, P., KALANI, A., MEDINA, I., FAMILTSEVA, A. & TYAGI, S. C. 2015. Cardiosome mediated regulation of MMP9 in diabetic heart: role of mir29b and mir455 in exercise. *J Cell Mol Med,* 19**,** 2153-61.

CHEN, L., WANG, Y., PAN, Y., ZHANG, L., SHEN, C., QIN, G., ASHRAF, M., WEINTRAUB, N., MA, G. & TANG, Y. 2013. Cardiac progenitor-derived exosomes protect ischemic myocardium from acute ischemia/reperfusion injury. *Biochem Biophys Res Commun,* 431**,** 566-71.

CHEN, L., ZHAO, L., SAMANTA, A., MAHMOUDI, S. M., BUEHLER, T., CANTILENA, A., VINCENT, R. J., GIRGIS, M., BREEDEN, J., ASANTE, S., XUAN, Y. T. & DAWN, B. 2017. STAT3 balances myocyte hypertrophy vis-a-vis autophagy in response to Angiotensin II by modulating the AMPKalpha/mTOR axis. *PLoS One,* 12**,** e0179835.

CHEN, X. L., DODD, G., THOMAS, S., ZHANG, X., WASSERMAN, M. A., ROVIN, B. H. & KUNSCH, C. 2006. Activation of Nrf2/ARE pathway protects endothelial cells from oxidant injury and inhibits inflammatory gene expression. *Am J Physiol Heart Circ Physiol,* 290**,** H1862-70.

CHEN, Z., TAN, F., ERDOS, E. G. & DEDDISH, P. A. 2005. Hydrolysis of angiotensin peptides by human angiotensin I-converting enzyme and the resensitization of B2 kinin receptors. *Hypertension,* 46**,** 1368-73.

CHO, H., HARRISON, K., SCHWARTZ, O. & KEHRL, J. H. 2003. The aorta and heart differentially express RGS (regulators of G-protein signalling) proteins that selectively regulate sphingosine 1-phosphate, angiotensin II and endothelin-1 signalling. *The Biochemical journal,* 371**,** 973-980.

CHOBANIAN, A. V., BAKRIS, G. L., BLACK, H. R., CUSHMAN, W. C., GREEN, L. A., IZZO, J. L., JR., JONES, D. W., MATERSON, B. J., OPARIL, S., WRIGHT, J. T., JR. & ROCCELLA, E. J. 2003. The Seventh Report of the Joint National Committee on Prevention, Detection, Evaluation, and Treatment of High Blood Pressure: the JNC 7 report. *Jama,* 289**,** 2560-72.

CHOW, B. S., KOCAN, M., BOSNYAK, S., SARWAR, M., WIGG, B., JONES, E. S., WIDDOP, R. E., SUMMERS, R. J., BATHGATE, R. A., HEWITSON, T. D. & SAMUEL, C. S. 2014. Relaxin requires the angiotensin II type 2 receptor to abrogate renal interstitial fibrosis. *Kidney Int,* 86**,** 75-85.

CHRISTIANSON, H. C., SVENSSON, K. J., VAN KUPPEVELT, T. H., LI, J. P. & BELTING, M. 2013. Cancer cell exosomes depend on cell-surface heparan sulfate proteoglycans for their internalization and functional activity. *Proc Natl Acad Sci U S A,* 110**,** 17380-5.

CICILINI, M. A., RAMOS, P. S., VASQUEZ, E. C. & CABRAL, A. M. 1994. Heart prolyl endopeptidase activity in one-kidney, one clip hypertensive rats. *Braz J Med Biol Res,* 27**,** 2821-30.

CLAYCOMB, W. C., LANSON, N. A., JR., STALLWORTH, B. S., EGELAND, D. B., DELCARPIO, J. B., BAHINSKI, A. & IZZO, N. J., JR. 1998. HL-1 cells: a cardiac muscle cell line that contracts and retains phenotypic characteristics of the adult cardiomyocyte. *Proceedings of the National Academy of Sciences of the United States of America,* 95**,** 2979-2984.

COHN, J. N., FERRARI, R. & SHARPE, N. 2000. Cardiac remodeling--concepts and clinical implications: a consensus paper from an international forum on cardiac remodeling. Behalf of an International Forum on Cardiac Remodeling. *J Am Coll Cardiol,* 35**,** 569-82.

COLOMBO, M., RAPOSO, G. & THERY, C. 2014. Biogenesis, secretion, and intercellular interactions of exosomes and other extracellular vesicles. *Annu Rev Cell Dev Biol,* 30**,** 255-89.

CONSENSUS 1987. Effects of enalapril on mortality in severe congestive heart failure. Results of the Cooperative North Scandinavian Enalapril Survival Study (CONSENSUS). *N Engl J Med,* 316**,** 1429-35.

CORDAZZO, C., NERI, T., PETRINI, S., LOMBARDI, S., BALIA, C., CIANCHETTI, S., CARMAZZI, Y., PAGGIARO, P., PEDRINELLI, R. & CELI, A. 2013. Angiotensin II induces the generation of procoagulant microparticles by human mononuclear cells via an angiotensin type 2 receptor-mediated pathway. *Thromb Res,* 131**,** e168-74.

COSENTINO, F., SAVOIA, C., DE PAOLIS, P., FRANCIA, P., RUSSO, A., MAFFEI, A., VENTURELLI, V., SCHIAVONI, M., LEMBO, G. & VOLPE, M. 2005. Angiotensin II type 2 receptors contribute to vascular responses in spontaneously hypertensive rats treated with angiotensin II type 1 receptor antagonists. *Am J Hypertens,* 18**,** 493-9.

COSSETTI, C., IRACI, N., MERCER, T. R., LEONARDI, T., ALPI, E., DRAGO, D., ALFARO-CERVELLO, C., SAINI, H. K., DAVIS, M. P., SCHAEFFER, J., VEGA, B., STEFANINI, M., ZHAO, C., MULLER, W., GARCIA-VERDUGO, J. M., MATHIVANAN, S., BACHI, A., ENRIGHT, A. J., MATTICK, J. S. & PLUCHINO, S. 2014. Extracellular vesicles from neural stem cells transfer IFN-gamma via Ifngr1 to activate Stat1 signaling in target cells. *Mol Cell,* 56**,** 193-204.

COSTA, M. A., LOPEZ VERRILLI, M. A., GOMEZ, K. A., NAKAGAWA, P., PENA, C., ARRANZ, C. & GIRONACCI, M. M. 2010. Angiotensin-(1-7) upregulates cardiac nitric oxide synthase in spontaneously hypertensive rats. *Am J Physiol Heart Circ Physiol,* 299**,** H1205-11.

CRACKOWER, M. A., SARAO, R., OUDIT, G. Y., YAGIL, C., KOZIERADZKI, I., SCANGA, S. E., OLIVEIRA-DOS-SANTOS, A. J., DA COSTA, J., ZHANG, L., PEI, Y., SCHOLEY, J., FERRARIO, C. M., MANOUKIAN, A. S., CHAPPELL, M. C., BACKX, P. H., YAGIL, Y. & PENNINGER, J. M. 2002. Angiotensin-converting enzyme 2 is an essential regulator of heart function. *Nature,* 417**,** 822-8.

CUI, Z., CHEN, X., CHEN, L., WANG, M. & LIU, L. 1999. [Angiotensin II regulates the expression of collagens in rat heart]. *Zhongguo Yi Xue Ke Xue Yuan Xue Bao,* 21**,** 483-7.

D'AMORE, A., BLACK, M. J. & THOMAS, W. G. 2005. The angiotensin II type 2 receptor causes constitutive growth of cardiomyocytes and does not antagonize angiotensin II type 1 receptor-mediated hypertrophy. *Hypertension,* 46**,** 1347-54.

DATTA, R., BANSAL, T., RANA, S., DATTA, K., DATTA CHAUDHURI, R., CHAWLA-SARKAR, M. & SARKAR, S. 2017. Myocyte-Derived Hsp90 Modulates Collagen Upregulation via Biphasic Activation of STAT-3 in Fibroblasts during Cardiac Hypertrophy. *Mol Cell Biol,* 37.

DAUGHERTY, A., RATERI, D. L., LU, H., INAGAMI, T. & CASSIS, L. A. 2004. Hypercholesterolemia stimulates angiotensin peptide synthesis and contributes to atherosclerosis through the AT1A receptor. *Circulation,* 110**,** 3849-57.

DELLES, C., SCHIFFER, E., VON ZUR MUHLEN, C., PETER, K., ROSSING, P., PARVING, H. H., DYMOTT, J. A., NEISIUS, U., ZIMMERLI, L. U., SNELL-BERGEON, J. K., MAAHS, D. M., SCHMIEDER, R. E., MISCHAK, H. & DOMINICZAK, A. F. 2010. Urinary proteomic diagnosis of coronary artery disease: identification and clinical validation in 623 individuals. *J Hypertens,* 28**,** 2316-22.

DENDORFER, A., WOLFRUM, S., WAGEMANN, M., QADRI, F. & DOMINIAK, P. 2001. Pathways of bradykinin degradation in blood and plasma of normotensive and hypertensive rats. *Am J Physiol Heart Circ Physiol,* 280**,** H2182-8.

DESCHEPPER, C. F. 1994. Angiotensinogen: hormonal regulation and relative importance in the generation of angiotensin II. *Kidney Int,* 46**,** 1561-3.

DI VIZIO, D., MORELLO, M., DUDLEY, A. C., SCHOW, P. W., ADAM, R. M., MORLEY, S., MULHOLLAND, D., ROTINEN, M., HAGER, M. H., INSABATO, L., MOSES, M. A., DEMICHELIS, F., LISANTI, M. P., WU, H., KLAGSBRUN, M., BHOWMICK, N. A., RUBIN, M. A., D'SOUZA-SCHOREY, C. & FREEMAN, M. R.

2012. Large oncosomes in human prostate cancer tissues and in the circulation of mice with metastatic disease. *Am J Pathol,* 181**,** 1573-84.

DIAS-PEIXOTO, M. F., SANTOS, R. A., GOMES, E. R., ALVES, M. N., ALMEIDA, P. W., GRECO, L., ROSA, M., FAULER, B., BADER, M., ALENINA, N. & GUATIMOSIM, S. 2008. Molecular mechanisms involved in the angiotensin-(1-7)/Mas signaling pathway in cardiomyocytes. *Hypertension,* 52**,** 542-8.

DOMINICZAK, A. F., DEVLIN, A. M., BROSNAN, M. J., ANDERSON, N. H., GRAHAM, D., CLARK, J. S., MCPHADEN, A., HAMILTON, C. A. & REID, J. L. 1997. Left ventricular hypertrophy and arterial blood pressure in experimental models of hypertension. *Adv Exp Med Biol,* 432**,** 23-33.

DONG, B., ZHANG, Y. H., DONG, Q. L., YU, Q. T., ZHU, L., LI, S. Y., YANG, Y. P., ZHANG, C., FENG, J. B., LIU, C. X., SONG, H. D., PAN, C. M. & ZHANG, Y. 2009. [Overexpression of angiotensin converting enzyme 2 inhibits inflammatory response of atherosclerotic plaques in hypercholesterolemic rabbits]. *Zhonghua Xin Xue Guan Bing Za Zhi,* 37**,** 622-5.

DONNAN, G. A., FISHER, M., MACLEOD, M. & DAVIS, S. M. 2008. Stroke. *Lancet,* 371**,** 1612-23.

DONOGHUE, M., HSIEH, F., BARONAS, E., GODBOUT, K., GOSSELIN, M., STAGLIANO, N., DONOVAN, M., WOOLF, B., ROBISON, K., JEYASEELAN, R., BREITBART, R. E. & ACTON, S. 2000. A novel angiotensin-converting enzyme-related carboxypeptidase (ACE2) converts angiotensin I to angiotensin 1-9. *Circ Res,* 87**,** E1-9.

DORAYAPPAN, K. D. P., WANNER, R., WALLBILLICH, J. J., SAINI, U., ZINGARELLI, R., SUAREZ, A. A., COHN, D. E. & SELVENDIRAN, K. 2018. Hypoxia-induced exosomes contribute to a more aggressive and chemoresistant ovarian cancer phenotype: a novel mechanism linking STAT3/Rab proteins. *Oncogene,* 37**,** 3806-3821.

DU, G., HUANG, P., LIANG, B. T. & FROHMAN, M. A. 2004. Phospholipase D2 localizes to the plasma membrane and regulates angiotensin II receptor endocytosis. *Mol Biol Cell,* 15**,** 1024-30.

DUNN, K. W., KAMOCKA, M. M. & MCDONALD, J. H. 2011. A practical guide to evaluating colocalization in biological microscopy. *American journal of physiology. Cell physiology,* 300**,** C723-C742.

FARIA-COSTA, G., LEITE-MOREIRA, A. & HENRIQUES-COELHO, T. 2014. Cardiovascular effects of the angiotensin type 2 receptor. *Rev Port Cardiol,* 33**,** 439-49.

FARUQU, F. N., XU, L. & AL-JAMAL, K. T. 2018. Preparation of Exosomes for siRNA Delivery to Cancer Cells. *J Vis Exp*.

FASCIOLO, J. C., HOUSSAY, B. A. & TAQUINI, A. C. 1938. The blood-pressure raising secretion of the ischaemic kidney. *J Physiol,* 94**,** 281-93.

FERGUSON, A. V. & WASHBURN, D. L. 1998. Angiotensin II: a peptidergic neurotransmitter in central autonomic pathways. *Prog Neurobiol,* 54**,** 169-92.

FERREIRA, A. J., MORAES, P. L., FOUREAUX, G., ANDRADE, A. B., SANTOS, R. A. & ALMEIDA, A. P. 2011. The angiotensin-(1-7)/Mas receptor axis is expressed in sinoatrial node cells of rats. *J Histochem Cytochem,* 59**,** 761-8.

FISH, J. E., SANTORO, M. M., MORTON, S. U., YU, S., YEH, R. F., WYTHE, J. D., IVEY, K. N., BRUNEAU, B. G., STAINIER, D. Y. & SRIVASTAVA, D. 2008. miR-126 regulates angiogenic signaling and vascular integrity. *Dev Cell,* 15**,** 272-84.

FLORES-MUNOZ, M., GODINHO, B. M., ALMALIK, A. & NICKLIN, S. A. 2012a. Adenoviral delivery of angiotensin-(1-7) or angiotensin-(1-9) inhibits cardiomyocyte hypertrophy via the mas or angiotensin type 2 receptor. *PLoS One,* 7**,** e45564.

FLORES-MUÑOZ, M., SMITH, N. J., HAGGERTY, C., MILLIGAN, G. & NICKLIN, S. A. 2011. Angiotensin1-9 antagonises pro-hypertrophic signalling in cardiomyocytes via the angiotensin type 2 receptor. *J Physiol,* 589**,** 939-51.

FLORES-MUNOZ, M., WORK, L. M., DOUGLAS, K., DENBY, L., DOMINICZAK, A. F., GRAHAM, D. & NICKLIN, S. A. 2012b. Angiotensin-(1-9) attenuates cardiac fibrosis in the stroke-prone spontaneously hypertensive rat via the angiotensin type 2 receptor. *Hypertension,* 59**,** 300-7.

FORCE, T., POMBO, C. M., AVRUCH, J. A., BONVENTRE, J. V. & KYRIAKIS, J. M. 1996. Stress-activated protein kinases in cardiovascular disease. *Circ Res,* 78**,** 947-53.

FRANK, G. D., SAITO, S., MOTLEY, E. D., SASAKI, T., OHBA, M., KUROKI, T., INAGAMI, T. & EGUCHI, S. 2002. Requirement of Ca(2+) and PKCdelta for Janus kinase 2 activation by angiotensin II: involvement of PYK2. *Mol Endocrinol,* 16**,** 367-77.

FREY, U. H., KLAASSEN, M., OCHSENFARTH, C., MURKE, F., THIELMANN, M., KOTTENBERG, E., KLEINBONGARD, P., KLENKE, S., ENGLER, A., HEUSCH, G., GIEBEL, B. & PETERS, J. 2019. Remote ischaemic preconditioning increases serum extracellular vesicle concentrations with altered micro-RNA signature in CABG patients. *Acta Anaesthesiol Scand,* 63**,** 483-492.

FYHRQUIST, F., METSARINNE, K. & TIKKANEN, I. 1995. Role of angiotensin II in blood pressure regulation and in the pathophysiology of cardiovascular disorders. *J Hum Hypertens,* 9 Suppl 5**,** S19-24.

GABORIK, Z. & HUNYADY, L. 2004. Intracellular trafficking of hormone receptors. *Trends Endocrinol Metab,* 15**,** 286-93.

GALANDRIN, S., DENIS, C., BOULARAN, C., MARIE, J., M'KADMI, C., PILETTE, C., DUBROCA, C., NICAISE, Y., SEGUELAS, M. H., N'GUYEN, D., BANERES, J. L., PATHAK, A., SENARD, J. M. & GALES, C. 2016. Cardioprotective Angiotensin-(1-7) Peptide Acts as a Natural-Biased Ligand at the Angiotensin II Type 1 Receptor. *Hypertension,* 68**,** 1365-1374.

GALIS, Z. S. & KHATRI, J. J. 2002. Matrix metalloproteinases in vascular remodeling and atherogenesis: the good, the bad, and the ugly. *Circ Res,* 90**,** 251-62.

GASC, J. M., SHANMUGAM, S., SIBONY, M. & CORVOL, P. 1994. Tissue-specific expression of type 1 angiotensin II receptor subtypes. An in situ hybridization study. *Hypertension,* 24**,** 531-7.

GAVA, E., DE CASTRO, C. H., FERREIRA, A. J., COLLETA, H., MELO, M. B., ALENINA, N., BADER, M., OLIVEIRA, L. A., SANTOS, R. A. & KITTEN, G. T. 2012. Angiotensin-(1-7) receptor Mas is an essential modulator of extracellular matrix protein expression in the heart. *Regul Pept,* 175**,** 30-42.

GNECCHI, M., HE, H., LIANG, O. D., MELO, L. G., MORELLO, F., MU, H., NOISEUX, N., ZHANG, L., PRATT, R. E., INGWALL, J. S. & DZAU, V. J. 2005. Paracrine action accounts for marked protection of ischemic heart by Akt-modified mesenchymal stem cells. *Nature Medicine,* 11**,** 367.

GNECCHI, M., HE, H., NOISEUX, N., LIANG, O. D., ZHANG, L., MORELLO, F., MU, H., MELO, L. G., PRATT, R. E., INGWALL, J. S. & DZAU, V. J. 2006. Evidence supporting paracrine hypothesis for Akt-modified mesenchymal

stem cell-mediated cardiac protection and functional improvement. *Faseb j,* 20**,** 661-9.
GOMES, E. R., SANTOS, R. A. & GUATIMOSIM, S. 2012. Angiotensin-(1-7)-mediated signaling in cardiomyocytes. *Int J Hypertens,* 2012**,** 493129.
GORELIK, G., CARBINI, L. A. & SCICLI, A. G. 1998. Angiotensin 1-7 induces bradykinin-mediated relaxation in porcine coronary artery. *J Pharmacol Exp Ther,* 286**,** 403-10.
GORGENS, A., BREMER, M., FERRER-TUR, R., MURKE, F., TERTEL, T., HORN, P. A., THALMANN, S., WELSH, J. A., PROBST, C., GUERIN, C., BOULANGER, C. M., JONES, J. C., HANENBERG, H., ERDBRUGGER, U., LANNIGAN, J., RICKLEFS, F. L., EL-ANDALOUSSI, S. & GIEBEL, B. 2019. Optimisation of imaging flow cytometry for the analysis of single extracellular vesicles by using fluorescence-tagged vesicles as biological reference material. *J Extracell Vesicles,* 8**,** 1587567.
GRAHAM, D., MCBRIDE, M. W., GAASENBEEK, M., GILDAY, K., BEATTIE, E., MILLER, W. H., MCCLURE, J. D., POLKE, J. M., MONTEZANO, A., TOUYZ, R. M. & DOMINICZAK, A. F. 2007. Candidate genes that determine response to salt in the stroke-prone spontaneously hypertensive rat: congenic analysis. *Hypertension,* 50**,** 1134-41.
GRANGER, C. B., MCMURRAY, J. J., YUSUF, S., HELD, P., MICHELSON, E. L., OLOFSSON, B., OSTERGREN, J., PFEFFER, M. A. & SWEDBERG, K. 2003. Effects of candesartan in patients with chronic heart failure and reduced left-ventricular systolic function intolerant to angiotensin-converting-enzyme inhibitors: the CHARM-Alternative trial. *Lancet,* 362**,** 772-6.
GRANT, B. D. & DONALDSON, J. G. 2009. Pathways and mechanisms of endocytic recycling. *Nat Rev Mol Cell Biol,* 10**,** 597-608.
GRATTON, J. P., BERNATCHEZ, P. & SESSA, W. C. 2004. Caveolae and caveolins in the cardiovascular system. *Circ Res,* 94**,** 1408-17.
GRAY, M. O., LONG, C. S., KALINYAK, J. E., LI, H. T. & KARLINER, J. S. 1998. Angiotensin II stimulates cardiac myocyte hypertrophy via paracrine release of TGF-beta 1 and endothelin-1 from fibroblasts. *Cardiovasc Res,* 40**,** 352-63.
GRIENDLING, K. K., DELAFONTAINE, P., RITTENHOUSE, S. E., GIMBRONE, M. A., JR. & ALEXANDER, R. W. 1987. Correlation of receptor sequestration with sustained diacylglycerol accumulation in angiotensin II-stimulated cultured vascular smooth muscle cells. *J Biol Chem,* 262**,** 14555-62.
GRIENDLING, K. K., SORESCU, D. & USHIO-FUKAI, M. 2000. NAD(P)H oxidase: role in cardiovascular biology and disease. *Circ Res,* 86**,** 494-501.
GROBE, J. L., MECCA, A. P., MAO, H. & KATOVICH, M. J. 2006. Chronic angiotensin-(1-7) prevents cardiac fibrosis in DOCA-salt model of hypertension. *Am J Physiol Heart Circ Physiol,* 290**,** H2417-23.
GROSS, V. & LUFT, F. C. 2003. Exercising restraint in measuring blood pressure in conscious mice. *Hypertension,* 41**,** 879-81.
GUANG, C., PHILLIPS, R. D., JIANG, B. & MILANI, F. 2012. Three key proteases--angiotensin-I-converting enzyme (ACE), ACE2 and renin--within and beyond the renin-angiotensin system. *Arch Cardiovasc Dis,* 105**,** 373-85.
GUO, L., YIN, A., ZHANG, Q., ZHONG, T., O'ROURKE, S. T. & SUN, C. 2017. Angiotensin-(1-7) attenuates angiotensin II-induced cardiac hypertrophy via a Sirt3-dependent mechanism. *Am J Physiol Heart Circ Physiol,* 312**,** H980-h991.
GUO, W. G., SU, F. F., YUAN, L. J., YANG, G. D., SHI, X. Q., LI, R. Y., SHU, Q., LIU, X. T., LU, Z. F. & ZHENG, Q. S. 2010. Simvastatin inhibits angiotensin

II-induced cardiac cell hypertrophy: role of Homer 1a. *Clin Exp Pharmacol Physiol,* 37**,** 40-5.

GUPTA, S. & KNOWLTON, A. A. 2007. HSP60 trafficking in adult cardiac myocytes: role of the exosomal pathway. *Am J Physiol Heart Circ Physiol,* 292**,** H3052-6.

HANEY, M. J., KLYACHKO, N. L., ZHAO, Y., GUPTA, R., PLOTNIKOVA, E. G., HE, Z., PATEL, T., PIROYAN, A., SOKOLSKY, M., KABANOV, A. V. & BATRAKOVA, E. V. 2015. Exosomes as drug delivery vehicles for Parkinson's disease therapy. *J Control Release,* 207**,** 18-30.

HAO, L., REN, M., RONG, B., XIE, F., LIN, M.-J., ZHAO, Y.-C., YUE, X., HAN, W.-Q. & ZHONG, J.-Q. 2018. TWEAK/Fn14 mediates atrial-derived HL-1 myocytes hypertrophy via JAK2/STAT3 signalling pathway. *Journal of cellular and molecular medicine,* 22**,** 4344-4353.

HAREL, Z., GILBERT, C., WALD, R., BELL, C., PERL, J., JUURLINK, D., BEYENE, J. & SHAH, P. S. 2012. The effect of combination treatment with aliskiren and blockers of the renin-angiotensin system on hyperkalaemia and acute kidney injury: systematic review and meta-analysis. *Bmj,* 344**,** e42.

HAYEK, T., ATTIAS, J., COLEMAN, R., BRODSKY, S., SMITH, J., BRESLOW, J. L. & KEIDAR, S. 1999. The angiotensin-converting enzyme inhibitor, fosinopril, and the angiotensin II receptor antagonist, losartan, inhibit LDL oxidation and attenuate atherosclerosis independent of lowering blood pressure in apolipoprotein E deficient mice. *Cardiovasc Res,* 44**,** 579-87.

HEIJNEN, H. F., SCHIEL, A. E., FIJNHEER, R., GEUZE, H. J. & SIXMA, J. J. 1999. Activated platelets release two types of membrane vesicles: microvesicles by surface shedding and exosomes derived from exocytosis of multivesicular bodies and alpha-granules. *Blood,* 94**,** 3791-9.

HEMMING, M. L. & SELKOE, D. J. 2005. Amyloid beta-protein is degraded by cellular angiotensin-converting enzyme (ACE) and elevated by an ACE inhibitor. *J Biol Chem,* 280**,** 37644-50.

HESCHELER, J., MEYER, R., PLANT, S., KRAUTWURST, D., ROSENTHAL, W. & SCHULTZ, G. 1991. Morphological, biochemical, and electrophysiological characterization of a clonal cell (H9c2) line from rat heart. *Circ Res,* 69**,** 1476-86.

HILZ, H., WIEGERS, U. & ADAMIETZ, P. 1975. Stimulation of proteinase K action by denaturing agents: application to the isolation of nucleic acids and the degradation of 'masked' proteins. *Eur J Biochem,* 56**,** 103-8.

HIRSCH, A. T., TALSNESS, C. E., SCHUNKERT, H., PAUL, M. & DZAU, V. J. 1991. Tissue-specific activation of cardiac angiotensin converting enzyme in experimental heart failure. *Circ Res,* 69**,** 475-82.

HONIGBERG, M. C. & GIVERTZ, M. M. 2019. Peripartum cardiomyopathy. *Bmj,* 364**,** k5287.

HOOD, J. L., SCOTT, M. J. & WICKLINE, S. A. 2014. Maximizing exosome colloidal stability following electroporation. *Anal Biochem,* 448**,** 41-9.

HSU, C., MOROHASHI, Y., YOSHIMURA, S., MANRIQUE-HOYOS, N., JUNG, S., LAUTERBACH, M. A., BAKHTI, M., GRONBORG, M., MOBIUS, W., RHEE, J., BARR, F. A. & SIMONS, M. 2010. Regulation of exosome secretion by Rab35 and its GTPase-activating proteins TBC1D10A-C. *J Cell Biol,* 189**,** 223-32.

HUANG, C. Y., KUO, W. W., CHUEH, P. J., TSENG, C. T., CHOU, M. Y. & YANG, J. J. 2004. Transforming growth factor-beta induces the expression of ANF and hypertrophic growth in cultured cardiomyoblast cells through ZAK. *Biochem Biophys Res Commun,* 324**,** 424-31.

HUANG, X., YUAN, T., TSCHANNEN, M., SUN, Z., JACOB, H., DU, M., LIANG, M., DITTMAR, R. L., LIU, Y., LIANG, M., KOHLI, M., THIBODEAU, S. N., BOARDMAN, L. & WANG, L. 2013. Characterization of human plasma-derived exosomal RNAs by deep sequencing. *BMC Genomics,* 14**,** 319.

HUENTELMAN, M. J., GROBE, J. L., VAZQUEZ, J., STEWART, J. M., MECCA, A. P., KATOVICH, M. J., FERRARIO, C. M. & RAIZADA, M. K. 2005. Protection from angiotensin II-induced cardiac hypertrophy and fibrosis by systemic lentiviral delivery of ACE2 in rats. *Exp Physiol,* 90**,** 783-90.

HUNTER, J. J. & CHIEN, K. R. 1999. Signaling pathways for cardiac hypertrophy and failure. *N Engl J Med,* 341**,** 1276-83.

HUNYADY, L. & CATT, K. J. 2006. Pleiotropic AT1 receptor signaling pathways mediating physiological and pathogenic actions of angiotensin II. *Mol Endocrinol,* 20**,** 953-70.

IKEDA, S., KONG, S. W., LU, J., BISPING, E., ZHANG, H., ALLEN, P. D., GOLUB, T. R., PIESKE, B. & PU, W. T. 2007. Altered microRNA expression in human heart disease. *Physiol Genomics,* 31**,** 367-73.

IRVINE, R. J., WHITE, J. & CHAN, R. 1997. The influence of restraint on blood pressure in the rat. *J Pharmacol Toxicol Methods,* 38**,** 157-62.

IZUMIYA, Y., ARAKI, S., USUKU, H., ROKUTANDA, T., HANATANI, S. & OGAWA, H. 2012. Chronic C-Type Natriuretic Peptide Infusion Attenuates Angiotensin II-Induced Myocardial Superoxide Production and Cardiac Remodeling. *Int J Vasc Med,* 2012**,** 246058.

JACKMAN, H. L., MASSAD, M. G., SEKOSAN, M., TAN, F., BROVKOVYCH, V., MARCIC, B. M. & ERDOS, E. G. 2002. Angiotensin 1-9 and 1-7 release in human heart: role of cathepsin A. *Hypertension,* 39**,** 976-81.

JACOB, R., DIERBERGER, B. & KISSLING, G. 1992. Functional significance of the Frank-Starling mechanism under physiological and pathophysiological conditions. *Eur Heart J,* 13 Suppl E**,** 7-14.

JANG, J. H., CHUN, J. N., GODO, S., WU, G., SHIMOKAWA, H., JIN, C. Z., JEON, J. H., KIM, S. J., JIN, Z. H. & ZHANG, Y. H. 2015. ROS and endothelial nitric oxide synthase (eNOS)-dependent trafficking of angiotensin II type 2 receptor begets neuronal NOS in cardiac myocytes. *Basic Res Cardiol,* 110**,** 21.

JANSEN, F., YANG, X., HOELSCHER, M., CATTELAN, A., SCHMITZ, T., PROEBSTING, S., WENZEL, D., VOSEN, S., FRANKLIN, B. S., FLEISCHMANN, B. K., NICKENIG, G. & WERNER, N. 2013. Endothelial microparticle-mediated transfer of MicroRNA-126 promotes vascular endothelial cell repair via SPRED1 and is abrogated in glucose-damaged endothelial microparticles. *Circulation,* 128**,** 2026-38.

JOHNS, D. W., PEACH, M. J., GOMEZ, R. A., INAGAMI, T. & CAREY, R. M. 1990. Angiotensin II regulates renin gene expression. *Am J Physiol,* 259**,** F882-7.

JOHNSEN, K. B., GUDBERGSSON, J. M., SKOV, M. N., CHRISTIANSEN, G., GUREVICH, L., MOOS, T. & DUROUX, M. 2016. Evaluation of electroporation-induced adverse effects on adipose-derived stem cell exosomes. *Cytotechnology,* 68**,** 2125-38.

JOHNSEN, K. B., GUDBERGSSON, J. M., SKOV, M. N., PILGAARD, L., MOOS, T. & DUROUX, M. 2014. A comprehensive overview of exosomes as drug delivery vehicles - endogenous nanocarriers for targeted cancer therapy. *Biochim Biophys Acta,* 1846**,** 75-87.

JOHNSON, G. 1868. 1. On certain points in the Anatomy and Pathology of Bright's Disease of the Kidney. 2. On the Influence of the Minute Blood-vessels upon the Circulation. *Medico-chirurgical transactions,* 51**,** 57-78.3.

JOHNSTON, A. P., BAKER, J., DE LISIO, M. & PARISE, G. 2011. Skeletal muscle myoblasts possess a stretch-responsive local angiotensin signalling system. *J Renin Angiotensin Aldosterone Syst,* 12**,** 75-84.

JOHNSTONE, R. M., ADAM, M., HAMMOND, J. R., ORR, L. & TURBIDE, C. 1987. Vesicle formation during reticulocyte maturation. Association of plasma membrane activities with released vesicles (exosomes). *J Biol Chem,* 262**,** 9412-20.

JONES, E. S., VINH, A., MCCARTHY, C. A., GASPARI, T. A. & WIDDOP, R. E. 2008. AT2 receptors: functional relevance in cardiovascular disease. *Pharmacol Ther,* 120**,** 292-316.

JY, W., GOMEZ-MARIN, O., SALERNO, T. A., PANOS, A. L., WILLIAMS, D., HORSTMAN, L. L. & AHN, Y. S. 2015. Presurgical levels of circulating cell-derived microparticles discriminate between patients with and without transfusion in coronary artery bypass graft surgery. *J Thorac Cardiovasc Surg,* 149**,** 305-11.

KAGIYAMA, S., EGUCHI, S., FRANK, G. D., INAGAMI, T., ZHANG, Y. C. & PHILLIPS, M. I. 2002. Angiotensin II-induced cardiac hypertrophy and hypertension are attenuated by epidermal growth factor receptor antisense. *Circulation,* 106**,** 909-12.

KAHLERT, C., MELO, S. A., PROTOPOPOV, A., TANG, J., SETH, S., KOCH, M., ZHANG, J., WEITZ, J., CHIN, L., FUTREAL, A. & KALLURI, R. 2014. Identification of double-stranded genomic DNA spanning all chromosomes with mutated KRAS and p53 DNA in the serum exosomes of patients with pancreatic cancer. *J Biol Chem,* 289**,** 3869-75.

KAR, S., GAO, L., BELATTI, D. A., CURRY, P. L. & ZUCKER, I. H. 2011. Central angiotensin (1-7) enhances baroreflex gain in conscious rabbits with heart failure. *Hypertension,* 58**,** 627-34.

KASSIRI, Z., ZHONG, J., GUO, D., BASU, R., WANG, X., LIU, P. P., SCHOLEY, J. W., PENNINGER, J. M. & OUDIT, G. Y. 2009. Loss of angiotensin-converting enzyme 2 accelerates maladaptive left ventricular remodeling in response to myocardial infarction. *Circ Heart Fail,* 2**,** 446-55.

KATZMANN, D. J., BABST, M. & EMR, S. D. 2001. Ubiquitin-dependent sorting into the multivesicular body pathway requires the function of a conserved endosomal protein sorting complex, ESCRT-I. *Cell,* 106**,** 145-55.

KEMP, B. A., HOWELL, N. L., GILDEA, J. J., KELLER, S. R., PADIA, S. H. & CAREY, R. M. 2014. AT(2) receptor activation induces natriuresis and lowers blood pressure. *Circ Res,* 115**,** 388-99.

KESSLER, S. P., GOMOS, J. B., SCHEIDEMANTEL, T. S., ROWE, T. M., SMITH, H. L. & SEN, G. C. 2002. The germinal isozyme of angiotensin-converting enzyme can substitute for the somatic isozyme in maintaining normal renal structure and functions. *J Biol Chem,* 277**,** 4271-6.

KIM-MITSUYAMA, S., YAMAMOTO, E., TANAKA, T., ZHAN, Y., IZUMI, Y., IZUMIYA, Y., IOROI, T., WANIBUCHI, H. & IWAO, H. 2005. Critical role of angiotensin II in excess salt-induced brain oxidative stress of stroke-prone spontaneously hypertensive rats. *Stroke,* 36**,** 1083-8.

KIM, H., YUN, N., MUN, D., KANG, J. Y., LEE, S. H., PARK, H., PARK, H. & JOUNG, B. 2018a. Cardiac-specific delivery by cardiac tissue-targeting peptide-expressing exosomes. *Biochem Biophys Res Commun,* 499**,** 803-808.

KIM, J., AHN, S., REN, X. R., WHALEN, E. J., REITER, E., WEI, H. & LEFKOWITZ, R. J. 2005. Functional antagonism of different G protein-coupled receptor

kinases for beta-arrestin-mediated angiotensin II receptor signaling. *Proc Natl Acad Sci U S A,* 102**,** 1442-7.

KIM, J. C., SON, M. J., LE, Q. A. & WOO, S. H. 2018b. Role of inositol 1,4,5-trisphosphate receptor type 1 in ATP-induced nuclear Ca(2+) signal and hypertrophy in atrial myocytes. *Biochem Biophys Res Commun,* 503**,** 2998-3002.

KIMES, B. W. & BRANDT, B. L. 1976. Properties of a clonal muscle cell line from rat heart. *Exp Cell Res,* 98**,** 367-81.

KOEKEMOER, A. L., CHONG, N. W., GOODALL, A. H. & SAMANI, N. J. 2009. Myocyte stress 1 plays an important role in cellular hypertrophy and protection against apoptosis. *FEBS Lett,* 583**,** 2964-7.

KOGA, H., SUGIYAMA, S., KUGIYAMA, K., WATANABE, K., FUKUSHIMA, H., TANAKA, T., SAKAMOTO, T., YOSHIMURA, M., JINNOUCHI, H. & OGAWA, H. 2005. Elevated levels of VE-cadherin-positive endothelial microparticles in patients with type 2 diabetes mellitus and coronary artery disease. *J Am Coll Cardiol,* 45**,** 1622-30.

KOOIJMANS, S. A. A., STREMERSCH, S., BRAECKMANS, K., DE SMEDT, S. C., HENDRIX, A., WOOD, M. J. A., SCHIFFELERS, R. M., RAEMDONCK, K. & VADER, P. 2013. Electroporation-induced siRNA precipitation obscures the efficiency of siRNA loading into extracellular vesicles. *J Control Release,* 172**,** 229-238.

KOSAKA, N., IGUCHI, H., YOSHIOKA, Y., HAGIWARA, K., TAKESHITA, F. & OCHIYA, T. 2012. Competitive interactions of cancer cells and normal cells via secretory microRNAs. *J Biol Chem,* 287**,** 1397-405.

KRAMER, K. & KINTER, L. B. 2003. Evaluation and applications of radiotelemetry in small laboratory animals. *Physiol Genomics,* 13**,** 197-205.

KURTZ, T. W., GRIFFIN, K. A., BIDANI, A. K., DAVISSON, R. L. & HALL, J. E. 2005. Recommendations for blood pressure measurement in humans and experimental animals. Part 2: Blood pressure measurement in experimental animals: a statement for professionals from the subcommittee of professional and public education of the American Heart Association council on high blood pressure research. *Hypertension,* 45**,** 299-310.

LAI, C. P., KIM, E. Y., BADR, C. E., WEISSLEDER, R., MEMPEL, T. R., TANNOUS, B. A. & BREAKEFIELD, X. O. 2015. Visualization and tracking of tumour extracellular vesicle delivery and RNA translation using multiplexed reporters. *Nat Commun,* 6**,** 7029.

LAI, R. C., ARSLAN, F., LEE, M. M., SZE, N. S., CHOO, A., CHEN, T. S., SALTO-TELLEZ, M., TIMMERS, L., LEE, C. N., EL OAKLEY, R. M., PASTERKAMP, G., DE KLEIJN, D. P. & LIM, S. K. 2010. Exosome secreted by MSC reduces myocardial ischemia/reperfusion injury. *Stem Cell Res,* 4**,** 214-22.

LAMICHHANE, T. N., RAIKER, R. S. & JAY, S. M. 2015. Exogenous DNA Loading into Extracellular Vesicles via Electroporation is Size-Dependent and Enables Limited Gene Delivery. *Mol Pharm,* 12**,** 3650-7.

LASKOWSKI, A., WOODMAN, O. L., CAO, A. H., DRUMMOND, G. R., MARSHALL, T., KAYE, D. M. & RITCHIE, R. H. 2006. Antioxidant actions contribute to the antihypertrophic effects of atrial natriuretic peptide in neonatal rat cardiomyocytes. *Cardiovasc Res,* 72**,** 112-23.

LATINI, R., TOGNONI, G., MAGGIONI, A. P., BAIGENT, C., BRAUNWALD, E., CHEN, Z. M., COLLINS, R., FLATHER, M., FRANZOSI, M. G., KJEKSHUS, J., KOBER, L., LIU, L. S., PETO, R., PFEFFER, M., PIZZETTI, F., SANTORO, E., SLEIGHT, P., SWEDBERG, K., TAVAZZI, L., WANG, W. & YUSUF, S. 2000.

Clinical effects of early angiotensin-converting enzyme inhibitor treatment for acute myocardial infarction are similar in the presence and absence of aspirin: systematic overview of individual data from 96,712 randomized patients. Angiotensin-converting Enzyme Inhibitor Myocardial Infarction Collaborative Group. *J Am Coll Cardiol,* 35**,** 1801-7.

LAULAGNIER, K., GRAND, D., DUJARDIN, A., HAMDI, S., VINCENT-SCHNEIDER, H., LANKAR, D., SALLES, J. P., BONNEROT, C., PERRET, B. & RECORD, M. 2004a. PLD2 is enriched on exosomes and its activity is correlated to the release of exosomes. *FEBS Lett,* 572**,** 11-4.

LAULAGNIER, K., MOTTA, C., HAMDI, S., ROY, S., FAUVELLE, F., PAGEAUX, J. F., KOBAYASHI, T., SALLES, J. P., PERRET, B., BONNEROT, C. & RECORD, M. 2004b. Mast cell- and dendritic cell-derived exosomes display a specific lipid composition and an unusual membrane organization. *Biochem J,* 380**,** 161-71.

LEE, T. H., CHENNAKRISHNAIAH, S., AUDEMARD, E., MONTERMINI, L., MEEHAN, B. & RAK, J. 2014. Oncogenic ras-driven cancer cell vesiculation leads to emission of double-stranded DNA capable of interacting with target cells. *Biochem Biophys Res Commun,* 451**,** 295-301.

LEE, Y., EL ANDALOUSSI, S. & WOOD, M. J. 2012. Exosomes and microvesicles: extracellular vesicles for genetic information transfer and gene therapy. *Hum Mol Genet,* 21**,** R125-34.

LEVY, B. I. 2005. How to explain the differences between renin angiotensin system modulators. *Am J Hypertens,* 18**,** 134s-141s.

LI, J., LI, Y., ZHANG, Y., HU, D., GAO, Y., SHANG, H. & XING, Y. 2017. The Inhibitory Effect of WenxinKeli on H9C2 Cardiomyocytes Hypertrophy Induced by Angiotensin II through Regulating Autophagy Activity. *Oxidative medicine and cellular longevity,* 2017**,** 7042872-7042872.

LI, J., XUE, H., LI, T., CHU, X., XIN, D., XIONG, Y., QIU, W., GAO, X., QIAN, M., XU, J., WANG, Z. & LI, G. 2019. Exosomes derived from mesenchymal stem cells attenuate the progression of atherosclerosis in ApoE(-/-) mice via miR-let7 mediated infiltration and polarization of M2 macrophage. *Biochem Biophys Res Commun,* 510**,** 565-572.

LI, K. Y. & ZHANG, Y. J. 2015. Valsartan-induced cardioprotection involves angiotensin II type 2 receptor upregulation in isolated ischaemia and reperfused rat hearts. *Acta Cardiol,* 70**,** 67-72.

LI, P., LIU, Z., XIE, Y., GU, H., DAI, Q., YAO, J. & ZHOU, L. 2018. Serum Exosomes Attenuate H2O2-Induced Apoptosis in Rat H9C2 Cardiomyocytes via ERK1/2. *J Cardiovasc Transl Res*.

LI, Y., LI, X.-H. & YUAN, H. 2012. Angiotensin II type-2 receptor-specific effects on the cardiovascular system. *Cardiovascular diagnosis and therapy,* 2**,** 56-62.

LI, Y., WU, J., HE, Q., SHOU, Z., ZHANG, P., PEN, W., ZHU, Y. & CHEN, J. 2009. Angiotensin (1-7) prevent heart dysfunction and left ventricular remodeling caused by renal dysfunction in 5/6 nephrectomy mice. *Hypertens Res,* 32**,** 369-74.

LIANG, B., PENG, P., CHEN, S., LI, L., ZHANG, M., CAO, D., YANG, J., LI, H., GUI, T., LI, X. & SHEN, K. 2013. Characterization and proteomic analysis of ovarian cancer-derived exosomes. *J Proteomics,* 80**,** 171-82.

LIBBY, P., RIDKER, P. M. & MASERI, A. 2002. Inflammation and atherosclerosis. *Circulation,* 105**,** 1135-43.

LIN, L., LIU, X., XU, J., WENG, L., REN, J., GE, J. & ZOU, Y. 2016. Mas receptor mediates cardioprotection of angiotensin-(1-7) against Angiotensin II-

induced cardiomyocyte autophagy and cardiac remodelling through inhibition of oxidative stress. *J Cell Mol Med,* 20**,** 48-57.

LINSEMAN, D. A., BENJAMIN, C. W. & JONES, D. A. 1995. Convergence of angiotensin II and platelet-derived growth factor receptor signaling cascades in vascular smooth muscle cells. *J Biol Chem,* 270**,** 12563-8.

LIU, C. & SU, C. 2019. Design strategies and application progress of therapeutic exosomes. *Theranostics,* 9**,** 1015-1028.

LIU, Z., LIU, J., XIAO, M., WANG, J., YAO, F., ZENG, W., YU, L., GUAN, Y., WEI, W., PENG, Z., ZHU, K., WANG, J., YANG, Z., ZHONG, J. & CHEN, J. 2018. Mesenchymal stem cell-derived microvesicles alleviate pulmonary arterial hypertension by regulating renin-angiotensin system. *J Am Soc Hypertens,* 12**,** 470-478.

LIVAK, K. J. & SCHMITTGEN, T. D. 2001. Analysis of relative gene expression data using real-time quantitative PCR and the 2(-Delta Delta C(T)) Method. *Methods,* 25**,** 402-8.

LLORENTE, A., SKOTLAND, T., SYLVANNE, T., KAUHANEN, D., ROG, T., ORLOWSKI, A., VATTULAINEN, I., EKROOS, K. & SANDVIG, K. 2013. Molecular lipidomics of exosomes released by PC-3 prostate cancer cells. *Biochim Biophys Acta,* 1831**,** 1302-9.

LOTVALL, J., HILL, A. F., HOCHBERG, F., BUZAS, E. I., DI VIZIO, D., GARDINER, C., GHO, Y. S., KUROCHKIN, I. V., MATHIVANAN, S., QUESENBERRY, P., SAHOO, S., TAHARA, H., WAUBEN, M. H., WITWER, K. W. & THERY, C. 2014. Minimal experimental requirements for definition of extracellular vesicles and their functions: a position statement from the International Society for Extracellular Vesicles. *J Extracell Vesicles,* 3**,** 26913.

LOYER, X., VION, A. C., TEDGUI, A. & BOULANGER, C. M. 2014. Microvesicles as cell-cell messengers in cardiovascular diseases. *Circ Res,* 114**,** 345-53.

LOYER, X., ZLATANOVA, I., DEVUE, C., YIN, M., HOWANGYIN, K. Y., KLAIHMON, P., GUERIN, C. L., KHELOUFI, M., VILAR, J., ZANNIS, K., FLEISCHMANN, B. K., HWANG, D. W., PARK, J., LEE, H., MENASCHE, P., SILVESTRE, J. S. & BOULANGER, C. M. 2018. Intra-Cardiac Release of Extracellular Vesicles Shapes Inflammation Following Myocardial Infarction. *Circ Res,* 123**,** 100-106.

LYU, L., WANG, H., LI, B., QIN, Q., QI, L., NAGARKATTI, M., NAGARKATTI, P., JANICKI, J. S., WANG, X. L. & CUI, T. 2015. A critical role of cardiac fibroblast-derived exosomes in activating renin angiotensin system in cardiomyocytes. *J Mol Cell Cardiol*.

MA, T., CHEN, Y., CHEN, Y., MENG, Q., SUN, J., SHAO, L., YU, Y., HUANG, H., HU, Y., YANG, Z., YANG, J. & SHEN, Z. 2018. MicroRNA-132, Delivered by Mesenchymal Stem Cell-Derived Exosomes, Promote Angiogenesis in Myocardial Infarction. *Stem Cells Int,* 2018**,** 3290372.

MAHOMED, F. 1877. On the sphygmographic evidence of arterio-capillary fibrosis. *Trans Path Soc.,* 28**,** 394-397.

MAJALAHTI, T., SUO-PALOSAARI, M., SARMAN, B., HAUTALA, N., PIKKARAINEN, S., TOKOLA, H., VUOLTEENAHO, O., WANG, J., PARADIS, P., NEMER, M. & RUSKOAHO, H. 2007. Cardiac BNP gene activation by angiotensin II in vivo. *Mol Cell Endocrinol,* 273**,** 59-67.

MALIK, Z. A., KOTT, K. S., POE, A. J., KUO, T., CHEN, L., FERRARA, K. W. & KNOWLTON, A. A. 2013. Cardiac myocyte exosomes: stability, HSP60, and proteomics. *American journal of physiology. Heart and circulatory physiology,* 304**,** H954-H965.

MALLAT, Z., LAMBEAU, G. & TEDGUI, A. 2010. Lipoprotein-associated and secreted phospholipases A(2) in cardiovascular disease: roles as biological effectors and biomarkers. *Circulation,* 122**,** 2183-200.

MANGI, A. A., NOISEUX, N., KONG, D., HE, H., REZVANI, M., INGWALL, J. S. & DZAU, V. J. 2003. Mesenchymal stem cells modified with Akt prevent remodeling and restore performance of infarcted hearts. *Nature Medicine,* 9**,** 1195.

MANN, D. & BRISTOW, M. 2005. Mechanisms and models in heart failure: the biomechanical model and beyond. *Circulation,* 111**,** 2837–2849.

MATHERS, C., STEVENS, G. & MASCARENHAS, M. 2009. *Global health risks : mortality and burden of disease attributable to selected major risks,* Geneva, Switzerland, World Health Organization.

MCCOLLUM, L. T., GALLAGHER, P. E. & ANN TALLANT, E. 2012. Angiotensin-(1-7) attenuates angiotensin II-induced cardiac remodeling associated with upregulation of dual-specificity phosphatase 1. *Am J Physiol Heart Circ Physiol,* 302**,** H801-10.

MCMURRAY, J. J., OSTERGREN, J., SWEDBERG, K., GRANGER, C. B., HELD, P., MICHELSON, E. L., OLOFSSON, B., YUSUF, S. & PFEFFER, M. A. 2003. Effects of candesartan in patients with chronic heart failure and reduced left-ventricular systolic function taking angiotensin-converting-enzyme inhibitors: the CHARM-Added trial. *Lancet,* 362**,** 767-71.

MCMURRAY, J. J., PACKER, M., DESAI, A. S., GONG, J., LEFKOWITZ, M. P., RIZKALA, A. R., ROULEAU, J., SHI, V. C., SOLOMON, S. D., SWEDBERG, K. & ZILE, M. R. 2013. Dual angiotensin receptor and neprilysin inhibition as an alternative to angiotensin-converting enzyme inhibition in patients with chronic systolic heart failure: rationale for and design of the Prospective comparison of ARNI with ACEI to Determine Impact on Global Mortality and morbidity in Heart Failure trial (PARADIGM-HF). *Eur J Heart Fail,* 15**,** 1062-73.

MCMURRAY, J. J. & PFEFFER, M. A. 2005. Heart failure. *Lancet,* 365**,** 1877-89.

MEHTA, P. K. & GRIENDLING, K. K. 2007. Angiotensin II cell signaling: physiological and pathological effects in the cardiovascular system. *Am J Physiol Cell Physiol,* 292**,** C82-97.

MENDIS, P. P. & NORRVING 2011. *Global atlas on cardiovascular disease prevention and control*, Geneva : World Health Organization in collaboration with the World Heart Federation and the World Stroke Organization, [2011] ©2011.

MERCURE, C., YOGI, A., CALLERA, G. E., ARANHA, A. B., BADER, M., FERREIRA, A. J., SANTOS, R. A., WALTHER, T., TOUYZ, R. M. & REUDELHUBER, T. L. 2008. Angiotensin(1-7) blunts hypertensive cardiac remodeling by a direct effect on the heart. *Circ Res,* 103**,** 1319-26.

MICHAILOV, M. L., SCHAD, H., DAHLHEIM, H., JACOB, I. C. & BRECHTELSBAUER, H. 1987. Renin-angiotensin system responses of acute graded hemorrhage in dogs. *Circ Shock,* 21**,** 217-24.

MISHRA, J. S., MORE, A. S., GOPALAKRISHNAN, K. & KUMAR, S. 2019. Testosterone plays a permissive role in angiotensin II-induced hypertension and cardiac hypertrophy in male rats. *Biol Reprod,* 100**,** 139-148.

MITTELBRUNN, M., GUTIERREZ-VAZQUEZ, C., VILLARROYA-BELTRI, C., GONZALEZ, S., SANCHEZ-CABO, F., GONZALEZ, M. A., BERNAD, A. & SANCHEZ-MADRID, F. 2011. Unidirectional transfer of microRNA-loaded exosomes from T cells to antigen-presenting cells. *Nat Commun,* 2**,** 282.

MONTECALVO, A., LARREGINA, A. T., SHUFESKY, W. J., STOLZ, D. B., SULLIVAN, M. L., KARLSSON, J. M., BATY, C. J., GIBSON, G. A., ERDOS, G., WANG, Z., MILOSEVIC, J., TKACHEVA, O. A., DIVITO, S. J., JORDAN, R., LYONS-WEILER, J., WATKINS, S. C. & MORELLI, A. E. 2012. Mechanism of transfer of functional microRNAs between mouse dendritic cells via exosomes. *Blood,* 119**,** 756-66.

MORELLI, A. E., LARREGINA, A. T., SHUFESKY, W. J., SULLIVAN, M. L., STOLZ, D. B., PAPWORTH, G. D., ZAHORCHAK, A. F., LOGAR, A. J., WANG, Z., WATKINS, S. C., FALO, L. D., JR. & THOMSON, A. W. 2004. Endocytosis, intracellular sorting, and processing of exosomes by dendritic cells. *Blood,* 104**,** 3257-66.

MORISHITA, M., TAKAHASHI, Y., NISHIKAWA, M. & TAKAKURA, Y. 2017. Pharmacokinetics of Exosomes-An Important Factor for Elucidating the Biological Roles of Exosomes and for the Development of Exosome-Based Therapeutics. *J Pharm Sci,* 106**,** 2265-2269.

MUKAKA, M. M. 2012. Statistics corner: A guide to appropriate use of correlation coefficient in medical research. *Malawi medical journal : the journal of Medical Association of Malawi,* 24**,** 69-71.

MUKOYAMA, M., NAKAJIMA, M., HORIUCHI, M., SASAMURA, H., PRATT, R. E. & DZAU, V. J. 1993. Expression cloning of type 2 angiotensin II receptor reveals a unique class of seven-transmembrane receptors. *J Biol Chem,* 268**,** 24539-42.

MULCAHY, L. A., PINK, R. C. & CARTER, D. R. 2014. Routes and mechanisms of extracellular vesicle uptake. *J Extracell Vesicles,* 3.

MULROW, P. J. 1999. Angiotensin II and aldosterone regulation. *Regul Pept,* 80**,** 27-32.

MURALIDHARAN-CHARI, V., CLANCY, J., PLOU, C., ROMAO, M., CHAVRIER, P., RAPOSO, G. & D'SOUZA-SCHOREY, C. 2009. ARF6-regulated shedding of tumor cell-derived plasma membrane microvesicles. *Curr Biol,* 19**,** 1875-85.

NABHAN, J. F., HU, R., OH, R. S., COHEN, S. N. & LU, Q. 2012. Formation and release of arrestin domain-containing protein 1-mediated microvesicles (ARMMs) at plasma membrane by recruitment of TSG101 protein. *Proc Natl Acad Sci U S A,* 109**,** 4146-51.

NAFTILAN, A. J. & OPARIL, S. 1978. Inhibition of renin release from rat kidney slices by the angiotensins. *Am J Physiol,* 235**,** F62-8.

NANBO, A., KAWANISHI, E., YOSHIDA, R. & YOSHIYAMA, H. 2013. Exosomes derived from Epstein-Barr virus-infected cells are internalized via caveola-dependent endocytosis and promote phenotypic modulation in target cells. *J Virol,* 87**,** 10334-47.

NARBUTE, K., PILIPENKO, V., PUPURE, J., DZIRKALE, Z., JONAVICE, U., TUNAITIS, V., KRIAUCIUNAITE, K., JARMALAVICIUTE, A., JANSONE, B., KLUSA, V. & PIVORIUNAS, A. 2019. Intranasal Administration of Extracellular Vesicles Derived from Human Teeth Stem Cells Improve Motor Symptoms and Normalize Tyrosine Hydroxylase Expression in the Substantia Nigra and Striatum of the 6-Hydroxydopamine-Treated Rats. *Stem Cells Transl Med*.

NEMETH, A., ORGOVAN, N., SODAR, B. W., OSTEIKOETXEA, X., PALOCZI, K., SZABO-TAYLOR, K. E., VUKMAN, K. V., KITTEL, A., TURIAK, L., WIENER, Z., TOTH, S., DRAHOS, L., VEKEY, K., HORVATH, R. & BUZAS, E. I. 2017. Antibiotic-induced release of small extracellular vesicles (exosomes) with surface-associated DNA. *Sci Rep,* 7**,** 8202.

NEUBAUER, B., MACHURA, K., CHEN, M., WEINSTEIN, L. S., OPPERMANN, M., SEQUEIRA-LOPEZ, M. L., GOMEZ, R. A., SCHNERMANN, J., CASTROP, H., KURTZ, A. & WAGNER, C. 2009. Development of vascular renin expression in the kidney critically depends on the cyclic AMP pathway. *Am J Physiol Renal Physiol,* 296**,** F1006-12.

NEVES, L. A., ALMEIDA, A. P., KHOSLA, M. C., CAMPAGNOLE-SANTOS, M. J. & SANTOS, R. A. 1997. Effect of angiotensin-(1-7) on reperfusion arrhythmias in isolated rat hearts. *Braz J Med Biol Res,* 30**,** 801-9.

OCARANZA, M. P. & JALIL, J. E. 2012. Protective Role of the ACE2/Ang-(1-9) Axis in Cardiovascular Remodeling. *Int J Hypertens,* 2012**,** 594361.

OCARANZA, M. P., LAVANDERO, S., JALIL, J. E., MOYA, J., PINTO, M., NOVOA, U., APABLAZA, F., GONZALEZ, L., HERNANDEZ, C., VARAS, M., LOPEZ, R., GODOY, I., VERDEJO, H. & CHIONG, M. 2010. Angiotensin-(1-9) regulates cardiac hypertrophy in vivo and in vitro. *J Hypertens,* 28**,** 1054-64.

OCARANZA, M. P., MOYA, J., BARRIENTOS, V., ALZAMORA, R., HEVIA, D., MORALES, C., PINTO, M., ESCUDERO, N., GARCIA, L., NOVOA, U., AYALA, P., DIAZ-ARAYA, G., GODOY, I., CHIONG, M., LAVANDERO, S., JALIL, J. E. & MICHEA, L. 2014. Angiotensin-(1-9) reverses experimental hypertension and cardiovascular damage by inhibition of the angiotensin converting enzyme/Ang II axis. *J Hypertens,* 32**,** 771-83.

OHYAMA, K., YAMANO, Y., SANO, T., NAKAGOMI, Y., HAMAKUBO, T., MORISHIMA, I. & INAGAMI, T. 1995. Disulfide bridges in extracellular domains of angiotensin II receptor type IA. *Regul Pept,* 57**,** 141-7.

OPPERMANN, M., FREEDMAN, N. J., ALEXANDER, R. W. & LEFKOWITZ, R. J. 1996. Phosphorylation of the type 1A angiotensin II receptor by G protein-coupled receptor kinases and protein kinase C. *J Biol Chem,* 271**,** 13266-72.

ORSBORNE, C., CHAGGAR, P. S., SHAW, S. M. & WILLIAMS, S. G. 2017. The renin-angiotensin-aldosterone system in heart failure for the non-specialist: the past, the present and the future. *Postgrad Med J,* 93**,** 29-37.

OSADA-OKA, M., SHIOTA, M., IZUMI, Y., NISHIYAMA, M., TANAKA, M., YAMAGUCHI, T., SAKURAI, E., MIURA, K. & IWAO, H. 2016. Macrophage-derived exosomes induce inflammatory factors in endothelial cells under hypertensive conditions. *Hypertension Research,* 40**,** 353.

OSTROWSKI, M., CARMO, N. B., KRUMEICH, S., FANGET, I., RAPOSO, G., SAVINA, A., MOITA, C. F., SCHAUER, K., HUME, A. N., FREITAS, R. P., GOUD, B., BENAROCH, P., HACOHEN, N., FUKUDA, M., DESNOS, C., SEABRA, M. C., DARCHEN, F., AMIGORENA, S., MOITA, L. F. & THERY, C. 2010. Rab27a and Rab27b control different steps of the exosome secretion pathway. *Nat Cell Biol,* 12**,** 19-30; sup pp 1-13.

OTANI, K., YOKOYA, M., KODAMA, T., HORI, K., MATSUMOTO, K., OKADA, M. & YAMAWAKI, H. 2018. Plasma exosomes regulate systemic blood pressure in rats. *Biochem Biophys Res Commun,* 503**,** 776-783.

PADIA, S. H., KEMP, B. A., HOWELL, N. L., GILDEA, J. J., KELLER, S. R. & CAREY, R. M. 2009. Intrarenal angiotensin III infusion induces natriuresis and angiotensin type 2 receptor translocation in Wistar-Kyoto but not in spontaneously hypertensive rats. *Hypertension,* 53**,** 338-43.

PARKIN, E. T., TURNER, A. J. & HOOPER, N. M. 2004. Secretase-mediated cell surface shedding of the angiotensin-converting enzyme. *Protein Pept Lett,* 11**,** 423-32.

PASCUCCI, L., COCCE, V., BONOMI, A., AMI, D., CECCARELLI, P., CIUSANI, E., VIGANO, L., LOCATELLI, A., SISTO, F., DOGLIA, S. M., PARATI, E.,

BERNARDO, M. E., MURACA, M., ALESSANDRI, G., BONDIOLOTTI, G. & PESSINA, A. 2014. Paclitaxel is incorporated by mesenchymal stromal cells and released in exosomes that inhibit in vitro tumor growth: a new approach for drug delivery. *J Control Release,* 192**,** 262-70.

PASQUET, J. M., DACHARY-PRIGENT, J. & NURDEN, A. T. 1996. Calcium influx is a determining factor of calpain activation and microparticle formation in platelets. *Eur J Biochem,* 239**,** 647-54.

PATEL, V. B., BODIGA, S., BASU, R., DAS, S. K., WANG, W., WANG, Z., LO, J., GRANT, M. B., ZHONG, J., KASSIRI, Z. & OUDIT, G. Y. 2012. Loss of angiotensin-converting enzyme-2 exacerbates diabetic cardiovascular complications and leads to systolic and vascular dysfunction: a critical role of the angiotensin II/AT1 receptor axis. *Circ Res,* 110**,** 1322-35.

PATEL, V. B., TAKAWALE, A., RAMPRASATH, T., DAS, S. K., BASU, R., GRANT, M. B., HALL, D. A., KASSIRI, Z. & OUDIT, G. Y. 2015. Antagonism of angiotensin 1-7 prevents the therapeutic effects of recombinant human ACE2. *J Mol Med (Berl),* 93**,** 1003-13.

PATON, J. F. & KASPAROV, S. 1999. Differential effects of angiotensin II on cardiorespiratory reflexes mediated by nucleus tractus solitarii - a microinjection study in the rat. *The Journal of physiology,* 521 Pt 1**,** 213-225.

PAUL, M., WAGNER, J. & DZAU, V. J. 1993. Gene expression of the renin-angiotensin system in human tissues. Quantitative analysis by the polymerase chain reaction. *J Clin Invest,* 91**,** 2058-64.

PERTL, C., EBLENKAMP, M., PERTL, A., PFEIFER, S., WINTERMANTEL, E., LOCHMULLER, H., WALTER, M. C., KRAUSE, S. & THIRION, C. 2013. A new web-based method for automated analysis of muscle histology. *BMC Musculoskelet Disord,* 14**,** 26.

PETER, A. K., BJERKE, M. A. & LEINWAND, L. A. 2016. Biology of the cardiac myocyte in heart disease. *Molecular biology of the cell,* 27**,** 2149-2160.

PETRIE, M. C., PADMANABHAN, N., MCDONALD, J. E., HILLIER, C., CONNELL, J. M. & MCMURRAY, J. J. 2001. Angiotensin converting enzyme (ACE) and non-ACE dependent angiotensin II generation in resistance arteries from patients with heart failure and coronary heart disease. *J Am Coll Cardiol,* 37**,** 1056-61.

PILZ, B., SHAGDARSUREN, E., WELLNER, M., FIEBELER, A., DECHEND, R., GRATZE, P., MEINERS, S., FELDMAN, D. L., WEBB, R. L., GARRELDS, I. M., JAN DANSER, A. H., LUFT, F. C. & MULLER, D. N. 2005. Aliskiren, a human renin inhibitor, ameliorates cardiac and renal damage in double-transgenic rats. *Hypertension,* 46**,** 569-76.

PIRONTI, G., STRACHAN, R. T., ABRAHAM, D., MON-WEI YU, S., CHEN, M., CHEN, W., HANADA, K., MAO, L., WATSON, L. J. & ROCKMAN, H. A. 2015. Circulating Exosomes Induced by Cardiac Pressure Overload Contain Functional Angiotensin II Type 1 Receptors. *Circulation,* 131**,** 2120-30.

PLEBANEK, M. P., MUTHARASAN, R. K., VOLPERT, O., MATOV, A., GATLIN, J. C. & THAXTON, C. S. 2015. Nanoparticle Targeting and Cholesterol Flux Through Scavenger Receptor Type B-1 Inhibits Cellular Exosome Uptake. *Sci Rep,* 5**,** 15724.

POLS, M. S. & KLUMPERMAN, J. 2009. Trafficking and function of the tetraspanin CD63. *Exp Cell Res,* 315**,** 1584-92.

POPOVIC, V. 1988. Adaptation to restraint in the rat. *Physiologist,* 31**,** S65-6.

PORRELLO, E. R., PFLEGER, K. D., SEEBER, R. M., QIAN, H., ORO, C., ABOGADIE, F., DELBRIDGE, L. M. & THOMAS, W. G. 2011. Heteromerization of

angiotensin receptors changes trafficking and arrestin recruitment profiles. *Cell Signal,* 23**,** 1767-76.

PORSTI, I., BARA, A. T., BUSSE, R. & HECKER, M. 1994. Release of nitric oxide by angiotensin-(1-7) from porcine coronary endothelium: implications for a novel angiotensin receptor. *Br J Pharmacol,* 111**,** 652-4.

PRESTON, R. A., JY, W., JIMENEZ, J. J., MAURO, L. M., HORSTMAN, L. L., VALLE, M., AIME, G. & AHN, Y. S. 2003. Effects of severe hypertension on endothelial and platelet microparticles. *Hypertension,* 41**,** 211-7.

QI, Y., SHENOY, V., WONG, F., LI, H., AFZAL, A., MOCCO, J., SUMNERS, C., RAIZADA, M. K. & KATOVICH, M. J. 2011. Lentivirus-mediated overexpression of angiotensin-(1-7) attenuated ischaemia-induced cardiac pathophysiology. *Exp Physiol,* 96**,** 863-74.

RANGHINO, A., CANTALUPPI, V., GRANGE, C., VITILLO, L., FOP, F., BIANCONE, L., DEREGIBUS, M. C., TETTA, C., SEGOLONI, G. P. & CAMUSSI, G. 2012. Endothelial progenitor cell-derived microvesicles improve neovascularization in a murine model of hindlimb ischemia. *Int J Immunopathol Pharmacol,* 25**,** 75-85.

RAPOSO, G. & STOORVOGEL, W. 2013. Extracellular vesicles: exosomes, microvesicles, and friends. *J Cell Biol,* 200**,** 373-83.

RATAJCZAK, M. Z., KUCIA, M., JADCZYK, T., GRECO, N. J., WOJAKOWSKI, W., TENDERA, M. & RATAJCZAK, J. 2012. Pivotal role of paracrine effects in stem cell therapies in regenerative medicine: can we translate stem cell-secreted paracrine factors and microvesicles into better therapeutic strategies? *Leukemia,* 26**,** 1166-73.

RAUTOU, P. E., LEROYER, A. S., RAMKHELAWON, B., DEVUE, C., DUFLAUT, D., VION, A. C., NALBONE, G., CASTIER, Y., LESECHE, G., LEHOUX, S., TEDGUI, A. & BOULANGER, C. M. 2011. Microparticles from human atherosclerotic plaques promote endothelial ICAM-1-dependent monocyte adhesion and transendothelial migration. *Circ Res,* 108**,** 335-43.

REDDI, V., ZAGLUL, A., PENTZ, E. S. & GOMEZ, R. A. 1998. Renin-expressing cells are associated with branching of the developing kidney vasculature. *J Am Soc Nephrol,* 9**,** 63-71.

REISS, K., CAPASSO, J. M., HUANG, H. E., MEGGS, L. G., LI, P. & ANVERSA, P. 1993. ANG II receptors, c-myc, and c-jun in myocytes after myocardial infarction and ventricular failure. *Am J Physiol,* 264**,** H760-9.

RENTZSCH, B., TODIRAS, M., ILIESCU, R., POPOVA, E., CAMPOS, L. A., OLIVEIRA, M. L., BALTATU, O. C., SANTOS, R. A. & BADER, M. 2008. Transgenic angiotensin-converting enzyme 2 overexpression in vessels of SHRSP rats reduces blood pressure and improves endothelial function. *Hypertension,* 52**,** 967-73.

REZENDE, P. C., SCUDELER, T. L., DA COSTA, L. M. & HUEB, W. 2015. Conservative strategy for treatment of stable coronary artery disease. *World J Clin Cases,* 3**,** 163-70.

RIBEIRO-RODRIGUES, T. M., LAUNDOS, T. L., PEREIRA-CARVALHO, R., BATISTA-ALMEIDA, D., PEREIRA, R., COELHO-SANTOS, V., SILVA, A. P., FERNANDES, R., ZUZARTE, M., ENGUITA, F. J., COSTA, M. C., PINTO-DO-Ó, P., PINTO, M. T., GOUVEIA, P., FERREIRA, L., MASON, J. C., PEREIRA, P., KWAK, B. R., NASCIMENTO, D. S. & GIRÃO, H. 2017. Exosomes secreted by cardiomyocytes subjected to ischaemia promote cardiac angiogenesis. *Cardiovascular Research,* 113**,** 1338-1350.

RICE, G. I., THOMAS, D. A., GRANT, P. J., TURNER, A. J. & HOOPER, N. M. 2004. Evaluation of angiotensin-converting enzyme (ACE), its homologue ACE2 and neprilysin in angiotensin peptide metabolism. *Biochem J,* 383**,** 45-51.

RIGAT, B., HUBERT, C., CORVOL, P. & SOUBRIER, F. 1992. PCR detection of the insertion/deletion polymorphism of the human angiotensin converting enzyme gene (DCP1) (dipeptidyl carboxypeptidase 1). *Nucleic acids research,* 20**,** 1433-1433.

ROCIC, P., GOVINDARAJAN, G., SABRI, A. & LUCCHESI, P. A. 2001. A role for PYK2 in regulation of ERK1/2 MAP kinases and PI 3-kinase by ANG II in vascular smooth muscle. *Am J Physiol Cell Physiol,* 280**,** C90-9.

ROHRWASSER, A., MORGAN, T., DILLON, H. F., ZHAO, L., CALLAWAY, C. W., HILLAS, E., ZHANG, S., CHENG, T., INAGAMI, T., WARD, K., TERREROS, D. A. & LALOUEL, J. M. 1999. Elements of a paracrine tubular renin-angiotensin system along the entire nephron. *Hypertension,* 34**,** 1265-74.

ROSS, R. 1999. Atherosclerosis--an inflammatory disease. *N Engl J Med,* 340**,** 115-26.

ROWE, B. P., SAYLOR, D. L., SPETH, R. C. & ABSHER, D. R. 1995. Angiotensin-(1-7) binding at angiotensin II receptors in the rat brain. *Regul Pept,* 56**,** 139-46.

RUILOPE, L. M. & SCHMIEDER, R. E. 2008. Left Ventricular Hypertrophy and Clinical Outcomes in Hypertensive Patients. *American Journal of Hypertension,* 21**,** 500-508.

SAHA, P., SHARMA, S., KORUTLA, L., DATLA, S. R., SHOJA-TAHERI, F., MISHRA, R., BIGHAM, G. E., SARKAR, M., MORALES, D., BITTLE, G., GUNASEKARAN, M., AMBASTHA, C., ARFAT, M. Y., LI, D., HABERTHEUER, A., HU, R., PLATT, M. O., YANG, P., DAVIS, M. E., VALLABHAJOSYULA, P. & KAUSHAL, S. 2019. Circulating exosomes derived from transplanted progenitor cells aid the functional recovery of ischemic myocardium. *Sci Transl Med,* 11.

SAMAK, M., FATULLAYEV, J., SABASHNIKOV, A., ZERIOUH, M., SCHMACK, B., FARAG, M., POPOV, A. F., DOHMEN, P. M., CHOI, Y. H., WAHLERS, T. & WEYMANN, A. 2016. Cardiac Hypertrophy: An Introduction to Molecular and Cellular Basis. *Med Sci Monit Basic Res,* 22**,** 75-9.

SAMPAIO, W. O., SOUZA DOS SANTOS, R. A., FARIA-SILVA, R., DA MATA MACHADO, L. T., SCHIFFRIN, E. L. & TOUYZ, R. M. 2007. Angiotensin-(1-7) through receptor Mas mediates endothelial nitric oxide synthase activation via Akt-dependent pathways. *Hypertension,* 49**,** 185-92.

SANTOS, R. A., BRUM, J. M., BROSNIHAN, K. B. & FERRARIO, C. M. 1990. The renin-angiotensin system during acute myocardial ischemia in dogs. *Hypertension,* 15**,** I121-7.

SANTOS, R. A., CAMPAGNOLE-SANTOS, M. J. & ANDRADE, S. P. 2000. Angiotensin-(1-7): an update. *Regul Pept,* 91**,** 45-62.

SANTOS, R. A., FERREIRA, A. J., NADU, A. P., BRAGA, A. N., DE ALMEIDA, A. P., CAMPAGNOLE-SANTOS, M. J., BALTATU, O., ILIESCU, R., REUDELHUBER, T. L. & BADER, M. 2004. Expression of an angiotensin-(1-7)-producing fusion protein produces cardioprotective effects in rats. *Physiol Genomics,* 17**,** 292-9.

SANTOS, R. A., SIMOES E SILVA, A. C., MARIC, C., SILVA, D. M., MACHADO, R. P., DE BUHR, I., HERINGER-WALTHER, S., PINHEIRO, S. V., LOPES, M. T., BADER, M., MENDES, E. P., LEMOS, V. S., CAMPAGNOLE-SANTOS, M. J., SCHULTHEISS, H. P., SPETH, R. & WALTHER, T. 2003. Angiotensin-(1-7) is an endogenous ligand for the G protein-coupled receptor Mas. *Proc Natl Acad Sci U S A,* 100**,** 8258-63.

SARKIS, A., LOPEZ, B. & ROMAN, R. J. 2004. Role of 20-hydroxyeicosatetraenoic acid and epoxyeicosatrienoic acids in hypertension. *Curr Opin Nephrol Hypertens,* 13**,** 205-14.

SAUTER, A., MACHURA, K., NEUBAUER, B., KURTZ, A. & WAGNER, C. 2008. Development of renin expression in the mouse kidney. *Kidney Int,* 73**,** 43-51.

SAVERGNINI, S. Q., BEIMAN, M., LAUTNER, R. Q., DE PAULA-CARVALHO, V., ALLAHDADI, K., PESSOA, D. C., COSTA-FRAGA, F. P., FRAGA-SILVA, R. A., COJOCARU, G., COHEN, Y., BADER, M., DE ALMEIDA, A. P., ROTMAN, G. & SANTOS, R. A. 2010. Vascular relaxation, antihypertensive effect, and cardioprotection of a novel peptide agonist of the MAS receptor. *Hypertension,* 56**,** 112-20.

SCHALEKAMP, M. A., ADMIRAAL, P. J. & DERKX, F. H. 1989. Estimation of regional metabolism and production of angiotensins in hypertensive subjects. *Br J Clin Pharmacol,* 28 Suppl 2**,** 105S-112S; discussion 112S-113S.

SCHLUTER, K. D. & WENZEL, S. 2008. Angiotensin II: a hormone involved in and contributing to pro-hypertrophic cardiac networks and target of anti-hypertrophic cross-talks. *Pharmacol Ther,* 119**,** 311-25.

SCHMIEDER, R. E., MARTUS, P. & KLINGBEIL, A. 1996. Reversal of left ventricular hypertrophy in essential hypertension. A meta-analysis of randomized double-blind studies. *Jama,* 275**,** 1507-13.

SCHWARZ, H., BUMPUS, F. M. & PAGE, I. H. 1957. Synthesis of a Biologically Active Octapeptide Similar to Natural Isoleucine Angiotonin Octapeptide1. *Journal of the American Chemical Society,* 79**,** 5697-5703.

SEKO, T., ITO, M., KUREISHI, Y., OKAMOTO, R., MORIKI, N., ONISHI, K., ISAKA, N., HARTSHORNE, D. J. & NAKANO, T. 2003. Activation of RhoA and inhibition of myosin phosphatase as important components in hypertension in vascular smooth muscle. *Circ Res,* 92**,** 411-8.

SEQUEIRA LOPEZ, M. L., PENTZ, E. S., ROBERT, B., ABRAHAMSON, D. R. & GOMEZ, R. A. 2001. Embryonic origin and lineage of juxtaglomerular cells. *Am J Physiol Renal Physiol,* 281**,** F345-56.

SHAMKHLOVA, M., TRUBITSYNA, N. P., KATSAIA, G. V., GONCHAROV, N. P., MALYSHEVA, N. M., IL'IN, A. V., NIKANKINA, L. V., KOSHEL, L. V. & SHESTAKOVA, M. V. 2008. [The angiotensin II inhibition escape phenomenon in patients with type 2 diabetes and diabetic nephropathy]. *Ter Arkh,* 80**,** 49-52.

SHEN, Z., ZHANG, Z., WANG, X. & YANG, K. 2018. VEGFB-VEGFR1 ameliorates Ang II-induced cardiomyocyte hypertrophy through Ca(2+) -mediated PKG I pathway. *J Cell Biochem,* 119**,** 1511-1520.

SHI, Y., YANG, Y., GUO, Q., GAO, Q., DING, Y., WANG, H., XU, W., YU, B., WANG, M., ZHAO, Y. & ZHU, W. 2019. Exosomes Derived from Human Umbilical Cord Mesenchymal Stem Cells Promote Fibroblast-to-Myofibroblast Differentiation in Inflammatory Environments and Benefit Cardioprotective Effects. *Stem Cells Dev*.

SHTAM, T. A., KOVALEV, R. A., VARFOLOMEEVA, E. Y., MAKAROV, E. M., KIL, Y. V. & FILATOV, M. V. 2013. Exosomes are natural carriers of exogenous siRNA to human cells in vitro. *Cell Commun Signal,* 11**,** 88.

SIPIDO, K. R. & MARBAN, E. 1991. L-type calcium channels, potassium channels, and novel nonspecific cation channels in a clonal muscle cell line derived from embryonic rat ventricle. *Circ Res,* 69**,** 1487-99.

SKEGGS, L. T., JR., KAHN, J. R. & SHUMWAY, N. P. 1956. The preparation and function of the hypertensin-converting enzyme. *J Exp Med,* 103**,** 295-9.

SNYDER, R. A., WATT, K. W. & WINTROUB, B. U. 1985. A human platelet angiotensin I-processing system. Identification of components and inhibition of angiotensin-converting enzyme by product. *J Biol Chem,* 260**,** 7857-60.

SOLETI, R., ANDRIANTSITOHAINA, R. & MARTINEZ, M. C. 2018. Impact of polyphenols on extracellular vesicle levels and effects and their properties as tools for drug delivery for nutrition and health. *Arch Biochem Biophys,* 644**,** 57-63.

SOLOMON, S. D., APPELBAUM, E., MANNING, W. J., VERMA, A., BERGLUND, T., LUKASHEVICH, V., CHERIF PAPST, C., SMITH, B. A. & DAHLOF, B. 2009. Effect of the direct Renin inhibitor aliskiren, the Angiotensin receptor blocker losartan, or both on left ventricular mass in patients with hypertension and left ventricular hypertrophy. *Circulation,* 119**,** 530-7.

SOMSEL RODMAN, J. & WANDINGER-NESS, A. 2000. Rab GTPases coordinate endocytosis. *J Cell Sci,* 113 Pt 2**,** 183-92.

SOUZA, A. P., SOBRINHO, D. B., ALMEIDA, J. F., ALVES, G. M., MACEDO, L. M., PORTO, J. E., VENCIO, E. F., COLUGNATI, D. B., SANTOS, R. A., FERREIRA, A. J., MENDES, E. P. & CASTRO, C. H. 2013. Angiotensin II type 1 receptor blockade restores angiotensin-(1-7)-induced coronary vasodilation in hypertrophic rat hearts. *Clin Sci (Lond),* 125**,** 449-59.

STUFFERS, S., SEM WEGNER, C., STENMARK, H. & BRECH, A. 2009. Multivesicular endosome biogenesis in the absence of ESCRTs. *Traffic,* 10**,** 925-37.

SUN, J., ZHANG, Z., MA, T., YANG, Z., ZHANG, J., LIU, X., LU, D., SHEN, Z., YANG, J. & MENG, Q. 2018a. Endothelial progenitor cell-derived exosomes, loaded with miR-126, promoted deep vein thrombosis resolution and recanalization. *Stem Cell Res Ther,* 9**,** 223.

SUN, X., SHAN, A., WEI, Z. & XU, B. 2018b. Intravenous mesenchymal stem cell-derived exosomes ameliorate myocardial inflammation in the dilated cardiomyopathy. *Biochem Biophys Res Commun,* 503**,** 2611-2618.

SVENSSON, K. J., CHRISTIANSON, H. C., WITTRUP, A., BOURSEAU-GUILMAIN, E., LINDQVIST, E., SVENSSON, L. M., MORGELIN, M. & BELTING, M. 2013. Exosome uptake depends on ERK1/2-heat shock protein 27 signaling and lipid Raft-mediated endocytosis negatively regulated by caveolin-1. *J Biol Chem,* 288**,** 17713-24.

SYLOW, L., NIELSEN, I. L., KLEINERT, M., MOLLER, L. L., PLOUG, T., SCHJERLING, P., BILAN, P. J., KLIP, A., JENSEN, T. E. & RICHTER, E. A. 2016. Rac1 governs exercise-stimulated glucose uptake in skeletal muscle through regulation of GLUT4 translocation in mice. *J Physiol,* 594**,** 4997-5008.

TALLANT, E. A., FERRARIO, C. M. & GALLAGHER, P. E. 2005. Angiotensin-(1-7) inhibits growth of cardiac myocytes through activation of the mas receptor. *Am J Physiol Heart Circ Physiol,* 289**,** H1560-6.

TANG, K., ZHANG, Y., ZHANG, H., XU, P., LIU, J., MA, J., LV, M., LI, D., KATIRAI, F., SHEN, G. X., ZHANG, G., FENG, Z. H., YE, D. & HUANG, B. 2012. Delivery of chemotherapeutic drugs in tumour cell-derived microparticles. *Nat Commun,* 3**,** 1282.

TAURINO, C., MILLER, W. H., MCBRIDE, M. W., MCCLURE, J. D., KHANIN, R., MORENO, M. U., DYMOTT, J. A., DELLES, C. & DOMINICZAK, A. F. 2010. Gene expression profiling in whole blood of patients with coronary artery disease. *Clin Sci (Lond),* 119**,** 335-43.

THAKUR, B. K., ZHANG, H., BECKER, A., MATEI, I., HUANG, Y., COSTA-SILVA, B., ZHENG, Y., HOSHINO, A., BRAZIER, H., XIANG, J., WILLIAMS, C., RODRIGUEZ-BARRUECO, R., SILVA, J. M., ZHANG, W., HEARN, S., ELEMENTO, O., PAKNEJAD, N., MANOVA-TODOROVA, K., WELTE, K., BROMBERG, J., PEINADO, H. & LYDEN, D. 2014. Double-stranded DNA in exosomes: a novel biomarker in cancer detection. *Cell Res,* 24**,** 766-9.

THÉRY, C., AMIGORENA, S., RAPOSO, G. & CLAYTON, A. 2006. Isolation and characterization of exosomes from cell culture supernatants and biological fluids. *Curr Protoc Cell Biol,* Chapter 3**,** Unit 3.22.

THERY, C., BOUSSAC, M., VERON, P., RICCIARDI-CASTAGNOLI, P., RAPOSO, G., GARIN, J. & AMIGORENA, S. 2001. Proteomic analysis of dendritic cell-derived exosomes: a secreted subcellular compartment distinct from apoptotic vesicles. *J Immunol,* 166**,** 7309-18.

THÉRY, C., WITWER, K. W., AIKAWA, E., ALCARAZ, M. J., ANDERSON, J. D., ANDRIANTSITOHAINA, R., ANTONIOU, A., ARAB, T., ARCHER, F., ATKIN-SMITH, G. K., AYRE, D. C., BACH, J.-M., BACHURSKI, D., BAHARVAND, H., BALAJ, L., BALDACCHINO, S., BAUER, N. N., BAXTER, A. A., BEBAWY, M., BECKHAM, C., BEDINA ZAVEC, A., BENMOUSSA, A., BERARDI, A. C., BERGESE, P., BIELSKA, E., BLENKIRON, C., BOBIS-WOZOWICZ, S., BOILARD, E., BOIREAU, W., BONGIOVANNI, A., BORRÀS, F. E., BOSCH, S., BOULANGER, C. M., BREAKEFIELD, X., BREGLIO, A. M., BRENNAN, M. Á., BRIGSTOCK, D. R., BRISSON, A., BROEKMAN, M. L. D., BROMBERG, J. F., BRYL-GÓRECKA, P., BUCH, S., BUCK, A. H., BURGER, D., BUSATTO, S., BUSCHMANN, D., BUSSOLATI, B., BUZÁS, E. I., BYRD, J. B., CAMUSSI, G., CARTER, D. R. F., CARUSO, S., CHAMLEY, L. W., CHANG, Y.-T., CHEN, C., CHEN, S., CHENG, L., CHIN, A. R., CLAYTON, A., CLERICI, S. P., COCKS, A., COCUCCI, E., COFFEY, R. J., CORDEIRO-DA-SILVA, A., COUCH, Y., COUMANS, F. A. W., COYLE, B., CRESCITELLI, R., CRIADO, M. F., D'SOUZA-SCHOREY, C., DAS, S., DATTA CHAUDHURI, A., DE CANDIA, P., DE SANTANA, E. F., DE WEVER, O., DEL PORTILLO, H. A., DEMARET, T., DEVILLE, S., DEVITT, A., DHONDT, B., DI VIZIO, D., DIETERICH, L. C., DOLO, V., DOMINGUEZ RUBIO, A. P., DOMINICI, M., DOURADO, M. R., DRIEDONKS, T. A. P., DUARTE, F. V., DUNCAN, H. M., EICHENBERGER, R. M., EKSTRÖM, K., EL ANDALOUSSI, S., ELIE-CAILLE, C., ERDBRÜGGER, U., FALCÓN-PÉREZ, J. M., FATIMA, F., FISH, J. E., FLORES-BELLVER, M., FÖRSÖNITS, A., FRELET-BARRAND, A., et al. 2018. Minimal information for studies of extracellular vesicles 2018 (MISEV2018): a position statement of the International Society for Extracellular Vesicles and update of the MISEV2014 guidelines. *Journal of Extracellular Vesicles,* 7**,** 1535750.

THOMAS, W. G., BRANDENBURGER, Y., AUTELITANO, D. J., PHAM, T., QIAN, H. & HANNAN, R. D. 2002. Adenoviral-directed expression of the type 1A angiotensin receptor promotes cardiomyocyte hypertrophy via transactivation of the epidermal growth factor receptor. *Circ Res,* 90**,** 135-42.

THOMAS, W. G., MOTEL, T. J., KULE, C. E., KAROOR, V. & BAKER, K. M. 1998. Phosphorylation of the angiotensin II (AT1A) receptor carboxyl terminus: a role in receptor endocytosis. *Mol Endocrinol,* 12**,** 1513-24.

THUM, T., GALUPPO, P., WOLF, C., FIEDLER, J., KNEITZ, S., VAN LAAKE, L. W., DOEVENDANS, P. A., MUMMERY, C. L., BORLAK, J., HAVERICH, A., GROSS, C., ENGELHARDT, S., ERTL, G. & BAUERSACHS, J. 2007. MicroRNAs in the human heart: a clue to fetal gene reprogramming in heart failure. *Circulation,* 116**,** 258-67.

THUM, T., GROSS, C., FIEDLER, J., FISCHER, T., KISSLER, S., BUSSEN, M., GALUPPO, P., JUST, S., ROTTBAUER, W., FRANTZ, S., CASTOLDI, M., SOUTSCHEK, J., KOTELIANSKY, V., ROSENWALD, A., BASSON, M. A., LICHT, J. D., PENA, J. T., ROUHANIFARD, S. H., MUCKENTHALER, M. U., TUSCHL, T., MARTIN, G. R., BAUERSACHS, J. & ENGELHARDT, S. 2008. MicroRNA-21 contributes to myocardial disease by stimulating MAP kinase signalling in fibroblasts. *Nature,* 456**,** 980-4.

TIAN, C., GAO, L., ZIMMERMAN, M. C. & ZUCKER, I. H. 2018. Myocardial infarction-induced microRNA-enriched exosomes contribute to cardiac Nrf2 dysregulation in chronic heart failure. *American Journal of Physiology-Heart and Circulatory Physiology,* 314**,** H928-H939.

TIAN, J., GUO, X., LIU, X. M., LIU, L., WENG, Q. F., DONG, S. J., KNOWLTON, A. A., YUAN, W. J. & LIN, L. 2013. Extracellular HSP60 induces inflammation through activating and up-regulating TLRs in cardiomyocytes. *Cardiovasc Res,* 98**,** 391-401.

TIGERSTEDT, R. & BERGMAN, P. Q. 1898. Niere und Kreislauf1. *Skandinavisches Archiv Für Physiologie,* 8**,** 223-271.

TIMMERMANS, P. B., WONG, P. C., CHIU, A. T., HERBLIN, W. F., BENFIELD, P., CARINI, D. J., LEE, R. J., WEXLER, R. R., SAYE, J. A. & SMITH, R. D. 1993. Angiotensin II receptors and angiotensin II receptor antagonists. *Pharmacol Rev,* 45**,** 205-51.

TIMMERS, L., LIM, S. K., ARSLAN, F., ARMSTRONG, J. S., HOEFER, I. E., DOEVENDANS, P. A., PIEK, J. J., EL OAKLEY, R. M., CHOO, A., LEE, C. N., PASTERKAMP, G. & DE KLEIJN, D. P. 2007. Reduction of myocardial infarct size by human mesenchymal stem cell conditioned medium. *Stem Cell Res,* 1**,** 129-37.

TIPNIS, S. R., HOOPER, N. M., HYDE, R., KARRAN, E., CHRISTIE, G. & TURNER, A. J. 2000. A human homolog of angiotensin-converting enzyme. Cloning and functional expression as a captopril-insensitive carboxypeptidase. *J Biol Chem,* 275**,** 33238-43.

TOKUDA, K., KAI, H., KUWAHARA, F., YASUKAWA, H., TAHARA, N., KUDO, H., TAKEMIYA, K., KOGA, M., YAMAMOTO, T. & IMAIZUMI, T. 2004. Pressure-independent effects of angiotensin II on hypertensive myocardial fibrosis. *Hypertension,* 43**,** 499-503.

TOUYZ, R. M., HE, G., DENG, L. Y. & SCHIFFRIN, E. L. 1999. Role of extracellular signal-regulated kinases in angiotensin II-stimulated contraction of smooth muscle cells from human resistance arteries. *Circulation,* 99**,** 392-9.

TOWLER, P., STAKER, B., PRASAD, S. G., MENON, S., TANG, J., PARSONS, T., RYAN, D., FISHER, M., WILLIAMS, D., DALES, N. A., PATANE, M. A. & PANTOLIANO, M. W. 2004. ACE2 X-ray structures reveal a large hinge-bending motion important for inhibitor binding and catalysis. *J Biol Chem,* 279**,** 17996-8007.

TRAJKOVIC, K., HSU, C., CHIANTIA, S., RAJENDRAN, L., WENZEL, D., WIELAND, F., SCHWILLE, P., BRUGGER, B. & SIMONS, M. 2008. Ceramide triggers budding of exosome vesicles into multivesicular endosomes. *Science,* 319**,** 1244-7.

TRAMS, E. G., LAUTER, C. J., SALEM, N., JR. & HEINE, U. 1981. Exfoliation of membrane ecto-enzymes in the form of micro-vesicles. *Biochim Biophys Acta,* 645**,** 63-70.

TRIOULIER, Y., TORCH, S., BLOT, B., CRISTINA, N., CHATELLARD-CAUSSE, C., VERNA, J. M. & SADOUL, R. 2004. Alix, a protein regulating endosomal trafficking, is involved in neuronal death. *J Biol Chem,* 279**,** 2046-52.

VALADI, H., EKSTROM, K., BOSSIOS, A., SJOSTRAND, M., LEE, J. J. & LOTVALL, J. O. 2007. Exosome-mediated transfer of mRNAs and microRNAs is a novel mechanism of genetic exchange between cells. *Nat Cell Biol*, 9, 654-9.

VALENCIA-NUNEZ, D. M., KREUTLER, W., MOYA-GONZALEZ, J., ALADOS-ARBOLEDAS, P., MUNOZ-CARVAJAL, I., CARMONA, A., RAMIREZ-CHAMOND, R. & CARRACEDO-ANON, J. 2017. Endothelial vascular markers in coronary surgery. *Heart Vessels,* 32, 1390-1399.

VAN DEUN, J., MESTDAGH, P., AGOSTINIS, P., AKAY, O., ANAND, S., ANCKAERT, J., MARTINEZ, Z. A., BAETENS, T., BEGHEIN, E., BERTIER, L., BERX, G., BOERE, J., BOUKOURIS, S., BREMER, M., BUSCHMANN, D., BYRD, J. B., CASERT, C., CHENG, L., CMOCH, A., DAVELOOSE, D., DE SMEDT, E., DEMIRSOY, S., DEPOORTER, V., DHONDT, B., DRIEDONKS, T. A., DUDEK, A., ELSHARAWY, A., FLORIS, I., FOERS, A. D., GARTNER, K., GARG, A. D., GEEURICKX, E., GETTEMANS, J., GHAZAVI, F., GIEBEL, B., KORMELINK, T. G., HANCOCK, G., HELSMOORTEL, H., HILL, A. F., HYENNE, V., KALRA, H., KIM, D., KOWAL, J., KRAEMER, S., LEIDINGER, P., LEONELLI, C., LIANG, Y., LIPPENS, L., LIU, S., LO CICERO, A., MARTIN, S., MATHIVANAN, S., MATHIYALAGAN, P., MATUSEK, T., MILANI, G., MONGUIO-TORTAJADA, M., MUS, L. M., MUTH, D. C., NEMETH, A., NOLTE-'T HOEN, E. N., O'DRISCOLL, L., PALMULLI, R., PFAFFL, M. W., PRIMDAL-BENGTSON, B., ROMANO, E., ROUSSEAU, Q., SAHOO, S., SAMPAIO, N., SAMUEL, M., SCICLUNA, B., SOEN, B., STEELS, A., SWINNEN, J. V., TAKATALO, M., THAMINY, S., THERY, C., TULKENS, J., VAN AUDENHOVE, I., VAN DER GREIN, S., VAN GOETHEM, A., VAN HERWIJNEN, M. J., VAN NIEL, G., VAN ROY, N., VAN VLIET, A. R., VANDAMME, N., VANHAUWAERT, S., VERGAUWEN, G., VERWEIJ, F., WALLAERT, A., WAUBEN, M., WITWER, K. W., ZONNEVELD, M. I., DE WEVER, O., VANDESOMPELE, J. & HENDRIX, A. 2017. EV-TRACK: transparent reporting and centralizing knowledge in extracellular vesicle research. *Nat Methods,* 14, 228-232.

VAN KATS, J. P., DANSER, A. H., VAN MEEGEN, J. R., SASSEN, L. M., VERDOUW, P. D. & SCHALEKAMP, M. A. 1998. Angiotensin production by the heart: a quantitative study in pigs with the use of radiolabeled angiotensin infusions. *Circulation,* 98, 73-81.

VAN KATS, J. P., DE LANNOY, L. M., JAN DANSER, A. H., VAN MEEGEN, J. R., VERDOUW, P. D. & SCHALEKAMP, M. A. 1997. Angiotensin II type 1 (AT1) receptor-mediated accumulation of angiotensin II in tissues and its intracellular half-life in vivo. *Hypertension,* 30, 42-9.

VAN KRALINGEN, J. C., MCFALL, A., ORD, E. N. J., COYLE, T. F., BISSETT, M., MCCLURE, J. D., MCCABE, C., MACRAE, I. M., DAWSON, J. & WORK, L. M. 2019. Altered Extracellular Vesicle MicroRNA Expression in Ischemic Stroke and Small Vessel Disease. *Transl Stroke Res*.

VANDERGRIFF, A. C., HENSLEY, M. T. & CHENG, K. 2015. Isolation and cryopreservation of neonatal rat cardiomyocytes. *J Vis Exp*.

VARAGIC, J., AHMAD, S., BROSNIHAN, K. B., GROBAN, L., CHAPPELL, M. C., TALLANT, E. A., GALLAGHER, P. E. & FERRARIO, C. M. 2010. Decreased cardiac Ang-(1-7) is associated with salt-induced cardiac remodeling and dysfunction. *Ther Adv Cardiovasc Dis,* 4, 17-25.

VERANO-BRAGA, T., SCHWAMMLE, V., SYLVESTER, M., PASSOS-SILVA, D. G., PELUSO, A. A., ETELVINO, G. M., SANTOS, R. A. & ROEPSTORFF, P. 2012. Time-resolved quantitative phosphoproteomics: new insights into Angiotensin-(1-7) signaling networks in human endothelial cells. *J Proteome Res,* 11, 3370-81.

VERDECCHIA, P., SCHILLACI, G., BORGIONI, C., CIUCCI, A., GATTOBIGIO, R., ZAMPI, I., REBOLDI, G. & PORCELLATI, C. 1998. Prognostic significance of serial changes in left ventricular mass in essential hypertension. *Circulation,* 97**,** 48-54.

VESTAD, B., LLORENTE, A., NEURAUTER, A., PHUYAL, S., KIERULF, B., KIERULF, P., SKOTLAND, T., SANDVIG, K., HAUG, K. B. F. & ØVSTEBØ, R. 2017. Size and concentration analyses of extracellular vesicles by nanoparticle tracking analysis: a variation study. *Journal of extracellular vesicles,* 6**,** 1344087-1344087.

VILAS-BOAS, W. W., RIBEIRO-OLIVEIRA, A., JR., PEREIRA, R. M., RIBEIRO RDA, C., ALMEIDA, J., NADU, A. P., SIMOES E SILVA, A. C. & DOS SANTOS, R. A. 2009. Relationship between angiotensin-(1-7) and angiotensin II correlates with hemodynamic changes in human liver cirrhosis. *World J Gastroenterol,* 15**,** 2512-9.

VRIJSEN, K. R., SLUIJTER, J. P., SCHUCHARDT, M. W., VAN BALKOM, B. W., NOORT, W. A., CHAMULEAU, S. A. & DOEVENDANS, P. A. 2010. Cardiomyocyte progenitor cell-derived exosomes stimulate migration of endothelial cells. *J Cell Mol Med,* 14**,** 1064-70.

WAHLGREN, J., DE, L. K. T., BRISSLERT, M., VAZIRI SANI, F., TELEMO, E., SUNNERHAGEN, P. & VALADI, H. 2012. Plasma exosomes can deliver exogenous short interfering RNA to monocytes and lymphocytes. *Nucleic Acids Res,* 40**,** e130.

WALDENSTRÖM, A., GENNEBÄCK, N., HELLMAN, U. & RONQUIST, G. 2012. Cardiomyocyte microvesicles contain DNA/RNA and convey biological messages to target cells. *PLoS One,* 7**,** e34653.

WANG, F., YUAN, Y., YANG, P. & LI, X. 2017a. Extracellular vesicles-mediated transfer of miR-208a/b exaggerate hypoxia/reoxygenation injury in cardiomyocytes by reducing QKI expression. *Mol Cell Biochem,* 431**,** 187-195.

WANG, T., GILKES, D. M., TAKANO, N., XIANG, L., LUO, W., BISHOP, C. J., CHATURVEDI, P., GREEN, J. J. & SEMENZA, G. L. 2014a. Hypoxia-inducible factors and RAB22A mediate formation of microvesicles that stimulate breast cancer invasion and metastasis. *Proc Natl Acad Sci U S A,* 111**,** E3234-42.

WANG, X., GU, H., HUANG, W., PENG, J., LI, Y., YANG, L., QIN, D., ESSANDOH, K., WANG, Y., PENG, T. & FAN, G. C. 2016. Hsp20-Mediated Activation of Exosome Biogenesis in Cardiomyocytes Improves Cardiac Function and Angiogenesis in Diabetic Mice. *Diabetes,* 65**,** 3111-28.

WANG, X., HUANG, W., LIU, G., CAI, W., MILLARD, R. W., WANG, Y., CHANG, J., PENG, T. & FAN, G. C. 2014b. Cardiomyocytes mediate anti-angiogenesis in type 2 diabetic rats through the exosomal transfer of miR-320 into endothelial cells. *J Mol Cell Cardiol,* 74**,** 139-50.

WANG, X. L., ZHAO, Y. Y., SUN, L., SHI, Y., LI, Z. Q., ZHAO, X. D., XU, C. G., JI, H. G., WANG, M., XU, W. R. & ZHU, W. 2018. Exosomes derived from human umbilical cord mesenchymal stem cells improve myocardial repair via upregulation of Smad7. *Int J Mol Med,* 41**,** 3063-3072.

WANG, Y., WEI, S., WANG, Y.-L., LIU, M., SHANG, M., ZHANG, Q., WU, Y.-N., LIU, M.-L., SONG, J.-Q. & LIU, Y.-X. 2017b. Protective effects of circulating microvesicles derived from myocardial ischemic rats on apoptosis of cardiomyocytes in myocardial ischemia/reperfusion injury. *Oncotarget,* 8**,** 54572-54582.

WATKINS, S. J., BORTHWICK, G. M. & ARTHUR, H. M. 2011. The H9C2 cell line and primary neonatal cardiomyocyte cells show similar hypertrophic responses in vitro. *In Vitro Cell Dev Biol Anim,* 47**,** 125-31.

WEATHERALL, E., HAUER, P., VOGEL, R. & WILLMOTT, G. R. 2016. Pulse Size Distributions in Tunable Resistive Pulse Sensing. *Analytical Chemistry,* 88**,** 8648-8656.

WEBER, K. T. 1989. Cardiac interstitium in health and disease: the fibrillar collagen network. *J Am Coll Cardiol,* 13**,** 1637-52.

WEST, N., GUZIK, T., BLACK, E. & CHANNON, K. 2001. Enhanced superoxide production in experimental venous bypass graft intimal hyperplasia: role of NAD(P)H oxidase. *Arterioscler Thromb Vasc Biol,* 21**,** 189-94.

WHALEY-CONNELL, A., HABIBI, J., REHMER, N., ARDHANARI, S., HAYDEN, M. R., PULAKAT, L., KRUEGER, C., FERRARIO, C. M., DEMARCO, V. G. & SOWERS, J. R. 2013. Renin inhibition and AT(1)R blockade improve metabolic signaling, oxidant stress and myocardial tissue remodeling. *Metabolism,* 62**,** 861-72.

WIDDOP, R. E., GARDINER, S. M., KEMP, P. A. & BENNETT, T. 1992. Inhibition of the haemodynamic effects of angiotensin II in conscious rats by AT2-receptor antagonists given after the AT1-receptor antagonist, EXP 3174. *Br J Pharmacol,* 107**,** 873-80.

WILENSKY, R. L. & HAMAMDZIC, D. 2007. The molecular basis of vulnerable plaque: potential therapeutic role for immunomodulation. *Curr Opin Cardiol,* 22**,** 545-51.

WITWER, K. W., SOEKMADJI, C., HILL, A. F., WAUBEN, M. H., BUZAS, E. I., DI VIZIO, D., FALCON-PEREZ, J. M., GARDINER, C., HOCHBERG, F., KUROCHKIN, I. V., LOTVALL, J., MATHIVANAN, S., NIEUWLAND, R., SAHOO, S., TAHARA, H., TORRECILHAS, A. C., WEAVER, A. M., YIN, H., ZHENG, L., GHO, Y. S., QUESENBERRY, P. & THERY, C. 2017. Updating the MISEV minimal requirements for extracellular vesicle studies: building bridges to reproducibility. *J Extracell Vesicles,* 6**,** 1396823.

WONG, N. D. 2014. Epidemiological studies of CHD and the evolution of preventive cardiology. *Nat Rev Cardiol,* 11**,** 276-89.

WONG, W. T., TIAN, X. Y., XU, A., NG, C. F., LEE, H. K., CHEN, Z. Y., AU, C. L., YAO, X. & HUANG, Y. 2010. Angiotensin II type 1 receptor-dependent oxidative stress mediates endothelial dysfunction in type 2 diabetic mice. *Antioxid Redox Signal,* 13**,** 757-68.

WU, B. X., CLARKE, C. J. & HANNUN, Y. A. 2010. Mammalian neutral sphingomyelinases: regulation and roles in cell signaling responses. *Neuromolecular Med,* 12**,** 320-30.

WU, G., ZHAO, G. & HE, Y. 2003. Distinct pathways for the trafficking of angiotensin II and adrenergic receptors from the endoplasmic reticulum to the cell surface: Rab1-independent transport of a G protein-coupled receptor. *J Biol Chem,* 278**,** 47062-9.

WYNNE, B. M., LABAZI, H., LIMA, V. V., CARNEIRO, F. S., WEBB, R. C., TOSTES, R. C. & GIACHINI, F. R. 2018. Mesenteric arteries from stroke-prone spontaneously hypertensive rats exhibit an increase in nitric-oxide-dependent vasorelaxation. *Can J Physiol Pharmacol,* 96**,** 719-727.

XIN, H., LI, Y., CUI, Y., YANG, J. J., ZHANG, Z. G. & CHOPP, M. 2013. Systemic administration of exosomes released from mesenchymal stromal cells promote functional recovery and neurovascular plasticity after stroke in rats. *J Cereb Blood Flow Metab,* 33**,** 1711-5.

XU, P., COSTA-GONCALVES, A. C., TODIRAS, M., RABELO, L. A., SAMPAIO, W. O., MOURA, M. M., SANTOS, S. S., LUFT, F. C., BADER, M., GROSS, V., ALENINA, N. & SANTOS, R. A. 2008. Endothelial dysfunction and elevated blood pressure in MAS gene-deleted mice. *Hypertension,* 51**,** 574-80.

YAMADA, K., IYER, S. N., CHAPPELL, M. C., GANTEN, D. & FERRARIO, C. M. 1998. Converting enzyme determines plasma clearance of angiotensin-(1-7). *Hypertension,* 32**,** 496-502.

YAMAMOTO, K., OHISHI, M., KATSUYA, T., ITO, N., IKUSHIMA, M., KAIBE, M., TATARA, Y., SHIOTA, A., SUGANO, S., TAKEDA, S., RAKUGI, H. & OGIHARA, T. 2006. Deletion of angiotensin-converting enzyme 2 accelerates pressure overload-induced cardiac dysfunction by increasing local angiotensin II. *Hypertension,* 47**,** 718-26.

YAN, C., KIM, D., AIZAWA, T. & BERK, B. C. 2003. Functional interplay between angiotensin II and nitric oxide: cyclic GMP as a key mediator. *Arterioscler Thromb Vasc Biol,* 23**,** 26-36.

YAN, X., ZHAO, R., FENG, X., MU, J., LI, Y., CHEN, Y., LI, C., YAO, Q., CAI, L., JIN, L., HAN, C. & ZHANG, D. 2019. Sialyltransferase7A promotes angiotensin II-induced cardiomyocyte hypertrophy via HIF-1alpha-TAK1 signaling pathway. *Cardiovasc Res*.

YÁÑEZ-MÓ, M., SILJANDER, P. R. M., ANDREU, Z., BEDINA ZAVEC, A., BORRÀS, F. E., BUZAS, E. I., BUZAS, K., CASAL, E., CAPPELLO, F., CARVALHO, J., COLÁS, E., CORDEIRO-DA SILVA, A., FAIS, S., FALCON-PEREZ, J. M., GHOBRIAL, I. M., GIEBEL, B., GIMONA, M., GRANER, M., GURSEL, I., GURSEL, M., HEEGAARD, N. H. H., HENDRIX, A., KIERULF, P., KOKUBUN, K., KOSANOVIC, M., KRALJ-IGLIC, V., KRÄMER-ALBERS, E.-M., LAITINEN, S., LÄSSER, C., LENER, T., LIGETI, E., LINĒ, A., LIPPS, G., LLORENTE, A., LÖTVALL, J., MANČEK-KEBER, M., MARCILLA, A., MITTELBRUNN, M., NAZARENKO, I., NOLTE-'T HOEN, E. N. M., NYMAN, T. A., O'DRISCOLL, L., OLIVAN, M., OLIVEIRA, C., PÁLLINGER, É., DEL PORTILLO, H. A., REVENTÓS, J., RIGAU, M., ROHDE, E., SAMMAR, M., SÁNCHEZ-MADRID, F., SANTARÉM, N., SCHALLMOSER, K., STAMPE OSTENFELD, M., STOORVOGEL, W., STUKELJ, R., VAN DER GREIN, S. G., HELENA VASCONCELOS, M., WAUBEN, M. H. M. & DE WEVER, O. 2015. Biological properties of extracellular vesicles and their physiological functions. *Journal of Extracellular Vesicles,* 4**,** 27066.

YANG, C. W., LU, L. C., CHANG, C. C., CHO, C. C., HSIEH, W. Y., TSAI, C. H., LIN, Y. C. & LIN, C. S. 2017. Imbalanced plasma ACE and ACE2 level in the uremic patients with cardiovascular diseases and its change during a single hemodialysis session. *Ren Fail,* 39**,** 719-728.

YANG, J., CHEN, C., REN, H., HAN, Y., HE, D., ZHOU, L., HOPFER, U., JOSE, P. A. & ZENG, C. 2012. Angiotensin II AT(2) receptor decreases AT(1) receptor expression and function via nitric oxide/cGMP/Sp1 in renal proximal tubule cells from Wistar-Kyoto rats. *J Hypertens,* 30**,** 1176-84.

YIM, H. E. & YOO, K. H. 2008. Renin-Angiotensin system - considerations for hypertension and kidney. *Electrolyte Blood Press,* 6**,** 42-50.

YU, L., YUAN, K., PHUONG, H. T., PARK, B. M. & KIM, S. H. 2016. Angiotensin-(1-5), an active mediator of renin-angiotensin system, stimulates ANP secretion via Mas receptor. *Peptides,* 86**,** 33-41.

YU, L., ZHENG, M., WANG, W., ROZANSKI, G. J., ZUCKER, I. H. & GAO, L. 2010. Developmental changes in AT1 and AT2 receptor-protein expression in rats. *J Renin Angiotensin Aldosterone Syst,* 11**,** 214-21.

YUSUF, S., PITT, B., DAVIS, C. E., HOOD, W. B. & COHN, J. N. 1991. Effect of enalapril on survival in patients with reduced left ventricular ejection fractions and congestive heart failure. *N Engl J Med,* 325**,** 293-302.

YUSUF, S., PITT, B., DAVIS, C. E., HOOD, W. B., JR. & COHN, J. N. 1992. Effect of enalapril on mortality and the development of heart failure in asymptomatic patients with reduced left ventricular ejection fractions. *N Engl J Med,* 327**,** 685-91.

ZENG, W., CHEN, W., LENG, X., HE, J. G. & MA, H. 2009. Chronic angiotensin-(1-7) administration improves vascular remodeling after angioplasty through the regulation of the TGF-beta/Smad signaling pathway in rabbits. *Biochem Biophys Res Commun,* 389**,** 138-44.

ZHANG, C., HEIN, T. W., WANG, W. & KUO, L. 2003. Divergent roles of angiotensin II AT1 and AT2 receptors in modulating coronary microvascular function. *Circ Res,* 92**,** 322-9.

ZHANG, F., HU, Y., XU, Q. & YE, S. 2010. Different effects of angiotensin II and angiotensin-(1-7) on vascular smooth muscle cell proliferation and migration. *PLoS One,* 5**,** e12323.

ZHANG, W., MA, Y., ZHANG, Y., YANG, J., HE, G. & CHEN, S. 2019. Photo-Oxidative Blue-Light Stimulation in Retinal Pigment Epithelium Cells Promotes Exosome Secretion and Increases the Activity of the NLRP3 Inflammasome. *Curr Eye Res,* 44**,** 67-75.

ZHANG, W., ZHOU, X., YAO, Q., LIU, Y., ZHANG, H. & DONG, Z. 2017a. HIF-1-mediated production of exosomes during hypoxia is protective in renal tubular cells. *Am J Physiol Renal Physiol,* 313**,** F906-f913.

ZHANG, X., WANG, G., DUPRE, D. J., FENG, Y., ROBITAILLE, M., LAZARTIGUES, E., FENG, Y. H., HEBERT, T. E. & WU, G. 2009. Rab1 GTPase and dimerization in the cell surface expression of angiotensin II type 2 receptor. *J Pharmacol Exp Ther,* 330**,** 109-17.

ZHANG, X., WANG, X., ZHU, H., KRANIAS, E. G., TANG, Y., PENG, T., CHANG, J. & FAN, G. C. 2012. Hsp20 functions as a novel cardiokine in promoting angiogenesis via activation of VEGFR2. *PLoS One,* 7**,** e32765.

ZHANG, Z. Z., CHENG, Y. W., JIN, H. Y., CHANG, Q., SHANG, Q. H., XU, Y. L., CHEN, L. X., XU, R., SONG, B. & ZHONG, J. C. 2017b. The sirtuin 6 prevents angiotensin II-mediated myocardial fibrosis and injury by targeting AMPK-ACE2 signaling. *Oncotarget,* 8**,** 72302-72314.

ZHAO, J., LI, X., HU, J., CHEN, F., QIAO, S., SUN, X., GAO, L., XIE, J. & XU, B. 2019. Mesenchymal Stromal Cell-Derived Exosomes Attenuate Myocardial Ischemia-Reperfusion Injury through miR-182-Regulated Macrophage Polarization. *Cardiovasc Res*.

ZHENG, S. L., RODDICK, A. J. & AYIS, S. 2017. Effects of aliskiren on mortality, cardiovascular outcomes and adverse events in patients with diabetes and cardiovascular disease or risk: A systematic review and meta-analysis of 13,395 patients. *Diab Vasc Dis Res,* 14**,** 400-406.

ZHONG, J., BASU, R., GUO, D., CHOW, F. L., BYRNS, S., SCHUSTER, M., LOIBNER, H., WANG, X. H., PENNINGER, J. M., KASSIRI, Z. & OUDIT, G. Y. 2010. Angiotensin-converting enzyme 2 suppresses pathological hypertrophy, myocardial fibrosis, and cardiac dysfunction. *Circulation,* 122**,** 717-28, 18 p following 728.

ZHOU, Y., JIANG, Y. & KANG, Y. J. 2007. Copper inhibition of hydrogen peroxide-induced hypertrophy in embryonic rat cardiac H9c2 cells. *Exp Biol Med (Maywood),* 232**,** 385-9.

ZISMAN, L. S., KELLER, R. S., WEAVER, B., LIN, Q., SPETH, R., BRISTOW, M. R. & CANVER, C. C. 2003. Increased angiotensin-(1-7)-forming activity in failing human heart ventricles: evidence for upregulation of the angiotensin-converting enzyme Homologue ACE2. *Circulation,* 108**,** 1707-12.